NOTE TO USERS

This reproduction is the best copy available.

UMI®

University of Alberta

Structural and Functional Investigation of the Ubiquitin Conjugation Enzymes and Their Variants: Insights Into the Mechanism of Poly-Ubiquitin Chain Formation.

By

©

Sean A. McKenna

A thesis submitted to the Faculty of Graduate Studies and Research in partial fulfillment of the requirements for the degree of Doctor of Philosophy

Department of Biochemistry

Edmonton, Alberta

Spring 2004

Canada

ABSTRACT

The protein ubiquitination machinery is responsible for the covalent modification of target proteins with ubiquitin (Ub) chains, which results in a wide variety of cellular outcomes. Emerging evidence has indicated that at least some of this functional diversity stems from the conformation of the poly-Ub chain that is assembled, which in turn is dictated by the isopeptide bond formation between the C-terminal Gly of one Ub in the chain to one of seven surface exposed Lys residues on the next. For example, the typical Gly^{76}-Lys^{48} connectivity signals for proteasomal degradation of ubiquitinated proteins. However, the molecular mechanism responsible for the formation of specific poly-Ub chains remains largely elusive. In this dissertation, structural and functional insights into the mechanism of poly-Ub chain formation are presented, with a particular emphasis on the nature of the interactions between Ub and members of the Ub-conjugation machinery.

Ubc13/Uev heterodimers are believed to be responsible for the assembly of non-canonical Lys^{63}-linked poly-Ub chains that serve as novel signals in processes including DNA repair and NF-κB signaling. In this dissertation, human Ubc13/Mms2 and Ubc13/Uev1a heterodimers were used as model systems to probe the nature of the protein-protein interactions that lead to efficient formation of a specific poly-Ub chain linkage (*i.e.* Gly^{76}-Lys^{63}). NMR experiments were employed to delineate surfaces of interaction between these protein complexes and Ub, which suggested a model in which the heterodimers could serve as a structural scaffold upon which specific poly-Ub chain linkages are formed. The thermodynamics and kinetics of the interactions between Ub and its conjugation machinery were subsequently determined by NMR and ITC approaches. Dynamic properties of these protein-protein interfaces were examined using backbone ^{15}N-relaxation NMR experiments. Finally, a comparison between proteins responsible for Lys^{63} and Lys^{48}-linked poly-Ub chains was accomplished in order to establish whether common protein-protein interactions are responsible for all types of poly-Ub chain formation. Using these varied approaches, we have

developed a molecular model that can demonstrate the clear structural biases that result in the selection of a specific Lys residue on Ub as the site of isopeptide bond formation by the protein ubiquitination machinery.

For Ian

ACKNOWLEDGEMENT

I would like to thank the following people/groups/organizations:

(i)   First and foremost, the Natural Sciences and Engineering Research Council of Canada (NSERC), the Alberta Heritage Foundation for Medical Research (AHFMR), the Izaak Walter Killam Foundation, and the University of Alberta for providing financial and travel support throughout my doctoral studies.

(ii)   Members of the Ellison and Sypracopoulos labs, particularly Bobby "the Badger" Varelas, Trevor "the Armadillo" Moraes and Chris Ptak for their valuable input with respect to experimental design and execution, and in the writing and editing of this manuscript.

(iii)   Dr. Mike Ellison and Dr. Leo Spyracopoulos for providing interesting and enjoyable lab environments, as well as for supervision and direction throughout my graduate career.

(iv)   Dr. Wei Xiao and Landon Pastushok from the University of Saskatchewan for providing me with the Ubc13/Uev system upon which most of my research is based.

(v)   Dr. Gary Shaw and Kathy Hamilton (University of Western Ontario), Dr. Brian Sykes, Deryck Webb, Yanni Batsiolas and Robert Boyko (University of Alberta), and Dr. Lewis Kay (University of Toronto) for their NMR expertise and assistance.

(vi)   Dr. Dave Bryce for showing me that science can be fun. Panther.

(vi)   Bruce, Debbie, Lindsey McKenna for their support, enthusiasm, and encouragement for the last 28 years.

Last, but certainly not least, I would like to thank Murdie and Jake for constantly reminding me not to take anything too seriously. Their unique outlooks on life have made me a much more well-rounded person.

TABLE OF CONTENTS

LIST OF TABLES

LIST OF FIGURES

LIST OF SYMBOLS, NOMENCLATURE, OR ABBREVIATIONS

2D	two-dimensional
3D	three-dimensional
Ala	alanine
AMP	adenosine monophosphate
APC	anaphase promoting complex
Arg	arginine
Asn	asparigine
Asp	aspartic acid
ATP	adenosine triphosphate
CSI	chemical shift index
BCA	bicinchoninic acid
cDNA	complimentary DNA
CP	core particle
C-terminal	carboxy terminal
Cys	cysteine
DNA	deoxyribonucleic acid
DSS	2,2-dimethyl-2silapentane-5-sulfonate
DTT	dithiothreitol
DUB	deubiquitinating enzyme
E1	ubiquitin-activating enzyme
E2	ubiquitin-conjugating enzyme
E3	ubiquitin-protein ligase
E6AP	E6-associated protein
E. coli	*Escherichia coli*
EDTA	ethylene diamine tetraacetic acid
evolume	ellipsoid volume
Gln	glutamine
Glu	glutaminc acid
Gly	glycine

GST	glutathione *S*-transferase
HECT	homolgous to C-terminal domain of E6-AP
His	histidine
HSQC	heteronuclear single quantum coherence
IKK	IκB kinase
Ile	isoleucine
IPTG	isopropyl-β-D-thiogalactopyranoside
ITC	isothermal titration calorimetry
K_D	dissociation constant
k_{off}	off-rate constant
k_{on}	on-rate constant
LB	Luria-Bertani broth
Leu	leucine
Lys	lysine
Met	methionine
N-terminal	amino terminal
Nf-κB	nuclear factor kappa B
NMR	nuclear magnetic resonance
NOE	nuclear Overhauser enhancement
NOESY	nuclear Overhauser effect spectroscopy
OD	optical density
PAGE	polyacrylamide gel electrophoresis
PBS	phosphate-buffered saline
PCR	polymerase chain reaction
PCNA	proliferating cell nuclear antigen
PEST	sequence rich in Pro, Glu, Ser, Thr
Phe	phenylalanine
PMSF	phenylmethylsulfonylfluoride

Poly-Ub	poly-ubiquitin
PP$_I$	pyrophosphate
Pro	proline
RING	really interesting new gene
RMSD	root mean square deviation
RP	regulatory particle
S^2	generalized order parameter
S. cerevisiae	*Saccharomyces cerevisiae*
Ser	serine
SCF	Skp1-Cullin/Cdc53-F-box protein
SDS	sodium dodecyl sulfate
ssDNA	single-stranded DNA
SUMO	small ubiquitin-related modifier
TCA	trichloroacetic acid
Thr	Threonine
TOCSY	total correlated spectroscopy
Trp	tryptophan
Tyr	Tyrosine
*Ub	^{35}[S]-ubiquitin
Ub	ubiquitin
Ub$_2$	diubiquitin
Ub$_3$	triubiquitin
Ubc	ubiquitin-conjugating enzyme
Uev	ubiquitin-conjugating enzyme variant
Val	valine
VBC	von-Hippel Lindau-Elongin B anc C
WT	wild-type

SOFTWARE PROGRAMS

Adobe Acrobat 5.0
pdf preparation and manipulation (Mac OS 10.2.6);
available at: www.adobe.com

Adobe Illustrator 10
Figure preparation (Mac OS 10.2.6);
available at: www.adobe.com

BiGGER
Protein-protein soft-docking algorithm (Windows 98);
available at: www.cqfb.fct.unl.pt/bioin/chemera/Chemera/Bigger.html

Canvas 8
Figure preparation (Mac OS 10.2.6);
available at: www.deneba.com

CorelDraw 10
NMR spectrum figure preparation (Mac OS 10.2.6);
available at: www.corel.com

Cricket Graph III 1.53
Speadsheet and graphing software (Mac OS 9.2.1);
available at: www.quikerwit.com

EndNote 6
Reference management software (Mac OS 10.2.6);
available at: www.endnote.com

GRASP v.12
Performs surface electrostatic potential representations (Unix);
available at: http://trantor.bioc.columbia.edu/grasp/

gridit 0.8
Determination of rotational diffusion tensor parameters (Unix);
available upon request (written in-house)

Accelerys INSIGHT II
3D graphical environment for molecular modeling (Unix);
available at: www.accelerys.com/insight

KaleidaGraph 3.6
Technical graphing and data analysis (Mac OS 10.2.6);
available at: www.synergy.com

Macvector 7.0
Sequence analysis and alignment package (Mac OS 9.2.1);
available at: www.accelerys.com/products/macvactor

Mathematica 5
Equation generation and editing software (Unix/Linux)
available at: www.wolfram.com

Microcal Origin v 5.0
Isothermal titration calorimetry data processing (PC Windows 98);
available at: www.microcal.com

Microsoft Excel 10.1.0
Spreadsheet for data analysis (Mac OS 10.2.6);
available at: www.microsoft.com

Microsoft Word 10.1.1
Word processing software (Mac OS 10.2.6);
available at: www.microsoft.com

Modelfree v 4.15
Optimizing modelfree parameters to heteronuclear relaxation data (Linux);
available at: www.cpmcnet.columbia.edu/dept/gsas/biochem/labs/palmer/software/modelfree.html

nmrDraw 2.1
Companion graphical interface for NMRPipe (Linux);
available at: spin.niddk.nih.gov/bax/software/NMRPipe

NMRPipe
NMR spectral processing and analysis (Linux);
available at: spin.niddk.nih.gov/bax/software/NMRPipe

NMRView 5.1.1
Visualization and analysis of NMR data (Linux);
available at: www.nmrview.com

PIPP
NMR spectrum peak-picking software (Unix/Linux);
available at: http://spin/niddk.nih.gov/clore/

VNMR
NMR spectrometer programming, acquisition, and control software (Unix);
available at: www.varianinc.com

xcrvfit
Curve fitting software used for the determination of K_D values (Unix);
available at: http://canopus.pence.ualberta.ca/ftp/xcrvfit/

CHAPTER 1:

Introduction

1.1 PROTEIN UBIQUITINATION

1.1.1 Biological outcomes of protein ubiquitination

The posttranslational covalent modification of intracellular proteins represents a remarkably efficient mechanism for altering their biological activities via the alteration of surface features on the protein. Examples include protein phosphorylation (1-3), glycosylation (protein targeting and sorting mechanisms) (4), acetylation (regulatory role in DNA recognition, protein-protein interactions, and protein stability) (5), lipidation (target proteins to membrane destinations) (6-8), methylation (bacterial chemotaxis) (9, 10), and carboxylation (blood coagulation cascades) (11).

The focus of this thesis is the posttranslational modification of surface exposed Lys residues by polymers of the small protein ubiquitin (Ub). The most prevalent and best documented outcome of protein ubiquitination is to target substrates for rapid degradation by the 26S proteasome, thereby downregulating the activity of crucial regulatory proteins (12, 13). The degradation of poly-ubiquitinated proteins has proven to be a hallmark of a variety of processes, such as cell cycle control (*14, 15*), induction of the inflammatory response (*16, 17*), and NF–κB-dependent signal transduction (*18*). Not surprisingly, defects in Ub-dependent proteolysis have been implicated as a causative factor in cancers (*19-24*) and numerous inherited diseases, including Liddle's syndrome, Angelman syndrome, Cystic fibrosis, Alzheimer's disease, and Parkinson's disease (*24-31*). Ubiquitination is also involved in non-proteasomal processes, including DNA repair (*32-34*), ribosome biogenesis (*35, 36*), endocytosis of cell surface proteins (*37*), the function of certain transcription factors (*38*), and the initiation of the inflammatory response (*39*). These pathways are often signaled by mono-ubiquitination or non-canonical poly-Ub chains. Therefore, the study of the

mechanisms regulating the attachment of Ub onto target proteins is of profound scientific and therapeutic interest. For comprehensive reviews, see (*12, 13, 40-44*).

1.1.2 Protein ubiquitination cascade

Protein ubiquitination involves a three-step mechanism whereby Ub is passed sequentially as an activated thiolester intermediate from a Ub-activating enzyme (E1) to a Ub-conjugating enzyme (E2), and finally to the protein target with the help of a Ub-protein ligase (E3) (Fig. 1.1A) (12, 13). First, in an ATP-dependent step, a thiolester intermediate between the C-terminal tail of Ub (Gly^{76}) and the active-site Cys of the E1 is formed, activating the C-terminus of Ub for nucleophilic attack. A subsequent transthiolesterification reaction transfers the Ub to the active-site Cys of the E2, forming another thiolester derivative with the C-terminus of Ub. Often in combination with an E3 enzyme, Ub is then transferred to the ε-amino of a Lys on the target protein, forming a covalent isopeptide bond. Multi-Ub chains can then be repetitively assembled onto a Lys residue of Ub already conjugated onto the target protein, which is often portrayed as the attachment of one Ub molecule to the next in step-wise fashion via Gly^{76}-Lys linkages (Fig. 1.1B).

The arrangement of the protein ubiquitination cascade is hierarchical in that a single E1 activates Ub for a larger, but limited number of E2s (11 known in *S. cerevisiae*, at least 19 in humans) (*12, 13*). In turn, the association of a specific E2 with one of several different E3s is though to dictate substrate specificity (*12, 13*). Therefore, the combinatorial assembly of a number of E1, E2, and E3 proteins is responsible for the ubiquitination of a large spectrum of different proteins.
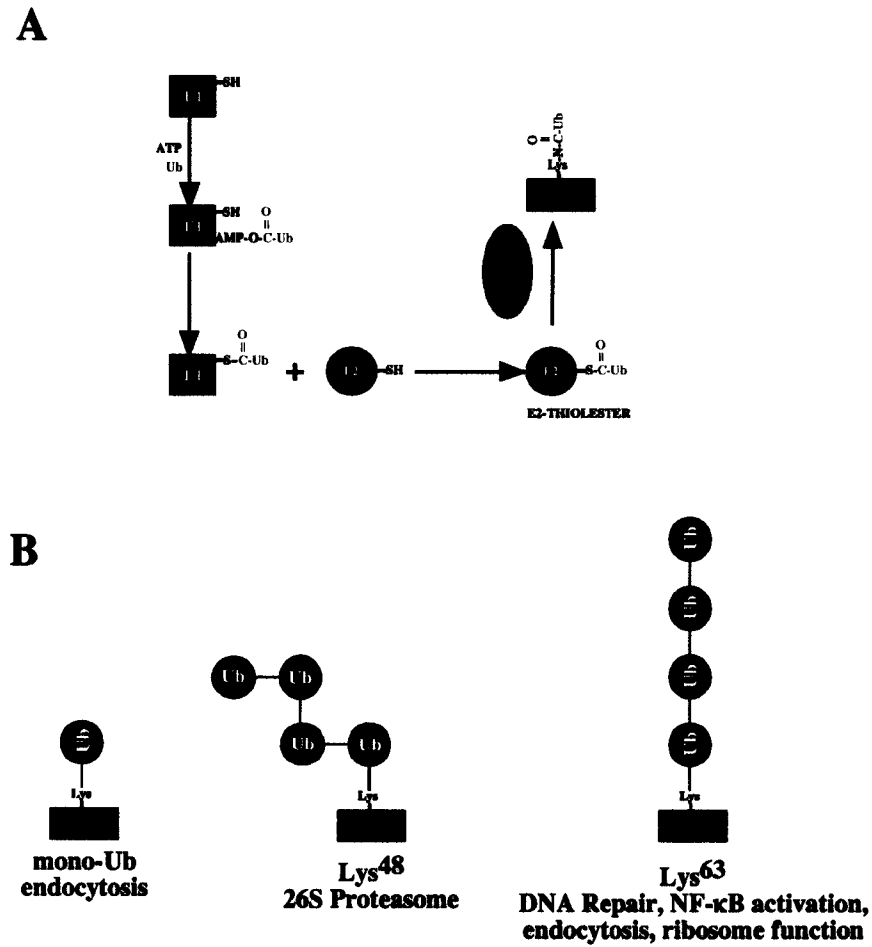
Figure 1.1 The protein ubiquitination cascade. (A) The E1 enzyme (blue) is responsible for the ATP-dependant activation of Ub, resulting in the formation of a thiolester association. Ub is subsequently transferred to the active-site Cys of an E2 enzyme (green) in a transthiolesterification reaction. With subsequent aid of an E3 enzyme (orange), Ub forms an isopeptide bond with a surface-exposed Lys on the target substrate. (B) Examples of different poly-Ub chain linkages and their biological outcomes are shown.

1.2 UBIQUITIN

1.2.1 Ubiquitin structure

Ub is an abundant 76 residue protein, and one of the most highly conserved proteins amongst eukaryotes. The tertiary structure of Ub is highly compact resulting from being tightly hydrogen bonded, and can be thought of as a rigid core with an unstructured C-terminal tail that contains the catalytic Gly^{76} residue (*45, 46*) (Fig. 1.2). The core of the Ub molecule is comprised of a highly ordered $\beta\beta\alpha\beta\beta\alpha\beta$ fold, and contains seven Lys residues, five of which have been implicated in poly-Ub chain assembly (Lys^6, Lys^{11}, Lys^{29}, Lys^{48}, and Lys^{63}) (*33, 47-51*). Lys^{48}, the site of canonical proteasomal poly-Ub chain formation, is also the most exposed of the Lys residues, as it is located within a highly contorted turn-rich region of the protein (*45, 46*). Specific and distinct patches on the surface of Ub have also been identified as requisite for growth in vegetative yeast cells (*52*), mediating endocytosis (*52*), interaction with the proteasome (*53*), interaction with E1 enzymes (*54*), and association with E2 enzymes (*55, 56*). Therefore, the very high conservation (only 3 residues are different between human and yeast proteins at positions 19, 24, and 28 (*57*)) of Ub across eukaryotes is presumably a function of the specific interactions which it is required to make with the E1, E2, and E3 proteins.

1.2.2 Ub-like proteins

The Ub structure has been classified as a superfold based on its structural homology with numerous other proteins (*58*). This structural conservation has been observed despite a striking lack of sequence identity among family members and are therefore found in proteins that are completely unrelated to Ub or Ub-related processes (*59-65*). On the other hand, certain members of the Ub superfold family, or "Ub-like" proteins, appear to function in systems analogous to the typical Ub-conjugation pathways. These observations have been confirmed and expanded biochemically to include up to 11 small molecules that can be covalently attached to amino groups on other
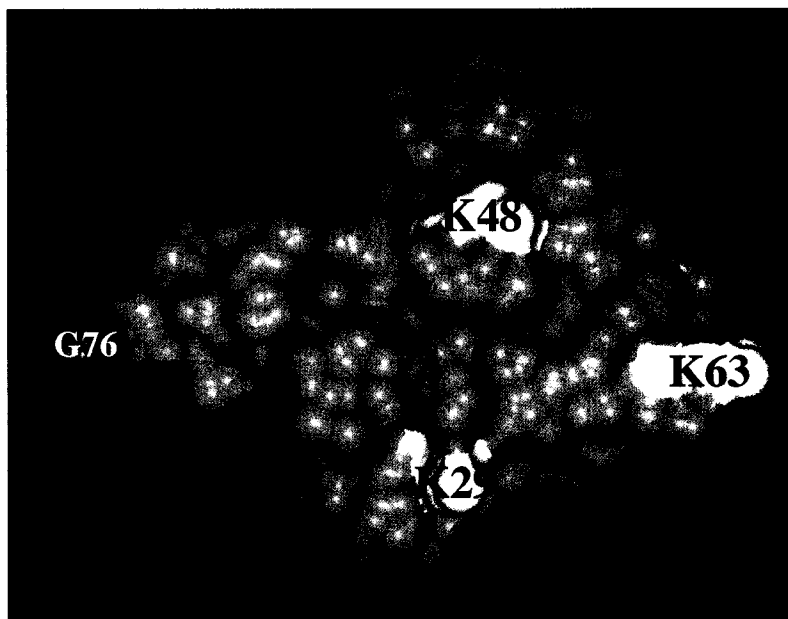
Figure 1.2 The 3D structure of ubiquitin. Shown is the Connolly projection of Ub based on its determined 3D structure (45). Principal residues involved in the formation of poly-Ub chains have been emphasized, including the C-terminal Gly[76] (green) and surface exposed Lys residues (yellow).

proteins posttranslationally (12), of which the three best characterized are SUMO, Nedd8, and Apg12.

The small Ub-related modifier (SUMO/sentrin/Smt3p) has 18% sequence identity to Ub, and appears to modify proteins that are primarily localized to the nucleus or nuclear envelope including (i) PML, a RING finger-containing E3 enzyme, which results in nuclear localization (*66*), (ii) p53, SP100, and HIPK2, which result in increased nuclear levels (*67*), (iii) RanGAP1, the Rab GTPase-activating protein, which targets it to the nuclear pore complex (*67-69*), (iv) IkBα, which precludes its ubiquitination and degradation (*70*), and (v) the proliferating cell nuclear antigen, PCNA, which blocks its ubiquitination and hence DNA repair activity (*71*). SUMO's overall structure closely resembles that of Ub, featuring the typical ββαββαβ fold of the ubiquitin superfamily (*72-74*). SUMO also possesses a long and flexible N-terminus that protrudes from the core of the protein and is absent in Ub. Furthermore, Lys^{48} is absent in the structures of SUMO, and is instead replaced by Gln^{69}, which accounts for the observation that only a single SUMO molecule, as opposed to chains, is conjugated onto target substrates (*72-74*). SUMO conjugation is accomplished by an E1 homologue, AOS1-UBA2 (*75, 76*), and a SUMO specific E2, Ubc9 (*70, 75-77*). Recent hypotheses have indicated that sumoylation and ubiquitination of target proteins at identical Lys residues may play antagonistic roles, thereby affecting the activity of crucial regulatory proteins (*70, 71*).

Nedd8/Rub1, on the other hand, demonstrates a 60% sequence identity to Ub, and its major target is Cdc53/Cul-1, a component of the SCF E3 complex, such that its activity is upregulated (*76, 78-84*). The 3D structure of Nedd8 closely resembles that of Ub with the addition of a C-terminal extension (*85, 86*). Furthermore, Arg^{72} in Ub is replaced by Ala^{72} in Nedd8. This substitution has been demonstrated to inhibit the interaction with Ub's E1 enzyme, thereby directing it into alternative pathways (*85, 86*). Nedd8 conjugation is accomplished by a dimer, APPBP1-UBA3 (*75, 76*), and a Nedd8 specific E2, Ubc12 (*12, 67, 75*).

Apg12, a Ub-like modifier which is conserved in all eukaryotes, is conjugated to the Lys residues of a specific target (Apg5), and thereby plays a central role in autophagosome vesicle formation (*87-89*). Apg12 is specifically activated by an E1 analogue, Apg7, and a single E2, Apg10, is responsible for thiolester formation (*87-89*). Apg12 is unrelated by sequence to Ub.

Taken together, the covalent modification of protein targets by Ub or Ub-like proteins represent a set of mechanistically conserved processes each resulting in distinct biological outcomes.

1.3 UBIQUITIN-ACTIVATING ENZYMES (E1s)

The first step in the protein ubiquitination cascade is catalyzed by the ubiquitin-activating enzyme, or E1, which must first form a thiolester intermediate with Ub in order to efficiently transfer Ub to an E2 enzyme (12). In most organisms, including humans, a single E1 enzyme is responsible for Ub activation for the entire spectrum of E2s (*90, 91*).

The chemistry of the E1 reaction has been well characterized. In the first stage of Ub activation, hydrolysis between the α and β phosphoryl group of ATP drives the formation of a Ub-adenylate at Gly^{76} of Ub (*92-96*):

$$E1 + ATP + Ub \xleftrightarrow{\text{Mg}^{2+}} E1\bullet AMP\text{-}Ub + PP_i$$

[eq. 1.1]

The adenlyate subsequently acts as the donor of Ub to the active-site Cys of E1 in the formation of a thiolester intermediate, and proceeds in the absence of Mg^{2+} (*93, 95-97*):

$$E1\bullet AMP\text{-}Ub \longleftrightarrow E1\text{-}Ub + AMP$$

[eq. 1.2]

Finally, the E1-Ub thiolester undergoes another round of adenylate formation, yielding a complex which contains two molecules of C-terminally activated Ub:

$$E1\text{-}Ub + ATP + Ub \xleftrightarrow{\text{Mg}^{2+}} E1\text{-}Ub\bullet AMP\text{-}Ub + PP_i$$

[eq. 1.3]
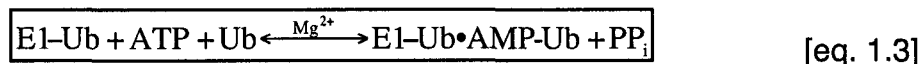
E1 is an extremely efficient enzyme relative to the downstream reactions which must be catalyzed by the E2s and E3s. The entire process encompassing ATP binding to transthiolesterification of the E2 occurs at rates which are 10- to

100- fold faster than the catalytic rate of substrate ubiquitination (*98, 99*). These rates are likely required due to the markedly higher concentrations of total E2 versus E1 present in cells; E1 allows for sufficient production of activated Ub such that it is not the rate limiting step (*100*).

While E1 enzymology has been well characterized, the molecular framework for understanding the activation of Ub, and other Ub-like proteins has only recently been uncovered. The first step towards uncovering a structural basis for Ub activation came from the examination of the *Escherichia coli* (*E. coli*) molybdenum cofactor biosynthesis pathways, specifically the MoeB and MoaD proteins. Together, these proteins function in an evolutionarily conserved manner to Ub-activation in eukaryotes by E1 (MoeB) and Ub (MoaD) proteins (*101, 102*). The crystal structure of the MoeB-MoaD complex in its apo, ATP-bound, and MoaD-adenylate forms revealed important insights, particularly with respect to the nature of the protein-protein interactions within a E1 adenylate ternary complex (*103*).

The structural basis for activation of Ub by Ub-adenylate, E1~Ub thiolester formation, and the mechanism of Ub transfer to an E2 were uncovered by examination of the E1 for Nedd8 in humans (APPBP1-UBA3) (*104*). This study revealed that each individual E1 activity is specified by a unique E1 domain: an adenylation domain that resembles the MoeB enzyme from bacteria (*103*), a catalytic domain that contains the active-site Cys and is responsible for thiolester formation, and a domain which is responsible for E2 recognition that mimics the structure of Ub (Fig. 1.3) (*104*). Together, these domains contribute to the formation of two distinct clefts that facilitate the coordination of nucleotide and protein binding to the E1 in such a manner that each of E1's reactions drive the next in an "assembly-line" fashion.
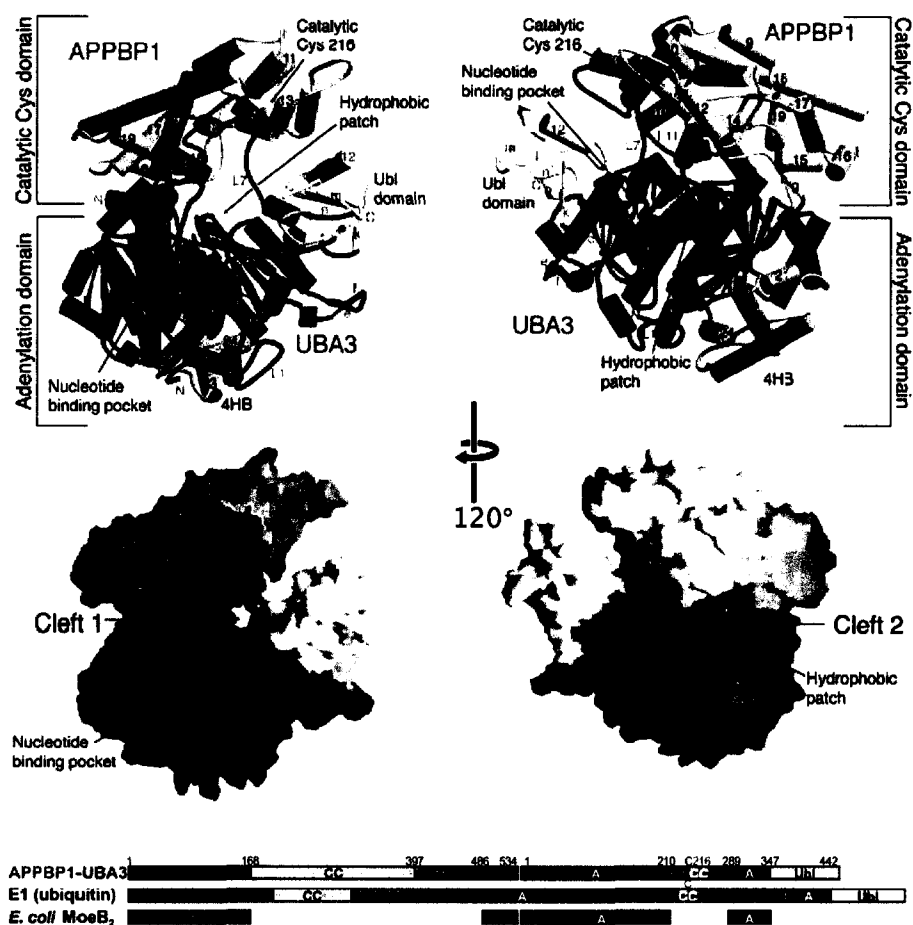
Figure 1.3 The structure of an E1 complex. Two views of the structure of the APPBP1-UBA3 complex, with the structural elements in the top panel, and surface representations below. APPBP1 is blue, whereas UBA3 is red, with domains shaded differently. Catalytic Cys^{216} is yellow. The primary sequences of APPBP1, the E1 of Ub, and the crystallographic MoeB dimer are shaded according to structure in the schematic diagram (bottom). A, adenylation domain; CC, catalytic cysteine domain; 4HB, 4-helix bundle in APPBP1; Ubl, Ub-like domain in UBA3. The adenylation, catalytic Cys, and Ub-like domains together contribute to a broad, deep groove in the structure that is divided into two clefts which coordinate nucleotide and protein binding. Figure used with permission from (104).

1.4 UBIQUITIN-CONJUGATION ENZYMES (E2s)

1.4.1 Mechanism and classification of the E2s

In the second step of the protein ubiquitination cascade, E2 enzymes forge thiolester linkages with Ub upon its transfer from an E1 enzyme via transthiolesterification (*12, 13*).

$$\boxed{\text{E1-Ub•AMP-Ub} + \text{E2} \longleftrightarrow \text{E1•AMP-Ub} + \text{E2-Ub}}$$ [eq. 1.4]

E2 enzymes share a conserved core domain of approximately 150 residues, whose distinguishing feature is an active-site Cys that is responsible for thiolester formation with Ub or Ub-like proteins (Figure 1.4). E2s are distinguished from each other based on the presence or absence of C- and N-terminal extensions, which are though to mediate specific interactions with binding partners, including E3s, and therefore may account for their abilities to mediate distinct biological outcomes (*105*). Type I E2s (Ubc4, Ubc5, and Ubc13 in *S. cerevisiae*) lack extensions, whereas type II (Ubc1 and Ubc8), type III (Ubc7, Ubc9, Ubc11, and Ubc12), and type IV E2s (Rad6, Cdc34, and Ubc6) have respective C-terminal, N-terminal, or both C- and N-terminal additions to the core domain (*106*). A further distinguishing feature is the presence and character of two loop region insertions centered at residues 35 and 110, which are also thought to play an important role in mediating the diverse actions of the E2s despite a generally conserved primary amino acid sequence (*12, 13*).

1.4.2 E2 core domain structure

Numerous overlapping X-ray (*107-115*) and nuclear magnetic resonance (NMR) (*56*) structures of E2s have confirmed that the fold of the core E2 domain is highly conserved amongst family members, consisting of a four-stranded antiparallel β-sheet flanked by four α-helices and a short 3_{10} helix (Fig. 1.5). The active-site Cys sits on the loop that connects $\beta4$ to $\alpha2$, and is housed in a shallow groove formed by residues upstream of the loop on one side and residues of the $\alpha2$-$\alpha3$ loop on the other. Not surprisingly, the most highly conserved residues
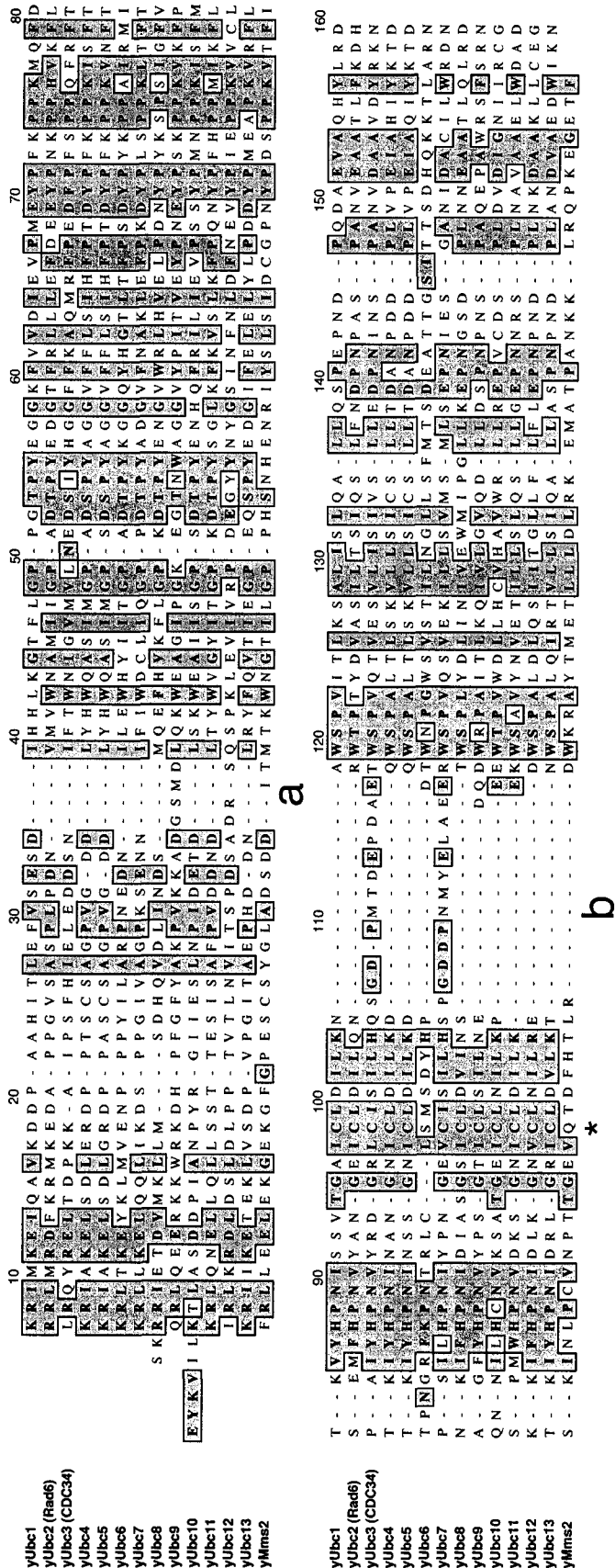
Figure 1.4 Multiple sequence alignment of the S. cerevisiae E2 enzymes. The core E2 domain without N- or C-terminal extensions from Ubc1(NP_010462), Rad6(A21906), CDC34(NP_010339), Ubc4(NP_010339), Ubc5(NP_009638), Ubc6(NP_011026), Ubc7(S28951), Ubc8(NP_010904), Ubc9(NP_010219), Ubc10(P29340), Ubc11(NP_014984), Ubc12(NP_013409), Ubc13(NP_010377), and Mms2(P53152) were used in the ClustalW multiple sequence alignment. Residues with significant sequence similarity are boxed in grey. Residue numbering is arbitrary. The active-site Cys (*) and variable loops (a and b) are also denoted.
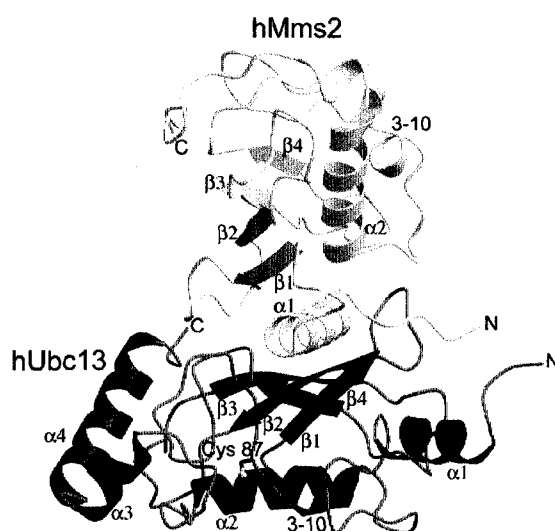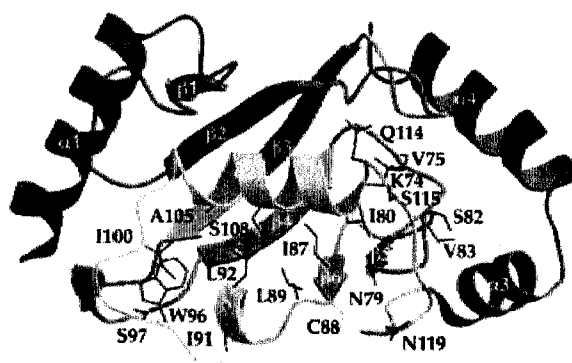
Figure 1.5 Structural properties of E2 enzymes. Two different examples of the conserved E2 fold are shown, including (top) the yeast Ubc1 catalytic core (109), and (bottom) the human Ubc13 protein (blue) which is heterodimerized to Mms2 (137). Each E2 consists of a four-stranded antiparallel β-sheet flanked by four α-helices, and are labeled accordingly. The active site Cys is also indicated in each case. The structure of an E2 variant, Mms2, is also shown (bottom, yellow), and adopts a similar fold to canonical E2's with the exception that it lacks the active site Cys and the two most C-terminal helices but contains an extended N-terminal tail.

amongst the E2 family members cluster to regions surrounding the active site (Fig. 1.4), whereas the most obvious divergence appears on the face of the molecule that is opposite the active-site Cys (*13*). Whether these divergent residues dictate specific functions of the E2s is not clearly understood (*116*). Unfortunately, structural information regarding the loops and termini of these E2s is sorely lacking, although recent studies have indicated that at least one E2 may employ its tail to interact with the core domain to effect regulation of thiolester formation (*117*).

The interactions within E2-Ub thiolester (*55, 109*) or E2-Ub oxyester (a more stable thiolester analog) (*56*) intermediates have been examined by NMR approaches. These studies have revealed that, as expected, the C-terminal tail of Ub and regions surrounding the active-site Cys of the E2 represent the principal areas of interaction. Notably absent from the proposed E2-Ub thiolester active-site region are side chains that could act as a general base to deprotonate the attacking thiol (of an E3) or amino group (of the target substrate Lys), and a group to stabilize the developing negative charge on Gly^{76} of Ub. Therefore, it appears as though these crucial catalytic residues involved in E1-E2 transthiolesterification lie mainly in the active-site of the E1 enzyme, and those responsible for the Ub transfer from E2 to E3 or E2 to target are housed primarily by E3 enzymes, although corroborating evidence does not support this claim as of present.

1.4.3 Additional characteristics of the E2s

Whereas significant inroads into our structural understanding of E2-thiolester formation have been made, information is sparse regarding the mechanism whereby E2s contribute directly to dictating poly-Ub chain formation. Limited results demonstrating the self-association and heterodimerization of E2s have been observed (*34, 118-124*), and are particularly interesting in light of the fact that a potential non-covalent interaction between Ub or Ub-like modifiers and their cognate E2 have been observed (*56, 125*). Taken together, it has been

hypothesized that E2-E2 associations, potentially associated with a specific E3, may somehow provide a scaffold upon which poly-Ub chains are built.

A final feature of the E2 enzymes is that they themselves are often a target for autoubiquitination on specific Lys residues (*109, 123, 126, 127*). While autoubiquitination may represent a non-specific transfer of Ub to a nearby primary amine (*128*), it is also possible that this modification represents a mechanism whereby the activity of the E2s may be self-regulated.

1.4.4 Ub-conjugating enzyme variants

In addition to the core family, several atypical E2s known as ubiquitin-conjugating enzyme variants (Uevs) have been identified (*129-132*). These proteins share significant sequence similarity with E2s, but lack the characteristic active-site Cys residue required for thiolester formation (Fig. 1.6). Despite this crucial difference, at least some Uevs possess the ability to bind Ub, and appear to function as either co-factors in poly-Ub chain formation or as Ub sensors (*34, 131-133*).

One such Uev, Mms2, forms a heterodimer with Ubc13, an E2 that functions in the error-free DNA postreplicative repair mechanism in both humans and yeast (*34, 130, 134, 135*). This E2-Uev heterodimer possesses unique catalytic abilities in that it is able to synthesize non-canonical Lys[63]-linked poly-Ub chains (*34, 136*). The crystal structure of the heterodimer reveals an asymmetric orientation in which the E2's β-sheet acts as a "saddle" upon which the Uev protein sits (using residues from α1 and loop-contained residues which connect β1 to β2) in order to bury ~1500 Å^2 of solvent accessible surface area (*111, 137*) (Fig. 1.5B). This orientation has led to the hypothesis that the heterodimer may act as a scaffold upon which Lys[63]-linked chains could be assembled (*111, 137, 138*). Mms2 itself adopts an E2-like fold, with the exception that it lacks the two C-terminal helices and contains an extended N-terminal tail (*137*) (Fig. 1.5B, yellow).

A

hUbc13	E2-like
hMms2	▪ E2-like
hUev1a	▬ E2-like
hTsg101	▸ E2-like ▬▬▬▬ / ▬▬

B

C-terminal
helices
↙

N-terminal
helix

←β-tongue
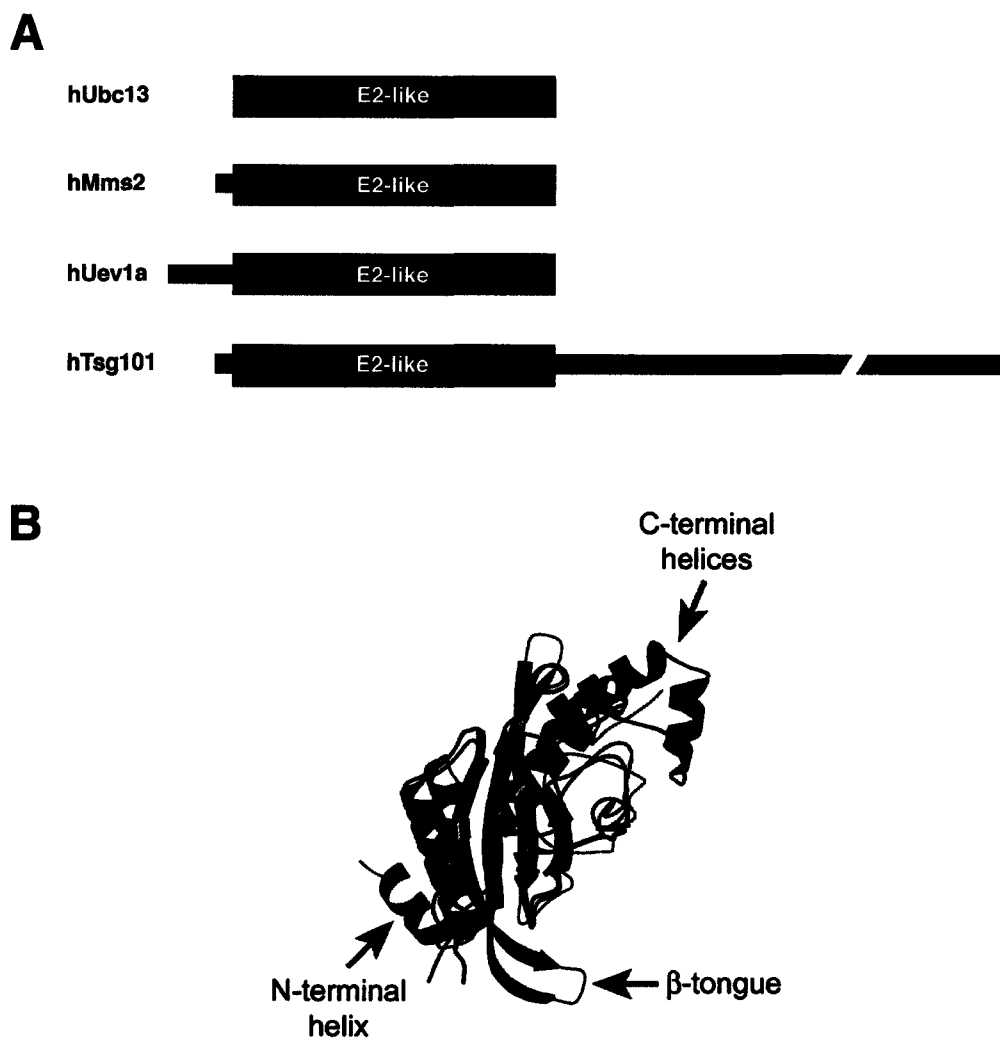
Figure 1.6 Comparison of Uev and E2 enzymes. (A) Schematic primary sequence alignment of an E2 (Ubc13) and the functionally relevant Uev proteins in humans. Each contains a conserved E2-like domain, while the Uev's possess additional N- and C-terminal extensions. (B) Superposition of the three dimensional structures of human Ubc13 (purple), human Mms2 (green), and human Tsg101 (yellow). The extra N-terminal helix (red arrow), β-hairpin "tongue" (blue arrow) and the missing C-terminal helices in Tsg101 are highlighted (140).

Another Uev, human Uev1a, is involved in NF-κB signal transduction, and also forms a heterodimer with Ubc13 which is responsible for Lys[63]-linked poly-Ub chain formation (*39, 139*). Preliminary structural work has indicated that Uev1a and Mms2 share similar structural features, both in terms of their interaction within the heterodimer and their respective structures[1].

A third Uev, Tsg101 (Vps23p in yeast), shares sequence and structural homology with Mms2 and Uev1a in its N-terminal region, whereas the remaining two-thirds of the protein is involved in interactions with other proteins (*131, 132, 140, 141*). Tsg101 plays a central role in the cellular vacuolar protein sorting pathway, which is responsible for the sorting of membrane-associated proteins through a series of endosomal compartments prior to delivery to the lysosome (*142, 143*). Tsg101 does not interact with an E2 to form poly-Ub chains, but instead appears to recognize and bind mono-ubiquitinated substrates for eventual incorporation into the lysosome (*133, 144*). The solution structure of the Tsg101 Uev domain resembles those of Mms2 and Uev1a, with the exception that it lacks C-terminal helices and possesses an extended β-hairpin that links β-strands 1 and 2. This extension is responsible for mediating the interaction between Tsg101 and Ub (*140, 141*) (Fig. 1.6B). Therefore, while the Uev domain may serve as a Ub-binding motif, each Uev may have evolved a different strategy for Ub binding.

Phylogenetic analysis indicates a deep separation and solid clustering of all Uev sequences within the E2 family tree (*145*). For example, full-length human *MMS2* cDNA is able to complement the yeast *mms2* mutant, suggesting that human Mms2 is indeed a functional homolog of yeast Mms2 (*130*). In all of the functional assays published to date, Mms2 and Uev1a can be employed interchangeably (*39, 139*). Furthermore, overexpression of a ciliated protist Uev is able to rescue the sensitivity of an *mms2* null mutant to various DNA damaging agents (*145*). Therefore, it appears as though the Uev family of proteins are functionally conserved from ancient organisms to humans.

---

[1] Trevor Moraes, unpublished observation (2003).

1.5 UBIQUITIN PROTEINS LIGASES (E3)

1.5.1 General features of the E3 family

The E3 enzyme complexes are the most numerous and varied components of the protein ubiquitination cascade in that they are responsible for recognition of both substrate and the E2 required for poly-Ub chain formation (*12, 13, 42*). In some cases (RING finger E3s), the E3 acts as a scaffold for both the E2 thiolester intermediate and the substrate such that transfer of Ub from the E2 to the substrate can proceed (*146, 147*). In other cases (HECT domain E3s), the E3 itself contains a catalytic Cys residue that accepts Ub from an E2 prior to acting as the proximal Ub donor to substrate (*148*). A third subset of E3s (U-box domain E4s) act as a chain elongation factors by binding previously assembled poly-Ub chains and helping the E2 thiolester intermediate transfer Ub to the elongating chain (*51, 149*). Therefore, the E3 proteins serve, either directly or indirectly, to catalyze the efficient transfer of activated Ub to the target substrate or the elongating poly-Ub chain.

The recognition of a particular substrate and its subsequent poly-ubiquitination by an E3 enzyme complex is thought to be directed by short sequence regions within the substrate. The first such "ubiquitination signal" to be discovered was the destruction box motif (RXALGXIXN; where X is any amino acid) in which the positioning of Arg and Lys residues represent the key determinants of specificity (*15, 150, 151*). Structural data in two cases has revealed that this motif generally adopts a well-defined conformation and remains surface exposed (*114, 116, 152, 153*). Another example of a ubiquitination signal that has been characterized is a hydrophobic surface on one face of an amphipathic α-helix, whose exposure can be regulated by interaction with accessory proteins (*152, 154*). Other examples of sequence motifs that may encourage ubiquitination include the identity of the N-terminal residue of a target protein (*155, 156*), and so-called PEST motifs, which contain sequences rich in Pro, Glu, Ser, and Thr (*157*). Despite these observations, many E3s appear to

be rather nonselective with respect to which Lys residue on the target substrate becomes ubiquitinated. In at least three cases, sequential single Lys to Arg mutants in target substrates had no effect on susceptibility to ubiquitination (*153, 158, 159*). Therefore, the manner in which E3s recognize specific substrates remains enigmatic.

1.5.2 RING-finger domain E3s

The RING-finger motif is defined by a characteristic pattern of Cys and His residues ($CX_2CX_{(9-39)}CX_{(1-3)}HX_{(2-3)}C/HX_2CX_{(4-48)}CX_2C$) which coordinates at least two zinc ions (*160, 161*). The RING Finger E3s each contain at least one RING domain that is responsible for interaction with an E2. These proteins are thought to function not catalytically (as in the HECT E3s) but rather as molecular scaffolds upon which the E2 thiolester and target substrate can be correctly oriented such that Ub transfer to the target can proceed efficiently (*160*).

RING E3s can be subdivided into two distinct varieties, namely single and multisubunit proteins. The single-subunit RING E3s require only their cognate E2 and target substrate for efficient poly-Ub chain formation (*13*). Single-subunit RING E3s have been shown to form complexes with UbcH7, UbcH8, UbcH5, Rad6/UbcH1, and Ubc13 (*21, 162-168*). The crystal structure of c-Cbl-UbcH7, a RING E3-E2 complex, supports its hypothesized role as a molecular scaffold wherein the RING domain is responsible primarily for the interaction with the E2 (Fig. 1.7A) (*169*). The structure suggests that substrate-E2 proximity is the crucial factor promoting poly-Ub chain formation, although the mechanism of transfer remains to be revealed. Residues linking its substrate recognition and RING domains are also required to mediate the E2 interaction, which may help to explain the specificity of each RING E3 for its cognate E2s.

Three examples of multisubunit RING E3s include the anaphase promoting complex (APC) (*170*), the von-Hippel Lindau-Elongin B and C (VBC)-Cul2 RING finger complex (*171-173*), and the Skp1-Cullin/Cdc53-F-box protein (SCF)-RING finger complexes (*146*). The structure of one such SCF complex

A

B
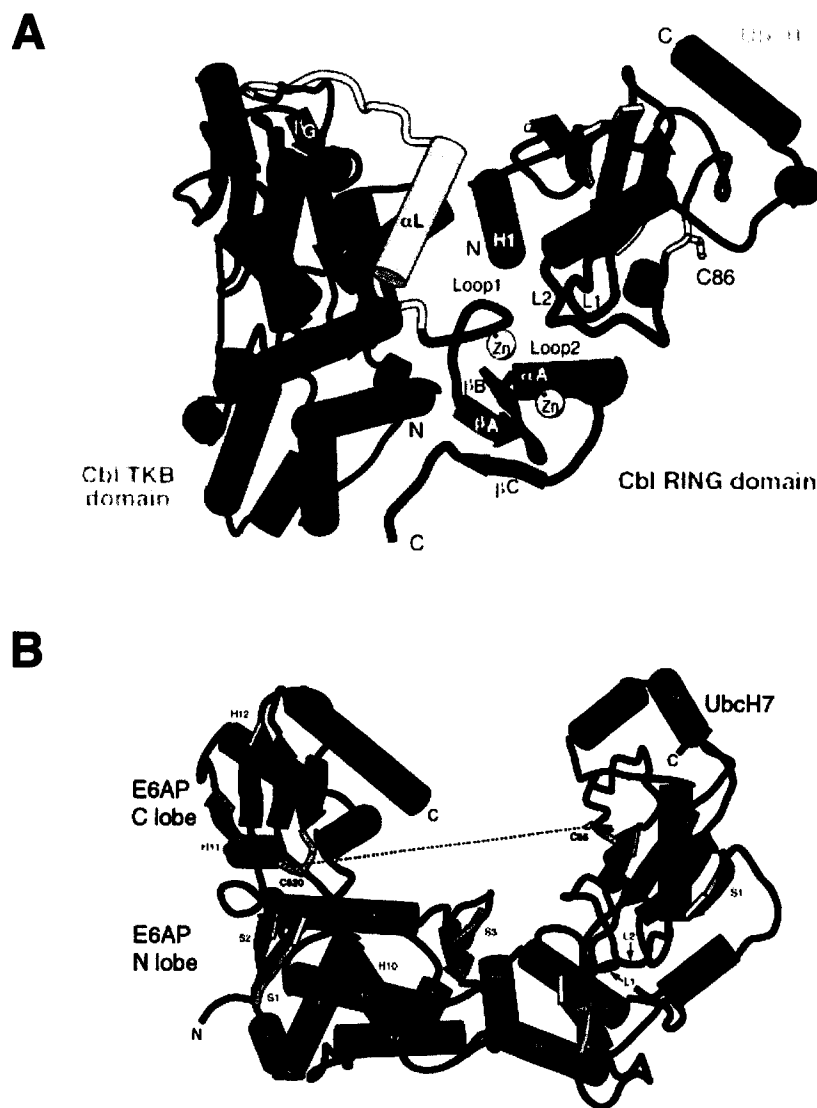
Figure 1.7   HECT and RING E3 interactions with their cognate E2 enzyme. (A) The interaction between UbcH7 (E2, blue) and c-Cbl (RING E3) is shown, with c-Cbl's RING domain red, the tyrosine kinase binding (TKB) domain green, and the linker region yellow. The active site Cys of UbcH7 (cyan) is indicated, as are the two zinc ions in the RING domain of the E3 (grey spheres)(169). (B) The interactions between UbcH7 (cyan), the E6AP HECT domain N lobe (red), and C lobe (green) are shown. The active site loops on each protein are colored yellow (177).

has revealed that, as in the case of single-subunit RING E3s, a molecular scaffold is assembled upon which the substrate and E2-thiolester complex may be brought into close proximity to facilitate the transfer of Ub (*105, 174*). The organization of the other multi-subunit RING E3s is analogous to that of the SCF, raising the possibility that a similar mechanism is employed to effect substrate ubiquitination (*12*).

1.5.3 HECT domain E3s

HECT E3 enzymes contain a ~350-residue C-terminal HECT domain whose sequence is homologous to the C-terminal domain of the first family member discovered, E6-associated protein (E6AP) (*175*). This HECT domain houses a strictly conserved catalytic Cys responsible for thiolester formation with Ub, which is positioned ~35 residues upstream of the C-terminus (*176*). The N-terminal portion of these E3s is responsible for interaction with its specific substrate(s) (*13*). Furthermore, it appears as though all HECT E3s employ a similar catalytic mechanism, and typically require UbcH7 or UbcH8 as their accompanying E2 (*175, 177-179*).

The structure of the E6AP-UbcH7 ubiquitination complex provided important insights into the mechanism and specificity of interaction mediated by HECT E3s (Fig. 1.7B) (*177*). The N-terminal lobe of E6AP forms a long, primarily α-helical arm, upon which the E2 and C-terminal lobe of E6AP interact at opposite ends. The highly-conserved active-site cleft of E6AP, which houses Cys^{820}, rests at the junction of the C- and N-terminal lobes, and sits 41 Å apart from the catalytic Cys of the E2. This orientation necessitates a large-scale structural rearrangement for efficient transthiolesterification of Ub from E2 to E3. Features of the N-terminal lobe can also account for the apparent preference for a specific E2 (*i.e.* UbcH7 and UbcH8) over others. It is interesting to note that similar surfaces on UbcH7 are employed for the interaction with both a HECT (*177*) and RING E3 (*169*) (Fig. 1.7).

1.6 DEUBIQUITINATING ENZYMES (DUBs)

Ubiquitin chains assembled on target substrates do not represent a static state, but rather a highly dynamic process whereby Ub is continuously being added and removed (12, 13). Therefore, the biological outcome of target poly-ubiquitination simply represents an enhanced rate of poly-Ub synthesis over deubiquitinating activity in the cell. All known deubiquitinating enzymes (DUBs) are ATP-independent Cys proteases, which specifically hydrolyze the amide bond between the ε-amino group of a Lys and the C-terminal Gly^{76} of Ub (12, 180, 181), and do so despite extremely high sequence diversity amongst family members.

The structures of several DUBs have been reported, and have shown similarities to typical Cys proteases in that they possess a catalytic triad in their active sites consisting of Cys, His and Asp residues (182-184). In one case, Ub binding induced a drastic conformational change in the active site that realigns the catalytic triad for catalysis (184). In another study, the surfaces of interaction between a DUB and Ub were mapped, and they appear to use primarily basic residues (Arg^{42}, Lys^{48}, Arg^{72}, and Lys^{74}) and a hydrophobic surface (Leu^{8}, Ile^{44}, Phe^{45}, Val^{70}, Leu^{71}, and Leu^{73}) on a single face of the Ub molecule to mediate the interaction with complimentary patches on the DUB (185, 186).

1.7 THE 26S PROTEASOME

Recognition, proteolysis, and recycling of substrates modified with Lys^{48}-linked chains is accomplished by the highly evolutionarily conserved 26S proteasome. This 2.5 MDa ATP-dependent protease holoenzyme consists of two major subcomplexes: the catalytic 20S core particle (CP), and the 19S regulatory particle (RP) (Fig. 1.8) (187, 188).

The 20S CP is a barrel-shaped stack of four structurally similar heptameric rings, with the two outer stacks (α-rings) mediating interactions with RPs, and the two inner stacks (β-rings) creating a sequestered chamber into which the

19S RP

20S RP

α7

β7

β7

α7
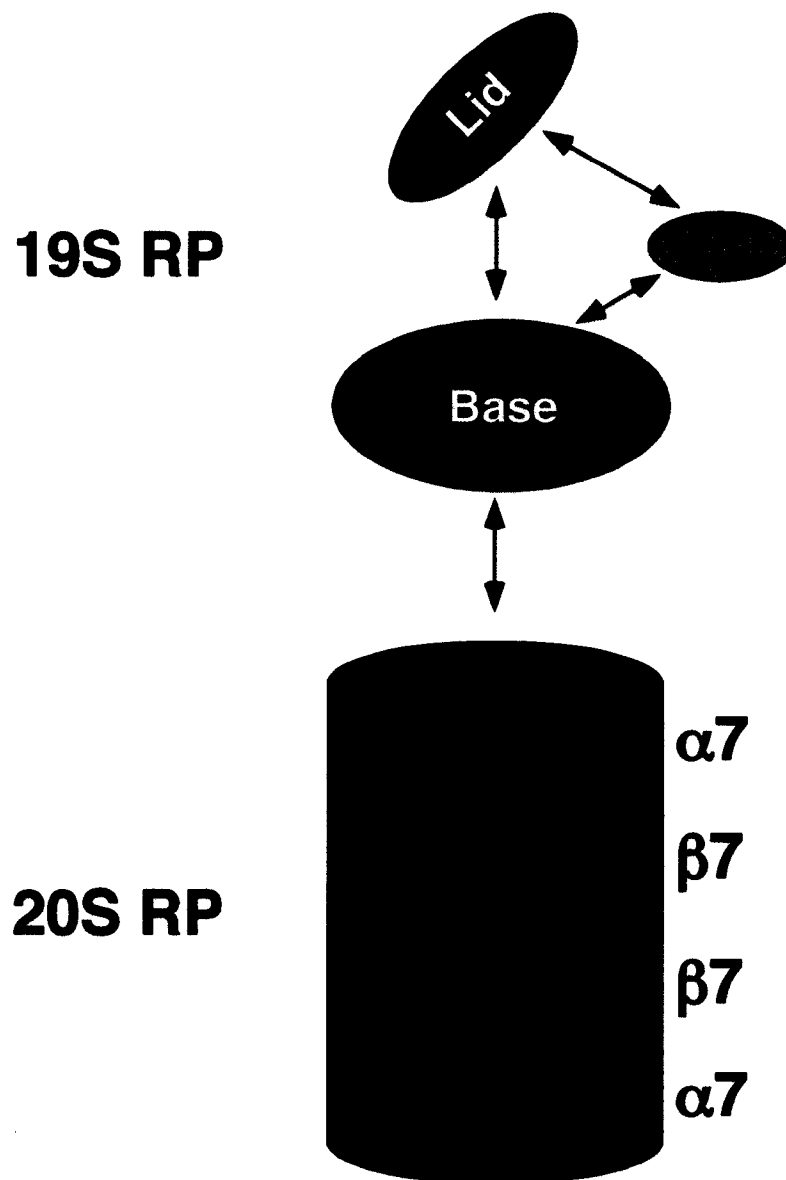
Figure 1.8 Structure of the proteasome. The core particle (CP) consists of four heptameric rings: two identical α-rings and two identical β-rings. Each ring contains seven distinct homologous subunits. Certain β-subunits contain the protease active-sites facing into the proteolytic chamber. The 19S regulatory particle (RP) is comprised of two eight-subunit complexes, the lid and the base. The base that contains all six proteasomal ATPases attaches to the α-ring of the CP. Rpn10 can stabilze the interaction between the base and the lid (12).

proteolytic Thr active-sites face (*189-191*). The 20S CP is remarkably efficient in that it can cleave peptide bonds after most amino acids, and typically generates peptides of seven to nine residues in length, which are subsequently hydrolyzed by downstream peptidases (*12*). Ub, however, is not proteolyzed but rather removed from substrates by DUBs within the proteasome and recycled back into the cellular pool (*192-194*).

The 19S RP contains two 8-subunit complexes; the lid and the base (*187, 188*). The base contains the proteasomal ATPase activity, and is thought to mediate the unfolding and translocation of the ubiquitinated peptide into the gated 20S CP (*195-198*). The lid complex contains no ATPase subunits, and is required for proper degradation of poly-ubiquitinated substrates (*199, 200*), but its role in poly-Ub chain binding remains unclear. The only well characterized subunit of the proteasome which has demonstrated significant affinity for Ub chains is Rpn10, an accessory protein which helps to stabilize the interactions between base and lid of the 19S RP (*201-205*). Spatial relationships amongst Ub moieties within a chain and the presentation of sufficient hydrophobic patches centered around Ile^{44} of Ub dictate that chains consisting of at least four Lys^{48}-linked Ub molecules are required for efficient binding to the proteasome (*50, 206*). Circumstantial observations indicate that a complimentary hydrophobic patch on Rpn10 in conjunction with the 19S RP may help mediate recognition of poly-ubiquitinated substrates prior to degradation (*12, 200, 207*).

1.8 UB CHAINS

1.8.1 Lys^{48}-linked chains

The conjugation of cellular proteins with Lys^{48}-linked poly-Ub chains typically results in their rapid degradation by the 26S proteasome (*12*). The structure of Lys^{48}-linked poly-Ub chains of varying lengths have been studied in both crystal (*208-210*) and solution phases (*211*). In each case, significantly different conformations of the chains were observed leading to the conclusion that Lys^{48}-linked poly-Ub chains appear to be inherently flexible, with the Ub

molecules behaving as rigid units connected by flexible tails. Furthermore, these dynamic chains appear to fluctuate between two distinct conformations, open and closed, which may serve to sequester or render accessible key hydrophobic residues (Leu^8, Ile^{44}, Val^{70}) required for interaction with recognition factors and the proteasome (211). These results have led to the hypothesis that poly-Ub recognition factors may sequester chains into the open conformation, thus stabilizing the interaction.

1.8.2 Alternatively assembled poly-Ub chains

Lys^{48}-linked poly-Ub comprise the canonical chain conformation. Recent studies have shown that alternative Lys residues (at positions 6, 11, 29, and 63) may also function in chain formation (12). Synthesis of these alternative chains does not appear to play a role in target substrate degradation, but rather in activation/inactivation (much like protein phosphorylation). Therefore, these alternative poly-Ub chain linkages represent a novel and apparently crucial function of the protein ubiquitination system.

Modification of proteins with Lys^{63}-linked chains play a role in a variety of processes and is by far best documented non-canonical chain linkage (Fig. 1.1B). These chains function in both NF-κB signal transduction (39, 139) and postreplicative DNA repair (33, 71). Assembly of Lys^{63}-linked chains on L28, a component of the large ribosomal subunit in yeast and humans, is required for ribosome function (36). Ubiquitination and endocytosis of several yeast plasma membrane proteins requires Lys^{63}-linked poly-Ub chains, ultimately leading to their downregulation via lysosomal degradation (212, 213). Lys^{63}-linked chains have also been implicated in the stress response (48) and mitochondrial DNA inheritance (214).

Poly-Ub chains connected via Lys^6, Lys^{11}, and Lys^{29} have also been observed in a limited number of cases. UbcH5A, a 120 kDa protein complex that behaves as an E1, E2, and E3 can synthesize unanchored Lys^{29}-linked poly-Ub chains (99, 215). Lys^{29}-linked chains have also been implicated in the

recruitment of chain elongation factors (51). Enzymes that catalyze the formation of chains linked through Lys^6 or Lys^{11} have also been observed, but their role remains to be uncovered.

The existence of poly-Ub chains linked through surface exposed Lys residues other than Lys^{48} suggests the distinct possibility that mechanisms exist that allow for the differential recognition of specific poly-Ub chain types from one another. Unfortunately, no structural or functional studies of alternative poly-Ub chain linkages have been published to date to confirm or refute this hypothesis.

1.9 FUNCTIONAL DIVERSITY OF POLY-UB CHAINS

This section is designed to emphasize the differential roles that various types of poly-Ub chains may play in distinct biological pathways, including the role of the canonical Lys^{48}-linked chains, non-canonical Lys^{63}-linked chains, mono-ubiquitination, and covalent attachment of Ub-like proteins. Two examples will be considered, the first being the Rad6 DNA repair pathway (section 1.9.1), which is discussed as it employs different types of chains that are assembled on a single target substrate. NF-κB signaling (section 1.9.2) is also discussed to highlight a system wherein distinct protein components within in a single signal transduction cascade are modified by either typical or atypical poly-Ub chains.

1.9.1 Rad6-dependent DNA repair

Eukaryotic genomes are highly vulnerable to spontaneous and environmental damage, and therefore employ repair systems to protect the integrity or their DNA (216, 217). Highly conserved DNA repair enzymes continuously monitor chromosomes for damage caused by exposure to mutagens, carcinogens, and cytotoxic compounds and function to repair the damage (216, 217). In the yeast S. cerevisiae, these DNA repair processes can be subdivided into three categories based on genetic epistatic analyses of DNA repair mutants: the Rad3, Rad52, and Rad6 groups (217-219). The Rad3 group

of mutants is responsible for nucleotide excision repair, whereas double-stranded break repair through mitotic or meiotic recombination is mediated by the *Rad52* group of mutants. DNA lesions are usually repaired via these nucleotide or base-excision repair mechanisms, but when these pathways become saturated or unable to repair such lesions prior to the onset of S-phase, the lesions persist during DNA replication, resulting in single-stranded DNA (ssDNA) breaks (*220-223*). Postreplicative repair by proteins of the *Rad6* group appear to function on stalled replication machinery that have encountered such single-stranded breaks (*217, 218, 224*). The Rad6 pathway functions to fix the ssDNA break, thereby removing the block to replication. Rad6-dependent postreplicative repair pathways are mediated by either (i) an error-prone mechanism in which the activity of Polζ, a mutagenic polymerase fills in damaged regions with low fidelity (*225*), or (ii) an error-free mechanism in which the activity of Polδ uses the information of the undamaged strand at the replication fork to repair the lesion (*217*).

Protein ubiquitination has been implicated in playing a key role in these postreplicative repair pathways, given that Rad6 is itself a Ub-conjugating enzyme (*12, 13, 226, 227*). Recent work has demonstrated that a logical target of this E2 is the proliferating cell nuclear cell antigen (PCNA) (*71*): a trimeric ring-shaped complex that that functions as a sliding clamp and processivity factor for DNA polymerases, including Polδ (Fig. 1.9) (*216, 217, 228*). PCNA may be modified in three different ways by the protein ubiquitination machinery, and each modification may alter its function in DNA repair by recruiting different repair components to the DNA.

Rad6 is recruited to regions of damage by an interaction with Rad18, a RING-finger E3 ssDNA-binding protein (*168, 229, 230*). Together they are responsible for the mono-ubiquitination of PCNA at Lys[164] (*71*) (Fig. 1.9). This mono-ubiquitination event is hypothesized to target stalled replication forks to initiate error-prone DNA repair (*71, 231*). Alternatively, PCNA may be subsequently modified at Lys[164] by non-canonical Lys[63]-linked poly-Ub chains,
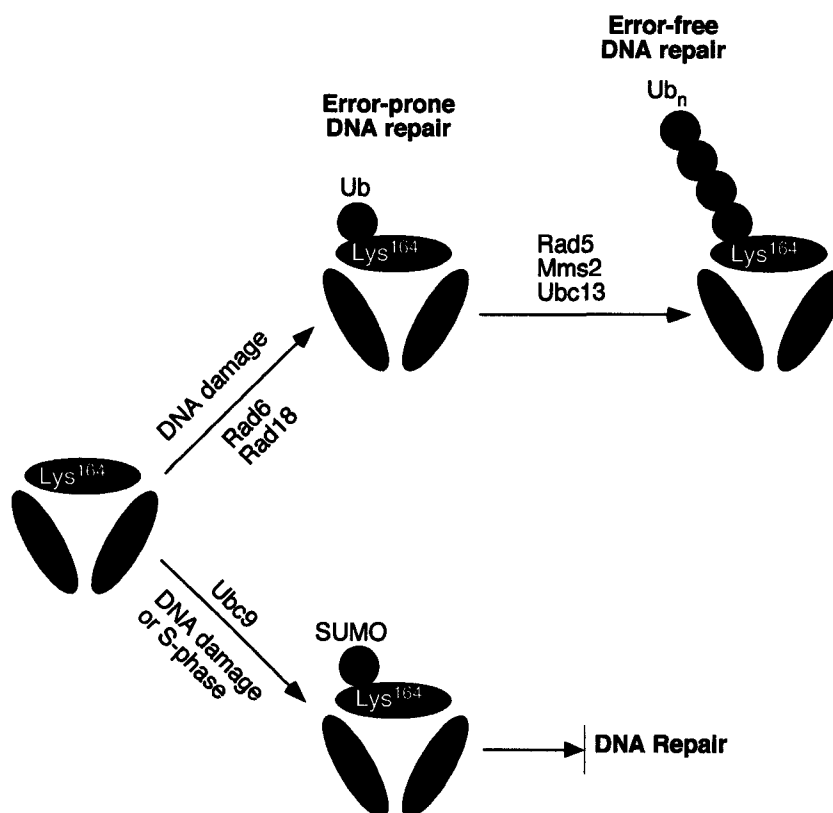
Figure 1.9 The role of ubiquitination in DNA repair pathways. PCNA forms a trimeric ring which binds DNA and acts as a processivity factor for DNA polymerases. Upon DNA damage, PCNA is monoubiquitinated on Lys^{164} in a reaction which is dependent on the Rad6/Rad18 (E2/E3) proteins. Monoubiquitinated PCNA is believed to target stalled replication forks to initiate error-prone repair. PCNA may be further modified at Lys^{164} by Lys^{63}-linked poly-Ub chains in an Mms2/Ubc13/Rad5 (Uev/E2/E3) dependent manner. This modification causes the induction of error-free DNA repair pathways. In a competing reaction, Lys^{164} may be modified by SUMO in both normal and damaged cells during S phase, and requires Ubc9 (E2).

which additionally requires the heterodimer Ubc13/Mms2, and Rad5 (*71*), a RING-finger E3 DNA-binding protein which recruits the heterodimer to ssDNA (*168, 229*). This modification is crucial for the initiation of error-free postreplicative DNA repair, and accounts for previous observations in which the proteolytic activity of proteasomes not required for DNA repair function by Ubc13/Mms2 (*34, 136*). The interplay between the two ubiquitin conjugation activities (Rad6 and Ubc13/Mms2) is further mediated by physical interactions that have been observed between the two RING-finger containing ssDNA binding proteins Rad18 and Rad5 (*168, 229*). Although the mechanism of Lys^{63} chain building and the role of these alternative chains remains to be confirmed (*e.g.* polymerase recruitment), the discovery of PCNA as a target represents the first protein substrate recognized and ubiquitinated by components of the Rad6 pathway.

Lys^{164} of PCNA can also become covalently modified by a single SUMO molecule via its cognate E2 (Ubc9), which appears to regulate normal DNA replication via inhibition of ubiquitination of PCNA (*71*). Furthermore, conservation of each of these modifications on PCNA have been observed in both yeast and humans, underscoring the highly conserved nature of DNA repair pathways in eukaryotes, and the crucial role that distinct ubiquitination processes play in these pathways (*71*).

1.9.2 NF-κB signal transduction

Another example where different modes of protein ubiquitination play a role in a biological process is found in NF-κB signal transduction. This pathway is different in that distinct modes of ubiquitination are used along the signaling cascade on different target proteins, eventually leading to NF-κB activation. The NF-κB family comprises a set of transcription factors regulate a wide variety of genes including cytokines, chemokines, adhesion molecules, acute phase proteins, inducible effector proteins, and regulators of apoptosis and cell proliferation, which together play a crucial role in the recognition of pathogens by

innate or adaptive immune responses (*17, 232, 233*). Upon agonist stimulation (*i.e.* tumor necrosis factor α, interleukin 1β) of cell-surface receptors, NF-κB mediated transcriptional activation of target genes is stimulated via an intricately regulated cascade whose ultimate purpose is to release the transcription factor from inhibitory molecules in the cytoplasm, thus allowing for nuclear translocation (Fig. 1.10). NF-κB-mediated transcriptional activation is meditated by protein ubiquitination in a variety of manners, and serves as an excellent example of the multitude of regulatory mechanisms protein ubiquitination possesses (Fig. 1.10).

NF-κB is composed of two subunits, p100 and p105 precursor proteins, which are sequestered in the cytoplasm (*234*). In order to activate transcription, p105 alone must find its way to the nucleus where transcription occurs (*235*). Degradation of p100, which unmasks p105's nuclear localization signal and thus allows for translocation, is accomplished via its conjugation with Lys^{48}-linked poly-Ub chains (*236*). Here, the ubiquitination signal serves to activate a protein, NF-κB, via the specific degradation of one of its subunits by the 26S proteasome.

A second example of the role ubiquitination plays in NF-κB signal transduction involves the ubiquitination and subsequent rapid degradation of IκB by the 26S proteasome. In order to reach the nucleus, NF-κB must escape its inhibitory binding partner, IκB, as this interaction results in a cytoplasmic localization of the two proteins (*232, 233, 237*). In response to external agonists, IκB proteins are rapidly phosphorylated at two specific serine residues (Ser^{32} and Ser^{36}) by an IκB kinase (IKK) (*238, 239*), and then tagged by Lys^{48}-linked poly-Ub chains (*17*). Recent studies have identified the IκB-E2 as a member of the Ubc4/5 family, and the IκB-E3 as an SCF complex which specifically binds phosphorylated IκB (*240*). Here, the ubiquitination signal serves to specifically degrade the IκB proteins via the 26S proteasome, again allowing for nuclear translocation of the transcription factor.

A third example of the regulatory role that protein ubiquitination plays in the NF-κB signal transduction pathway is decisively different from the latter two
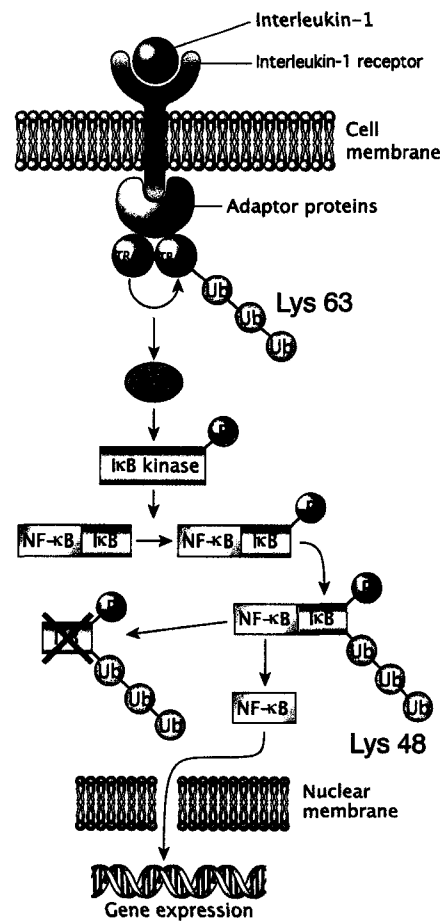
Figure 1.10 The role of ubiquitination in NF-κB signal transduction. In response to IL-1 binding to its receptor, a set of adaptor proteins bind to the receptor and recruit TRAF6 (E3) molecules, which subsequently become modified by Lys[63] poly-Ub chains, which is believed to activate the TAK1 kinase. Downstream, the IκB protein becomes poly-ubiquitinated with Lys[48]-linked chains, which ultimately leads to its destruction via the 26S proteasome and the release of the NF-κB transcription factor into the nucleus. Adapted from (237).

in that it plays an early and non-destructive role. IKK activation, which is required for the downstream phosphorylation of IκB, is accomplished by a complex that includes the protein kinase TAK1 (*18, 139, 241, 242*). In turn, TAK1 activation has been demonstrated to be dependent upon a RING-finger E3 protein ligase, TRAF6 (*39, 139*), which oligomerizes on the cytoplasmic side of the cell membrane upon stimuli of extracellular receptors (*243*) (Fig. 1.10). Most importantly, activation of TAK1 requires TRAF6 upon which non-canonical Lys[63]-linked poly-Ub chains have been conjugated after oligomerization, and these chains do not signal for degradation (*18, 39, 139, 236*). Although the manner in which these Lys[63]-linked chains are responsible for activation of TAK1 remains unknown, a specific E2-Uev heterodimer has been identified, Ubc13-Uev1a, which is responsible for the alternative chain formation. The RING-finger domain of TRAF6 itself is also required for the ubiquitination event (*39, 139*). Therefore, the assembly of Lys[63]-linked chains on TRAF6 represents its activation through non-proteasomal mechanisms.

1.10 OVERVIEW

The preceding introduction should provide a general framework upon which the results presented in this dissertation build. The research outlined in this thesis deals in a broad sense with employing the nature of the interactions between components of the protein ubiquitination machinery to provide insight into the mechanism of poly-Ub chain formation. Specifically, the fundamental nature of the interactions between E2 enzymes and Ub moieties will be addressed, as will the implications that these interactions have for canonical and non-canonical poly-Ub chain formation.

Initially, biochemical data will be presented outlining a novel E2-Uev heterodimer interaction, which is responsible for the formation of alternative Lys[63] poly-Ub chains (Chapter 2). Next, in order to probe that structural features of this E2-Uev heterodimer that are responsible for the assembly of Lys[63]-linked chains, the NMR chemical shift assignments for each of the heterodimer components will

be described (Chapter 3), followed by a detailed structural analysis of the interactions between Ub moieties and this heterodimer (Chapter 4). Additional data regarding the thermodynamic and kinetic bases for these interactions will be presented (Chapter 5), and complimented with an analysis of NMR-derived backbone dynamics of each of the proteins alone and in complex with each other (Chapter 6). A final chapter will deal with examining the biochemical and structural nature of Ub interactions with E2 enzymes responsible for the assembly of canonical Lys[48]-linked chains (Chapter 7). Finally, these results will be discussed in a cohesive manner, describing the potential mechanistic implications on poly-Ub chain catalysis (Chapter 8).

1.11 REFERENCES

1. Johnson, L. N., and Barford, D. (1993) *Annu Rev Biophys Biomol Struct 22*, 199-232.

2. Johnson, L. N., Barford, D., Owen, D. J., Noble, M. E., and Garman, E. F. (1997) *Adv Second Messenger Phosphoprotein Res 31*, 11-28.

3. Johnson, L. N., De Moliner, E., Brown, N. R., Song, H., Barford, D., Endicott, J. A., and Noble, M. E. (2002) *Pharmacol Ther 93*, 113-24.

4. Van den Steen, P., Rudd, P. M., Dwek, R. A., and Opdenakker, G. (1998) *Crit Rev Biochem Mol Biol 33*, 151-208.

5. Kouzarides, T. (2000) *Embo J 19*, 1176-9.

6. Casey, P. J. (1994) *Curr. Opi. Cell Biol. 6*, 219-225.

7. Rando, R. R. (1996) *Biochim Biophys Acta 1300*, 5-16.

8. Desrosiers, R. R., Gauthier, F., Lanthier, J., and Beliveau, R. (2000) *J Biol Chem 275*, 14949-57.

9. Adler, J. (1975) *Annu Rev Biochem 44*, 341-356.

10. Kim, S. H., Wang, W., Kim, K.K. (2002) *Proc Natl Acad Sci U S A 99*, 11611-11615.

11. Clarke, S. (1985) *Annu Rev Biochem 54*, 479-506.

12. Glickman, M. H., and Ciechanover, A. (2002) *Physiol Rev 82*, 373-428.

13. Pickart, C. M. (2001) *Annu Rev Biochem 70*, 503-33.

14. Peters, J.-M., King, R.W., Deshaies, R.J. (1998) *Ubiquitin and the Biology of the Cell*, Plenum Press, New York.

15. Koepp, D. M., Harper, J. W., and Elledge, S. J. (1999) *Cell 97*, 431-4.

16. Chen, Z., Hagler, J., Palombella, V. J., Melandri, F., Scherer, D., Ballard, D., and Maniatis, T. (1995) *Genes Dev 9*, 1586-97.

17. Ghosh, S., May, M. J., and Kopp, E. B. (1998) *Annu Rev Immunol 16*, 225-60.

18. Chen, Z. J., Parent, L., and Maniatis, T. (1996) *Cell 84*, 853-62.

19. Scheffner, M., and Whitaker, N. J. (2003) *Semin Cancer Biol 13*, 59-67.

20. Loda, M., Cukor, B., Tam, S. W., Lavin, P., Fiorentino, M., Draetta, G. F., Jessup, J. M., and Pagano, M. (1997) *Nat Med 3*, 231-4.

21. Joazeiro, C. A., Wing, S. S., Huang, H., Leverson, J. D., Hunter, T., and Liu, Y. C. (1999) *Science 286*, 309-12.

22. Waterman, H., Levkowitz, G., Alroy, I., and Yarden, Y. (1999) *J Biol Chem 274*, 22151-4.

23. Bignell, G. R., Warren, W., Seal, S., Takahashi, M., Rapley, E., Barfoot, R., Green, H., Brown, C., Biggs, P. J., Lakhani, S. R., Jones, C., Hansen, J., Blair, E., Hofmann, B., Siebert, R., Turner, G., Evans, D. G., Schrander-Stumpel, C., Beemer, F. A., van Den Ouweland, A., Halley, D., Delpech, B., Cleveland, M. G., Leigh, I., Leisti, J., and Rasmussen, S. (2000) *Nat Genet 25*, 160-5.

24. Maxwell, P. H., Wiesener, M. S., Chang, G. W., Clifford, S. C., Vaux, E. C., Cockman, M. E., Wykoff, C. C., Pugh, C. W., Maher, E. R., and Ratcliffe, P. J. (1999) *Nature 399*, 271-5.

25. Matsuura, T., Sutcliffe, J. S., Fang, P., Galjaard, R. J., Jiang, Y. H., Benton, C. S., Rommens, J. M., and Beaudet, A. L. (1997) *Nat Genet 15*, 74-7.

26. Shimura, H., Hattori, N., Kubo, S., Mizuno, Y., Asakawa, S., Minoshima, S., Shimizu, N., Iwai, K., Chiba, T., Tanaka, K., and Suzuki, T. (2000) *Nat Genet 25*, 302-5.

27. van Leeuwen, F. W., de Kleijn, D. P., van den Hurk, H. H., Neubauer, A., Sonnemans, M. A., Sluijs, J. A., Koycu, S., Ramdjielal, R. D., Salehi, A., Martens, G. J., Grosveld, F. G., Peter, J., Burbach, H., and Hol, E. M. (1998) *Science 279*, 242-7.

28. Lam, Y. A., Pickart, C. M., Alban, A., Landon, M., Jamieson, C., Ramage, R., Mayer, R. J., and Layfield, R. (2000) *Proc Natl Acad Sci U S A 97*, 9902-6.

29. Saigoh, K., Wang, Y. L., Suh, J. G., Yamanishi, T., Sakai, Y., Kiyosawa, H., Harada, T., Ichihara, N., Wakana, S., Kikuchi, T., and Wada, K. (1999) *Nat Genet 23*, 47-51.

30. Staub, O., Gautschi, I., Ishikawa, T., Breitschopf, K., Ciechanover, A., Schild, L., and Rotin, D. (1997) *Embo J 16*, 6325-36.

31. Kishino, T., Lalande, M., and Wagstaff, J. (1997) *Nat Genet 15*, 70-3.

32. Jentsch, S., McGrath, J. P., and Varshavsky, A. (1987) *Nature 329*, 131-4.

33. Spence, J., Sadis, S., Haas, A. L., and Finley, D. (1995) *Mol Cell Biol 15*, 1265-73.

34. Hofmann, R. M., and Pickart, C. M. (1999) *Cell 96*, 645-53.

35. Finley, D., Bartel, B., and Varshavsky, A. (1989) *Nature 338*, 394-401.

36. Spence, J., Gali, R. R., Dittmar, G., Sherman, F., Karin, M., and Finley, D. (2000) *Cell 102*, 67-76.

37. Hicke, L., and Riezman, H. (1996) *Cell 84*, 277-87.

38. Kaiser, P., Flick, K., Wittenberg, C., and Reed, S. I. (2000) *Cell 102*, 303-14.

39. Deng, L., Wang, C., Spencer, E., Yang, L., Braun, A., You, J., Slaughter, C., Pickart, C., and Chen, Z. J. (2000) *Cell 103*, 351-61.

40. Hershko, A., Ciechanover, A., and Varshavsky, A. (2000) *Nat Med 6*, 1073-81.

41. Varshavsky, A. (1997) *Trends Biochem Sci 22*, 383-7.

42. Hochstrasser, M. (1996) *Annu Rev Genet 30*, 405-39.

43. Hershko, A., and Ciechanover, A. (1992) *Annu Rev Biochem 61*, 761-807.

44. Jentsch, S. (1992) *Annu Rev Genet 26*, 179-207.

45. Vijay-Kumar, S., Bugg, C. E., Wilkinson, K. D., Vierstra, R. D., Hatfield, P. M., and Cook, W. J. (1987) *J Biol Chem 262*, 6396-9.

46. Weber, P. L., Brown, S. C., and Mueller, L. (1987) *Biochemistry 26*, 7282-90.

47. Chau, V., Tobias, J. W., Bachmair, A., Marriott, D., Ecker, D. J., Gonda, D. K., and Varshavsky, A. (1989) *Science 243*, 1576-83.

48. Arnason, T., and Ellison, M. J. (1994) *Mol Cell Biol 14*, 7876-83.

49. Johnson, E. S., Ma, P. C., Ota, I. M., and Varshavsky, A. (1995) *J Biol Chem 270*, 17442-56.

50. Baboshina, O. V., and Haas, A. L. (1996) *J Biol Chem 271*, 2823-31.

51. Koegl, M., Hoppe, T., Schlenker, S., Ulrich, H. D., Mayer, T. U., and Jentsch, S. (1999) *Cell 96*, 635-44.

52. Sloper-Mould, K. E., Jemc, J. C., Pickart, C. M., and Hicke, L. (2001) *J Biol Chem 276*, 30483-9.

53. Beal, R., Devereaux, Q., Xia, G., Rechsteiner, M., Pickart, C. (1996) *Proc Natl Acad Sci U S A 93*, 861-866.

54. Burch, T. J., and Haas, A. L. (1994) *Biochemistry 33*, 7300-8.

55. Hamilton, K. S., Ellison, M. J., and Shaw, G. S. (2000) *J Biomol NMR 18*, 319-27.

56. Miura, T., Klaus, W., Gsell, B., Miyamoto, C., and Senn, H. (1999) *J Mol Biol 290*, 213-28.

57. Ozkaynak, E., Finley, D., Solomon, M. J., and Varshavsky, A. (1987) *Embo J 6*, 1429-39.

58. Orengo, C. A., Jones, D. T., and Thornton, J. M. (1994) *Nature 372*, 631-4.

59. Achari, A., Hale, S. P., Howard, A. J., Clore, G. M., Gronenborn, A. M., Hardman, K. D., and Whitlow, M. (1992) *Biochemistry 31*, 10449-57.

60. Gallagher, T., Alexander, P., Bryan, P., and Gilliland, G. L. (1994) *Biochemistry 33*, 4721-9.

61. Tsukihara, T., Fukuyama, K., Mizushima, M., Harioka, T., Kusunoki, M., Katsube, Y., Hase, T., and Matsubara, H. (1990) *J Mol Biol 216*, 399-410.

62. Nassar, N., Horn, G., Herrmann, C., Scherer, A., McCormick, F., and Wittinghofer, A. (1995) *Nature 375*, 554-60.

63. Geyer, M., Herrmann, C., Wohlgemuth, S., Wittinghofer, A., and Kalbitzer, H. R. (1997) *Nat Struct Biol 4*, 694-9.

64. Kalhammer, G., Bahler, M., Schmitz, F., Jockel, J., and Block, C. (1997) *FEBS Lett 414*, 599-602.

65. Esser, D., Bauer, B., Wolthuis, R. M., Wittinghofer, A., Cool, R. H., and Bayer, P. (1998) *Biochemistry 37*, 13453-62.

66. Kamitani, T., Kito, K., Nguyen, H. P., Wada, H., Fukuda-Kamitani, T., and Yeh, E. T. (1998) *J Biol Chem 273*, 26675-82.

67. Yeh, E. T., Gong, L., and Kamitani, T. (2000) *Gene 248*, 1-14.

68. Mahajan, R., Delphin, C., Guan, T., Gerace, L., and Melchior, F. (1997) *Cell 88*, 97-107.

69. Melchior, F. (2000) *Annu Rev Cell Dev Biol 16*, 591-626.

70. Desterro, J. M., Rodriguez, M. S., and Hay, R. T. (1998) *Mol Cell 2*, 233-9.

71. Hoege, C., Pfander, B., Moldovan, G. L., Pyrowolakis, G., and Jentsch, S. (2002) *Nature 419*, 135-41.

72. Bayer, P., Arndt, A., Metzger, S., Mahajan, R., Melchior, F., Jaenicke, R., and Becker, J. (1998) *J Mol Biol 280*, 275-86.

73. Jin, C., Shiyanova, T., Shen, Z., and Liao, X. (2001) *Int J Biol Macromol 28*, 227-34.

74. Sheng, W., and Liao, X. (2002) *Protein Sci 11*, 1482-91.

75. Gong, L., and Yeh, E. T. (1999) *J Biol Chem 274*, 12036-42.

76. Liakopoulos, D., Doenges, G., Matuschewski, K., and Jentsch, S. (1998) *Embo J 17*, 2208-14.

77. Johnson, E. S., and Blobel, G. (1997) *J Biol Chem 272*, 26799-802.

78. Osaka, F., Saeki, M., Katayama, S., Aida, N., Toh, E. A., Kominami, K., Toda, T., Suzuki, T., Chiba, T., Tanaka, K., and Kato, S. (2000) *Embo J 19*, 3475-84.

79. Tateishi, K., Omata, M., Tanaka, K., and Chiba, T. (2001) *J Cell Biol 155*, 571-9.

80. Kamura, T., Koepp, D. M., Conrad, M. N., Skowyra, D., Moreland, R. J., Iliopoulos, O., Lane, W. S., Kaelin, W. G., Jr., Elledge, S. J., Conaway, R. C., Harper, J. W., and Conaway, J. W. (1999) *Science 284*, 657-61.

81. Kawakami, T., Chiba, T., Suzuki, T., Iwai, K., Yamanaka, K., Minato, N., Suzuki, H., Shimbara, N., Hidaka, Y., Osaka, F., Omata, M., and Tanaka, K. (2001) *Embo J 20*, 4003-12.

82. Wu, K., Chen, A., Tan, P., and Pan, Z. Q. (2002) *J Biol Chem 277*, 516-27.

83. Lyapina, S., Cope, G., Shevchenko, A., Serino, G., Tsuge, T., Zhou, C., Wolf, D. A., Wei, N., and Deshaies, R. J. (2001) *Science 292*, 1382-5.

84. Zhou, C., Seibert, V., Geyer, R., Rhee, E., Lyapina, S., Cope, G., Deshaies, R. J., and Wolf, D. A. (2001) *BMC Biochem 2*, 7.

85. Whitby, F. G., Xia, G., Pickart, C. M., and Hill, C. P. (1998) *J Biol Chem 273*, 34983-91.

86. Rao-Naik, C., delaCruz, W., Laplaza, J. M., Tan, S., Callis, J., and Fisher, A. J. (1998) *J Biol Chem 273*, 34976-82.

87. Furukawa, K., Mizushima, N., Noda, T., and Ohsumi, Y. (2000) *J Biol Chem 275*, 7462-5.

88. Ohsumi, Y. (2001) *Nat Rev Mol Cell Biol 2*, 211-6.

89. Klionsky, D. J., and Ohsumi, Y. (1999) *Annu Rev Cell Dev Biol 15*, 1-32.

90. Zacksenhaus, E., and Sheinin, R. (1990) *Embo J 9*, 2923-9.

91. McGrath, J. P., Jentsch, S., and Varshavsky, A. (1991) *Embo J 10*, 227-36.

92. Ciechanover, A., Heller, H., Katz-Etzion, R., and Hershko, A. (1981) *Proc Natl Acad Sci U S A 78*, 761-5.

93. Haas, A. L., Warms, J. V., Hershko, A., and Rose, I. A. (1982) *J Biol Chem 257*, 2543-8.

94. Pickart, C. M., Kasperek, E. M., Beal, R., and Kim, A. (1994) *J Biol Chem 269*, 7115-23.

95. Haas, A. L., Rose, I.A. (1982) *J. Biol. Chem. 257*, 10329-10337.

96. Haas, A. L., Warms, J.V.B., Rose, I,A. (1983) *Biochemistry 22*, 4388-4394.

97. Ciechanover, A., Elias, S., Heller, H., and Hershko, A. (1982) *J Biol Chem 257*, 2537-42.

98. Haas, A. L., and Rose, I. A. (1982) *J Biol Chem 257*, 10329-37.

99. Mastrandrea, L. D., You, J., Niles, E. G., and Pickart, C. M. (1999) *J Biol Chem 274*, 27299-306.

100. Hershko, A., Heller, H., Elias, S., and Ciechanover, A. (1983) *J Biol Chem 258*, 8206-14.

101. Rajagopalan, K. V. (1996) (Neidhardt, F. C., Ed.) pp 674-679, ASM Press, Washington, DC.

102. Rajagopalan, K. V. (1997) *Biochem. Soc. Trans. 25*, 757-761.

103. Lake, M. W., Wuebbens, M. M., Rajagopalan, K. V., and Schindelin, H. (2001) *Nature 414*, 325-9.

104. Walden, H., Podgorski, M. S., and Schulman, B. A. (2003) *Nature 422*, 330-4.

105. Schulman, B. A., Carrano, A. C., Jeffrey, P. D., Bowen, Z., Kinnucan, E. R., Finnin, M. S., Elledge, S. J., Harper, J. W., Pagano, M., and Pavletich, N. P. (2000) *Nature 408*, 381-6.

106. Ptak, C., Gwozd, C., Huzil, J. T., Gwozd, T. J., Garen, G., and Ellison, M. J. (2001) *Mol Cell Biol 21*, 6537-48.

107. Tong, H., Hateboer, G., Perrakis, A., Bernards, R., and Sixma, T. K. (1997) *J Biol Chem 272*, 21381-7.

108. Worthylake, D. K., Prakash, S., Prakash, L., and Hill, C. P. (1998) *J Biol Chem 273*, 6271-6.

109. Hamilton, K. S., Ellison, M. J., Barber, K. R., Williams, R. S., Huzil, J. T., McKenna, S., Ptak, C., Glover, M., and Shaw, G. S. (2001) *Structure (Camb) 9*, 897-904.

110. Lin, Y., Hwang, W. C., and Basavappa, R. (2002) *J Biol Chem 277*, 21913-21.

111. VanDemark, A. P., Hofmann, R. M., Tsui, C., Pickart, C. M., and Wolberger, C. (2001) *Cell 105*, 711-20.

112. Cook, W. J., Jeffrey, L. C., Xu, Y., and Chau, V. (1993) *Biochemistry 32*, 13809-17.

113. Cook, W. J., Jeffrey, L. C., Sullivan, M. L., and Vierstra, R. D. (1992) *J Biol Chem 267*, 15116-21.

114. Jiang, F., and Basavappa, R. (1999) *Biochemistry 38*, 6471-8.

115. Cook, W. J., Martin, P. D., Edwards, B. F., Yamazaki, R. K., and Chau, V. (1997) *Biochemistry 36*, 1621-7.

116. Yamanaka, A., Hatakeyama, S., Kominami, K., Kitagawa, M., Matsumoto, M., and Nakayama, K. (2000) *Mol Biol Cell 11*, 2821-31.

117. Merkley, N., and Shaw, G. S. (2003) *J Biomol NMR 26*, 147-55.

118. Varelas, X., Ptak, C., and Ellison, M. J. (2003) *Mol Cell Biol 23*, 5388-400.

119. Girod, P. A., Carpenter, T. B., van Nocker, S., Sullivan, M. L., and Vierstra, R. D. (1993) *Plant J 3*, 545-52.

120. Pickart, C. M., and Rose, I. A. (1985) *J Biol Chem 260*, 7903-10.

121. Gwozd, C. S., Arnason, T. G., Cook, W. J., Chau, V., and Ellison, M. J. (1995) *Biochemistry 34*, 6296-302.

122. Leggett, D. S., and Candido, P. M. (1997) *Biochem J 327 (Pt 2)*, 357-61.

123. Ptak, C., Prendergast, J. A., Hodgins, R., Kay, C. M., Chau, V., and Ellison, M. J. (1994) *J Biol Chem 269*, 26539-45.

124. Chen, P., Johnson, P., Sommer, T., Jentsch, S., and Hochstrasser, M. (1993) *Cell 74*, 357-69.

125. Liu, Q., Jin, C., Liao, X., Shen, Z., Chen, D. J., and Chen, Y. (1999) *J Biol Chem 274*, 16979-87.

126. Banerjee, A., Gregori, L., Xu, Y., and Chau, V. (1993) *J Biol Chem 268*, 5668-75.

127. Arnold, J. E., and Gevers, W. (1990) *Biochem J 267*, 751-7.

128. Pickart, C. M., and Rose, I. A. (1985) *J Biol Chem 260*, 1573-81.

129. Sancho, E., Vila, M. R., Sanchez-Pulido, L., Lozano, J. J., Paciucci, R., Nadal, M., Fox, M., Harvey, C., Bercovich, B., Loukili, N., Ciechanover, A., Lin, S. L., Sanz, F., Estivill, X., Valencia, A., and Thomson, T. M. (1998) *Mol Cell Biol 18*, 576-89.

130. Broomfield, S., Chow, B. L., and Xiao, W. (1998) *Proc Natl Acad Sci U S A 95*, 5678-83.

131. Garrus, J. E., von Schwedler, U. K., Pornillos, O. W., Morham, S. G., Zavitz, K. H., Wang, H. E., Wettstein, D. A., Stray, K. M., Cote, M., Rich, R. L., Myszka, D. G., and Sundquist, W. I. (2001) *Cell 107*, 55-65.

132. VerPlank, L., Bouamr, F., LaGrassa, T. J., Agresta, B., Kikonyogo, A., Leis, J., and Carter, C. A. (2001) *Proc Natl Acad Sci U S A 98*, 7724-9.

133. Katzmann, D. J., Babst, M., and Emr, S. D. (2001) *Cell 106*, 145-55.

134. Brusky, J., Zhu, Y., and Xiao, W. (2000) *Curr Genet 37*, 168-74.

135. Xiao, W., Lin, S. L., Broomfield, S., Chow, B. L., and Wei, Y. F. (1998) *Nucleic Acids Res 26*, 3908-14.

136. Hofmann, R. M., and Pickart, C. M. (2001) *J Biol Chem 276*, 27936-43.

137. Moraes, T. F., Edwards, R. A., McKenna, S., Pastushok, L., Xiao, W., Glover, J. N., and Ellison, M. J. (2001) *Nat Struct Biol 8*, 669-73.

138. Chan, N. L., and Hill, C. P. (2001) *Nat Struct Biol 8*, 650-2.

139. Wang, C., Deng, L., Hong, M., Akkaraju, G. R., Inoue, J., and Chen, Z. J. (2001) *Nature 412*, 346-51.

140. Pornillos, O., Alam, S. L., Davis, D. R., and Sundquist, W. I. (2002) *Nat Struct Biol 9*, 812-7.

141. Pornillos, O., Alam, S. L., Rich, R. L., Myszka, D. G., Davis, D. R., and Sundquist, W. I. (2002) *Embo J 21*, 2397-406.

142. Dupre, S., and Haguenauer-Tsapis, R. (2001) *Mol Cell Biol 21*, 4482-94.

143. Hicke, L. (2001) *Cell 106*, 527-30.

144. Hewitt, E. W., Duncan, L., Mufti, D., Baker, J., Stevenson, P. G., and Lehner, P. J. (2002) *Embo J 21*, 2418-29.

145. Villalobo, E., Morin, L., Moch, C., Lescasse, R., Hanna, M., Xiao, W., and Baroin-Tourancheau, A. (2002) *Mol Biol Evol 19*, 39-48.

146. Deshaies, R. J. (1999) *Annu Rev Cell Dev Biol 15*, 435-67.

147. Fang, S., Lorick, K. L., Jensen, J. P., and Weissman, A. M. (2003) *Semin Cancer Biol 13*, 5-14.

148. Zheng, N. (2003) *Structure (Camb) 11*, 5-6.

149. Hatakeyama, S., and Nakayama, K. I. (2003) *Biochem Biophys Res Commun 302*, 635-45.

150. Glotzer, M., Murray, A. W., and Kirschner, M. W. (1991) *Nature 349*, 132-8.

151. Yamano, H., Tsurumi, C., Gannon, J., and Hunt, T. (1998) *Embo J 17*, 5670-8.

152. Laney, J. D., and Hochstrasser, M. (1999) *Cell 97*, 427-30.

153. Lawson, T. G., Gronros, D. L., Evans, P. E., Bastien, M. C., Michalewich, K. M., Clark, J. K., Edmonds, J. H., Graber, K. H., Werner, J. A., Lurvey, B. A., and Cate, J. M. (1999) *J Biol Chem 274*, 9904-80.

154. Johnson, P. R., Swanson, R., Rakhilina, L., and Hochstrasser, M. (1998) *Cell 94*, 217-27.

155. Bachmair, A., Finley, D., and Varshavsky, A. (1986) *Science 234*, 179-86.

156. Varshavsky, A. (1996) *Proc Natl Acad Sci U S A 93*, 12142-9.

157. Rechsteiner, M., and Rogers, S. W. (1996) *Trends Biochem Sci 21*, 267-71.

158. Treier, M., Staszewski, L. M., and Bohmann, D. (1994) *Cell 78*, 787-98.

159. Hou, D., Cenciarelli, C., Jensen, J. P., Nguygen, H. B., and Weissman, A. M. (1994) *J Biol Chem 269*, 14244-7.

160. Borden, K. L. (2000) *J Mol Biol 295*, 1103-12.

161. Saurin, A. J., Borden, K. L., Boddy, M. N., and Freemont, P. S. (1996) *Trends Biochem Sci 21*, 208-14.

162. Lorick, K. L., Jensen, J. P., Fang, S., Ong, A. M., Hatakeyama, S., and Weissman, A. M. (1999) *Proc Natl Acad Sci U S A 96*, 11364-9.

163. Moynihan, T. P., Ardley, H. C., Nuber, U., Rose, S. A., Jones, P. F., Markham, A. F., Scheffner, M., and Robinson, P. A. (1999) *J Biol Chem 274*, 30963-8.

164. Fang, S., Jensen, J. P., Ludwig, R. L., Vousden, K. H., and Weissman, A. M. (2000) *J Biol Chem 275*, 8945-51.

165. Madura, K., Dohmen, R. J., and Varshavsky, A. (1993) *J Biol Chem 268*, 12046-54.

166. Xie, Y., and Varshavsky, A. (1999) *Embo J 18*, 6832-44.

167. Watkins, J. F., Sung, P., Prakash, S., and Prakash, L. (1993) *Genes Dev 7*, 250-61.

168. Ulrich, H. D., and Jentsch, S. (2000) *Embo J 19*, 3388-97.

169. Zheng, N., Wang, P., Jeffrey, P. D., and Pavletich, N. P. (2000) *Cell 102*, 533-9.

170. Page, A. M., and Hieter, P. (1999) *Annu Rev Biochem 68*, 583-609.

171. Iwai, K., Yamanaka, K., Kamura, T., Minato, N., Conaway, R. C., Conaway, J. W., Klausner, R. D., and Pause, A. (1999) *Proc Natl Acad Sci U S A 96*, 12436-41.

172. Lisztwan, J., Imbert, G., Wirbelauer, C., Gstaiger, M., and Krek, W. (1999) *Genes Dev 13*, 1822-33.

173. Pause, A., Peterson, B., Schaffar, G., Stearman, R., and Klausner, R. D. (1999) *Proc Natl Acad Sci U S A 96*, 9533-8.

174. Zheng, N., Schulman, B. A., Song, L., Miller, J. J., Jeffrey, P. D., Wang, P., Chu, C., Koepp, D. M., Elledge, S. J., Pagano, M., Conaway, R. C., Conaway, J. W., Harper, J. W., and Pavletich, N. P. (2002) *Nature 416*, 703-9.

175. Huibregtse, J. M., Scheffner, M., Beaudenon, S., and Howley, P. M. (1995) *Proc Natl Acad Sci U S A 92*, 5249.

176. Scheffner, M., Nuber, U., and Huibregtse, J. M. (1995) *Nature 373*, 81-3.

177. Huang, L., Kinnucan, E., Wang, G., Beaudenon, S., Howley, P. M., Huibregtse, J. M., and Pavletich, N. P. (1999) *Science 286*, 1321-6.

178. Nuber, U., Schwarz, S., Kaiser, P., Schneider, R., and Scheffner, M. (1996) *J Biol Chem 271*, 2795-800.

179. Kumar, S., Kao, W. H., and Howley, P. M. (1997) *J Biol Chem 272*, 13548-54.

180. Wilkinson, K. D., Tashayev, V. L., O'Connor, L. B., Larsen, C. N., Kasperek, E., and Pickart, C. M. (1995) *Biochemistry 34*, 14535-46.

181. Baker, R. T., Tobias, J. W., and Varshavsky, A. (1992) *J Biol Chem 267*, 23364-75.

182. Johnston, S. C., Riddle, S. M., Cohen, R. E., and Hill, C. P. (1999) *Embo J 18*, 3877-87.

183. Johnston, S. C., Larsen, C. N., Cook, W. J., Wilkinson, K. D., and Hill, C. P. (1997) *Embo J 16*, 3787-96.

184. Hu, M., Li, P., Li, M., Li, W., Yao, T., Wu, J. W., Gu, W., Cohen, R. E., and Shi, Y. (2002) *Cell 111*, 1041-54.

185. Sakamoto, T., Tanaka, T., Ito, Y., Rajesh, S., Iwamoto-Sugai, M., Kodera, Y., Tsuchida, N., Shibata, T., and Kohno, T. (1999) *Biochemistry 38*, 11634-42.

186. Rajesh, S., Sakamoto, T., Iwamoto-Sugai, M., Shibata, T., Kohno, T., and Ito, Y. (1999) *Biochemistry 38*, 9242-53.

187. Pickart, C. M., and VanDemark, A. P. (2000) *Nat Struct Biol 7*, 999-1001.

188. Baumeister, W., Walz, J., Zuhl, F., and Seemuller, E. (1998) *Cell 92*, 367-80.

189. Groll, M., Bajorek, M., Kohler, A., Moroder, L., Rubin, D. M., Huber, R., Glickman, M. H., and Finley, D. (2000) *Nat Struct Biol 7*, 1062-7.

190. Groll, M., and Huber, R. (2003) *Int J Biochem Cell Biol 35*, 606-16.

191. Whitby, F. G., Masters, E. I., Kramer, L., Knowlton, J. R., Yao, Y., Wang, C. C., and Hill, C. P. (2000) *Nature 408*, 115-20.

192. Hough, R., Pratt, G., and Rechsteiner, M. (1986) *J Biol Chem 261*, 2400-8.

193. Hough, R., and Rechsteiner, M. (1986) *J Biol Chem 261*, 2391-9.

194. Swaminathan, S., Amerik, A. Y., and Hochstrasser, M. (1999) *Mol Biol Cell 10*, 2583-94.

195. Braun, B. C., Glickman, M., Kraft, R., Dahlmann, B., Kloetzel, P. M., Finley, D., and Schmidt, M. (1999) *Nat Cell Biol 1*, 221-6.

196. Groll, M., Ditzel, L., Lowe, J., Stock, D., Bochtler, M., Bartunik, H. D., and Huber, R. (1997) *Nature 386*, 463-71.

197. Horwich, A. L., Weber-Ban, E. U., and Finley, D. (1999) *Proc Natl Acad Sci U S A 96*, 11033-40.

198. Strickland, E., Hakala, K., Thomas, P. J., and DeMartino, G. N. (2000) *J Biol Chem 275*, 5565-72.

199. Glickman, M. H., Rubin, D. M., Coux, O., Wefes, I., Pfeifer, G., Cjeka, Z., Baumeister, W., Fried, V. A., and Finley, D. (1998) *Cell 94*, 615-23.

200. Glickman, M. H., Rubin, D. M., Fried, V. A., and Finley, D. (1998) *Mol Cell Biol 18*, 3149-62.

201. Deveraux, Q., Jensen, C., and Rechsteiner, M. (1995) *J Biol Chem 270*, 23726-9.

202. Haracska, L., and Udvardy, A. (1997) *FEBS Lett 412*, 331-6.

203. van Nocker, S., Sadis, S., Rubin, D. M., Glickman, M., Fu, H., Coux, O., Wefes, I., Finley, D., and Vierstra, R. D. (1996) *Mol Cell Biol 16*, 6020-8.

204. van Nocker, S., Deveraux, Q., Rechsteiner, M., and Vierstra, R. D. (1996) *Proc Natl Acad Sci U S A 93*, 856-60.

205. Wilkinson, C. R., Ferrell, K., Penney, M., Wallace, M., Dubiel, W., and Gordon, C. (2000) *J Biol Chem 275*, 15182-92.

206. Thrower, J. S., Hoffman, L., Rechsteiner, M., and Pickart, C. M. (2000) *Embo J 19*, 94-102.

207. Glickman, M. H., Rubin, D. M., Fu, H., Larsen, C. N., Coux, O., Wefes, I., Pfeifer, G., Cjeka, Z., Vierstra, R., Baumeister, W., Fried, V., and Finley, D. (1999) *Mol Biol Rep 26*, 21-8.

208. Cook, W. J., Jeffrey, L. C., Carson, M., Chen, Z., and Pickart, C. M. (1992) *J Biol Chem 267*, 16467-71.

209. Cook, W., Jeffrey, L.C., Kasperek, E., Pickart, CM. (1994) *J. Mol. Biol. 236*, 601-609.

210. Phillips, C. L., Thrower, J., Pickart, C. M., and Hill, C. P. (2001) *Acta Crystallogr D Biol Crystallogr 57*, 341-4.

211. Varadan, R., Walker, O., Pickart, C., and Fushman, D. (2002) *J Mol Biol 324*, 637-47.

212. Galan, J. M., and Haguenauer-Tsapis, R. (1997) *Embo J 16*, 5847-54.

213. Springael, J. Y., Galan, J. M., Haguenauer-Tsapis, R., and Andre, B. (1999) *J Cell Sci 112 (Pt 9)*, 1375-83.

214. Fisk, H. A., and Yaffe, M. P. (1999) *J Cell Biol 145*, 1199-208.

215. You, J., and Pickart, C. M. (2001) *J Biol Chem 276*, 19871-8.

216. Wood, R. D., Mitchell, M., Sgouros, J., and Lindahl, T. (2001) *Science 291*, 1284-9.

217. Broomfield, S., Hryciw, T., and Xiao, W. (2001) *Mutat Res 486*, 167-84.

218. Prakash, S., Sung, P., and Prakash, L. (1993) *Annu Rev Genet 27*, 33-70.

219. Hoeijmakers, J. H. (2001) *Nature 411*, 366-74.

220. Rupp, W. D., Wilde, C. E., 3rd, Reno, D. L., and Howard-Flanders, P. (1971) *J Mol Biol 61*, 25-44.

221. Lehmann, A. R. (1972) *J. Mol. Biol. 66*, 319-337.

222. Prakash, L. (1981) *Mol Gen Genet 184*, 471-8.

223. di Caprio, L., Cox, B.S. (1981) *Mutat Res 82*, 69-85.

224. Ulrich, H. D. (2002) *Eukaryot Cell 1*, 1-10.

225. Nelson, J. R., Lawrence, C. W., and Hinkle, D. C. (1996) *Science 272*, 1646-9.

226. Pickart, C. M. (2002) *Nature 419*, 120-1.

227. Silver, E. T., Gwozd, T. J., Ptak, C., Goebl, M., and Ellison, M. J. (1992) *Embo J 11*, 3091-8.

228. Paunesku, T., Mittal, S., Protic, M., Oryhon, J., Korolev, S. V., Joachimiak, A., and Woloschak, G. E. (2001) *Int J Radiat Biol 77*, 1007-21.

229. Ulrich, H. D. (2003) *J Biol Chem 278*, 7051-8.

230. Bailly, V., Lamb, J., Sung, P., Prakash, S., and Prakash, L. (1994) *Genes Dev 8*, 811-20.

231. Matunis, M. J. (2002) *Mol Cell 10*, 441-2.

232. Zhang, G., and Ghosh, S. (2001) *J Clin Invest 107*, 13-9.

233. Ghosh, S., and Karin, M. (2002) *Cell 109 Suppl*, S81-96.

234. Karin, M., and Ben-Neriah, Y. (2000) *Annu Rev Immunol 18*, 621-63.

235. Xiao, G., Harhaj, E. W., and Sun, S. C. (2001) *Mol Cell 7*, 401-9.

236. Palombella, V. J., Rando, O. J., Goldberg, A. L., and Maniatis, T. (1994) *Cell 78*, 773-85.

237. Finley, D. (2001) *Nature 412*, 283, 285-6.

238. Brockman, J. A., Scherer, D. C., McKinsey, T. A., Hall, S. M., Qi, X., Lee, W. Y., and Ballard, D. W. (1995) *Mol Cell Biol 15*, 2809-18.

239. Brown, K., Gerstberger, S., Carlson, L., Franzoso, G., and Siebenlist, U. (1995) *Science 267*, 1485-8.

240. Maniatis, T. (1999) *Genes Dev 13*, 505-10.

241. Takaesu, G., Kishida, S., Hiyama, A., Yamaguchi, K., Shibuya, H., Irie, K., Ninomiya-Tsuji, J., and Matsumoto, K. (2000) *Mol Cell 5*, 649-58.

242. Ninomiya-Tsuji, J., Kishimoto, K., Hiyama, A., Inoue, J., Cao, Z., and Matsumoto, K. (1999) *Nature 398*, 252-6.

243. Cao, Z., Xiong, J., Takeuchi, M., Kurama, T., and Goeddel, D. V. (1996) *Nature 383*, 443-6.

CHAPTER 2:

Non-covalent interaction between Ub and the human DNA repair protein Mms2 is required for Ubc13-mediated poly-ubiquitination[1].

2.1 SUMMARY

Ub-conjugating enzyme variants share significant sequence similarity with typical E2 enzymes of the protein ubiquitination pathway, but lack their characteristic active-site Cys residue. The MMS2 gene of Saccharomyces cerevisiae encodes one such Ub-conjugating enzyme variant that is involved in the error-free DNA postreplicative repair pathway through its association with Ubc13, an E2. The Mms2/Ubc13 heterodimer is capable of linking Ub molecules to one another through an isopeptide bond between the C-terminus and Lys[63]. Using highly purified components, we show here that the human forms of Mms2 and Ubc13 associate into a heterodimer that is stable over a range of conditions. The Ub-thiolester form of the heterodimer can be produced by the direct activation of its Ubc13 subunit with E1, or by the association of Mms2 with the Ubc13~Ub thiolester. The activated heterodimer is capable of transferring its covalently bound ubiquitin to Lys[63] of an untethered ubiquitin molecule, resulting in Ub_2 as the predominant species. We also show here that the Ubc13 protein displays markedly different in vitro chain building and autoubiquitination properties. In ^{1}H-^{15}N-HSQC NMR experiments we have mapped the surface determinants of tethered and untethered ubiquitin that interact with Mms2 and Ubc13 in both their monomeric and dimeric forms. These results have identified a surface of untethered Ub which interacts with Mms2 in the monomeric and heterodimeric form. Furthermore, the C-terminal tail of Ub does not participate in this interaction. These results suggest that the role of Mms2 is to correctly orient

---

[1] The contents of this chapter are based on previously published research: McKenna *et. al.* (2001) *J. Biol. Chem.* **276**, 40120-40126.

either a target-bound or untethered Ub molecule such that its Lys^{63} is placed proximally to the C-terminus of the Ub molecule that is linked to the active site of Ubc13.

2.2 INTRODUCTION

The covalent attachment of Ub to proteins and their subsequent degradation by the 26S proteasome represents the most commonly ascribed role for the protein ubiquitination system (1). In this respect, Ub conjugation to target substrates participates in a variety of important eukaryotic processes, such as cell cycle control (2), DNA repair (3), ribosome biogenesis (4), and the inflammatory response (5). In recent years, the role of ubiquitination has expanded to involve functions apparently unrelated to 26S-dependent proteolysis, including endocytosis of cell surface proteins (6), and NF-κB dependant signal transduction (7). Therefore, the role of protein ubiquitination has broadened in scope.

Protein ubiquitination involves a cascade of enzymatic steps where Ub is passed sequentially as an activated thiolester intermediate from a Ub activating enzyme (E1) to a Ub conjugating enzyme (E2), and finally to the protein target with the help of a Ub protein ligase (E3) (1, 8). In the first step, a thiolester intermediate between the C-terminal tail of Ub (Gly^{76}) and the active-site Cys of the E1 is formed in an ATP-dependent manner. A subsequent transthiolesterification reaction transfers the Ub to the active-site Cys of the E2, forming another thiolester derivative with the C-terminus of Ub. In combination with an E3 enzyme, Ub is then transferred to a Lys residue of the target protein, forming a covalent isopeptide bond. Multi-Ub chains can then be assembled onto the mono-ubiquitinated protein, which is often portrayed as the conjugation of one Ub molecule to the next in step-wise fashion via Gly^{76}-Lys^{48} linkages (1).

Eukaryotic organisms possess multiple E2 and E3 enzymes (1). Within the family of known E2s, all share a highly similar catalytic core domain of approximately 150 amino acids, and are classified based on the presence or

absence of C- and N-terminal extensions (*9*). Numerous complementary structural studies have documented that the fold of the core domain is very well conserved among family members (*10-16*). Furthermore, interactions between E2s and Ub within the thiolester complex appear to be conserved among different E2 enzymes based on NMR chemical shift perturbation analysis (*17-20*). Therefore, in order for E2 enzymes to effect different target substrate ubiquitination, interactions with additional specificity factors are required. Target substrate specificity is thought to be dictated by different combinations of E2s and E3s in conjunction with auxiliary factors (*21-24*).

In addition to this core family, several atypical E2s known as Ub-conjugating enzyme variants (Uevs) have been identified (*25, 26*). These proteins share significant sequence similarity with E2s, but lack the characteristic active-site Cys residue required for thiolester formation. Based on their similarities to E2s, it has been hypothesized that Uev proteins may function as either dominant negative (*25*) or positive (*27*) regulators of E2 function. One such Uev, encoded by the *MMS2* gene in the yeast *S. cerevisiae*, is involved in error-free DNA postreplicative repair (*26*). Mms2 forms a heterodimer with Ubc13 (*27*), an E2 that functions in the error-free DNA postreplicative repair mechanism (*28*). Another Uev, encoded by the human *UEV1* gene, is involved in NF-κB signal transduction (*29*). Ubc13 is unique among known E2s in that it catalyzes the linkage of Ub molecules to one another via a Gly^{76}-Lys^{63} isopeptide bond in an Mms2-dependent manner (*27, 29*). *In vivo* results demonstrated that Lys^{63} chain assembly by the Ubc13/Uev heterodimer does not appear to be involved in proteasome-based degradation of target substrates (*29*). Furthermore, two chromatin-associated RING finger proteins, Rad5 and Rad18, are involved in the recruitment of Ubc13/Mms2 and Ubc2 (Rad6) to DNA (*30*). A model is emerging in which the Ubc13/Mms2 heterodimer plays a central role in the recruitment and/or regulation of factors involved in the error-free tolerance to DNA damage via ubiquitination (*31*).

Two human homologs of yeast Mms2, Uev1a (*32*) and human Mms2 (*31*),

have been identified and characterized. The full-length human *MMS2* cDNA is able to complement the yeast *mms2* mutant, suggesting that human Mms2 is indeed a functional homolog of yeast Mms2. In addition, a human *UBC13* cDNA was isolated as a homolog of the *Drosophila melanogaster bendless* gene (*33*). Human *UBC13* cDNA is also able to complement the yeast Ubc13 mutant[2]. Therefore, human equivalents of the yeast Ubc13 and Mms2 proteins have been identified, and their mechanism of activity remains to be determined.

In this chapter, we demonstrate that purified human Ubc13 and Mms2 proteins form a stable heterodimer, and have uncovered several mechanistic and structural aspects that are pertinent to its function.

2.3 EXPERIMENTAL PROCEDURES

2.3.1 Expression and purification of recombinant Mms2 and Ubc13

Both human *UBC13* and *MMS2* open reading frames were PCR amplified and cloned as *Bam*HI-*Sal*I fragments into the corresponding sites of a GST fusion vector pGEX6 (Pharmacia). In each case, the last codon of N-terminal GST sequence was separated from the first codon of Mms2 and Ubc13 by intervening DNA that encoded the linker peptide, Leu-Glu-Val-Leu-Phe-Gln-Gly-Pro-Leu-Gly-Ser. The linker peptide contained the cleavage site for the PreScission Protease (Pharmacia) that cleaves between Gln and Gly. Cleavage results in the separation of GST from Mms2 or Ubc13, which contain Gly-Pro-Leu-Gly-Ser appended to the N-terminus of the first codon. The DNA sequences were derived from plasmid-borne cloned versions for Mms2 (*31*) and Ubc13 (*33*) respectively. The DNA sequences of the human *UBC13* and *MMS2* coding regions were verified by sequencing each recombinant plasmid.

Proteins were expressed in the *E. coli* strain BL21(DE3)-RIL (Stratagene) that contained extra copies of the argU, ileY, and leuW tRNA genes in addition to the pGEX6-derived plasmids as described above. 2L cultures were grown at

---

[2] Landon Pastushok and Wei Xiao, unpublished observation (2002).

37°C to OD_{590}= 0.3 in LB media containing ampicillin (50 $\mu g/ml$) followed by induction with isopropyl ß-D-thiogalactopyranoside (IPTG) (0.4mM) for 5 hours at 37°C. Cells were harvested by centrifugation, and stored at –80°C. All subsequent steps were performed at 4°C. *S. Cerevisiae* Ubc13 and Mms2 were produced in an identical manner to that described for the human forms. The Ubc13Lys^{92}Arg mutant was produced by substituting the Lys^{92} for Arg^{92} in human Ubc13 via site-directed mutagenesis.

Cell pellets were resuspended in 50 mL of disruption buffer (20 mM Tris/Cl pH 7.9, 10 mM $MgCl_2$, 1 mM EDTA, 5% glycerol, 1 mM DTT, 0.3 M ammonium sulfate, 1 mM PMSF), lysed by two passages through a French Press, followed by centrifugation (40,000 rpm for 45 minutes). The supernatant was dialyzed against 4 L of 1XPBS buffer (140 mM NaCl, 2.7 mM KCl, 10 mM Na_2HPO_4, 1.8 mM KH_2PO_4 pH 7.3) overnight at 4°C and clarified through a 0.45 μm low protein binding filter (Millipore). The filtered lysate was applied slowly to a 5 mL Glutathione Sepharose 4B RediPack column (Pharmacia) equilibrated with 50 mL of 1XPBS buffer. The column was washed three times with 30 mL of 1XPBS buffer, and the retained protein was eluted with three washes of 5 mL of Glutathione Elution buffer (10 mM reduced glutathione, 50 mM Tris/Cl pH 8.0). Glutathione was removed from protein samples by dialysis against 4 L of PreScission Cleavage Buffer (50 mM Tris/Cl pH 7.0, 150 mM NaCl, 1 mM EDTA, 1 mM DTT) for 4 hours followed by the addition of PreScission Protease (Pharmacia) (40 units). Fusion proteins were completely cleaved after a 16 hour incubation at 4°C. Following cleavage, the sample was reapplied to the Glutathione Sepharose 4B column and eluted as described above. In this case, cleaved Ubc13 and Mms2 proteins appeared in the 1XPBS flow-through, while the GST tag and the PreScission Protease (which is also fused to GST) remained bound to the column. The flow-through was concentrated to 2 mL using an Ultrafree Centrifugal Filter Device (Millipore- 10 kDa molecular mass cutoff) and applied to a Hi-Load 16/60 Superdex 75 column (Pharmacia) equilibrated with 200 mL of Superdex 75 buffer (50 mM HEPES pH 7.5, 75 mM

NaCl, 1 mM EDTA, 1 mM DTT). Proteins were eluted at a flow rate of 1 mL/min, and collected in 1 mL fractions. Both Ubc13 and Mms2 eluted between 69-80 mL and were judged to be pure by SDS-PAGE. Samples were subsequently pooled and concentrated.

2.3.2 Expression and purification of recombinant Ub

Wild-type Ub, UbLys^{48}Arg, and UbLys^{63}Arg were overexpressed and purified in an identical manner. The UbLys^{48}Arg mutant was produced by substituting the Lys^{48} for Arg^{48} in Ub via site-directed mutagenesis. A similar strategy was employed for the UbLys^{63}Arg construct. Proteins were expressed in the *E. coli* strain *BL21(DE$_3$)-RP* (Stratagene) on a PET3a overexpression plasmid. 1 L cultures were grown at 37 °C to OD$_{590}$= 0.4-0.5 in LB media containing ampicillin (50 μg/ml) followed by induction with IPTG (0.4mM) for 5 hours at 37°C. Cells were harvested by centrifugation, and stored at –80 °C. All subsequent steps were performed at 4 °C.

Cell pellets were resuspended in 50 mL of disruption buffer (20 mM Tris/Cl pH 7.9, 10 mM MgCl$_2$, 1 mM EDTA, 5% glycerol, 1 mM DTT, 0.3 M ammonium sulfate, 1 mM PMSF), lysed by two passages through a French Press, followed by centrifugation (40,000 rpm for 45 minutes). The supernatant was dialyzed against 4 L of in Q-Sepharose A buffer (50 mM Tris pH 7.5, 1 mM EDTA, 1 mM DTT) overnight at 4°C and clarified through a 0.45 μm low protein binding filter (Millipore). The filtered lysate was applied to a Hi-Load Q-Sepharose ion exchange column (Pharmacia) equilibrated with Q-Sepharose A buffer. Ub does not bind the Q-Sepharose column, and elutes in the flow-through. The flow-through was concentrated to 2 mL using an Ultrafree Centrifugal Filter Device (Millipore- 5 kDa molecular mass cutoff) and applied to a Hi-Load 16/60 Superdex 75 column (Pharmacia) equilibrated with 200 mL of Superdex 75 buffer (50 mM HEPES pH 7.5, 75 mM NaCl, 1 mM EDTA, 1 mM DTT). Proteins were eluted at a flow rate of 1mL/min, and collected in 1mL fractions. Ub eluted between 87-102 mL and was judged to be pure by SDS-PAGE. Samples were

subsequently pooled and concentrated.

[35]S-labeled Ub (*Ub) was purified in a similar manner (34). It should be noted that in some of the *Ub preparations, radiolabeled contaminant bands exist, and are denoted in appropriate figure legends.

2.3.3 Expression and purification of S. cerevisiae E2 enzymes

S. cerevisiae E2s and their derivatives (Cdc34, cdc34$_{\Delta244}$, cdc34$_{\Delta209}$, Ubc1Δ, and Rad6Δ) were expressed and purified as described extensively in section 7.3.

2.3.4 Expression and purification of S. cerevisiae Uba1

S. cerevisiae E1 (Uba1) was contained on the pJD325 plasmid as a His$_6$-fusion protein, and was provided by Daniel Finley (Harvard Medical School). MHY501 yeast cells containing the aforementioned plasmid were grown in 4-8 L of SD media (Leu$^-$) to an OD$_{600}$= 0.1-0.2 at 30 °C. CuSO$_4$ was subsequently added to the media to a final concentration of 0.1 mM, and the cells were allowed to grow overnight. Cells were then harvested by centrifugation, washed, and then subsequently resuspended in disruption buffer (20 mM Tris/Cl pH 7.9, 10 mM MgCl$_2$, 1 mM EDTA, 5% glycerol, 1 mM DTT, 0.3 M ammonium sulfate, 1 mM PMSF), lysed by glass bead vortexing and sonication, followed by centrifugation (40,000 rpm for 45 minutes). The supernatant was dialyzed against 4 L of in Q-Sepharose A buffer (50 mM Tris pH 7.5, 1 mM EDTA, 1 mM DTT) overnight at 4° C.

The lysate was applied slowly to a 5 mL Hitrap Q-Sepharose HP anion exchange column (Pharmacia) equilibrated with Q-Sepharose A buffer. The protein was eluted with an NaCl gradient from 0-2 M using Q-Sepharose B buffer (50 mM Tris pH 7.5, 2M NaCl, 1 mM EDTA, 1 mM DTT). The His$_6$-fusion eluted at approximately 250-300 mM NaCl, as confirmed by SDS-PAGE, and appropriate fractions were pooled. The pooled fractions were subsequently applied to a 5 mL HiTrap chelating column (Pharmacia) charged with NiSO$_4$ and

equilibrated with His loading buffer (10 mM imidazole in 1XPBS). The bound protein was washed with 5 column volumes of His loading buffer, and eluted with 10 mL of His elution buffer (500 mM imidazole in 1XPBS). The eluate was concentrated to 2 mL using an Ultrafree Centrifugal Filter Device (Millipore- 10 kDa molecular mass cutoff) and applied to a Hi-Load 16/60 Superdex 75 column (Pharmacia) equilibrated with 200 mL of Superdex 75 buffer (50 mM HEPES pH 7.5, 75 mM NaCl, 1 mM EDTA, 1 mM DTT). Proteins were eluted at a flow rate of 1 mL/min, and collected in 1 mL fractions. Uba1 eluted at the column void volume (approximately 35 mL) and was judged to be pure by SDS-PAGE. Samples were subsequently pooled and concentrated.

Uba1 concentration was assayed using a standard Ub-activating activity assay which measures the ability of the enzyme to bind to and activate Ub moieties. A reaction containing a known volume of Uba1 and a known amount of ^{35}S-[Ub] in a 500 μL reaction containing Buffer C (10 mM HEPES pH 7.5, 5 mM MgCl$_2$, 5 mM ATP) was incubated at 30 °C for one hour. The reaction was then applied to a HR 10/30 Superdex 75 gel filtration column (Pharmacia) equilibrated with Superdex 75 buffer lacking DTT. The incorporation of radioactivity into the Uba1~(Ub)$_2$ peak was employed to determine the concentration of Uba1.

2.3.5 Heterodimer purification

The Ubc13/Mms2 heterodimer was purified from its monomer components by mixing Ubc13 and Mms2 (500 μL each at 1 mg/mL) at 25 °C, followed by Hi-Load 16/60 Superdex 75 column chromatography as described above. The heterodimer eluted between 61-70 mL.

2.3.6 Thiolester purification

The Ubc13~[^{35}S]-Ub (Ubc13~*Ub) thiolester was formed as follows. A reaction (0.5 mL) containing E1 (200 nM), *Ub (4 μM), and Ubc13 (4 μM) in Buffer C (10 mM HEPES pH 7.5, 5 mM MgCl$_2$, 5 mM ATP), supplemented with the protease inhibitors and an ATP regeneration system (34), was incubated at

30° C for 30 minutes. The thiolester was then purified by size exclusion chromatography using a Superdex 75 HR 10/30 column, as described above. Peak fractions corresponding to Ubc13~*Ub were assayed for concentration based on the specific activity of ^{35}S-[Ub] contained within the thiolester.

2.3.7 Thiolester assays

All thiolester reactions were carried out in buffer C as described above. E1 and *Ub were incubated at 30 °C for 30 minutes with either Ubc13, Mms2 or the Ubc13/Mms2 heterodimer (500 μL- final). The concentration of each component is noted in the appropriate figure legend. DTT (10 mM) was added to one half of the reaction and the components of the treated and untreated samples were separated by Superdex 75 chromatography and analyzed as described above (HR 10/30 column at 0.5 mL/min).

Kinetic measurements of thiolester formation were performed at 30 °C by removing aliquots (0.5 mL) at designated times from a mother liquor. Upon removal, aliquots were immediately quenched with EDTA (10 mM). The components of each aliquot were then separated by gel exclusion chromatography (Superdex 75 HR 10/30 column at 0.5 mL/min). Concentrations were determined from the specific activity of radio-labeled Ub contained in each fraction (0.5 mL).

2.3.8 Conjugation reactions

All Ub conjugation reactions (0.5 mL) were performed at 30° C for 4-5 hours in buffer C. The concentration of each component is noted in the figure legends. Reactions were terminated by the addition of trichloroacetic acid (TCA) (10%- final) and processed for SDS-PAGE (18%) and autoradiography as previously described (37).

2.3.9 NMR spectroscopy

All of the NMR spectra were obtained using a Varian Unity INOVA 500 MHz spectrometer at 30° C. The 2D ^1H-^{15}N-HSQC NMR spectra were acquired using the sensitivity-enhanced gradient pulse scheme developed by Lewis E. Kay and co-workers (35, 36). The ^1H and ^{15}N sweep widths were 6000 and 1550 Hz, respectively. Spectral processing and analyses were accomplished with the programs NMRPipe (37) and PIPP (38) respectively.

All NMR samples were prepared to a final volume of 500 μL, and contained HEPES (50 mM, pH 7.5), NaCl (75 mM), EDTA (1 mM), and DSS (1 mM) in the presence of 9:1 H_2O:D_2O. In each sample ^{15}N-UbLys^{48}Arg (300 μM) was employed as the NMR-detectable species. Purification of this species is described elsewhere (19). These reaction conditions represent those employed for obtaining the ^1H-^{15}N HSQC NMR spectrum for UbLys^{48}Arg alone. The NMR resonance assignments for UbLys^{48}Arg at pH 7.5 have been described previously (19).

Non-covalent interactions between ^{15}N-UbLys^{48}Arg and Ubc13 were detected by including Ubc13 (310 μM) in addition to reagents mentioned above. Similarly, non-covalent interactions between ^{15}N-UbLys^{48}Arg and Mms2 were detected by inclusion of Mms2 (310 μM). Non-covalent interactions between ^{15}N-UbLys^{48}Arg and the Ubc13/Mms2 heterodimer were detected by adding both Ubc13 and Mms2 (310 μM) to the NMR sample.

Interactions between ^{15}N-UbLys^{48}Arg and Ubc13 in the Ubc13~^{15}N-UbLys^{48}Arg thiolester were determined by including Ubc13 (310 μM), ATP (5 mM), MgCl$_2$ (5 mM), and E1 (1 μM) to the NMR sample. Covalent interactions between ^{15}N-UbLys^{48}Arg and the Ubc13/Mms2 heterodimer within the Mms2/Ubc13~^{15}N-UbLys^{48}Arg thiolester were delineated by inclusion of Ubc13 (310 μM), MMS2 (310 μM), ATP (5 mM), MgCl$_2$ (5 mM), and E1 (1 μM) into the NMR sample. Prior to the commencement of NMR analysis, a time course was performed to determine the kinetics of thiolester relative to conjugate formation (data not shown). We determined that thiolester formation is rapid (minutes)

whereas the formation of conjugate is slow (hours). Furthermore, the onset of conjugate formation can be clearly identified based on the accumulation of new peaks emanating from the mixed population of Ub species. The ^{1}H-^{15}N HSQC NMR experiments were therefore performed between 10 and 120 minutes after the addition of E1 in order to minimize the impact of possible side-reactions.

2.4 RESULTS

2.4.1 Human Ubc13 and Mms2 form a heterodimer

Our initial goal was to overexpress and purify human Ubc13 and Mms2 in high yield for the purposes of mechanistic and structural investigations. GST derivatives of Ubc13 and Mms2 were constructed and overexpressed in *E. coli*. Following elution from a glutathione column, the GST tag was proteolytically cleaved from both Ubc13 and Mms2, leaving 5 additional amino acids at each N-terminus. The GST component of each cleaved mixture was removed by a second glutathione column step followed by size exclusion chromatography. Both Ubc13 and Mms2 eluted as a single peak at an approximate molecular mass of 18 kDa (Fig. 2.1B). SDS-PAGE of these peaks revealed that Ubc13 and Mms2 had been purified to virtual homogeneity (Fig. 2.1A). Mms2 appeared to migrate at a slightly larger molecular mass than expected, although the calculated molecular weight of Mms2 used in this study (16.8 kDa) is less than that of Ubc13 (17.6 kDa). A faint high molecular mass band was also observed, mainly associated with Mms2, which we attributed to aggregation based on the fact that no corresponding higher molecular mass species eluted from the size exclusion column.

S. cerevisiae Ubc13 and Mms2 have been previously shown to form a heterodimer using partially purified proteins (27) or in yeast two-hybrid and coimmunoprecipitation assays (30, 31). To determine whether the purified human counterparts interact, equimolar amounts of Ubc13 and Mms2 were combined and fractionated by size-exclusion chromatography. The combined monomers were found to elute as a single peak of 40 kDa, which corresponded
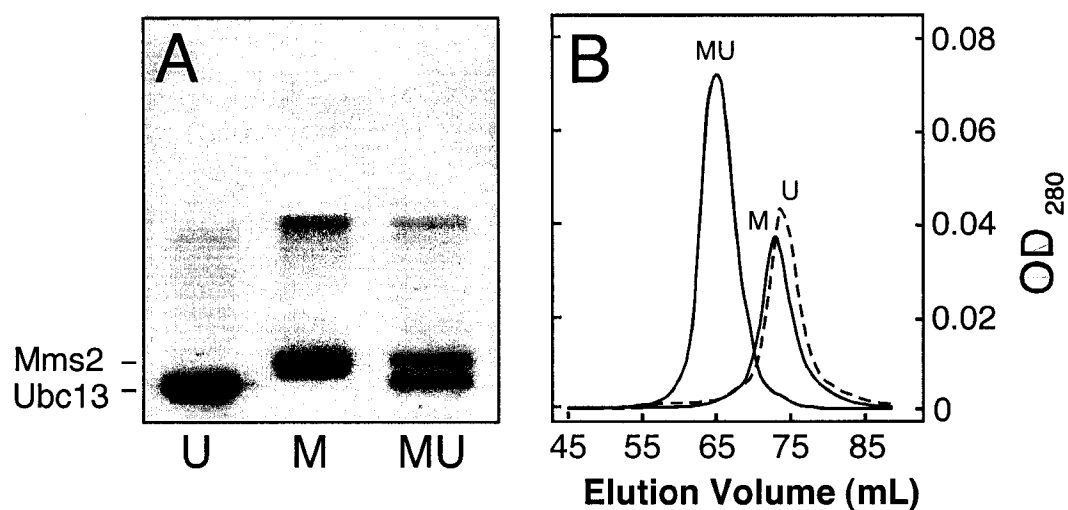
Figure 2.1 Human Ubc13 and Mms2 form a stable heterodimer. (A) Coomassie blue stained 18% SDS-PAGE demonstrating purified Ubc13 (U) (10 μg), Mms2 (M) (10 μg), and the Ubc13/Mms2 heterodimer (MU) (20 μg) from (B). (B) Size exclusion column elution profiles of purified Ubc13 (U, solid line), Mms2 (M, dashed line), and the Ubc13/Mms2 heterodimer (MU, solid line). In each case, 500 μg of Ubc13, Mms2, or both were employed.

approximately to the expected molecular mass of a heterodimer consisting of one molecule of each of Ubc13 and Mms2 (Fig. 2.1B). The absence of peaks of similar mass from control samples containing either Ubc13 or Mms2 alone eliminated the possibility of homodimer formation (data not shown). The 1:1 stoichiometry of the heterodimer was confirmed by quantifying the Ubc13 and Mms2 bands following separation by SDS-PAGE (Fig. 2.1A). The heterodimer was completely stable over a range of NaCl concentration (up to 1 M) suggesting a strong hydrophobic interaction between monomers (data not shown). Ubc13 was able to heterodimerize with both human Uev1a and yeast Mms2 (Fig. 2.2A). However, Mms2 failed to form heterodimers with other E2s from *S. cerevisiae* including Cdc34 derivatives, Rad6Δ, and Ubc1Δ (Fig. 2.2B). Thus, the interaction between human Ubc13 and Uevs appears to be highly specific.

2.4.2 Ub Thiolester Formation

In the absence of a reducing agent, a reaction containing E1, E2 and radio-labeled Ub results in the formation of an E2~Ub thiolester that can be separated by size exclusion chromatography and detected by autoradiography. The chromatographic profile of these reactions typically reveals three peaks that correspond to free Ub, the E2~Ub thiolester and the E1~Ub$_2$ thiolester. When Ubc13 was used in the thiolester reaction, three peaks were observed corresponding to E1~Ub$_2$ (120 kDa), E2~Ub (28 kDa), and free Ub (9 kDa) (Fig. 2.3A). The disappearance of the Ubc13~Ub peak upon DTT treatment coupled with an increase in the free Ub peak is consistent with the lability of the thiolester bond in the presence of reducing agents (data not shown). By comparison, Mms2 was found to be unreactive with respect to E2~Ub formation under identical conditions (Fig. 2.3A). This result was expected as Mms2 lacks the canonical active-site Cys required for thiolester formation (*31*).

Ubc13 can also exist as a Ub thiolester in the heterodimeric form with Mms2. The thiolated heterodimer can either be produced by combining purified Ubc13 thiolester with Mms2 (Fig. 2.3B), or by thiolating the heterodimer directly

A

hUbc13	+ hMms2	**+**
	+ yMms2	**+**
	+ Uev1a	**+**
	+Croc-1B	**-**

B

hMms2	+ hUbc13	**+**
	+ yUbc13	**+**
	+ Cdc34	**-**
	+ cdc34$_{\Delta244}$	**-**
	+ cdc34$_{\Delta209}$	**-**
	+ Ubc1Δ	**-**
	+ Rad6Δ	**-**

Figure 2.2 The interaction between Ubc13 and the Uevs is specific. In all cases (+) denotes an observable interaction, whereas (-) denotes no heterodimerization observed. No homodimerization of any components was observed. (A) Interactions between hUbc13 and the Uevs. Equimolar mixtures of hUbc13 and each of the Uev proteins listed were mixed and loaded onto a Hi-Load Superdex 75 column size exclusion column in order to determine whether heterodimerization was occurring. (B) Interactions between hMms2 and other E2 enzymes. Identical protocol as described for (A) was employed. All truncations (i.e. cdc34$_{\Delta209}$) refer to C-terminal truncations (see experimental procedures).
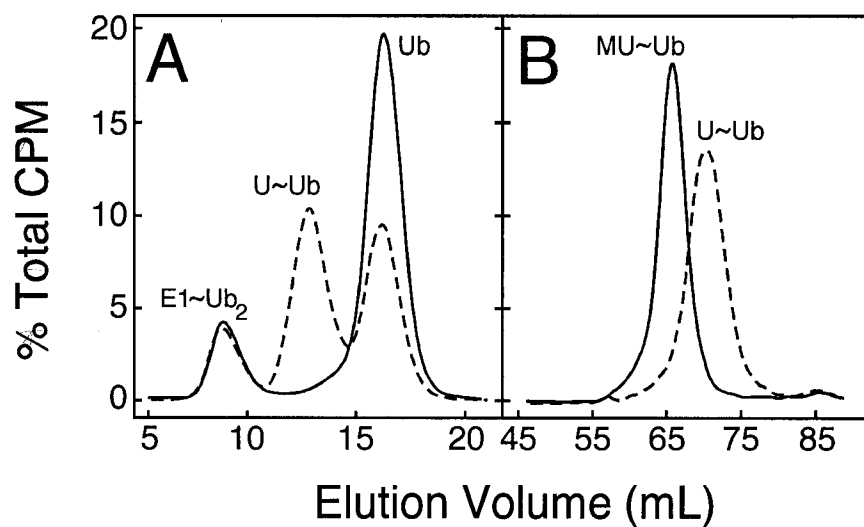
Figure 2.3 Ubc13, not Mms2, supports Ub thiolester formation. All reactions contain *Ub as the detectable species. (A) Size exclusion column profiles of a 500 μL reaction containing E1 (100 nM), *Ub (1 μM), and either Ubc13 (1 μM, dashed line) or Mms2 (1 μM, solid line) in Buffer C was reacted at 30° C for 30 minutes and loaded onto a Superdex 75 HR10/30 column. Peaks are labeled E1~Ub$_2$ (E1 thioletser), U~Ub (Ubc13~Ub thiolester), and Ub (free Ub). (B) An 800 μL mixture containing either purified Ubc13~*Ub (0.5 μM) alone (dashed line), or Ubc13~*Ub (0.5 μM) and Mms2 (2.5 μM) (solid line) was reacted at 30° C for 30 minutes prior to loading onto a Hi-Load Superdex 75 column. Peaks are labeled either MU~Ub (Mms2/Ubc13~Ub) or U~Ub (Ubc13~Ub).

(data not shown). Therefore, the heterodimer and thiolester are structurally compatible.

The elution properties (Fig. 2.3B) of the heterodimer and heterodimer thiolester are uncharacteristic of a simple molecular mass relationship. First, the apparent molecular mass of the heterodimer is slightly larger than its actual mass (40kDa compared to 35kDa). Second, the addition of Ub to the heterodimer upon thiolation increases its apparent mass by only 4 kDa, less than one half the molecular mass of Ub.

The rate of Ubc13~Ub thiolester formation differs in the presence or absence of Mms2, as Mms2 inhibits the rate of thiolester formation approximately two-fold (Fig. 2.4A,B). Furthermore, in the presence of Mms2 only the heterodimeric form of the Ubc13~Ub thiolester is observed. These results indicate that: i) Ubc13 in the heterodimeric form is less reactive to thiolester formation than the monomeric form, and that ii) heterodimer formation may well precede thiolester formation. Interestingly, the Ubc13~Ub component of the heterodimer is less labile than the monomeric form of Ubc13~Ub based on the relative release of free Ub with respect to time (Fig. 2.4C).

2.4.3 The heterodimer conjugates Ub molecules via Lys^{63}

A previous study has shown that yeast Ubc13/Mms2 catalyzes the linkage of Ub molecules via Lys^{63} (27). We tested the conjugation characteristics of the human heterodimer in reactions that contained E1, *Ub, and combinations of Ubc13 and Mms2. The radiolabeled products were then separated by SDS-PAGE (Fig. 2.5A). A reaction containing both Ubc13 and Mms2 resulted in the formation of di- and tri-ubiquitin (Ub_2 and Ub_3, respectively) which were absent in either the Ubc13 or Mms2 alone reactions. The use of either wild-type Ub or UbLys^{48}Arg in these reactions resulted in similar yields of free Ub chains, which eliminated the possibility that the Ub moieties of the dimer were linked through Lys^{48}.
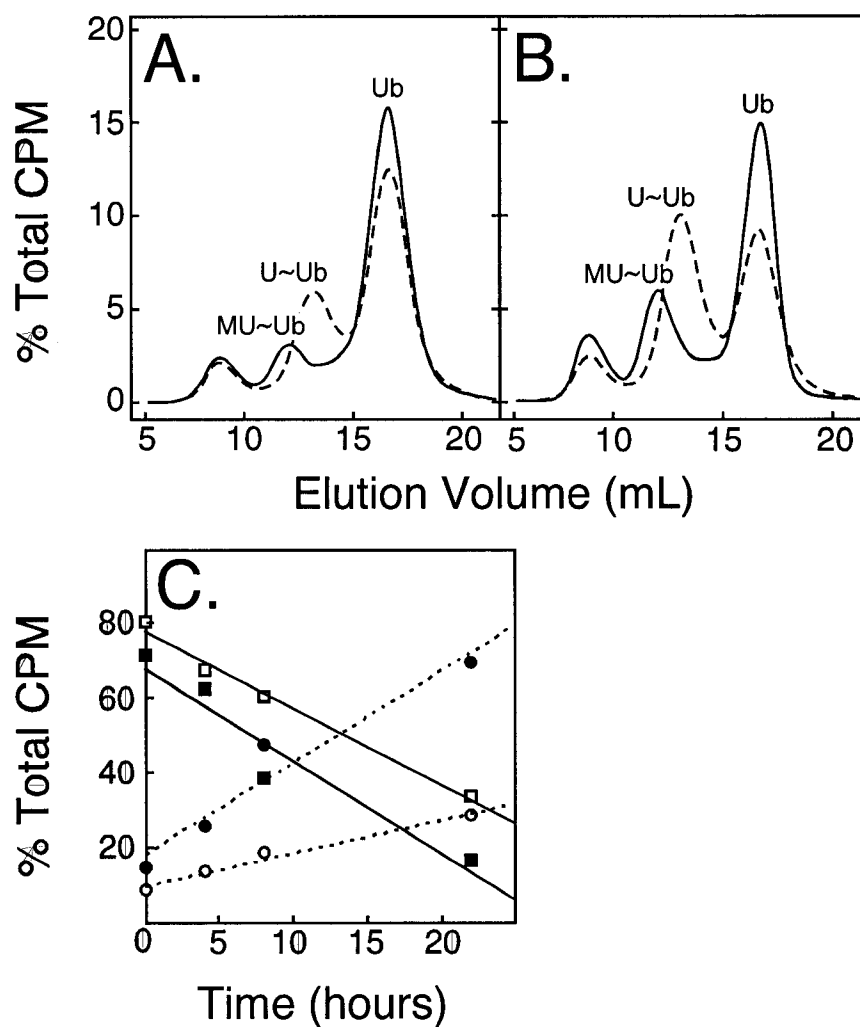
Figure 2.4 Mms2 impedes thiolester formation, while increasing its stability. Several identical reactions (500 μL), each containing E1 (100 nM), *Ub (2 μM), and either Ubc13 (1 μM, dashed line) or both Ubc13 (1 μM) and Mms2 (1 μM) (solid line) were incubated at 30°C for (A) 10, or (B) 20 minutes. Reactions were quenched by the addition of 10 mM EDTA prior to loading onto a Superdex 75 HR10/30 column. Peaks are labeled as in Figure 2.3. (C) Ubc13~Ub thiolester stability. Ubc13~*Ub (500 nM) was purified and incubated at 30°C in the presence (open symbols) or absence (closed symbols) of Mms2 (500 nM). Aliquots were removed, and fractionated by size exclusion chromatography in order to identify species containing radiolabeled Ub. The amount of thiolester product (solid lines) and free Ub (dashed lines) are shown. Lines represent regression analysis of duplicate experiments, and have assumed linear kinetics. Ubc13-Ub conjugate formation has been omitted for clarity.
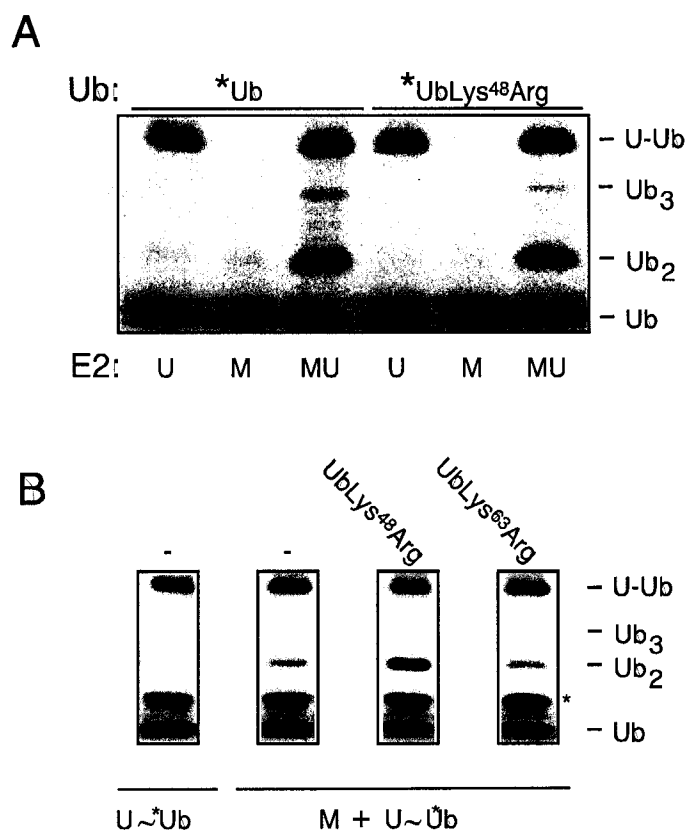
Figure 2.5 The Ubc13/Mms2 heterodimer synthesizes free Ub chains. *In vitro* ubiquitination reactions were performed using *Ub in combination with 18% SDS-PAGE and autoradiography. All reactions were precipitated with TCA and solubilized in SDS-PAGE load buffer. Contaminants present in some of the *Ub preparations are denoted (*). (A) Either Ubc13 (U, 250 nM), Mms2 (M, 250 nM), or both were included in reactions (500 μL total volume) containing E1 (25 nM) and either wild-type Ub (1.25 μM) or UbLys^{48}Arg (1.25 μM). reactions proceeded for 5 hr at 30°C. Prominent bands include U-Ub (Ub conjugated onto Ubc13), Ub$_2$, Ub$_3$, and free Ub. (B) A reaction containing purified Ubc13~*Ub (250 nM), Mms2 (250 nM), and either (i) no free Ub, (ii) free unlabeled UbLys^{48}Arg (2 μM), or (iii) free unlabeled UbLys^{63}Arg (2 μM) was reacted for 4 hours at 30° C.

The formation of Ub and longer chains by the heterodimer could occur by one of two mechanisms. Two heterodimer thiolester molecules could, for example, interact such that one donates its Ub to the other. Alternatively, the thiolester could target free Ub (*i.e.* not covalently attached to either Ubc13 or Mms2). To distinguish between these two possibilities, the following experiment was performed. Purified Ubc13~*Ub thiolester was incubated in the presence or absence of unlabeled free UbLys^{48}Arg, and the formation of Ub$_2$ was initiated by the addition of Mms2. As seen in Fig. 2.5B, the yield of Ub$_2$ increases significantly when UbLys^{48}Arg is added to the reaction. Thus free Ub is the preferred substrate for Ub$_2$ formation. We attribute the presence of trace amounts of Ub$_2$ lacking an obvious source of free Ub to the Ub that arises from thiolester hydrolysis during the time interval following thiolester purification and prior to the addition of Mms2 (Fig. 2.5B). Notably, the level of Ub$_2$ in a reaction in which UbLys^{63}Arg is employed as the source of free Ub is comparable to the control reaction in which free Ub has been omitted. Together, these results illustrate that Ub$_2$ is formed specifically by the transfer of Ub from the thiolester to Lys^{63} of a free molecule of Ub.

2.4.4 Human Ubc13 autoubiquitinates itself in vitro

Given that the reactions were treated with reducing agent (DTT) prior to loading onto the gel, the presence of a 26 kDa conjugate species that was unique to the Ubc13 reactions indicated that Ubc13 undergoes autoubiquitination. Human Ubc13 contains two potential sites for autoubiquitination at Lys^{92} and Lys^{94} which, based on preliminary structural determinations, are in reasonable proximity to the active-site. Lys^{92} was identified as the site of Ub conjugation, as its mutation to Arg completely eliminated conjugate formation, while not significantly affecting the amount of free-chains produced (Fig. 2.6A).

A

B
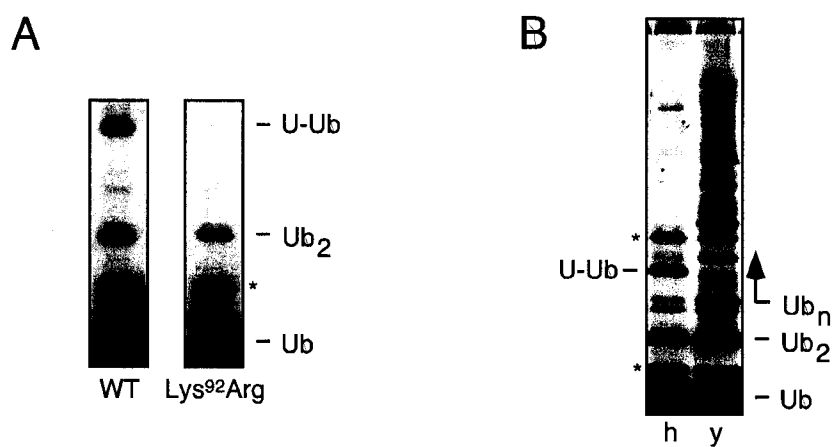
Figure 2.6 Interesting aspects of Ubc13's chain building function. (A) Human Ubc13 autoubiquitnates itself on Lys^{92}. Either wild-type (WT) or Ubc13Lys^{92}Arg (250 nM) was included in reactions containing E1 (25 nM), *Ub (1 μM) and Mms2 (250 nM). Reactions proceeded for 4 hr at 30° C. (B) Differences between the human and yeast Ubc13 proteins. Either human (h) or *S. cerevisiae* (y) Ubc13 (200 nM) and hMms2 (200 nM) were included in reactions containing E1 (15 nM), and *Ub (2 μM). Reactions proceeded for 5 hr at 30° C.

2.4.5 Human and S. cerevisiae Ubc13/Mms2 complexes possess different in vitro activities.

Previous studies have demonstrated that the *S. cerevisiae* Ubc13/Mms2 complex appears to be more effective (*27*) at producing longer chains when compared to the human counterparts in the absence of any other activator proteins (*29*). Upon direct comparison of the *in vitro* activities of both human and *S. cerevisiae* complexes, it is clear that the *S. cerevisiae* complex does in fact synthesize much longer chains when compared to the human proteins (Fig. 2.6B). Furthermore, we can report that the formation of the Ubc13 conjugate is only observed with the human, and not the yeast protein.

2.4.6 NMR-derived footprints of the Ub contact surface

By comparing the assigned two-dimensional ^{1}H-^{15}N-HSQC NMR spectra of ^{15}N-UbLys^{48}Arg alone or in combination with unlabeled Ubc13 and/or Mms2, we have been able to map the interacting surface of Ub in i) a non-covalent complex with Mms2, ii) a non-covalent complex with the Mms2/Ubc13 heterodimer, iii) as a thiolester with Ubc13, and iv) as a thiolester with the heterodimer.

The relative decrease in cross-peak intensities in the ^{1}H-^{15}N HSQC NMR spectrum that occur upon complex formation were determined for each amino acid residue in ^{15}N-UbLys^{48}Arg. Normally, cross-peak intensity decreases in proportion to the size of the protein or protein-protein complex due to peak broadening as a result of increased rotational tumbling time. A decrease in peak intensity beyond this effect likely reflects changes in chemical environment that occur due to protein-protein interactions (*39*).

^{1}H-^{15}N-HSQC NMR spectroscopy was used to determine if Ub associates with Ubc13 and/or Mms2 in a non-covalent fashion; that is in the absence of E1 and ATP/Mg^{2+}. The ^{1}H-^{15}N-HSQC NMR spectrum of ^{15}N-UbLys^{48}Arg alone is indistinguishable from the spectrum acquired in the presence of Ubc13. This observation indicates the lack of an interaction between Ub and Ubc13 at a
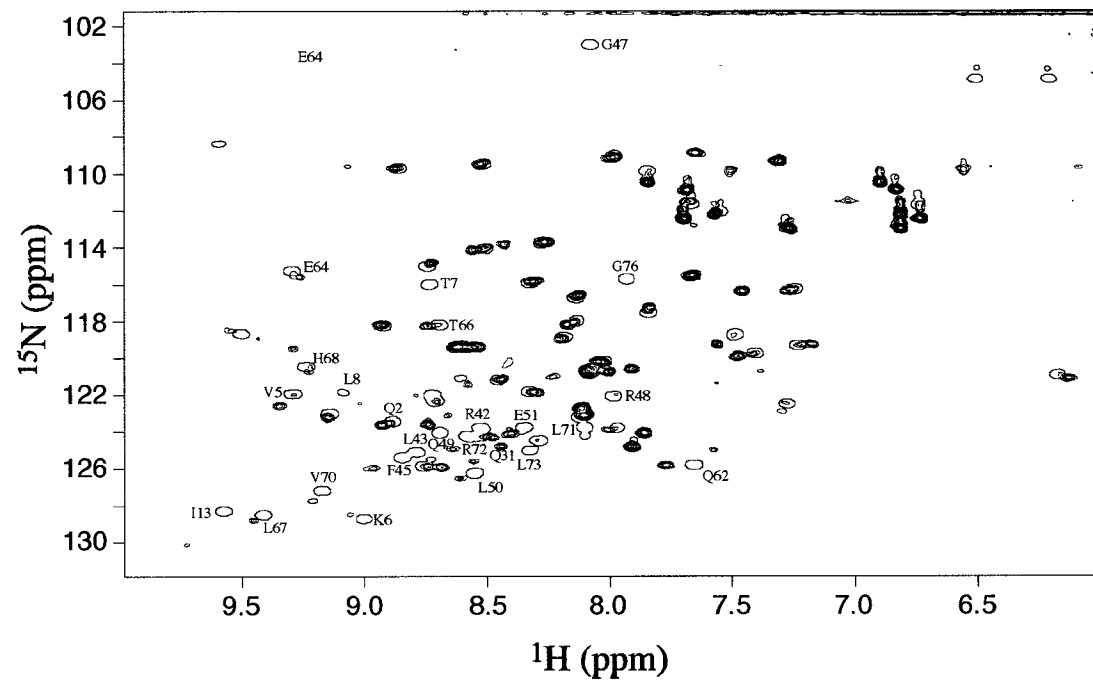
Figure 2.7 Superposition of ^{1}H-^{15}N HSQC NMR spectra of ^{15}N-labeled Ub, free and in complex with Ubc13. 500 μL NMR samples including either ^{15}N-UbLys^{48}Arg (300 nM, blue), or ^{15}N-UbLys^{48}Arg (300 μM), E1 (1 μM), and Ubc13 (310 μM) (green, 20 contours). Samples were studied at 30° C, pH 7.5, and included 1% DSS and a mixture of 9:1 H$_2$O:D$_2$O. Only selected backbone amide resonances which were affected by complex formation are labeled.

concentration 300 μM (data not shown). In the presence of either Mms2 or the Mms2/Ubc13 heterodimer, the ^{1}H-^{15}N-HSQC NMR spectrum of ^{15}N-UbLys^{48}Arg undergoes two types of changes (Fig. 2.7). First, a global reduction in peak intensities is observed when compared with ^{15}N-UbLys^{48}Arg alone. A 57% average reduction in peak intensity is observed in the presence of Mms2, and a 70% average reduction in peak intensity is observed in the presence of the heterodimer. Each of these results appears reasonable based on the predicted increase in molecular mass of the non-covalent protein complexes. Second, a marked decrease of peak intensity was observed over and above these average decreases that correspond to specific residues that cluster to one face of Ub (Fig. 2.8). It can be concluded from these findings that Ub interacts with Mms2 and the Mms2/Ubc13 heterodimer through non-covalent contacts, and that a similar contact surface is used by Ub in each case.

The interactions of ^{15}N-UbLys^{48}Arg with the Ubc13 thiolester or within the heterodimeric thiolester complex were also examined using ^{1}H-^{15}N-HSQC NMR spectroscopy. The incorporation of ^{15}N-UbLys^{48}Arg into each of the two thiolester forms resulted in an average reduction of ^{1}H-^{15}N-HSQC NMR cross-peak intensity (relative to ^{15}N-UbLys^{48}Arg alone) of 88% for Ubc13~Ub and 91% in the case of the heterodimer thiolester. Upon comparison of the two thiolester forms, residues corresponding to the largest reductions in cross-peak intensity are clustered on similar surfaces of Ub (Fig. 2.8). The most notable difference exhibited by the thiolester-linked forms of Ub, when compared to the unlinked, is that the C-terminal tail makes extensive contacts in the former but not in the latter. Excluding the C-terminal tail as well as obvious differences in detail, Ub utilizes an analogous contact surface in both the thiolester and untethered complexes described above.

2.5 DISCUSSION

The present work illustrates that like its yeast counterpart, the human form of the Mms2/Ubc13 heterodimer links Ub molecules together via Lys^{63}. This work
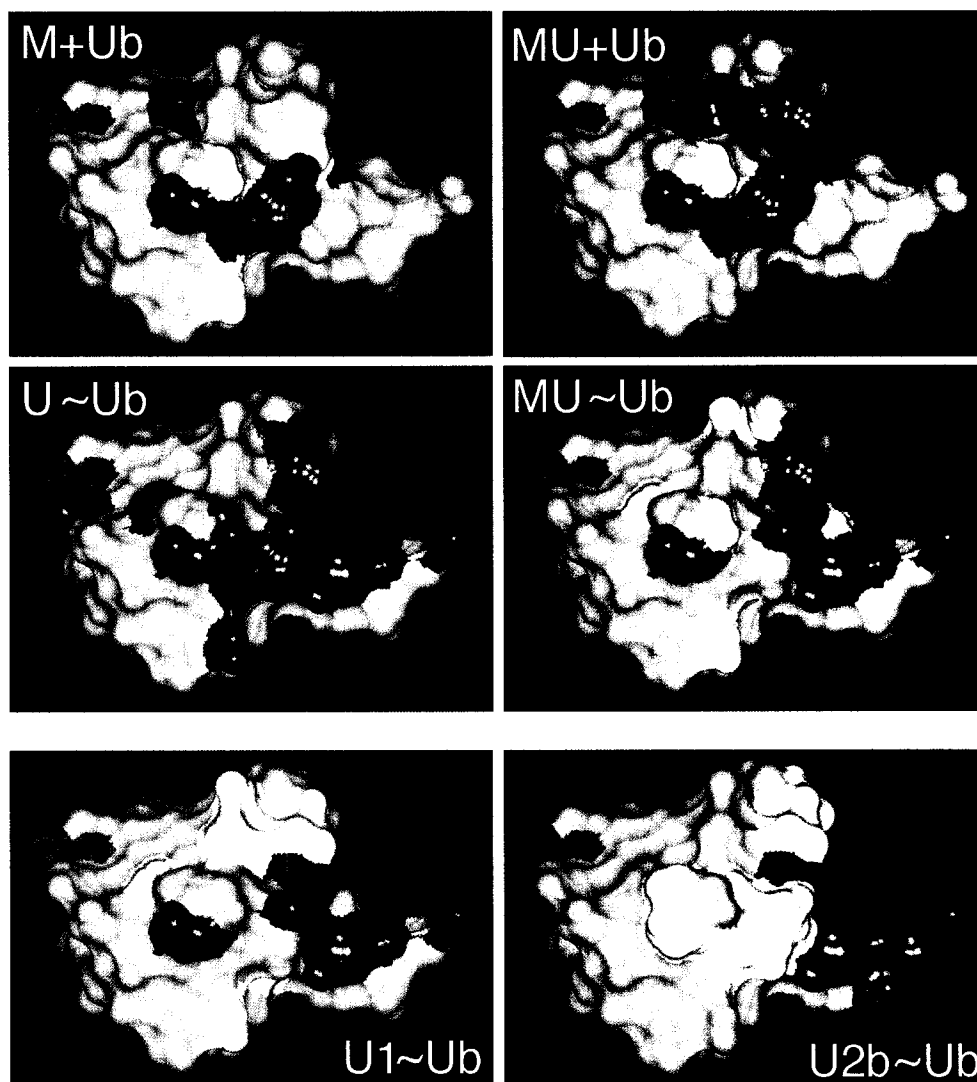
Figure 2.8 Connolly surface of the binding interfaces on Ub. The surface of Ub is presented, and residues whose HSQC NMR peak height intensities are affected by complex formation moderately (yellow, corresponding to $\geq 20\%$ reduction when compared to average decreases in peak height intensity upon complex formation) and more significantly (red, corresponding to a disappearance of intensity beyond detection limits) are colored. Lys[63] is colored in green as a point of reference. (M+Ub) Non-covalent interaction between Ub and Mms2. (MU+Ub) Non-covalent interaction between Ub and the Ubc13/Mms2 heterodimer. (U~Ub) Interactions between Ub and Ubc13 in the Ubc13~Ub thiolester. (MU~Ub) Interactions between Ub and the Ubc13/Mms2 heterodimer within the Mms2/Ubc13~Ub thiolester. (U1~Ub) Interactions between Ub and yeast Ubc1 within the Ubc1~Ub thiolester (19). (U2b~Ub) Interactions between Ub and human Ubc2b within the hUbc2b~Ub thiolester (18).

also extends previous studies on these proteins (27) with a more comprehensive understanding of how their structures relate to their functions.

The human heterodimer is formed rapidly and quantitatively by combining Mms2 and Ubc13. Furthermore the association of these subunits is significant (K_D ~ 50 nM, see Chapter 5), and stable over a wide range of salt concentration. The Ub thiolester form of the heterodimer can be created in either of two ways: 1) by direct activation of the Ubc13 subunit by E1, or 2) by assembly of the heterodimer from Mms2 and Ubc13~Ub thiolester. The rate of dimer assembly *in vitro* exceeds the rate of thiolester formation. Thus, the first pathway may be the preferred route of thiolester formation *in vivo*.

While the Ubc13 component of the heterodimer is less reactive to activation than its monomeric counterpart, it is more stable with respect to hydrolysis. One explanation for these observations is that the active-site Cys and the C-terminus of Ub become less accessible to E1 and solvent when incorporated into the heterodimer.

The human and *S. cerevisiae* Ubc13/Mms2 complexes demonstrate markedly different *in vitro* activities with respect to both chain formation and autoubiquitination. Lys[92] of human Ubc13 becomes autoubiquitinated, a phenomenon that occurs with other Ub-conjugating enzymes, namely *S. cerevisiae* Ubc1, which undergoes conjugate formation on an analogous Lys at position 93 (40). In contrast, no conjugate formation was observed upon yeast Ubc13, but chains of significantly greater length were formed in the presence of Mms2. Recent reports have also indicated that murine Ubc13, which shares high sequence identity with the human protein, acts in a manner analogous to the human protein (41).

The Ub conjugation studies taken together with the results of the NMR spectroscopy experiments are consistent with a mechanistic model that can account for the linkage between Ub molecules via Lys[63] (Fig. 2.9). The model portrays one Ub molecule linked to the active-site Cys of the Ubc13 subunit making non-covalent contacts primarily with Ubc13. The other Ub molecule is not
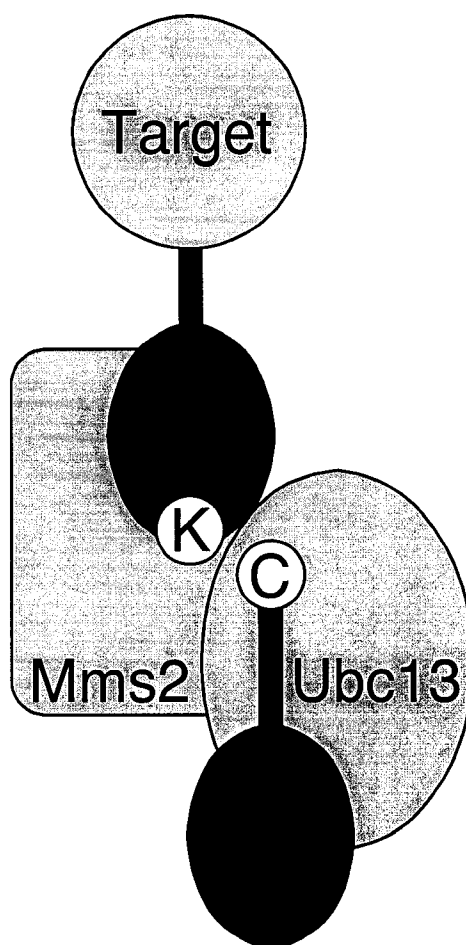
Figure 2.9 Model of Ubc13/Mms2 catalyzed ubiquitination of target substrates. Heterodimer formation between Ubc13 and Mms2 proceeds rapidly, followed by the formation of thiolester between the active-site Cys of Ubc13 and the C-terminal tail of Ub (C). Mms2 may serve to correctly position a second Ub, via a non-covalent binding site, such that the transfer of thiolester linked Ub to Lys[63] (K) of the second may proceed. Target substrates may be bound to the non-covalently bound Ub, or alternatively may become ubiquitinated via a downstream mechanism.

covalently tethered but makes its principal non-covalent contacts with the Mms2 subunit. The variation in the Ub contact surfaces that are observed when either the Mms2 or Ubc13 monomers assume their heterodimeric forms may reflect adjustments of Ub on the E2 surface and/or additional contacts that are formed with the second protein. The Ub molecule bound to Mms2 is oriented such that Lys[63] is close to the active site of Ubc13, thereby facilitating linkage with the C-terminus of the thiolester linked Ub molecule of Ubc13. Unlike the Ubc13-bound Ub molecule, the C-terminal region of the Mms2-bound Ub molecule is not sequestered. From the model presented herein, we speculate that the C-terminal region of Mms2-bound Ub is sterically free, thereby allowing for coupling to a suitable target without interference from heterodimer. This raises the possibility that subsequent Ub molecules are added to the Ub molecule of a mono-ubiquitinated substrate.

Recently, the high-resolution X-ray crystal structures of both the human (*42*) and *S. cerevisiae* (*43*) Ubc13/Mms2 heterodimer have been solved, and both structures propose models that could accommodate the active-site tethered and non-covalently bound Ub molecules. In combination with the data presented, these structures establish a foundation for the assembly of Lys[63] chains by the Ubc13/Mms2 heterodimer. Furthermore, an E2-recognition domain in an E1 analogue structurally resembles Ub, indicating a potential non-covalent interaction between at least some of the E2s and Ub (*44*). Therefore, a precedent has been established for a non-covalent interaction between E2s and Ub mediating an important stage in the protein ubiquitination cascade.

As will be described in upcoming chapters of this dissertation, the mechanistic model proposed in Fig. 2.9 has subsequently been confirmed by structural, kinetic, and thermodynamic approaches, and significant insights into the mechanism of poly-Ub chain formation have been gained as a result.

2.6 REFERENCES

1.	Hochstrasser, M. (1996) *Annu Rev Genet 30*, 405-39.

2.	Peters, J.-M., King, R.W., Deshaies, R.J. (1998) *Ubiquitin and the Biology of the Cell*, Plenum Press, New York.

3.	Jentsch, S., McGrath, J. P., and Varshavsky, A. (1987) *Nature 329*, 131-4.

4.	Finley, D., Bartel, B., and Varshavsky, A. (1989) *Nature 338*, 394-401.

5.	Chen, Z., Hagler, J., Palombella, V. J., Melandri, F., Scherer, D., Ballard, D., and Maniatis, T. (1995) *Genes Dev 9*, 1586-97.

6.	Hicke, L., and Riezman, H. (1996) *Cell 84*, 277-87.

7.	Chen, Z. J., Parent, L., and Maniatis, T. (1996) *Cell 84*, 853-62.

8.	Hershko, A., Heller, H., Elias, S., and Ciechanover, A. (1983) *J Biol Chem 258*, 8206-14.

9.	Jentsch, S. (1992) *Annu Rev Genet 26*, 179-207.

10.	Cook, W. J., Jeffrey, L. C., Xu, Y., and Chau, V. (1993) *Biochemistry 32*, 13809-17.

11.	Cook, W. J., Martin, P. D., Edwards, B. F., Yamazaki, R. K., and Chau, V. (1997) *Biochemistry 36*, 1621-7.

12.	Giraud, M. F., Desterro, J. M., and Naismith, J. H. (1998) *Acta Crystallogr D Biol Crystallogr 54 (Pt 5)*, 891-8.

13.	Jiang, F., and Basavappa, R. (1999) *Biochemistry 38*, 6471-8.

14.	Tong, H., Hateboer, G., Perrakis, A., Bernards, R., and Sixma, T. K. (1997) *J Biol Chem 272*, 21381-7.

15.	Worthylake, D. K., Prakash, S., Prakash, L., and Hill, C. P. (1998) *J Biol Chem 273*, 6271-6.

16.	Huang, L., Kinnucan, E., Wang, G., Beaudenon, S., Howley, P. M., Huibregtse, J. M., and Pavletich, N. P. (1999) *Science 286*, 1321-6.

17.	Liu, Q., Jin, C., Liao, X., Shen, Z., Chen, D. J., and Chen, Y. (1999) *J Biol Chem 274*, 16979-87.

18. Miura, T., Klaus, W., Gsell, B., Miyamoto, C., and Senn, H. (1999) *J Mol Biol 290*, 213-28.

19. Hamilton, K. S., Ellison, M. J., Barber, K. R., Williams, R. S., Huzil, J. T., McKenna, S., Ptak, C., Glover, M., and Shaw, G. S. (2001) *Structure (Camb) 9*, 897-904.

20. Hamilton, K. S., Ellison, M. J., and Shaw, G. S. (2000) *J Biomol NMR 18*, 319-27.

21. Deshaies, R. J. (1999) *Annu Rev Cell Dev Biol 15*, 435-67.

22. Feldman, R. M., Correll, C. C., Kaplan, K. B., and Deshaies, R. J. (1997) *Cell 91*, 221-30.

23. Kumar, S., Kao, W. H., and Howley, P. M. (1997) *J Biol Chem 272*, 13548-54.

24. Nuber, U., Schwarz, S., Kaiser, P., Schneider, R., and Scheffner, M. (1996) *J Biol Chem 271*, 2795-800.

25. Sancho, E., Vila, M. R., Sanchez-Pulido, L., Lozano, J. J., Paciucci, R., Nadal, M., Fox, M., Harvey, C., Bercovich, B., Loukili, N., Ciechanover, A., Lin, S. L., Sanz, F., Estivill, X., Valencia, A., and Thomson, T. M. (1998) *Mol Cell Biol 18*, 576-89.

26. Broomfield, S., Chow, B. L., and Xiao, W. (1998) *Proc Natl Acad Sci U S A 95*, 5678-83.

27. Hofmann, R. M., and Pickart, C. M. (1999) *Cell 96*, 645-53.

28. Brusky, J., Zhu, Y., and Xiao, W. (2000) *Curr Genet 37*, 168-74.

29. Deng, L., Wang, C., Spencer, E., Yang, L., Braun, A., You, J., Slaughter, C., Pickart, C., and Chen, Z. J. (2000) *Cell 103*, 351-61.

30. Ulrich, H. D., and Jentsch, S. (2000) *Embo J 19*, 3388-97.

31. Xiao, W., Lin, S. L., Broomfield, S., Chow, B. L., and Wei, Y. F. (1998) *Nucleic Acids Res 26*, 3908-14.

32. Rothofsky, M. L., and Lin, S. L. (1997) *Gene 195*, 141-9.

33. Yamaguchi, T., Kim, N. S., Sekine, S., Seino, H., Osaka, F., Yamao, F., and Kato, S. (1996) *J Biochem (Tokyo) 120*, 494-97.

34. Ptak, C., Prendergast, J. A., Hodgins, R., Kay, C. M., Chau, V., and Ellison, M. J. (1994) *J Biol Chem 269*, 26539-45.

35. Kay, L. E., Keifer, P., Saarinen, T. (1992) *J. Am. Chem. Soc. 114*, 10663-10665.

36. Zhang, O., Kay, L. E., Olivier, J. P., and Forman-Kay, J. D. (1994) *J Biomol NMR 4*, 845-58.

37. Delaglio, F., Grzesiek, S., Vuister, G. W., Zhu, G., Pfeifer, J., and Bax, A. (1995) *J Biomol NMR 6*, 277-93.

38. Garrett, F., Grzesiek, S., Vuister, G.W., Zhu, G., Pfeifer, J., Bax, A. (1995) *J. Biol. NMR 6*, 277.

39. Zuiderweg, E. R. (2002) *Biochemistry 41*, 1-7.

40. Hodgins, R., Gwozd, C., Arnason, T., Cummings, M., and Ellison, M. J. (1996) *J Biol Chem 271*, 28766-71.

41. Ashley, C., Pastushok, L., McKenna, S., Ellison, M. J., and Xiao, W. (2002) *Gene 285*, 183-91.

42. Moraes, T. F., Edwards, R. A., McKenna, S., Pastushok, L., Xiao, W., Glover, J. N., and Ellison, M. J. (2001) *Nat Struct Biol 8*, 669-73.

43. VanDemark, A. P., Hofmann, R. M., Tsui, C., Pickart, C. M., and Wolberger, C. (2001) *Cell 105*, 711-20.

44. Walden, H., Podgorski, M. S., and Schulman, B. A. (2003) *Nature 422*, 330-4.

CHAPTER 3:

Sequence-specific ^{1}H, ^{13}C, and ^{15}N resonance assignments of the human Ub-conjugation enzyme, Ubc13, and its heterodimerization partner, Mms2.

3.1 SUMMARY

The molecular mechanism responsible for the formation and recognition of poly-Ub chains remains largely elusive, particularly with respect to the selection of specific isopeptide bond formation between the C-terminus of one Ub molecule and one of several surface-exposed Lys residues of another. In humans, a heterodimer consisting of a catalytically active E2 (Ubc13) and an inert Uev (Mms2) are thought to mediate the assembly of Lys^{63}-linked chains by providing a scaffold upon which Ub moieties can be proximally oriented. In order to test this hypothesis, the nature of the protein-protein interactions that lead to successful formation of Lys^{63}-linked poly-Ub chains must be delineated within the Ubc13/Mms2 system. Based on the inherent lability of thiolester linkages and the weak non-covalent interaction between Ub and Mms2, NMR approaches appear most feasible for structural determinations. The results presented in this chapter detail the NMR chemical shift assignments for both Mms2 and Ubc13. Each protein displays a well-resolved and disperse spectrum characteristic of the E2-family of proteins. Furthermore, chemical shift index calculations confirm that the protein is well-folded and secondary structural elements are conserved in both solution and crystalline phases. The results presented herein form the basis for the determination of the surfaces of interaction, kinetics, thermodynamics, and backbone dynamics within the Ubc13/Mms2 heterodimer complex investigated in future chapters.

3.2 INTRODUCTION

The covalent attachment of poly-Ub chains to target proteins represents

an efficient mechanism for their subsequent regulation and/or degradation, and is involved in a variety of processes from cell cycle control to DNA repair (*1*). Poly-Ub chains are formed by the conjugation of one Ub molecule to the next in a stepwise fashion through formation of an isopeptide bond between the C-terminal Gly^{76} of a donor Ub and the ε-amino group of a specific surface lysine of an acceptor Ub. The use of different Ub surface Lys residues leads to topologically distinct Ub chains that assume different biological roles. For instance, assembly of Lys^{48} linked chains signal for degradation of a target substrate by the 26S proteasome, which is the best characterized pathway in protein ubiquitination (*1*). In contrast, atypical Lys^{63} linked ubiquitin chains do not target proteins for degradation, rather they appear to regulate the activity of key enzymes in both error-free postreplicative DNA repair (*2, 3*) and NF-κB signaling (*4, 5*). Formation of the atypical Lys^{63} linkage is thought to be catalyzed by a stable heterodimer of Ub conjugation enzymes, Ubc13 and Mms2.

Biochemical studies indicate that human Ubc13 forms an activated thiolester linkage with the C-terminus of a donor molecule of ubiquitin such that it can be readily transferred (*6*). Human Mms2 may serve to position an acceptor molecule of ubiquitin such that Lys^{63} linked chains are specifically formed when a ubiquitin molecule is donated from the active-site of hUbc13. The tetrameric system composed of two molecules of Ub bound to the hUbc13/hMms2 heterodimer (51 kDa) represents a formidable challenge in terms of NMR-based structural investigations, because of the labile Ubc13~Ub thiolester bond and the weak non-covalent interaction between ubiquitin and Mms2. In future chapters, chemical shift perturbation titrations to determine the kinetics and thermodynamics of the system, and even backbone amide dynamics will be investigated by NMR experiments in an attempt to delineate the surfaces on each component of the tetramer which are important in forming protein-protein interactions. A necessary, and time-consuming, precursor to these experiments is the assignment of all relevant chemical shift resonances. In this chapter, sequence specific backbone amide (complete) and side chain (partial)

assignments are presented for both human Ubc13 and Mms2 in their monomeric forms. These data represent an important first step towards developing an understanding of this unique mechanism of poly-Ub chain formation.

3.3 EXPERIMENTAL PROCEDURES

3.3.1 Protein expression and purification

The expression and purification of both human Ubc13 and Mms2 have been described in detail in section 2.3.1, with minor modifications noted below. The gene coding for Ubc13 was subcloned into the GST fusion vector pGEX6 (Amersham Pharmacia Biotech), and transformed into *E. coli* BL21(DE_3)-RIL cells. Bacteria were grown at 25 °C in minimal media containing $^{15}NH_4Cl$ as the sole nitrogen source and either $^{13}C_6$-glucose or unlabelled glucose. Expression was induced in the presence of 0.4 mM IPTG after 24 hours of growth. Following induction for 24 hours, cells were harvested and lysed by two passages through a French press. The lysate was clarified by centrifugation (40,000 rpm for 45 minutes) and filtration (0.45 μM low-protein binding, Millipore). Each protein was then purified from the crude lysate by retention on and elution from a glutathione-Sepharose column, followed by Precission protease (Amersham Pharmacia Biotech) removal of the GST tag. The cleaved GST and protease were subsequently retained on a glutathione-Sepharose column, while the purified Ubc13 or Mms2 was not. Each protein was then purified by size exclusion chromatography using a Hi-Load 16/60 Superdex 75 column. Homogeneity was confirmed by SDS-PAGE. The purified protein (50 mM HEPES, 150 mM NaCl, 1 mM EDTA, 1 mM DTT, pH 7.5) was then concentrated in preparation for NMR experiments. For $^{13}C/^{15}N$ labeling, the protein yield was approximately 10 mg per liter of original culture.

3.3.2 NMR spectroscopy

NMR samples contained approximately 0.5 mM Ubc13 or Mms2, 50 mM HEPES (pH 7.5), 150 mM NaCl, 1 mM EDTA, 1 mM DTT, and 1 mM 2,2-

dimethyl-2-silapentanesulfonic acid (DSS) in 9:1 $H_2O:D_2O$. Spectra were recorded on a Varian Unity INOVA 600 MHz spectrometer at 30 °C at the Institute for Biomolecular Design at the University of Alberta, Edmonton. All chemical shifts were referenced to internal DSS. Processing of NMR data was accomplished using the VNMR software package (Varian) and NMRPipe (7). ^1H, ^{15}N, and ^{13}C assignments were made using the NMRView software program (8).

3.3.3 Assignment strategy

The flowchart depicted in Figure 3.1 summarizes the strategy employed to accomplish the complete backbone and partial side chain resonance assignment of both Mms2 and Ubc13. Sequence specific backbone assignments for $^1H^N$, $^{13}C^\alpha$, $^{13}C^\beta$ and ^{15}N nuclei for each protein were first obtained from triple resonance CBCA(CO)NH (9), HNCACB (9) and (H)C(CO)NH-TOCSY (10) experiments. An example of the quality of the data and the approach taken is depicted for the HNCACB experiment in Figure 3.2. Backbone amide ^1H and ^{15}N assignments were then confirmed by HNHA (11) and ^{15}N NOESY-HSQC (12) experiments, which also allowed for $^1H^\alpha$ assignments. ^{13}C side chain assignments were obtained from (H)C(CO)NH-TOCSY in tandem with HNCACB and CBCA(CO)NH experiments, while side chain and backbone proton assignments were obtained from combinations CBCA(CO)NH, HNCACB, HNHA, (H)C(CO)NH-TOCSY, ^{15}N NOESY-HSQC and HCCH-TOCSY (13) experiments.

The X-ray diffraction structures of both human (14) and S. cerevisiae (15) Ubc13 and Mms2 have been previously solved, and show extensive structural similarities. The human structures were employed in tandem with the HNHA and ^{15}N-edited NOESY experiments in order to confirm the sequential $^1H^\alpha$ assignments made.

3.4 RESULTS AND DISCUSSION

3.4.1 Extent of assignments for human Ubc13

Human Ubc13 contains 152 amino acids, of which 14 are Pro residues. In

$^1H^N$, $^{13}C\alpha$, $^{13}C\beta$, ^{15}NH
by
CBCA(CO)NH, HNCACB, (H)C(CO)NH-TOCSY

Confirm $^1H^N$, ^{15}NH
by
HNHA, ^{15}N-NOESY-HSQC

^{13}C Side Chain
by
(H)C(CO)NH-TOCSY

^1H Side Chain
by
HNHA, ^{15}N-NOESY-HSQC, HCCH-TOCSY
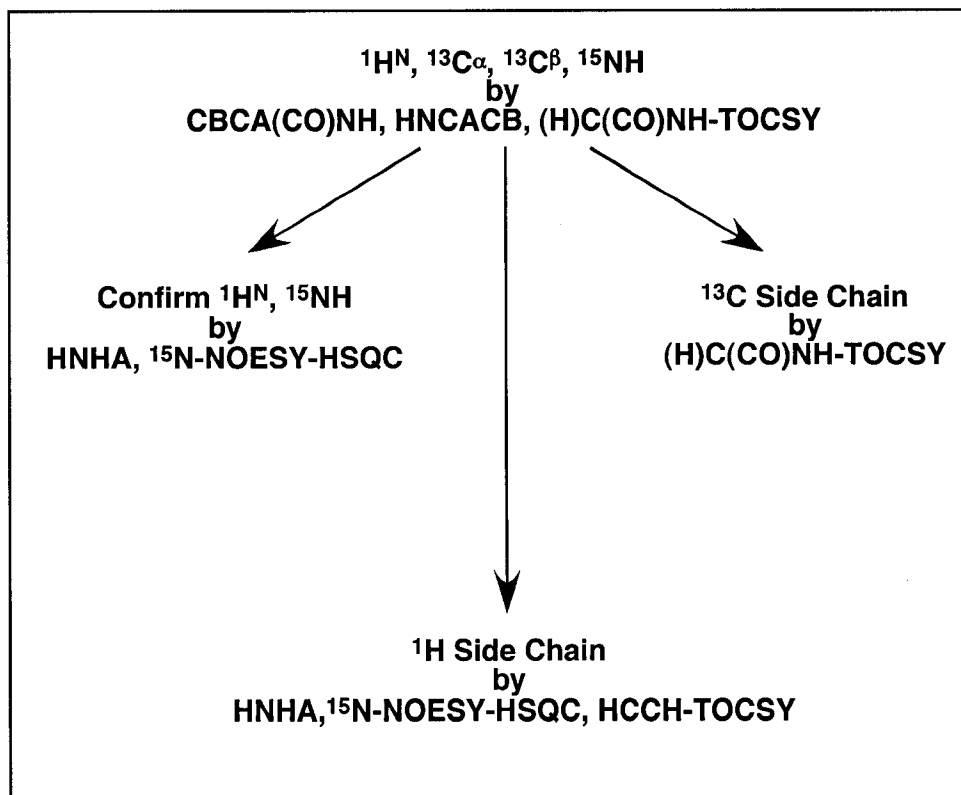
Figure 3.1 NMR resonance assignment strategy for human Ubc13 and Mms2. Shown is the schematic representation of the NMR experiments employed in order to effect the complete backbone and partial side chain resonance assignments in Ubc13 and Mms2. ^{15}N- and $^{15}N^{13}C$-labeled proteins were used as applicable for the particular experiment.
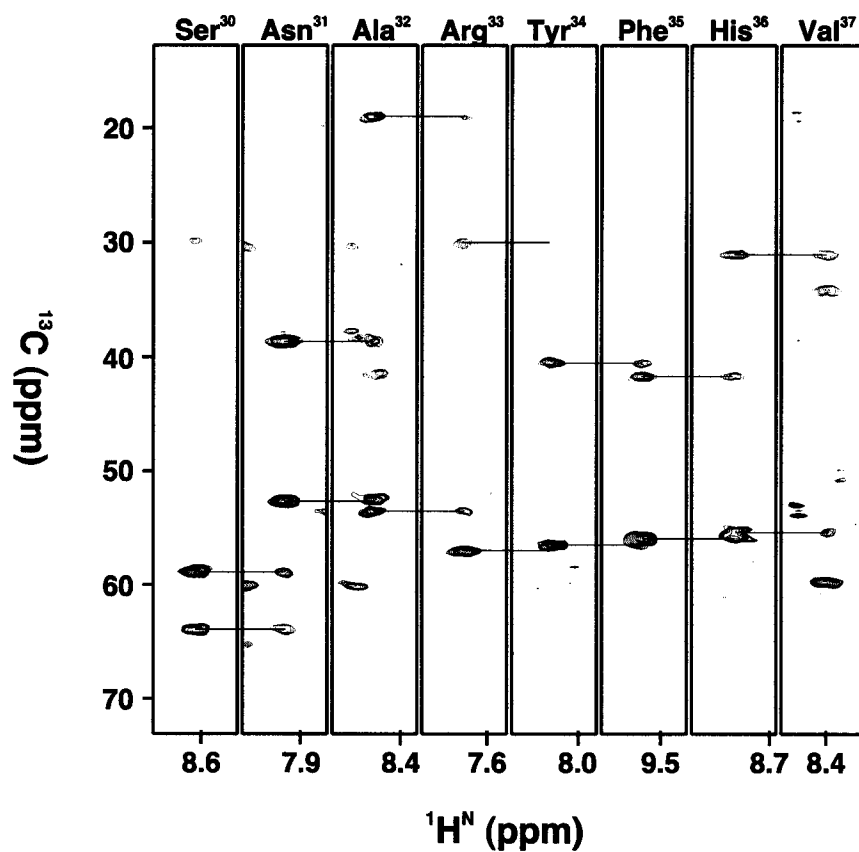
Figure 3.2 Sequential NMR assignment of ^{15}N-^{13}C- labeled human Ubc13. As an example of the techniques used to assign both Mms2 and Ubc13, strip plots corresponding to eight sequential amino acid residues in Ubc13 for the HNCACB NMR experiment are shown. Each strip contains the resonance cross-peak corresponding to the C^{α} and C^{β} for both residue i (linked to the strip ahead of it in sequence) and i-1 (linked to the strip before it in sequence). The unique characteristics of the primary amino acid sequence for each residue in the protein allows for the assignment of these resonances, which correspond to a given $^{1}H^{N}$ chemical shift (x-axis) and a given ^{15}N chemical shift (z-axis, not shown for simplicity).

addition, cleavage of the fusion protein leaves a 5 amino acid N-terminal extension on Ubc13. Spectral analysis allowed for the assignment of 132 out of 138 (152 minus 14 Pro residues) backbone amide $^1H^N$ and ^{15}N residues (96%); Gly^3, Arg^6, Arg^7, Glu^{60}, Ile^{91}, and Asn^{155} could not be assigned unambiguously by the methodology employed. Furthermore, $^1H^N$ and ^{15}N assignments for the N-terminal GST extension were not identified. The assigned 2D ^1H-^{15}N HSQC is shown in Fig. 3.3, and demonstrates a disperse and fairly well resolved spectrum for a 17 kDa protein at sub-millimolar concentrations. For those residues whose backbone amide assignments were completed, all $^{13}C^\alpha$ and $^{13}C^\beta$ assignments were also determined. $^1H^\alpha$ assignments were made with the exception of Ala^2, Gly^3, Asn^{31}, Glu^{61}, Ala^{66}, Met^{72}, Asn^{79}, Asp^{89}, Ile^{101}, Asp^{124}, and Val^{125} (92%). The vast majority of side chain ^1H and ^{13}C assignments assignments were also completed (data not shown). A tabulation of the ^{15}N, $^1H^N$, $^{13}C^\alpha$, and $^{13}C^\beta$ chemical shifts on a per-residue basis can be found in Table 3.1.

3.4.2 Extent of assignments for human Mms2

Human Mms2 contains 145 amino acids, of which 11 are Pro residues. As in the case with Ubc13, cleavage of the fusion protein leaves a 5 amino acid N-terminal extension on Mms2. Spectral analysis allowed for the assignment of 128 out of 134 (145 minus 11 Pro residues) backbone amide $^1H^N$ and ^{15}N residues (96%); Val^3, Asp^{28}, Glu^{75}, Asn^{93}, Ser^{94}, and Lys^{129} could not be assigned unambiguously by the methodology employed. Furthermore, $^1H^N$ and ^{15}N assignments for the N-terminal GST extension were not identified. The assigned 2D ^1H-^{15}N HSQC is shown in Fig. 3.4, and, much like Ubc13 demonstrates a disperse and fairly well resolved spectrum for a 17 kDa protein at sub-millimolar concentrations. All $^{13}C^\alpha$ and $^{13}C^\beta$ assignments were determined with the following exceptions: Gly^{27}, Asp^{76}, and Asn^{93} (98%). $^1H^\alpha$ assignments were made with the exception of Val^3, Gly^6, Asp^{28}, Glu^{75}, Asn^{93}, Ser^{94}, Ile^{115}, and Lys^{129} (94%). The vast majority of side chain ^1H and ^{13}C assignments assignments were also

Figure 3.3 The assigned 2D ^{1}H-^{15}N HSQC spectrum of Ubc13 in the amide region. ^{15}N-Ubc13 (500 μM) is shown, with the spectrum recorded on a 600 MHz Varian Inova spectrometer at 30° C. Backbone amide residue assignments are denoted beside each resonance cross-peak.
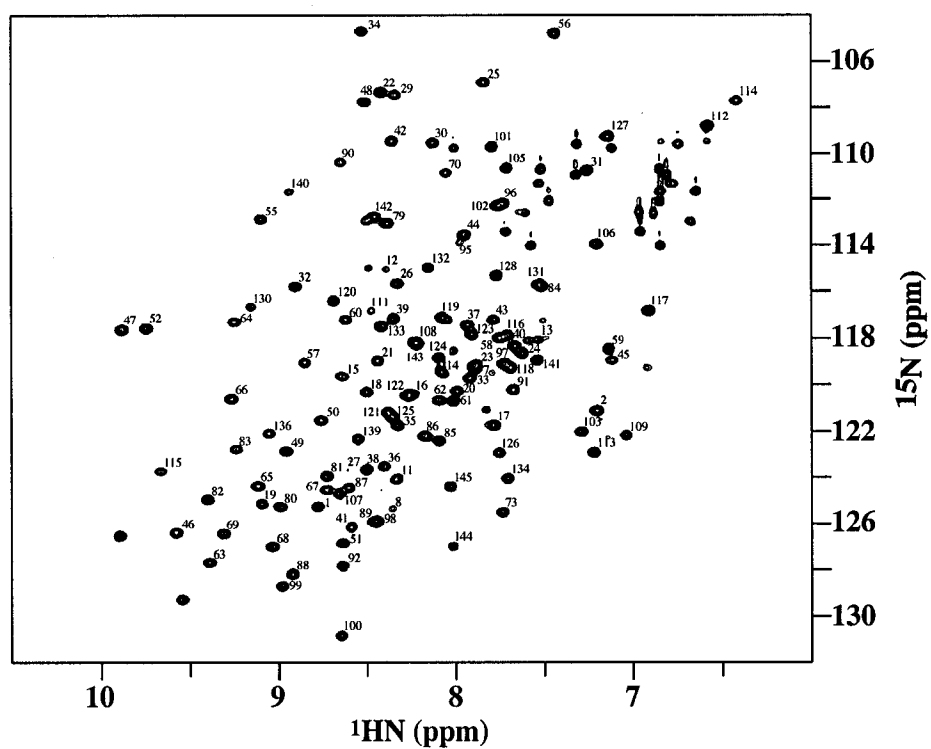
Figure 3.4 The assigned 2D ^{1}H-^{15}N-HSQC spectrum of Mms2 in the amide region. ^{15}N-Mms2 (500 μM) is shown, with the spectrum recorded on a 600 MHz Varian Inova spectrometer at 30° C. Backbone amide residue assignments are denoted beside each resonance cross-peak.

completed (data not shown). A listing of the ^{15}N, ^{1}H^{N}, ^{13}C$^{\alpha}$, and ^{13}C$^{\beta}$ chemical shifts on a per-residue basis can be found in Table 3.2.

3.4.3 NMR-based calculations of secondary structure for Ubc13 and Mms2

The ^{13}C$^{\alpha}$, ^{13}C$^{\beta}$, and ^{1}H$^{\alpha}$ chemical shifts for Mms2 and Ubc13 were employed to calculate the chemical shift index (CSI), whose value provides a measure of the deviation between the observed chemical shifts and their random coil values, and is indicative of the type of secondary structure (16). The comparison between secondary structural elements as determined by X-ray crystallography and from the CSI calculations are shown in Fig. 3.5. There is close correlation between types of secondary structure determined in the solution and crystal states, with the exception that the 3$_{10}$ helix in both proteins is not predicted by CSI. Taken together, these results indicate the likelihood that the chemical shift assignments are reliable for use in future experimentation.

3.4.4 Potential uses for chemical shift assignments of Ubc13 and Mms2

As will be presented in future chapters of this dissertation, there are a variety of important structural, mechanistic, and hence biologically relevant questions with respect to poly-Ub chain formation which can be answered using a number of NMR-based approaches. As a result, the resonance assignments detailed in this Chapter were used to determine the surfaces of interaction within the Ubc13/Mms2/Ub$_{2}$ complex (Chapter 4), the thermodynamics and kinetics governing these interactions (Chapter 5), and the characterization of the backbone amide dynamics of each of these proteins (Chapter 6).

With respect to future directions, the complete side chain assignments for each of these proteins should be performed in order to be able to characterize the nature of protein-protein interactions within this system more extensively. The data would be a prerequisite to solving three-dimensional structures of Ub-bound complexes within the Ubc13/Mms2 system. The chemical shift
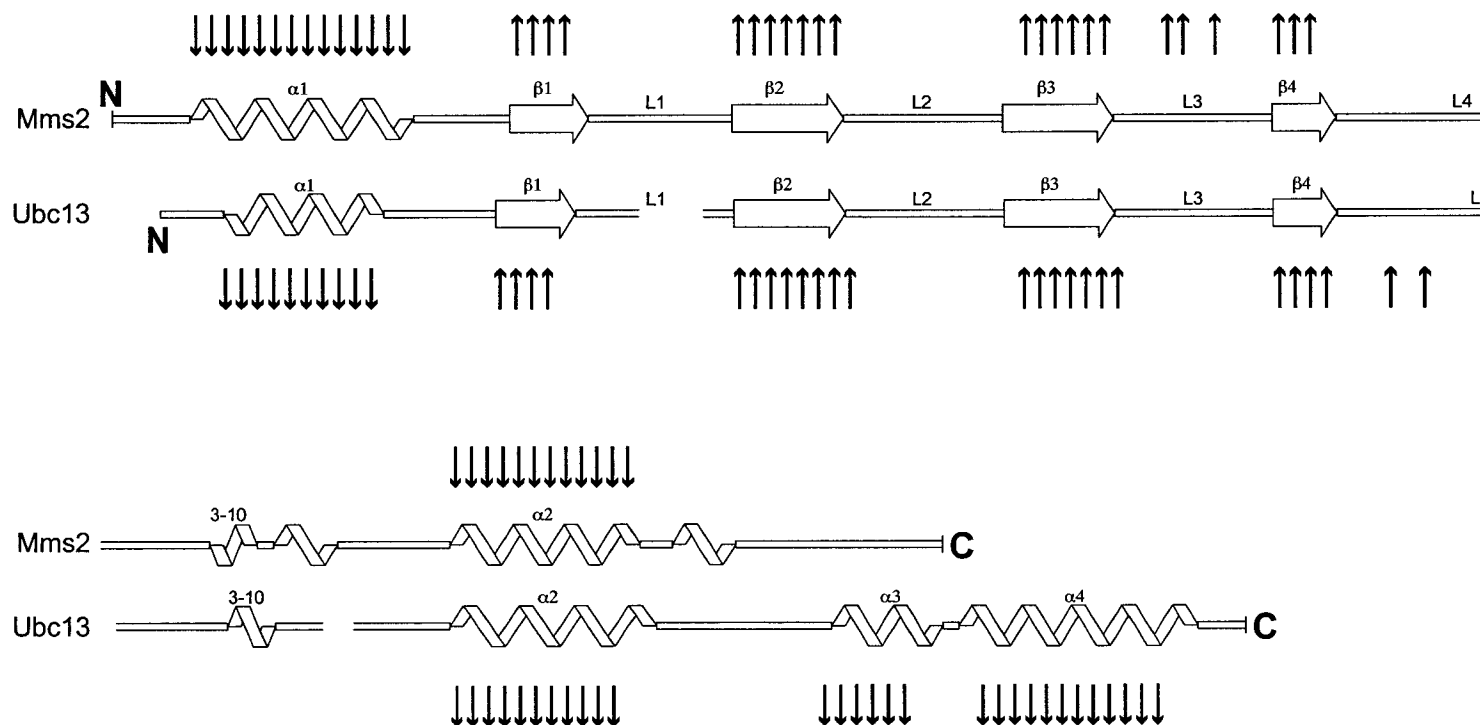
Figure 3.5 Solution and crystal phases of human Mms2 and Ubc13 show high correlation with respect to secondary structure determination. The ribbon diagram of each protein is shown, with the secondary structural elements as determined by X-ray crystallography (14) highlighted. Above (Mms2) and below (Ubc13) each sequence alignment, the average chemical shift index (CSI) values are shown, and were determined from $^{13}C^{\alpha}$, $^{13}C^{\beta}$, and $^{1}H^{\alpha}$ chemical shifts using the program NMRview with the Wishart peptide database (16), pH 7.5, and 303 K. Scores of +1 (up arrow), -1 (down arrow), and 0 (no arrow) correspond to α-helices, β-sheets, and random coil secondary structure elements respectively.

assignments of both hUbc13 and hMms2 in the context of heterodimerization should also be addressed.

Table 3.1 Resonance assignments for human Ubc13. Resonance assignments, shown in units of ppm, are tabulated for each of the 152 residues of Ubc13. While partial side chain assignments were also made, they are not included for simplicity. Dashes (-) represent unassigned resonances.

Residue Number	^{15}N	^{1}H^{N}	^{13}C$^{\alpha}$	^{13}C$^{\beta}$
Met 1	123.2	7.84	55.7	32.7
Ala 2	123.5	8.01	52.9	14.9
Gly 3	-	-	45.2	-
Leu 4	122.5	7.89	53.0	42.8
Pro 5	-	-	-	-
Arg 6	-	-	59.4	29.9
Arg 7	-	-	59.1	30.5
Ile 8	115.6	7.31	65.9	38.0
Ile 9	124.2	7.67	65.5	38.0
Lys10	119.2	8.57	59.4	31.9
Glu 11	118.5	8.49	61.5	31.7
Thr 12	115.9	8.33	68.6	68.2
Gln 13	119.7	8.44	59.4	28.2
Arg 14	118.7	8.01	59.1	29.8
Leu 15	121.4	8.08	57.6	42.2
Leu 16	116.5	7.71	56.6	41.8
Ala 17	120.0	7.84	53.9	19.9
Glu 18	118.2	8.01	53.0	30.3
Pro 19	-	-	62.9	32.6
Val 20	125.7	9.38	60.1	32.9
Pro 21	-	-	64.5	31.7
Gly 22	111.9	8.55	45.7	-
Ile 23	120.2	8.25	60.9	40.5
Lys 24	129.5	9.03	54.9	34.7
Ala 25	127.1	8.37	51.3	21.6
Glu 26	120.6	8.49	52.8	32.8
Pro 27	-	-	61.7	31.5
Asp 28	123.9	8.72	64.6	43.7
Glu 29	124.4	8.70	58.9	29.9
Ser 30	113.8	8.61	59.2	64.2
Asn 31	119.8	7.94	52.9	38.8
Ala 32	126.1	8.47	53.8	19.1
Arg 33	111.2	7.66	57.3	30.2
Tyr 34	119.0	8.06	56.8	40.7
Phe 35	120.7	9.54	56.2	41.9
His 36	122.3	8.78	55.5	31.2
Val 37	126.4	8.40	60.0	34.2
Val 38	127.6	9.29	61.3	34.6
Ile 39	126.8	9.45	60.4	41.4
Ala 40	130.1	8.47	51.6	19.1
Gly 41	110.5	9.26	44.3	-

Residue Number	^{15}N	^{1}H^{N}	^{13}C$^{\alpha}$	^{13}C$^{\beta}$
Pro 42	-	-	-	-
Gln 43	125.9	7.70	57.6	28.9
Asp 44	119.8	9.36	56.6	39.4
Ser 45	115.4	7.90	57.5	65.6
Pro 46	-	-	63.7	32.5
Phe 47	115.2	7.28	55.6	39.5
Glu 48	123.2	7.40	58.4	30.2
Gly 49	115.9	9.26	45.1	-
Gly 50	106.6	8.42	44.8	-
Thr 51	118.7	9.18	62.0	70.1
Phe 52	123.2	8.73	57.2	41.2
Lys 53	123.0	9.27	55.7	33.9
Leu 54	124.4	9.52	54.9	45.8
Glu 55	121.9	8.77	54.9	33.7
Leu 56	127.8	8.30	53.9	45.6
Phe 57	126.5	9.37	54.8	43.0
Leu 58	126.9	8.36	50.1	41.3
Pro 59	-	-	-	-
Glu 60	-	-	60.4	29.3
Glu 61	114.2	8.75	56.9	29.4
Tyr 62	124.9	8.28	58.4	39.6
Pro 63	-	-	64.2	33.4
Met 64	125.5	9.03	57.2	30.6
Ala 65	120.0	6.78	49.8	22.5
Ala 66	119.7	7.25	49.3	18.2
Pro 67	-	-	62.2	31.8
Lys 68	120.5	8.76	54.7	33.2
Val 69	122.7	8.65	59.7	34.8
Arg 70	122.3	8.44	54.7	33.7
Phe 71	124.1	10.2	60.0	40.3
Met 72	121.1	9.46	54.9	32.8
Thr 73	118.9	7.48	62.7	71.8
Lys 74	128.5	8.60	58.3	33.2
Ile75	120.0	8.10	60.5	40.9
Tyr 76	133.4	8.81	57.7	37.2
His 77	123.0	7.90	54.2	35.6
Pro 78	-	-	64.4	32.2
Asn 79	118.0	10.89	53.4	40.7
Val 80	120.0	7.34	60.9	34.7
Asp 81	126.0	8.46	52.8	41.7
Lys 82	115.4	8.24	58.5	32.3
Leu 83	120.7	8.15	54.6	42.0
Gly 84	109.4	8.35	46.1	-
Arg 85	121.2	8.57	57.0	29.8
Ile 86	-	-	60.4	41.0
Cys 87	128.3	8.79	57.8	26.7
Leu 88	126.0	7.26	53.8	46.3
Asp 89	129.2	9.31	58.1	39.2
Ile 90	116.5	8.38	64.1	38.4

Residue Number	^{15}N	^{1}H^N	^{13}C$^\alpha$	^{13}C$^\beta$
Leu 91	113.3	7.27	54.0	41.4
Lys 92	122.9	7.88	56.3	33.0
Asp 93	120.5	8.81	56.0	40.8
Lys 94	115.4	7.76	54.7	31.8
Trp 95	120.7	7.34	59.4	30.1
Ser 96	120.7	5.46	54.5	65.0
Pro 97	-	-	63.9	31.8
Ala 98	119.1	7.35	52.8	19.0
Leu 99	119.2	7.40	54.2	41.5
Gln 100	111.2	7.14	53.9	32.6
Ile 101	123.9	9.97	66.8	37.7
Arg 102	117.7	9.26	60.4	30.6
Thr 103	113.1	7.12	66.1	68.8
Val 104	122.8	7.81	67.1	31.6
Leu 105	117.7	8.13	58.4	40.6
Leu 106	118.4	8.28	58.2	42.3
Ser 107	116.4	8.08	62.8	63.2
Ile 108	123.4	8.10	65.6	37.7
Gln 109	119.7	8.04	60.4	30.4
Ala 110	120.5	8.17	54.9	18.1
Leu 111	120.1	7.66	56.5	42.8
Leu 112	119.3	7.68	58.0	41.3
Ser 113	110.4	7.29	60.8	63.9
Ala 114	124.1	7.85	50.0	19.2
Pro 115	-	-	62.9	32.0
Asn 116	116.8	8.73	49.7	39.2
Pro 117	-	-	63.7	32.4
Asp 118	116.8	7.64	55.1	41.1
Asp 119	120.9	7.12	52.5	41.9
Pro 120	-	-	64.0	33.0
Leu 121	119.0	8.32	54.7	43.0
Ala 122	123.2	7.63	52.0	18.8
Asn 123	124.4	8.13	54.9	41.3
Asp 124	121.3	7.08	56.9	39.6
Val 125	122.1	7.80	65.5	31.8
Ala 126	122.1	8.24	55.9	19.0
Glu 127	116.6	8.03	59.6	29.3
Gln 128	120.4	7.77	58.7	28.5
Trp 129	120.7	8.47	61.5	28.7
Lys 130	112.9	7.93	58.4	33.3
Thr 131	111.4	8.06	64.2	70.3
Asn 132	122.8	8.46	52.2	38.1
Glu 133	125.8	8.51	60.4	30.5
Ala 134	118.3	8.37	55.5	18.0
Gln 135	117.6	7.32	57.8	29.0
Ala 136	125.6	8.00	55.1	17.2
Ile 137	117.5	8.15	65.4	37.7
Glu 138	119.2	7.47	59.5	29.0
Thr 139	120.2	8.29	66.7	68.4

Residue Number	^{15}N	^{1}H^N	^{13}C$^\alpha$	^{13}C$^\beta$
Ala 140	125.1	8.66	56.0	18.8
Arg 141	121.7	8.69	59.9	30.6
Ala 142	125.0	8.39	55.6	17.8
Trp 143	119.4	9.74	61.0	29.1
Thr 144	124.8	8.66	68.2	68.6
Arg 145	120.1	7.62	58.9	30.1
Leu 146	117.0	7.99	57.3	42.8
Tyr 147	112.4	8.05	57.7	40.8
Ala 148	121.8	8.06	51.1	21.8
Met 149	116.8	7.65	55.1	34.3
Asn 150	-	-	57.2	37.0
Asn 151	124.4	8.13	53.6	38.6
Ile 152	124.5	7.58	62.8	39.5

Table 3.2 Resonance assignments for human Mms2. Resonance assignments, shown in units of ppm, are tabulated for each of the 145 residues of Mms2. While partial side chain assignments were also made, they are not included for simplicity. Dashes (-) represent unassigned resonances.

Residue Number	^{15}N	^{1}H^{N}	^{13}C$^{\alpha}$	^{13}C$^{\beta}$
Met 1	125.4	8.78	58.5	28.9
Ala 2	121.2	7.21	48.2	20.6
Val 3	-	-	61.4	34.0
Ser 4	127.9	7.90	57.9	63.9
Thr 5	123.0	8.07	61.6	69.9
Gly 6	127.0	7.76	45.3	-
Val 7	119.5	7.90	62.3	33.0
Lys 8	125.5	8.39	56.1	33.03
Val 9	124.7	8.42	59.9	33.2
Pro 10	-	-	56.1	33.0
Arg 11	124.1	8.33	59.9	33.1
Asn 12	115.0	8.48	56.9	37.2
Phe 13	118.1	7.54	60.8	38.8
Arg 14	119.6	8.08	57.5	28.5
Leu 15	119.8	8.65	58.6	43.0
Leu 16	120.5	8.24	58.3	41.6
Glu 17	121.9	7.79	59.9	29.5
Glu18	120.4	8.51	61.6	29.5
Leu 19	125.2	9.10	58.9	42.8
Glu 20	120.2	8.00	59.6	29.5
Glu 21	119.1	8.45	59.7	29.9
Gly 22	107.5	8.42	45.4	-
Gln 23	119.3	7.89	57.8	28.8
Lys 24	118.7	7.63	57.9	33.3
Gly 25	107.0	7.85	45.2	-
Val 26	115.8	8.33	61.3	33.4
Gly 27	123.7	8.61	-	-
Asp 28	-	-	53.5	41.1
Gly 29	107.5	8.35	46.2	-
Thr 30	109.7	8.13	64.3	70.6
Val 31	110.9	7.26	59.3	36.1
Ser 32	115.9	8.91	57.8	65.4
Trp 33	119.8	7.92	57.9	32.3
Gly 34	104.9	8.54	45.2	-
Leu 35	121.8	8.33	55.1	42.5
Glu 36	123.6	8.41	59.0	30.5
Asp 37	117.5	7.94	52.7	43.0
Asp 38	123.8	8.51	56.0	40.6
Glu 39	117.4	8.36	56.2	29.5
Asp 40	118.5	7.67	53.5	40.4
Met 41	126.3	8.59	56.6	32.0

Residue Number	^{15}N	^{1}H^{N}	^{13}C$^{\alpha}$	^{13}C$^{\beta}$
Thr 42	109.5	8.37	62.5	70.2
Leu 43	117.4	7.80	56.4	39.9
Thr 44	113.7	7.95	66.0	69.4
Arg 45	119.3	7.12	57.2	31.3
Trp 46	126.5	9.58	56.6	30.9
Thr 47	117.8	9.89	60.2	70.6
Gly 48	107.9	8.53	44.2	-
Met 49	122.9	8.96	54.6	36.2
Ile 50	121.6	8.77	60.6	44.9
Ile 51	127.0	8.64	60.4	37.5
Gly 52	117.7	9.75	44.9	-
Pro 53	-	-	-	-
Pro 54	-	-	62.7	32.3
Arg 55	113.0	9.11	57.5	26.6
Thr 56	104.9	7.45	60.2	74.2
Asn 57	119.1	8.86	53.9	36.4
Tyr 58	118.1	7.76	56.7	38.7
Glu 59	118.6	7.14	57.9	30.9
Asn 60	117.3	8.63	55.2	37.4
Arg 61	120.8	8.02	56.4	31.7
Ile 62	120.8	8.09	60.7	38.6
Tyr 63	127.8	9.39	58.6	40.7
Ser 64	117.5	9.25	57.7	64.4
Leu 65	124.5	9.12	5.8	46.5
Lys 66	120.7	9.27	55.5	35.2
Val 67	124.6	8.74	60.7	35.4
Glu 68	127.1	9.04	54.6	32.3
Cys 69	126.5	9.32	58.2	27.9
Gly 70	110.9	8.05	45.6	-
Pro 71	-	-	65.0	32.9
Lys 72	114.7	8.70	54.9	32.8
Tyr 73	125.6	7.74	57.7	40.0
Pro 74	-	-	-	-
Glu 75	-	-	55.9	29.9
Ala 76	128.5	8.05	-	-
Pro 77	-	-	-	-
Pro 78	-	-	61.7	32.6
Ser 79	113.2	8.39	57.3	64.3
Val 80	125.4	8.99	61.3	34.6
Arg 81	124.0	8.74	54.2	34.3
Phe 82	125.1	9.41	60.0	39.7
Val 83	122.9	9.24	64.9	33.0
Thr 84	116.0	7.52	63.4	70.8
Lys 85	122.5	8.10	58.9	33.0
Ile 86	122.3	8.18	60.3	41.9
Asn 87	124.5	8.62	50.84	38.7
Met 88	128.3	8.92	56.4	36.5
Asn 89	126.0	8.46	56.5	38.4
Gly 90	110.5	8.65	45.1	-

Residue Number	¹⁵N	¹Hᴺ	¹³Cᵅ	¹³Cᵝ
Ile 91	120.3	7.68	59.0	36.8
Asn 92	128.0	8.64	55.1	39.7
Asn 93	-	-	-	-
Ser 94	-	-	59.9	64.3
Ser 95	113.9	7.98	57.3	66.9
Gly 96	112.3	7.74	46.2	-
Met 97	119.2	7.73	56.6	32.6
Val 98	126.0	8.45	62.6	32.2
Asp 99	128.8	8.98	53.8	41.0
Ala 100	131.0	8.65	54.9	19.4
Arg 101	109.9	7.80	58.0	30.0
Ser 102	112.4	7.77	59.6	64.9
Ile 103	122.1	7.29	55.4	37.4
Pro 104	-	-	67.4	32.1
Val 105	110.7	7.71	64.4	31.5
Leu 106	114.0	7.21	56.2	42.1
Ala 107	124.8	8.66	54.9	19.1
Lys 108	118.2	8.23	53.6	31.0
Trp 109	122.3	7.05	59.6	30.6
Gln 110	123.9	5.17	52.4	31.8
Asn 111	117.0	8.47	54.0	37.4
Ser 112	108.9	6.58	57.5	63.1
Tyr 113	123.0	7.23	53.7	35.2
Ser 114	107.9	6.43	56.3	65.3
Ile 115	123.8	9.68	67.1	38.0
Lys 116	118.0	7.71	59.9	31.5
Val 117	117.0	6.92	65.7	32.6
Val 118	119.4	7.70	67.1	31.4
Leu 119	117.3	8.09	58.3	41.0
Gln 120	116.5	8.69	59.5	28.6
Glu 121	121.2	8.39	58.8	28.9
Leu 122	120.6	8.27	58.5	42.0
Arg 123	118.0	7.91	59.5	29.5
Arg 124	119.0	8.09	59.6	30.0
Leu 125	121.5	8.36	57.7	41.5
Met 126	123.0	7.76	59.6	32.6
Met 127	109.4	7.15	55.4	33.9
Ser 128	115.5	7.77	58.6	64.5
Lys 129	-	-	60.1	32.5
Glu 130	116.9	9.16	58.9	28.9
Asn 131	115.8	7.53	54.2	41.1
Met 132	115.1	8.16	60.4	33.6
Lys 133	117.6	8.42	54.2	31.9
Leu 134	124.1	7.71	53.8	40.5
Pro 135	-	-	62.8	31.6
Gln 136	122.3	9.05	52.5	29.1
Pro 137	-	-	-	-
Pro 138	-	-	63.2	32.1
Glu 139	122.5	8.56	57.7	30.1

Residue Number	¹⁵N	¹Hᴺ	¹³Cᵅ	¹³Cᵝ
Gly 140	111.9	8.93	45.4	-
Gln 141	119.0	7.54	56.2	29.9
Thr 142	112.9	8.46	59.7	72.2
Tyr 143	118.4	8.23	60.6	38.6
Asn 144	127.1	8.01	53.4	39.2
Asn 145	124.5	8.03	54.9	40.6

3.5 REFERENCES

1. Glickman, M. H., and Ciechanover, A. (2002) *Physiol Rev 82*, 373-428.

2. Brusky, J., Zhu, Y., and Xiao, W. (2000) *Curr Genet 37*, 168-74.

3. Hofmann, R. M., and Pickart, C. M. (1999) *Cell 96*, 645-53.

4. Wang, C., Deng, L., Hong, M., Akkaraju, G. R., Inoue, J., and Chen, Z. J. (2001) *Nature 412*, 346-51.

5. Deng, L., Wang, C., Spencer, E., Yang, L., Braun, A., You, J., Slaughter, C., Pickart, C., and Chen, Z. J. (2000) *Cell 103*, 351-61.

6. McKenna, S., Spyracopoulos, L., Moraes, T., Pastushok, L., Ptak, C., Xiao, W., and Ellison, M. J. (2001) *J Biol Chem 276*, 40120-6.

7. Delaglio, F., Grzesiek, S., Vuister, G. W., Zhu, G., Pfeifer, J., and Bax, A. (1995) *J Biomol NMR 6*, 277-93.

8. Johnson, B. A., Blevins, R.A. (1994) *J. Chem. Phys. 29*, 1012-1014.

9. Muhandiram, R. D., Kay, L.E. (1994) *J. Mag. Res. 103*, 203-216.

10. Logan, T. M., Olejniczak, E.T., Xu, R.X., Fesik, S.W. (1993) *J Biomol NMR 3*, 225-231.

11. Vuister, G. W., Bax, A. (1993) *J. Am. Chem. Soc. 115*, 7772-7777.

12. Zhang, O., Kay, L.E., Olivier, J.P., Forman-Kay, J.D. (1994) *J Biomol NMR 4*, 845-858.

13. Kay, L. E., Xu, G.-Y., Singer, A.U., Muhandiram, D.R., Forman-Kay, J.D. (1993) *J Magn Reson 101*, 333-337.

14. Moraes, T. F., Edwards, R. A., McKenna, S., Pastushok, L., Xiao, W., Glover, J. N., and Ellison, M. J. (2001) *Nat Struct Biol 8*, 669-73.

15. VanDemark, A. P., Hofmann, R. M., Tsui, C., Pickart, C. M., and Wolberger, C. (2001) *Cell 105*, 711-20.

16. Wishart, D. S., Sykes, B. D., and Richards, F. M. (1992) *Biochemistry 31*, 1647-51.

CHAPTER 4:

An NMR based model of the Ub-bound human Ub-conjugation complex Mms2/Ubc13: The structural basis for Lys[63] chain catalysis[1].

4.1 SUMMARY

A heterodimer composed of the catalytically active Ub conjugating enzyme Ubc13 and its catalytically inactive paralogue, Mms2, forms the catalytic core for the synthesis of an alternative type of multi-Ub chain where Ub molecules are tandemly linked to one another through a Lys[63] isopeptide bond. This type of linkage, as opposed to the more typical Lys[48]-linked chains, serves as a non-proteolytic marker of protein targets involved in error-free post-replicative DNA repair and NF-κB signal transduction. Using a two dimensional ^{1}H-^{15}N nuclear magnetic resonance approach, we have mapped: 1) the interaction between the subunits of the human Ubc13/Mms2 heterodimer and 2) the interactions between each of the subunits or heterodimer with a non-covalently bound acceptor Ub or a thiolester-linked donor Ub. Using these NMR-derived constraints and an unbiased docking approach, we have assembled the four components of this catalytic complex into a three dimensional model that agrees well with its catalytic function.

4.2 INTRODUCTION

The post-translational modification of intracellular proteins by ubiquitination fulfills an important regulatory function in many cellular pathways. Protein ubiquitination involves a cascade of enzymatic steps where Ub is passed sequentially as an activated thiolester from a Ub activating enzyme (E1) to a Ub

---

[1] The contents of this chapter are based on previously published research: McKenna *et. al.* (2003) *J. Biol. Chem.* **278**, 40120-40126.

conjugating enzyme (E2), and finally to the protein target with the help of a Ub protein ligase (E3) (*1, 2*).

The assembly of poly-Ub chains onto a targeted protein has proven to be a hallmark of a variety of processes, such as cell cycle control (*3*), DNA repair (*4*), ribosome biogenesis (*5*), the inflammatory response (*6*), endocytosis of cell surface proteins (*7*), and NF-κB-dependent signal transduction (*8*). These chains are synthesized in an E2-dependent reaction where each Ub within the chain is covalently bound to its neighbor by an isopeptide bond that links the C-terminus to a surface Lys of its target-proximal Ub partner. Previous observations have demonstrated that these chains can exist in different configurations that are defined by the specific lysine residue that links each Ub molecule within the chain (*9-14*).

The most prevalent and best-documented examples of protein ubiquitination use the Lys[48]-linked chain configuration to target proteins for degradation by the 26S proteasome (*2*). Recently, however, a non-proteolytic ubiquitination pathway has come to light that results in the substrate-tethered assembly of multi-Ub chains where Ub molecules are tandemly linked to one another through Lys[63] (*12, 15-19*). This pathway plays a key role in error-free DNA post-replicative repair (*20-22*) endocytosis (*15*), polysome stability (*17*), and is an important component of NF-κB signal transduction (*18, 19*).

The error-free repair and NF-κB pathways both catalyze the assembly of Lys[63] chains using a conserved E2 heterodimer, composed of a catalytically active Ubc13 subunit, and a catalytically inactive E2-like subunit termed Ubiquitin Enzyme Variant (Uev). Uev proteins share significant sequence similarity with other E2s, but lack the characteristic active-site Cys residue required for thiolester formation. In the error-free repair pathway of *S. cerevisiae*, two chromatin-associated RING finger proteins, Rad5 and Rad18, recruit the Ubc13/Mms2 heterodimer and Rad6 (Ubc2) to DNA (*23*). In very recent work, Hoege *et al.* (*24*) have demonstrated that a target of this pathway is the yeast proliferating cell nuclear antigen (PCNA), which is first mono-ubiquitinated

through Rad6 and Rad18 and then poly-ubiquitinated by Ubc13/Mms2 in conjunction with Rad5. In NF-κB signal transduction, Traf6, a RING domain E3 protein, functions together with the Ubc13/Uev heterodimer (containing either Uev1a or the functionally equivalent Mms2) in the formation of Lys[63]-linked poly-Ub chains that are required for the activation of IκB kinase (IKK), a key signal transducer in the NF-κB pathway (*18, 19*).

Insight into the mechanism of Lys[63] chain assembly and its relationship to structure recently became possible with the simultaneous determination of both *S. cerevisiae* (*25*) and human (*26*) Ubc13/Mms2 heterodimer structures by X-ray crystallography, and an NMR-based approach for mapping the protein-protein interactions within the Ub bound complex (*27*). Using the previously determined assignments for Ub in ^{1}H-^{15}N HSQC NMR experiments, we were able to footprint the surface of Ub that interacted with the human Ubc13/Mms2 heterodimer and each of its subunits in either the thiolester-linked or unlinked forms (*27*). The results of this study were consistent with a two binding site model in which an "acceptor" molecule of Ub bound non-covalently to Mms2 was positioned in an orientation such that a second Ub molecule that was linked to Ubc13 as a thiolester could be transferred to Lys[63] of the accepting Ub molecule. The NMR assignments of both Mms2 and Ubc13 is an obvious prerequisite for footprinting the surfaces of the heterodimer that interact with both the covalently linked and unlinked forms of Ub. In the present work we have determined the footprint that both Ub molecules make on the surface of the Ubc13/Mms2 heterodimer. Taken together with previous work, a compelling model is presented for the tetrameric structure that places Lys[63] of the accepting Ub molecule in catalytic proximity of the C-terminus of the donor Ub molecule.

4.3 EXPERIMENTAL PROCEDURES

4.3.1 Protein expression and purification

Human Ubc13 and Mms2 were expressed and purified as described in section 2.3.1 with the following exceptions. Proteins were expressed in the *E.*

coli strain *BL21(DE₃)-RP* (Stratagene), and 2 L cultures were grown at 25 °C to OD_{590}= 0.3 in minimal media containing $^{15}NH_4Cl$ as the sole nitrogen source and induced with IPTG (0.4 mM) for an additional 24 hours at 25 °C. *S. cerevisiae* UbLys⁴⁸Arg, UbLys⁶³Arg, and Uba1 (E1) were expressed and purified as described previously (*27*).

4.3.2 NMR spectroscopy

All NMR spectra were obtained using a Varian Unity INOVA 600 MHz spectrometer at 30 °C. The 2D ^{1}H-^{15}N-HSQC NMR spectra were acquired using the sensitivity-enhanced gradient pulse scheme developed by Kay and co-workers (*28, 29*). The ^{1}H and ^{15}N sweep widths were 8000 and 2200 Hz, respectively. A minimum of 64 transients were collected for each spectrum. All NMR samples were prepared to include HEPES (50 mM, pH 7.5), NaCl (75 mM), EDTA (1 mM), DTT (1 mM), and DSS (1 mM) in the presence of 9:1 $H_2O:D_2O$.

Spectral processing was accomplished with the NMRPipe program (*30*). The NMRview program (*31*) was employed in the assignment of all 2D ^{1}H-^{15}N-HSQC NMR crosspeaks. To calculate the total average change in backbone amide ^{1}H^N and ^{15}N chemical shifts for each resonance, the following equation was applied (*32*):

$$\Delta\delta_{total} = \sqrt{\left(\Delta\delta^{15}N\right)^2 + \left(\Delta\delta^1H_N\right)^2}$$ [eq. 4.1]

where $\Delta\delta^{15}N$ and $\Delta\delta^1H_N$ are the chemical shift changes in Hertz. The average change in total chemical shift was then calculated for each identified residue, with the exception of those whose resonances had broadened past detectability in the 2D ^{1}H-^{15}N-HSQC NMR spectra. The standard deviation associated with each dataset was also calculated.

4.3.3 ^{15}N-Mms2 chemical shift perturbation experiments

An outline of all NMR chemical shift perturbation experiments is shown in Figure 4.1. An initial 2D ^{1}H-^{15}N-HSQC spectrum was acquired for ^{15}N-Mms2 (250
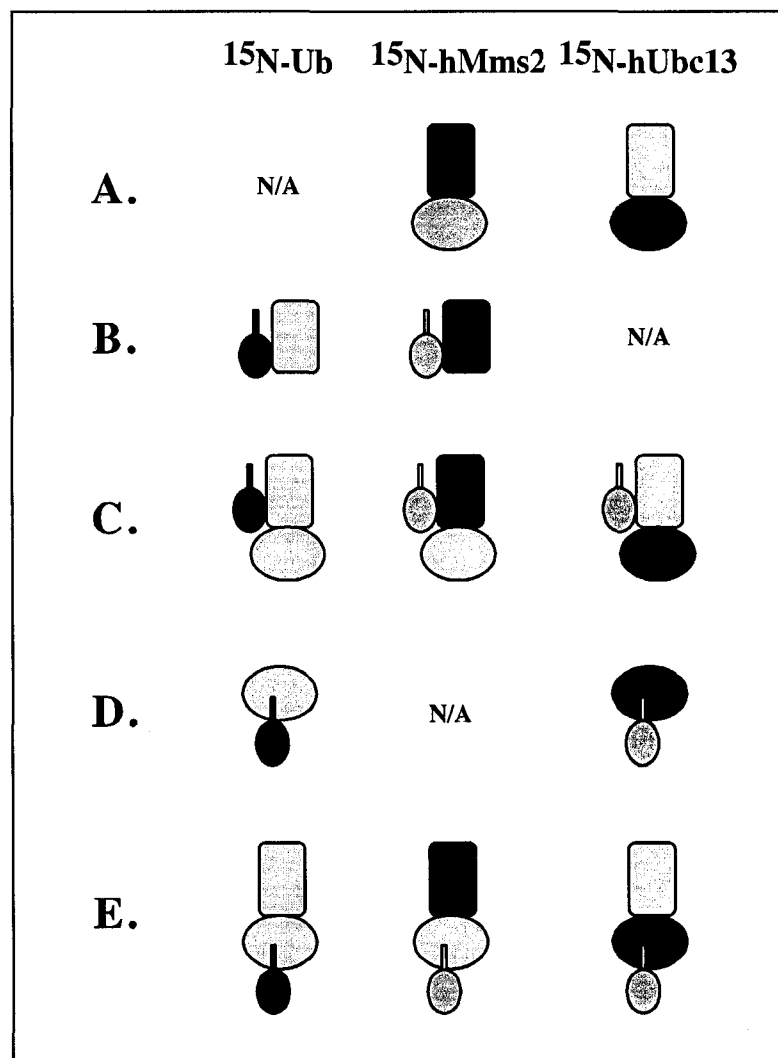
Figure 4.1 Outline of the NMR experiments performed in order to probe the surfaces of interaction within the Ubc13/Mms2/Ub complexes. Ub is represented by a small ellipse with a tail, the Mms2 component by a large ellipse, and the Ubc13 component by a rectangle. 15N-labeled components in each experiment are colored black, whereas unlabeled proteins are grey. The interactions to be examined include those between (A) the Ubc13/Mms2 interface, (B) Ub and Mms2 non-covalently, (C) Ub and Ubc13/Mms2 non-covalently, (D) Ub and Ubc13 in the thiolester complex, and (E) Ub and Ubc13/Mms2 heterodimer within the thiolester complex.

μM) as a point of reference for subsequent chemical shift perturbation experiments. The spectrum also served to confirm the proper folding and lack of aggregation of ^{15}N-Mms2.

The interactions between ^{15}N-Mms2 and Ubc13 were examined by inclusion of a slight excess of unlabeled Ubc13 (300 μM) to the sample described above for ^{15}N-Mms2 alone. The NMR tube was allowed to equilibrate for 1 hour at 30 °C to ensure heterodimerization would proceed to completion. A 2D ^{1}H-^{15}N-HSQC spectrum was then acquired for the sample.

Non-covalent interactions between ^{15}N-Mms2 (250 μM) and Ub were examined by including unlabeled UbLys^{48}Arg (600 μM) into NMR samples in the presence or absence of unlabeled Ubc13 (300 μM). A 2D ^{1}H-^{15}N-HSQC spectrum was then acquired for each sample. Chemical shift assignments in the 2D ^{1}H-^{15}N-HSQC spectra were again completed assuming that the closest cross peak represented the correct change in chemical shift. The 2D ^{1}H-^{15}N-HSQC NMR reference spectrum used when calculating changes caused by Ub were either (i) ^{15}N-Mms2 alone to examine the changes cause in Mms2 by itself or (ii) ^{15}N-Mms2/Ubc13 in order to probe the changes in chemical shift in Mms2 in the context of the heterodimer.

4.3.4 ^{15}N-Ubc13 chemical shift perturbation experiments.

An outline of all NMR chemical shift perturbation experiments is shown in Figure 4.1. As in the case of Mms2, an initial 2D ^{1}H-^{15}N-HSQC NMR spectrum was acquired as a point of reference, and confirmed the proper folding and lack of aggregation of ^{15}N-Ubc13 (300 μM).

The interactions between ^{15}N-Ubc13 and Mms2 were examined by inclusion of a slight excess of unlabeled Mms2 (330 μM) to the sample described above for ^{15}N-Ubc13 alone. Sample equilibration and acquisition were performed as described for the ^{15}N-Mms2 samples.

Thiolester-linked interactions between ^{15}N-Ubc13 (300μM) and Ub (330 μM) were examined in situ by inclusion of S. cerevisiae E1 (0.3 μM), ATP (5

mM), and $MgCl_2$ (5 mM) as described in section 2.3.9. Addition of Mms2 (330 μM) to this sample allowed for the examination of the Mms2/^{15}N-Ubc13~Ub species. Studies described elsewhere (Chapter 2) (27) have shown that thiolester formation is rapid (minutes) whereas the formation of Ub-conjugate on Ubc13 is slow (hours). Furthermore, the onset of conjugate formation can be clearly identified based on the accumulation of new peaks emanating from the mixed population of Ub species. The 2D ^{1}H-^{15}N-HSQC NMR experiments were therefore performed between 10 and 120 minutes after the addition of E1 in order to minimize the impact of possible side-reactions. UbLys[63]Arg was employed as the Ub species in order to eliminate the possibility of chain formation by the Ubc13/Mms2 heterodimer, and hence eliminate further complication of the spectra. The 2D ^{1}H-^{15}N-HSQC NMR reference spectrum used when calculating changes caused by Ub in thiolester complexes were either (i) ^{15}N-Ubc13 alone to examine the changes caused in Ubc13 by itself or (ii) ^{15}N-Ubc13/Mms2 in order to probe the changes in chemical shift in Ubc13 in the context of the heterodimer.

Non-covalent interactions between ^{15}N-Ubc13 and Ub were detected by including unlabeled UbLys[63]Arg into NMR samples in the presence or absence of unlabeled Ubc13 under conditions identical to thiolester formation with the exception that E1, ATP, and $MgCl_2$ were omitted. A 2D ^{1}H-^{15}N-HSQC NMR spectrum was then acquired for each sample. However, no changes in ^{15}N-Ubc13 cross peaks were observed in either case, and therefore no further analysis was performed.

4.3.5 Molecular modeling

Molecular modeling of the surfaces of interaction was accomplished with the BiGGER soft-docking algorithm (33, 34) using the unbound structures of Ub (target) (35) and the Ubc13/Mms2 heterodimer (probe) (26). The BiGGER algorithm systematically searches the complete 6-dimensional binding spaces of both target and probe, and then evaluates these solutions in terms of a global scoring function consisting of geometric complementarity, electrostatic

interactions, desolvation energy, and the pairwise propensities of amino acid side chains to interact across molecular interfaces. Docking parameters in this initial search included a 15° angular step, 5000 maximum solutions, and 300 minimum atomic contacts. The top 5000 solutions based on global score were then filtered using the NMR chemical shift perturbation data in the following manner. First, surface-exposed residues on Mms2 and Ub, respectively, which produced significant $\Delta\delta_{total}$ values upon non-covalent interaction were determined, and the number of atomic contacts between these two groups within a 5 Å distance cutoff in each of the top 5000 solutions as determined by global score was evaluated. The top solution based on these criteria was then accepted as the "correct" orientation, and subsequently underwent minimization using the INSIGHTII suite of programs. The thiolester bound Ub placement upon the heterodimer was then determined in an identical manner using $\Delta\delta_{total}$ values.

4.4 RESULTS

When engaged in catalysis, the Ubc13/Mms2 heterodimer necessarily exists as part of a tetramer that is composed of the heterodimer in association with two Ub molecules. One Ub molecule is linked as a thiolester to the active site of Ubc13 (the donor) while the other Ub molecule interacts non-covalently with Mms2 (the acceptor). While a high-resolution crystallographic structure for the heterodimer has been determined (*26*), a crystallographic structure for the Ub-bound tetramer is unlikely. This conclusion is based both on the instability of the Ubc13~Ub thiolester bond (*36*) and the relatively weak interaction that exists between the acceptor Ub and Mms2 ($K_D \sim 100\ \mu M$, see Chapter 5). Based on these considerations, we have pursued an alternative NMR-based approach to determine the structure of the Ubc13/Mms2-Ub$_2$ tetramer. The tetramer has three major protein-protein interfaces: 1) the Mms2/Ubc13 interface, 2) the Mms2-Ub (acceptor) interface and, 3) the Ubc13~Ub (donor) interface. In this and previous studies (*27*), we have used ^{1}H-^{15}N HSQC NMR spectroscopy to

observe the chemical shift perturbations that are induced upon interaction to define the footprint that each protein makes with its partner.

The method that we have chosen here relies upon the comparison of ^{1}H-^{15}N HSQC NMR spectra for each protein component in an unbound form and bound to its partner. To simplify the analysis, only one component of the complex is ^{15}N-labeled in any given experiment. Backbone amide ^{1}H$_N$ and ^{15}N chemical shifts are sensitive to a variety of factors including hydrogen bonding, electrostatic interactions, and aromatic ring current effects, to name a few. Therefore changes to chemical shifts that can result from differences in chemical environment upon complex formation can be used to identify residues that are either directly involved at the binding interface or correspond to long-range structural changes.

A necessary precursor to chemical shift mapping is the complete assignment of backbone amide ^{1}H-^{15}N cross peaks in the ^{1}H-^{15}N HSQC NMR spectra for a given component of the complex. Recently, we have completed the full backbone chemical shift assignments for both Ubc13 and Mms2 (Chapter 3). Each protein exhibits well dispersed and resolved ^{1}H-^{15}N HSQC NMR spectra at 600 MHz, as is shown for Mms2 (Fig. 4.2). Furthermore, the spectra retain these qualities fairly well upon formation of higher order complexes of up to 42.5 kDa, though the signal-to-noise ratio is reduced as expected, due to increased linewidths. Chemical shift assignments in the 2D ^{1}H-^{15}N-HSQC NMR spectra were made relative to the appropriate reference spectrum, assuming that the closest shifted cross peak represented the correct one. This approach was required due primarily to the lability of complexes containing thiolester linkages.

4.4.1 Mapping the heterodimer interface

The recent report of the human Mms2/Ubc13 heterodimer structure by X ray crystallography (26) presented a rare opportunity to evaluate an NMR-based approach to map protein-protein surface interactions when compared to a known high resolution structure. To map the interface between Ubc13 and Mms2, two

heterodimer complexes were prepared *in situ*: one containing ^{15}N-Ubc13 with unlabeled Mms2, and the other containing ^{15}N-Mms2 with unlabeled Ubc13. The Ubc13/Mms2 heterodimerization (34 kDa) proceeds efficiently upon equimolar addition of each protein, and results in the formation of a stable complex that remains associated during high-resolution size-exclusion chromatography (*27*). Residues whose backbone amide ^{1}H and ^{15}N chemical shifts exhibited a perturbation upon complex formation were identified, and quantified in terms of the total change in chemical shift, $\Delta\delta_{total}$. The major $\Delta\delta_{total}$ upon heterodimerization for either ^{15}N-Mms2 or ^{15}N-Ubc13 are associated with residues found at the heterodimer interface (Fig. 4.3B, 4.4B), indicating the similarity of this interface in both the crystalline and solution phases. Residues resulting in the greatest effect on $\Delta\delta_{total}$ for interactions within the heterodimer or between the heterodimer and Ub (see below) have been summarized in Figure 4.5 according to sequence and secondary structure.

In the case of ^{15}N-Mms2, the major changes to $\Delta\delta_{total}$ upon heterodimerization are associated with residues found at the heterodimer interface (Fig. 4.6A). These include: Val^{7} and Val^{9} in the N-terminal extension, Val^{12}, Ala^{13}, Arg^{14}, Glu^{17}, Glu^{18}, Glu^{20}, Gly^{22}, Lys^{24} in the α1 helix, and Leu^{35}, Glu^{36}, Asp^{37}, Glu^{39}, Asp^{40}, Met^{41}, Thr^{42} situated in the loop connecting strands β1 and β2. No other significant $\Delta\delta_{total}$ were observed, apart from a few residues (Val^{26}, for example) that undergo structural rearrangement, but are not found within the dimer interface. From these observations, it is apparent that the NMR-derived footprint of the Mms2 portion of the binding interface corresponds well to that of the X-ray crystallographic structure (*26*).

In the case of ^{15}N-Ubc13, the major changes to $\Delta\delta_{total}$ upon heterodimerization are also associated with residues found at the heterodimer interface (Fig. 4.6B). These include the solvent-exposed face formed by strands β2 to β4 (Arg^{33}, Tyr^{34}, Leu^{56}, Phe^{57}, Arg^{70}, Phe^{71}), the loop L1 (Asp^{28}, Glu^{29}, Ser^{30}, Ala^{32}) and the loop L4 (Met^{72}, Lys^{74}, Ile^{75}, Tyr^{76}, Asp^{81}, Lys^{82}, Leu^{83}, Gly^{84}, and
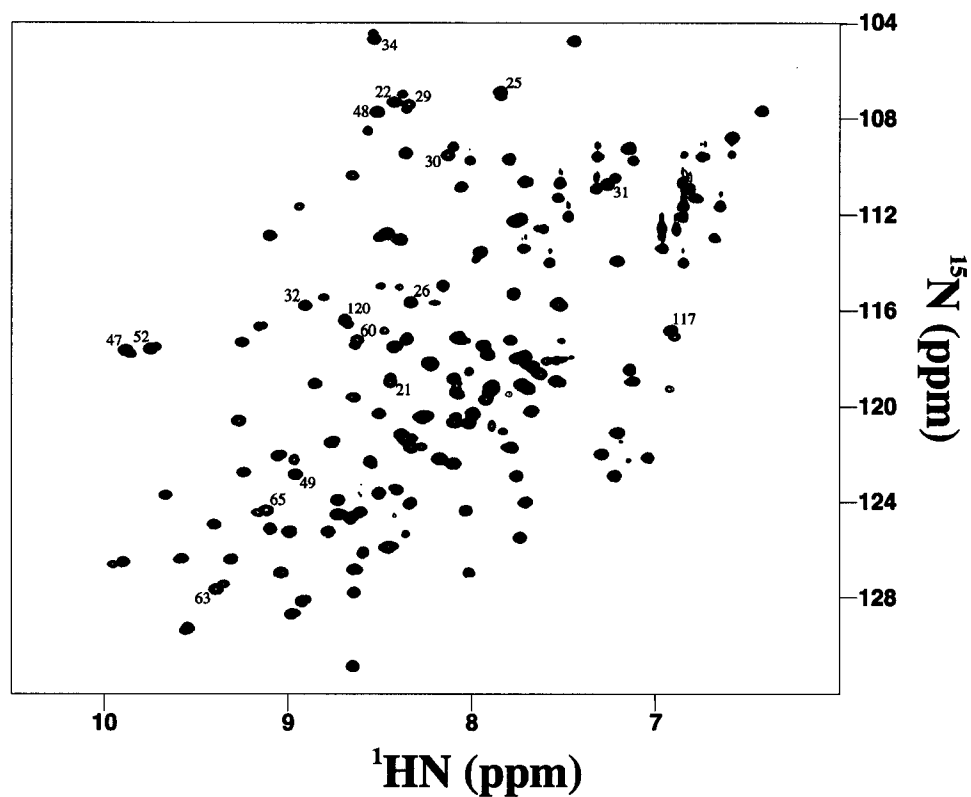
Figure 4.2 Superposition of ^{1}H-^{15}N HSQC spectra of ^{15}N-labeled Mms2, free and in complex with Ub. ^{1}H-^{15}N HSQC NMR spectra resulting from either ^{15}N-Mms2 (black), or ^{15}N-Mms2 and Ub (red) are overlaid, and a number of representative backbone amide cross-peaks which are affected by complex formation are labeled.
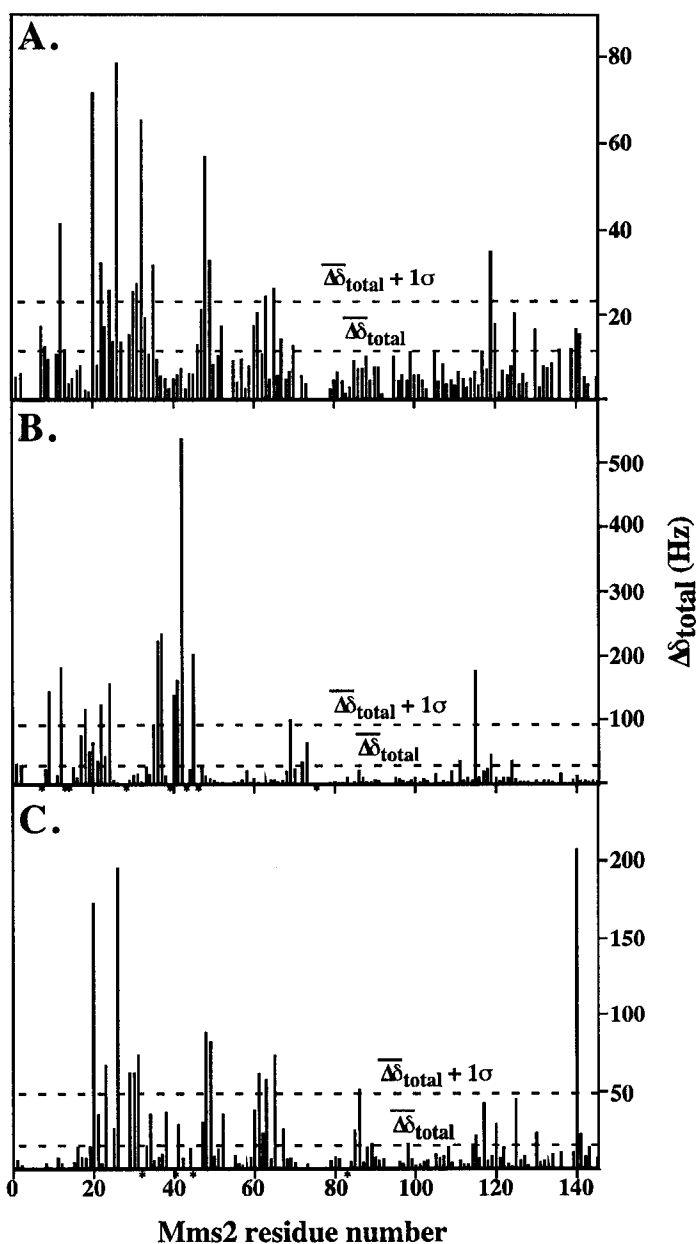
Figure 4.3 Binding-induced NMR chemical shift perturbation analysis of Mms2 with Ub. Comparison of backbone amide ^1H and ^{15}N chemical shift of Mms2 in the absence or presence of (A) Ub and (B) Ubc13, or (C) the comparison between ^{15}N-Mms2/Ubc13 heterodimer and this heterodimer in the presence of Ub. The total change in chemical shift, $\Delta\delta_{total}$, was calculated for Mms2 interacting with various binding partners and plotted as a function of primary amino acid sequence. Dashed lines represent the average change in $\Delta\delta_{total}$ and one standard deviation unit above this average. Residues whose change in chemical shift could not be identified are indicated with an asterisk (*).
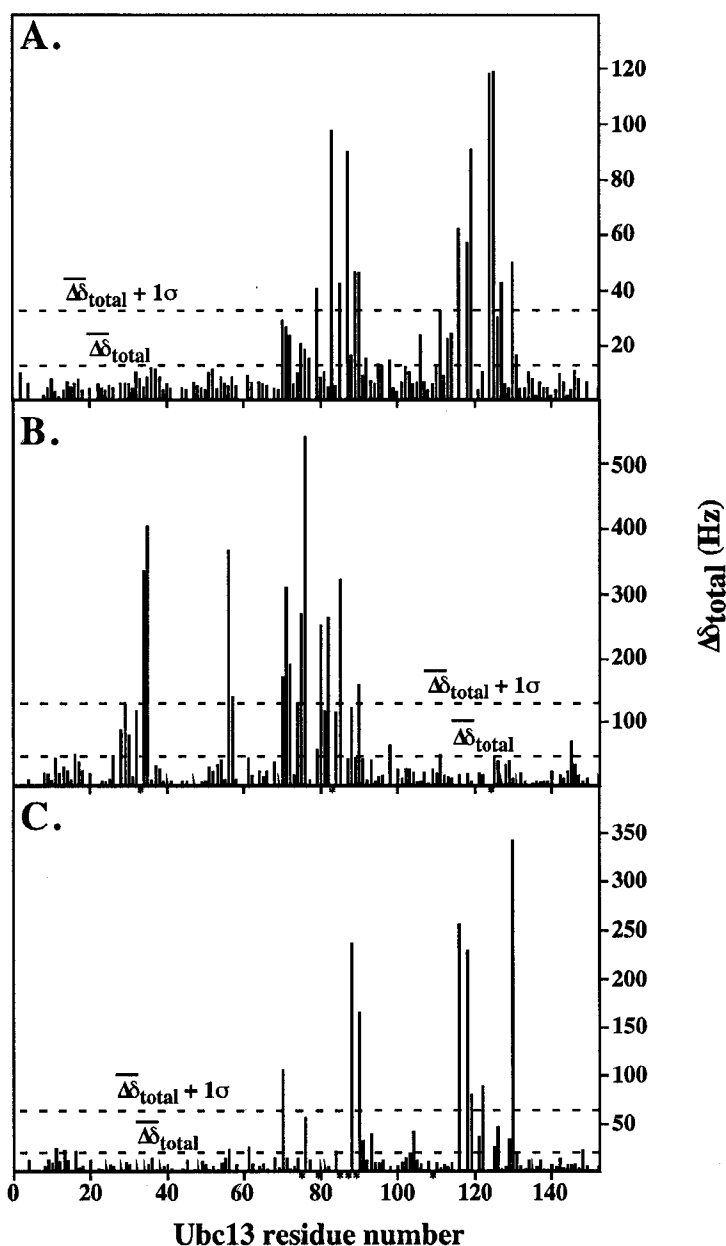
Figure 4.4   Binding-induced NMR chemical shift perturbation analysis of Ubc13 with Ub. Comparison of backbone amide ^{1}H and ^{15}N chemical shifts of Ubc13 in the absence or presence of (A) thiolester-linked Ub and (B) Mms2, or (C) the comparison between Mms2/^{15}N-Ubc13 heterodimer and the heterodimer in the presence of thiolester-linked Ub.   The total change in chemical shift, $\Delta\delta_{total}$, was calculated for Mms2 interacting with various binding partners and plotted as a function of primary amino acid sequence.   Dashed lines represent the average change in $\Delta\delta_{total}$ and one standard deviation unit above this average.   Resdiues whose change in chemical shift could not be identified are indicated with an asterisk (*).

Figure 4.5 Sequence alignments of the important interfacial residues in Ubc13 and Mms2 as determined by ^{1}H-^{15}N HSQC NMR chemical shift perturbation. Residues experiencing the greatest $\Delta\delta_{total}$ upon formation of Mms2/Ubc13 heterodimer are colored in yellow and blue respectively, and are compared with interfacial residues in the crystal structure (boxed) (26). Mms2 residues experiencing the most significant $\Delta\delta_{total}$ upon formation of non-covalent interaction with Ub are labeled in red, as are residues in Ubc13 upon formation of the thiolester adduct with Ub. For comparison, residues deemed responsible for interaction between yeast Ubc1 and Ub in the thiolester complex are also colored red (38).

Figure 4.6 Surfaces of interaction in the Ubc13/Mms2 heterodimer. Ribbon presentation of the Ubc13/Mms2 backbone in which residues affected by heterodimer formation are colored using a linear gradient from white ($\Delta\delta_{total}=0$) to dark red ($\Delta\delta_{total} \geq \Delta\delta_{total(av)+1\sigma}$ as determined by ^{1}H-^{15}N HSQC NMR chemical shift perturbation (see Fig. 4.3B and 4.4B). Residues whose $\Delta\delta_{total}$ could not be determined unambiguously due to broadening or extreme changes in chemical shift are colored orange. The active-site Cys[87] of Ubc13 is colored in green as a point of reference. (A) Interaction surface of ^{15}N-Mms2 (top) with unlabeled Ubc13 (yellow, bottom). (B) Interaction surface of ^{15}N-Ubc13 (bottom) with unlabeled Mms2 (blue, top).

Arg[85]). Interestingly, regions that precede and follow the active-site Cys of Ubc13 (Cys[87]), also show significant changes to $\Delta\delta_{total}$ (Leu[83], Gly[84], Arg[85], Leu[88], Ile[90]), indicative of a change in chemical environment (see Discussion).

4.4.2 The non-covalent interaction between Mms2 and Ub

Mms2 and Ubc13 have each been observed to exist in a monomeric state and in a heterodimeric state (23, 27), whereas homodimerization has not been observed. Therefore an examination of the non-covalent interaction between Ub and the Mms2 subunit is of interest. The chemical shift perturbations that result from the interaction of the ^{15}N-Mms2 subunit with unlabeled acceptor Ub are shown in Figure 4.3A. The greatest effects on $\Delta\delta_{total}$ upon interaction with Ub are observed at the N-terminal portion of Mms2. Specifically, the affected residues are located in helix $\alpha 1$ (Glu[20], Gly[22], Lys[24]), sections of strand $\beta 1$ (Val[31], Ser[32], Leu[35]), strand $\beta 2$ (Thr[47], Gly[48], Met[49]), strand $\beta 3$ (Tyr[63], Leu[65]), helix $\alpha 2$ (Leu[119]) as well as the loop joining helix $\alpha 1$ to strand $\beta 1$ (Val[26], Thr[30]). Intermediate effects on $\Delta\delta_{total}$ are found close in sequence to the greatest changes and include the C-terminal portion of $\alpha 1$ (Gln[23]), sections of $\beta 1$ (Trp[33]), $\beta 2$ (Trp[46]), L2 prior to $\beta 3$ (Asn[60], Arg[61]), $\beta 3$ (Val[67], Gly[70]) and the loop joining $\alpha 1$ to $\beta 1$ (Gly[25], Gly[27], Gly[29]). Intermediate changes are also found in $\alpha 2$ (Gln[120], Leu[125], Glu[130]) and the C-terminus (Gly[140], Gln[141]).

As expected, many of the residues in Mms2 that exhibit the greatest backbone amide chemical shift perturbations are located on the surface of the protein, and contain surface exposed side chains that may be involved in non-covalent interactions with Ub (Fig. 4.7A). These residues cluster onto one face of Mms2, forming three distinct patches. Interestingly, no significant changes in chemical shift were observed for residues on the opposite surface of Mms2. The first patch is perpendicular to the Ubc13/Mms2 interface, and is composed of residues at the C-terminal end of $\alpha 1$ and the loop that joins $\alpha 1$ to $\beta 1$ (Glu[20], Glu[21], Gly[22], Gln[23], Lys[24], Gly[25], Val[26], Gly[27], Gly[29], Val[31]), portions of $\beta 1$ (Ser[32], Trp[33],

Leu^{35}), β2 (Thr^{47}, Gly^{48}, Met^{49}), and β3 (Arg^{61}, Tyr^{63}, Leu^{65}). The second patch is found at the C-terminal portion of Mms2 (Glu^{139}, Gly^{140}, Met^{141}). Notably, the total surface area of both these Mms2 patches corresponds well with the complementary patch on Ub that has previously been demonstrated to interact with Mms2 (27). Additionally, the combined electrostatic surface potential of the Mms2 patches is complementary to that found on Ub (Fig. 4.7C). Interestingly, the third patch involves Mms2 residues that would normally interact with Ubc13 in the heterodimer, and include Val^{7}, Lys^{8}, (greatest $\Delta\delta_{total}$) and other N-terminal amino acids of Mms2 (intermediate $\Delta\delta_{total}$).

Our previous findings indicated that the Ub contact surface with Mms2 remained largely the same when alone or in complex with Ubc13 (27). When we next examined the ^{15}N-Mms2–Ub interaction as a heterodimer with Ubc13 we similarly found that the Mms2 residues that undergo change on Ub binding closely parallel those of the individual subunit with some notable exceptions (Fig. 4.3C). As with Mms2 alone, many of the major $\Delta\delta_{total}$ are found near the C-terminus of α1 (Glu^{20}, Gln^{23}), the loop that joins it to β1 (Val^{26}, Gly^{29}, Thr^{30}), β1 (Val^{31}), β2 (Gly^{48}, Met^{49}), and β3 (Arg^{61}, Tyr^{63}, Leu^{65}). Residues with intermediate values of $\Delta\delta_{total}$ are also similar, including α1 (Leu^{19}, Glu^{21}), the loop joining α1 to β1 (Gly^{25}), β1 (Trp^{33}, Gly^{34}), β2 (Thr^{47}, Gly^{52}), β3 (Asn^{60}, Ile^{62}, Val^{67}), α2 (Ser^{114}, Ile^{115}, Val^{117}, Gln^{120}, Leu^{125}, Glu^{130}), and the C-terminus (Gln^{141}). The backbone amide ^{1}H-^{15}N HSQC NMR cross peaks for three residues [L1 (Asp^{37}) and β2 (Arg^{45}, Ile^{50})] either experienced large changes in chemical shift, rendering identification difficult, or their intensities were severely diminished due to line-broadening as a result of complex formation.

In contrast to the Mms2 subunit alone, none of the N-terminal residues situated at the heterodimer interface undergo significant change upon Ub binding, whereas significant change is detected within L1 (Asp^{38}, Asp^{40}, Met^{41}, Arg^{45}). Notably, the region surrounding the vestigial active site of Mms2 does not appear to play a role in Ub binding. This result clearly distinguishes the Mms2-Ub
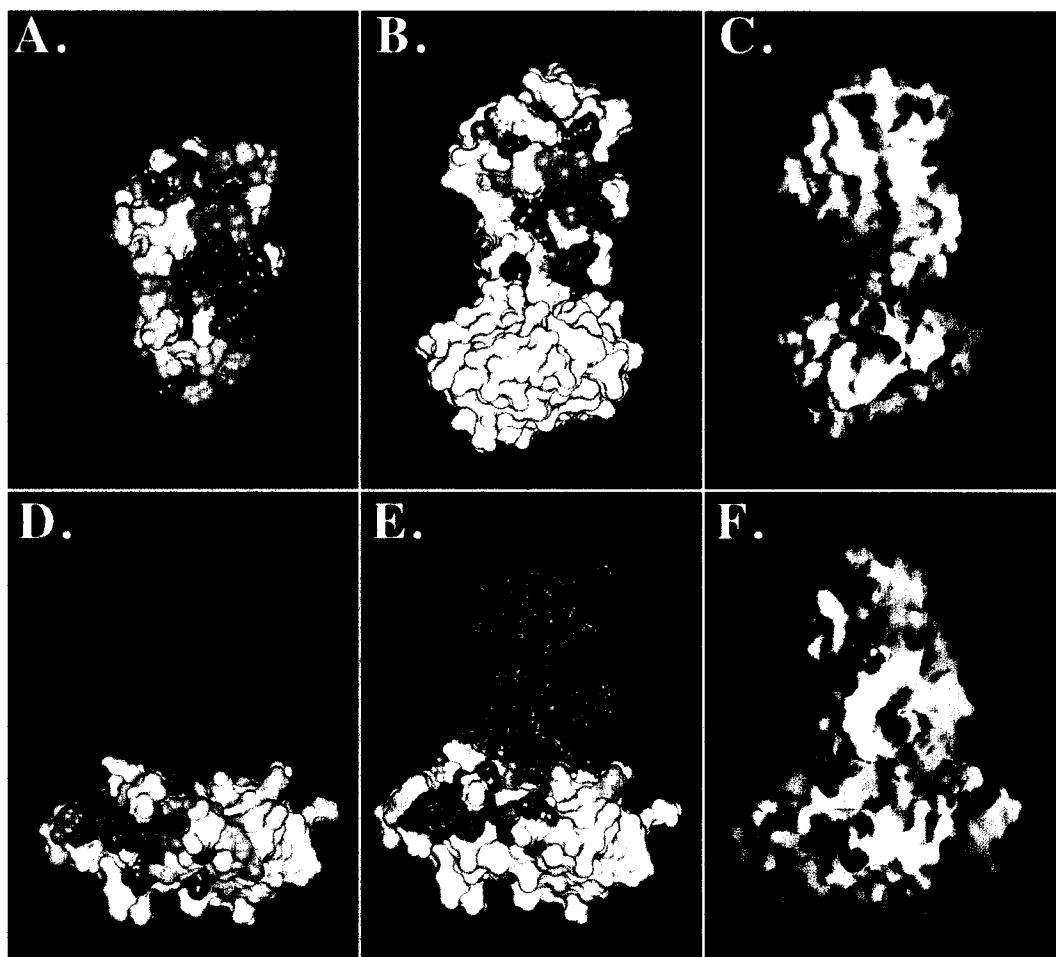
Figure 4.7 Connolly surface of the binding interfaces on Mms2 or Ubc13 upon interaction with Ub. The surface of Mms2 is presented either (A) alone, or (B) in the context of Mms2/Ubc13 heterodimer (Ubc13, yellow). The surface of Ubc13 is presented either (D) alone, or (E) in the context of Mms2/Ubc13 heterodimer (Mms2, blue). Residues affected by non-covalent interaction with Ub are colored with a linear gradient from white ($\Delta\delta_{total}=0$) to dark red ($\Delta\delta_{total}\geq\Delta\delta_{total(av)+1\sigma}$) (see Fig. 4.3 and 4.4). Residues whose $\Delta\delta_{total}$ could not be determined unambiguously due to broadening or extreme changes in chemical shift are colored orange. The active-site Cys[87] of Ubc13 is colored green as a point of reference. Electrostatic surface potential of the Mms2/Ubc13 heterodimer (C) and (F) shown in the same orientation as (B) and (E) respectively. The relative electrostatic potentials are displayed as a linear gradient, from acidic (-10, red), to neutral (0,white), to basic (+10, blue) as determined by the program GRASP.

interaction from other previously reported E2-Ub interactions. The changes in the surface characteristics of the Mms2 component of the heterodimer upon Ub binding are shown in Fig. 4.7B.

4.4.3 The interaction between Ubc13 and thiolester-linked Ub

The major changes to the ^{15}N-Ubc13 subunit that result from thiolester formation with Ub are found in and around the active-site (Cys^{87}) (Fig. 4.4A). These include: the active-site Cys itself, L4 (Asn^{79}, Leu^{83}, Arg^{85}) to the N-terminal side of Cys^{87}, the 3_{10} helix C-terminal to Cys^{87} (Asp^{89}, Ile^{90}), the loop preceding helix α3 (Leu^{111}, Asn^{116}, Asp^{118}, Asp^{119}), and helix α3 (Asp^{124}, Val^{125}, Glu^{127}, Lys^{130}). Intermediate perturbations of $\Delta\delta_{total}$ are found around and inter-digitated with the major changes described above. These include: L4 (Met^{72}, Ile^{75}, Tyr^{76}, His^{77}), near the active site (Leu^{88}), the 3_{10} helix (Lys^{92}, Trp^{95}, Ser^{96}, Ala^{98}), the loop preceding α3 (Ser^{113}, Ala^{114}), and α3 (Ala^{126}, Thr^{131}).

Heterodimerization of ^{15}N-Ubc13 with Mms2 results in somewhat less $\Delta\delta_{total}$ upon thiolester formation when compared with the thiolester formed with ^{15}N-Ubc13 alone (Fig. 4.4C when compared to 4.4A). It is noted, however, that a number of cross peaks in the ^{1}H-^{15}N HSQC NMR spectra of the heterodimer thiolester remain unassigned due to line broadening or large changes in chemical shift upon complex formation. The major and intermediate changes to $\Delta\delta_{total}$ occur within secondary structural regions including L4 (Lys^{74}, Ile^{75}, Tyr^{76}, His^{79}, Leu^{83}, Gly^{84}, Arg^{85}), the active-site (Cys^{87}), the 3_{10} helix (Leu^{88}, Asp^{89}, Ile^{90}, Leu^{91}, Asp^{93}), the loop preceding α3 helix (Asn^{116}, Asp^{118}, Leu^{121}, Ala^{122}, Asp^{124}) and the α3 helix (Val^{125}, Ala^{126}, Trp^{129}, Lys^{130}, Thr^{131}).

Surfaces involved in the interaction between Ubc13 and its thiolester-linked Ub were determined by mapping the major $\Delta\delta_{total}$ for the ^{15}N-Ubc13 subunit alone or in complex with Mm2s onto a surface projection of the Ubc13 crystal structure (Fig. 4.7D,E). In the absence of Mms2 (Fig. 4.7D), the greatest effect is found around the active site (Cys^{87}) where the majority of affected residues have

solvent exposed side chains [L4: (Arg[70], Leu[83], Arg[85], Ile[86], Cys[87], Asp[89]), α2: (Leu[106], Gln[109], Ala[110], Leu[111]), α3 and preceding loop: (Asn[116], Asp[118], Asp[119], Asp[124], Ala[126], Glu[127], Lys[130])].

From Figure 4.7E, it is apparent that Ubc13 exhibits a similar Ub dependent pattern of backbone amide chemical shift changes when present with Mms2. Significantly, all of the solvent exposed residues important in thiolester formation present themselves on only one face of the Ubc13 molecule regardless of dimerization state. We conclude from these results that residues mediating the Ubc13~Ub thiolester interaction is largely unaffected by the presence or absence of Mms2. These results are consistent with our previous NMR experiments demonstrating that both the C-terminal tail and a slightly basic surface on Ub form contacts with Ubc13 within the Ubc13~Ub thiolester regardless of the presence of Mms2 (27).

4.4.4 Modeling the tetramer

The soft-docking algorithm BiGGER (33, 34) was employed to generate models for the Ubc13/Mms2/Ub$_2$ tetramer based on geometric complementarity, electrostatic interactions, desolvation energy, and the pair wise propensities of amino acid side chains to interact across interfaces. Surface residues from the heterodimer (results presented herein) and Ub (section 2.4.6), that exhibited the greatest change to $\Delta\delta_{total}$ upon complex formation were incorporated as constraints into the BiGGER docking program (Fig. 4.8). The C-terminus of the donor Ub was not covalently linked to the active site of Ubc13. The top ten structures based on these criteria were subsequently averaged, and the resulting structure was subjected to energy minimization using the INSIGHTII suite of programs. The final structure of the model is shown in Figure 4.9.

The non-covalent interaction between acceptor Ub and the heterodimer involves primarily hydrophobic contacts between Ub and Mms2. The surface exposed residues of the β-sheet of the acceptor Ub, and the loops connecting strands within the sheet, constitute the contact interface with Mms2, while Mms2
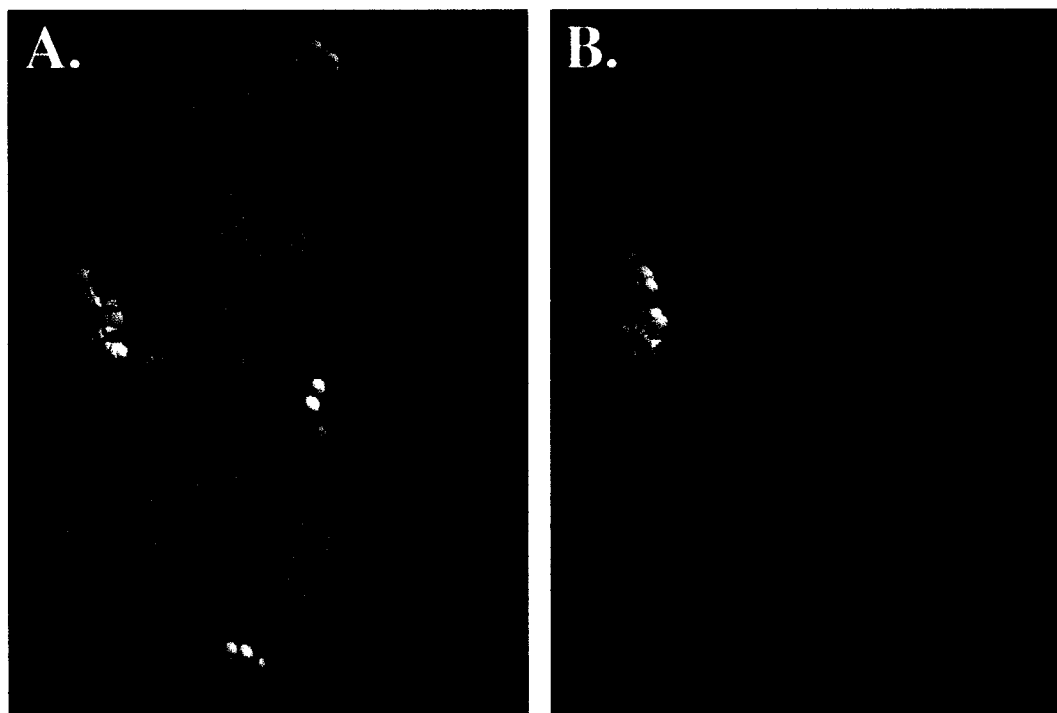
Figure 4.8 Molecular modeling of the non-covalent interaction between the Ubc13/Mms2 heterodimer and Ub. (A) The BiGGER soft-docking algorithm, in combination with the unbound structures of Ub (probe) and the Ubc13/Mms2 heterodimer (target) was used to generate 5000 potential solutions based on a combination of factors including geometric complementarity, electrostatic interactions, desolvation energy, and the pariwise propensities of side chains to interact across molecular interfaces. The heterodimer structure (blue sticks) is shown relative to the center of mass of the top 100 solutions (spheres), which are colored from green to red as the score of the solution increases. (B) The top 100 solutions when in addition to the scheme presented in (A), NMR constraints based on $\Delta\delta_{total}$ results are incorporated, demonstrating a single Ub binding site.
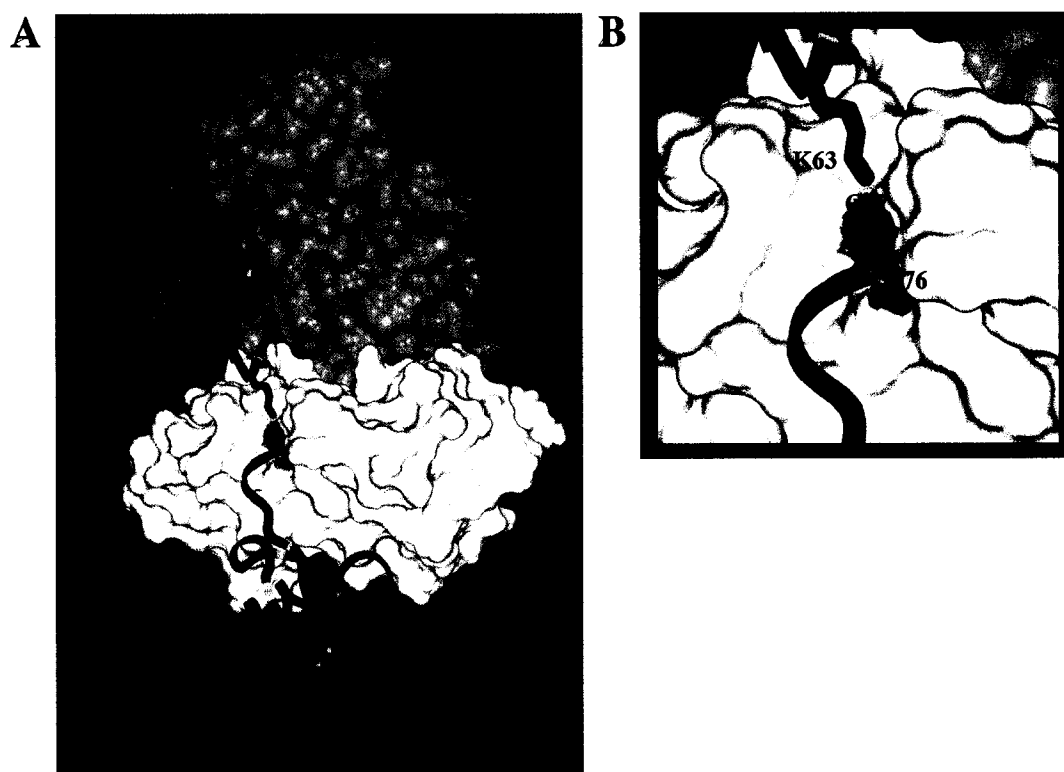
Figure 4.9 NMR-derived model of the tetrameric Ub-conjugating enzyme complex. (A) The surfaces of interaction between either acceptor (top) or donor (bottom) Ub molecules (red, ribbon) and the Ubc13 (yellow)/Mms2 (blue) heterodimer are presented. Of specific interest is the active-site Cys^{87} of Ubc13 (green), Lys^{63} of the acceptor Ub (purple), and Gly^{76} of the donor Ub (purple). Residues hypothesized to represent the RING E3 binding domain are colored in white. The NMR-derived model was determined using the BiGGER docking algorithm and the INSIGHTII suite of programs as described in the Experimental section of this chapter. (B) Close-up of the model in the region surrounding Cys^{87} of Ubc13.

residues that contact the acceptor Ub are found in $\alpha 1, \beta 1, \beta 2$, and the loops connecting these secondary structural elements. The Mms2 surface involved in the interaction is located opposite to that containing the vestigial active site. The donor Ub makes contacts with Ubc13 through C-terminal residues 70-76, as well as some residues in $\beta 1$ and $\beta 3$. The Ubc13 residues that form contacts with the C-terminus of donor Ub are found within the active site, the loops preceding it, and residues in $\alpha 2$.

4.5 DISCUSSION

The NMR chemical shift perturbation results have been interpreted to produce a model of the tetramer using a molecular docking strategy that is tailored to this NMR-based approach. The accepting Ub molecule sits on a concave face of Mms2, a distinctive feature of both E2s and Uevs, with its C-terminal tail far removed from the vestigial active site of Mms2. In combination with Ubc13, the concave face of Mms2 narrows to form a channel or funnel as it approaches the active-site of Ubc13. The side-chain of Lys[63] for the acceptor Ub lies within this channel, placing the ε-nitrogen within 3 Å of the sulphur atom contained within the active-site Cys of Ubc13. The interaction between the accepting Ub and the heterodimer buries 2792 Å^2 of surface area, a rather large value in light of our observation that the interaction between the two is weak (K_D ~100 μM, see Chapter 5). The model likely overestimates the buried surface area of the acceptor Ub because the imposed chemical shift restraints force the contact regions to be maximized and may include residues that are affected indirectly through induced structural changes in the proteins.

There are two features of the accepting Ub-heterodimer interface that bear directly on its biochemical function. First, the C-terminal tail of the acceptor is neither constrained nor sterically hindered, raising the likelihood that it can serve as the poly-Ub chain anchor in either the free form or when attached to an appropriate protein target. Second, Lys[48] of the acceptor is buried within the

protein-protein interface, thereby excluding this residue as a potential site for chain assembly of the canonical type.

The donor Ub interacts exclusively with a hydrophobic concave surface that narrows to an acidic cleft on Ubc13 and culminating with the active-site Cys (Fig. 4.7F). The tail of the donor Ub lies within the active site cleft of the E2 placing the C-terminal carboxyl carbon of Gly[76], the active site sulphur and the ε-nitrogen of Lys[63] for the acceptor Ub molecule within 3.5 Å of each other.

In terms of the position and orientation of the components, the model presented here agrees moderately well with that proposed by VanDemark *et al.* (*25*) for the *S. cerevisiae* complex. It differs significantly however, from the model proposed by Pornillos *et al.* (*37*) who examined the non-covalent interaction between the human Tsg101 Uev domain and Ub by a similar approach to the one used here. The structural differences between the Ub-Mms2 interaction and Ub-Tsg101 interaction results from the presence of an extended β-hairpin that links strands 1 and 2 in Tsg101 that sequester Ub. The fact that this motif is absent in Mms2 illustrates that Uevs have evolved different strategies for Ub binding.

Our high confidence in this model stems from the NMR-constrained docking approach used here. The docking algorithm BiGGER is particularly well suited for these analyses because of its ability to use NMR chemical shift perturbation results as information to filter suitable models (*33, 34*). The BiGGER docking algorithm requires no information that constrains the orientation of the docking partners, and therefore represents a fairly unbiased approach for using NMR data to model the tetramer interactions. The validation of this approach lies in the predicted positions of the three atoms involved in linking the C-terminus of the donor Ub molecule to Lys[63] of the accepting Ub molecule: 1) the Cys sulfur atom of the Ubc13 active site, 2) The Gly[76] carboxyl group of the Ub donor molecule, and 3) the Lys[63] ε-nitrogen of the accepting Ub molecule. Each of these atoms are positioned within 3.5 Å of each other (Fig. 4.9).

The model presented here also agrees well with the findings of a previous mutagenesis study that used the *S. cerevisiae* Ubc13/Mms2 heterodimer (*25*). A Ubc13 substitution (Ala^{110}Arg) located on the surface of α3 near the center of the predicted interaction between Ubc13 and the donor Ub resulted in a 4-fold reduction in the rate of isopeptide bond formation. A Ubc13 substitution (Asp^{81}Ala) situated nearby the predicted position of Lys^{63} of the accepting Ub resulted in a diminished affinity of the acceptor Ub for the heterodimer *in vitro*. A Ub substitution (Ile^{44}Ala) located in the NMR-derived surface for the acceptor but not donor, results in reduced binding of Ub to the acceptor site on Mms2, whereas the interaction with Ubc13 remains unaffected. Conversely, an Mms2 substitution (Glu^{12}Arg) situated near the heterodimer interface but not predicted by the model to play a role in acceptor Ub binding, does not weaken the interaction of the acceptor Ub with the heterodimer *in vitro* (*25*).

The structure of the Ubc13~Ub thiolester presented here holds features in common with the models for the Ubc1~Ub thiolester from *S. cerevisiae* (*38, 39*) and the human Ubc2b~Ub serine ester (*36*), each derived by similar NMR-based approaches. All three E2s employ a common thiolester-binding motif (L4 around the active site, regions of α2, and the loop that joins α2 to α3) that constrains the C-terminal tail similarly amongst models. In contrast, the folded domain of Ub is positioned slightly differently on the each of the three E2s (Fig. 4.5). These differences are likely explained by properties associated with catalysis. The tail of the Ub donor must be bound to the E2 strongly enough to secure its alignment during isopeptide bond formation with the target, yet weakly enough to assure efficient transfer and subsequent turnover of the E2. E2 interactions with the rest of the Ub globular domain are therefore likely to be even weaker and can be imagined to vary significantly by differences of a few key surface residues from one E2 to the next.

An examination of high-resolution E2 structures has revealed that the active-site is part of an unstructured loop (*38, 40-46*). Our previous and present findings suggest that the interaction of Mms2 with Ubc13 alters the activity of

Ubc13 by altering the conformation of the Ubc13 active-site. We have previously shown that when Mms2 binds to Ubc13, both the rate of Ub thiolester formation with Ubc13 (reduced 2-fold in the presence of Mms2) and the stability of the resulting thiolester are measurably affected *in vitro* (Chapter 2). This observation raises the intriguing possibility that the interaction of an E2 with other proteins could order the loop in a particular conformation, thereby modulating its catalytic activity.

An examination of the chemical shift perturbation data reveals that there is communication between the acceptor and donor Ub binding sites. This is reflected by a change in chemical environment at residues that are known to play a key role in the active-site loop. For instance, residues in the active-site cleft of Ubc13 (Leu^{83}, Gly^{84}, Arg^{85}, Leu^{88}, Ile^{90}), show significant values of $\Delta\delta_{total}$ upon dimerization with Mms2. Three of these residues (Leu^{83}, Gly^{84}, and Arg^{85}) are directly involved in the heterodimer interface, whereas two of these residues (Leu^{88} and Ile^{90}) are remote from the interface. In addition, Ub thiolester formation within the heterodimer results in a significant shift of $\Delta\delta_{total}$ for the interfacial residues Leu^{83} and Arg^{85}. This observation suggests that the communication between the heterodimer interface and the active site is in fact occurring, that is, altering the interface alters the active site and *vice versa*. These results appear to be in contrast with those previously reported for *S. cerevisiae* Ubc13/Mms2, for which there appears to be little communication between the dimer interface and the active site. An RMSD of 0.8 Å for superimposition of all backbone C^{α} atoms between free and Mms2-bound Ubc13 was reported, with the active site cleft little changed (*25*). However, as chemical shift changes cannot be directly converted into 3D structural changes, further analyses will be required to establish the extent of similarities and differences between the human and *S. cerevisiae* protein complexes.

The arrangement of the four molecules within the tetramer poses no obvious steric problem for the interaction of Ubc13 with its functionally specific E3, Traf6. The interface between Ubc13 and Traf6 can be predicted on the basis

of the X-ray crystallographic structure for the E2-E3 complex UbcH7-c-Cbl (*47*). Both c-Cbl and Traf6 contain E2-binding RING-finger domains that share significant sequence identity. Traf6 likely sits on an 11-residue patch of Ubc13, with six residues identical to those employed by UbcH7 in its interaction with c-Cbl (Fig. 4.9A). Notably, none of these residues are involved in forming contacts between Ub and Ubc13.

Despite its small size and highly conserved fold, the E2 core domain family is apparently the centerpiece for several distinct biochemical functions that hinge on isopeptide bond formation. These functions include both target ubiquitination and the synthesis of multi-Ub chains that differ from one another in configuration. As a consequence of unknown evolutionary pressure, these proteins have apparently modeled and remodeled their surfaces with great economy and creativity. The functional repertoire of protein ubiquitination has been expanded by the ability of these proteins to interact with common or related partners in fundamentally different ways. This point is underscored in part by the present work. The E2 core fold has evolved at least two relevant and fundamentally different modes of Ub binding. Furthermore, the juxtaposition of these modes, through the interaction of a catalytically active fold with an inactive fold, provides the structural basis for Lys[63] multi-Ub chain synthesis.

4.6 REFERENCES

1. Hochstrasser, M. (1996) *Annu Rev Genet 30*, 405-39.

2. Glickman, M. H., and Ciechanover, A. (2002) *Physiol Rev 82*, 373-428.

3. Peters, J.-M., King, R.W., Deshaies, R.J. (1998) *Ubiquitin and the Biology of the Cell*, Plenum Press, New York.

4. Jentsch, S., McGrath, J. P., and Varshavsky, A. (1987) *Nature 329*, 131-4.

5. Finley, D., Bartel, B., and Varshavsky, A. (1989) *Nature 338*, 394-401.

6. Chen, Z., Hagler, J., Palombella, V. J., Melandri, F., Scherer, D., Ballard, D., and Maniatis, T. (1995) *Genes Dev 9*, 1586-97.

7. Hicke, L., and Riezman, H. (1996) *Cell 84*, 277-87.

8. Chen, Z. J., Parent, L., and Maniatis, T. (1996) *Cell 84*, 853-62.

9. Chau, V., Tobias, J. W., Bachmair, A., Marriott, D., Ecker, D. J., Gonda, D. K., and Varshavsky, A. (1989) *Science 243*, 1576-83.

10. Arnason, T., and Ellison, M. J. (1994) *Mol Cell Biol 14*, 7876-83.

11. Johnson, E. S., Ma, P. C., Ota, I. M., and Varshavsky, A. (1995) *J Biol Chem 270*, 17442-56.

12. Spence, J., Sadis, S., Haas, A. L., and Finley, D. (1995) *Mol Cell Biol 15*, 1265-73.

13. Baboshina, O. V., and Haas, A. L. (1996) *J Biol Chem 271*, 2823-31.

14. Koegl, M., Hoppe, T., Schlenker, S., Ulrich, H. D., Mayer, T. U., and Jentsch, S. (1999) *Cell 96*, 635-44.

15. Galan, J. M., and Haguenauer-Tsapis, R. (1997) *Embo J 16*, 5847-54.

16. Springael, J. Y., Galan, J. M., Haguenauer-Tsapis, R., and Andre, B. (1999) *J Cell Sci 112 (Pt 9)*, 1375-83.

17. Spence, J., Gali, R. R., Dittmar, G., Sherman, F., Karin, M., and Finley, D. (2000) *Cell 102*, 67-76.

18. Deng, L., Wang, C., Spencer, E., Yang, L., Braun, A., You, J., Slaughter, C., Pickart, C., and Chen, Z. J. (2000) *Cell 103*, 351-61.

19. Wang, C., Deng, L., Hong, M., Akkaraju, G. R., Inoue, J., and Chen, Z. J. (2001) *Nature 412*, 346-51.

20. Broomfield, S., Chow, B. L., and Xiao, W. (1998) *Proc Natl Acad Sci U S A 95*, 5678-83.

21. Hofmann, R. M., and Pickart, C. M. (1999) *Cell 96*, 645-53.

22. Brusky, J., Zhu, Y., and Xiao, W. (2000) *Curr Genet 37*, 168-74.

23. Ulrich, H. D., and Jentsch, S. (2000) *Embo J 19*, 3388-97.

24. Hoege, C., Pfander, B., Moldovan, G. L., Pyrowolakis, G., and Jentsch, S. (2002) *Nature 419*, 135-41.

25. VanDemark, A. P., Hofmann, R. M., Tsui, C., Pickart, C. M., and Wolberger, C. (2001) *Cell 105*, 711-20.

26. Moraes, T. F., Edwards, R. A., McKenna, S., Pastushok, L., Xiao, W., Glover, J. N., and Ellison, M. J. (2001) *Nat Struct Biol 8*, 669-73.

27. McKenna, S., Spyracopoulos, L., Moraes, T., Pastushok, L., Ptak, C., Xiao, W., and Ellison, M. J. (2001) *J Biol Chem 276*, 40120-6.

28. Kay, L. E., Keifer, P., Saarinen, T. (1992) *J. Am. Chem. Soc. 114*, 10663-10665.

29. Zhang, O., Kay, L. E., Olivier, J. P., and Forman-Kay, J. D. (1994) *J Biomol NMR 4*, 845-58.

30. Delaglio, F., Grzesiek, S., Vuister, G. W., Zhu, G., Pfeifer, J., and Bax, A. (1995) *J Biomol NMR 6*, 277-93.

31. Johnson, B. A., Blevins, R.A. (1994) *J. Chem. Phys. 29*, 1012-1014.

32. McKay, R. T., Tripet, B. P., Hodges, R. S., and Sykes, B. D. (1997) *J Biol Chem 272*, 28494-500.

33. Palma, P. N., Krippahl, L., Wampler, J. E., and Moura, J. J. (2000) *Proteins 39*, 372-84.

34. Morelli, X. J., Palma, P. N., Guerlesquin, F., and Rigby, A. C. (2001) *Protein Sci 10*, 2131-7.

35. Vijay-Kumar, S., Bugg, C. E., Wilkinson, K. D., Vierstra, R. D., Hatfield, P. M., and Cook, W. J. (1987) *J Biol Chem 262*, 6396-9.

36. Miura, T., Klaus, W., Gsell, B., Miyamoto, C., and Senn, H. (1999) *J Mol Biol 290*, 213-28.

37. Pornillos, O., Alam, S. L., Rich, R. L., Myszka, D. G., Davis, D. R., and Sundquist, W. I. (2002) *Embo J 21*, 2397-406.

38. Hamilton, K. S., Ellison, M. J., Barber, K. R., Williams, R. S., Huzil, J. T., McKenna, S., Ptak, C., Glover, M., and Shaw, G. S. (2001) *Structure (Camb) 9*, 897-904.

39. Hamilton, K. S., Ellison, M. J., and Shaw, G. S. (2000) *J Biomol NMR 18*, 319-27.

40. Cook, W. J., Jeffrey, L. C., Xu, Y., and Chau, V. (1993) *Biochemistry 32*, 13809-17.

41. Cook, W. J., Martin, P. D., Edwards, B. F., Yamazaki, R. K., and Chau, V. (1997) *Biochemistry 36*, 1621-7.

42. Tong, H., Hateboer, G., Perrakis, A., Bernards, R., and Sixma, T. K. (1997) *J Biol Chem 272*, 21381-7.

43. Worthylake, D. K., Prakash, S., Prakash, L., and Hill, C. P. (1998) *J Biol Chem 273*, 6271-6.

44. Giraud, M. F., Desterro, J. M., and Naismith, J. H. (1998) *Acta Crystallogr D Biol Crystallogr 54 (Pt 5)*, 891-8.

45. Jiang, F., and Basavappa, R. (1999) *Biochemistry 38*, 6471-8.

46. Huang, L., Kinnucan, E., Wang, G., Beaudenon, S., Howley, P. M., Huibregtse, J. M., and Pavletich, N. P. (1999) *Science 286*, 1321-6.

47. Zheng, N., Wang, P., Jeffrey, P. D., and Pavletich, N. P. (2000) *Cell 102*, 533-9.

CHAPTER 5:

Energetics and specificity of interactions within Ubc13/Uev/Ub human Ub-conjugation complexes[1]

5.1 SUMMARY

Lys[63]-linked poly-Ub chains appear to play a non-degradative signaling and/or recruitment role in a variety of key eukaryotic cellular processes including NF-κB signal transduction and DNA repair. A protein heterodimer composed of a catalytically active ubiquitin conjugating enzyme (Ubc13) and its homologue (Mms2 or Uev1a) forms a catalytic scaffold upon which a non-covalently associated acceptor Ub and thiolester-linked donor Ub are oriented such that Lys[63]-linked poly-Ub chain synthesis is facilitated. In this study, we have used 2D ^{1}H-^{15}N HSQC NMR spectroscopy, in combination with isothermal titration calorimetry, in order to determine the thermodynamics and kinetics of the interactions between various components of the Lys[63]-linked poly-Ub conjugation machinery. Mms2 and Uev1a interact *in vitro* with acceptor Ub to form 1:1 complexes with macroscopic dissociation constants of 99 ± 15 and 214 ± 14 μM respectively, and appear to bind Ub in a similar fashion. Interestingly, the Ubc13/Mms2 heterodimer associates with acceptor Ub in a 1:1 complex and binds with a dissociation constant of 28 ± 6 μM, significantly stronger than Mms2 alone. Furthermore, a dissociation constant of 49 ± 7 nM was determined for the interaction between Mms2 and Ubc13 using isothermal titration calorimetry. In connection with previous structural studies for this system, the thermodynamics and kinetics of acceptor Ub binding to the Ubc13/Mms2 heterodimer detailed in this study will allow for a more thorough rationalization of the mechanism of formation of Lys[63]-linked poly-Ub chains.

5.2 INTRODUCTION

Protein ubiquitination is a key post-translational modification event for a variety of intracellular proteins involved in numerous degradative and regulatory pathways including cell cycle control (1), NF-κB-dependent signal transduction (2, 3), DNA repair (4, 5), ribosome biogenesis (6), and endocytosis of cell surface proteins (7). The cellular protein ubiquitination machinery is responsible for the covalent formation of an isopeptide bond between the C-terminal carboxy group of Ub and the ε-amino group of a solvent-exposed Lys on a target substrate. Covalent attachment of Ub to target substrates is accomplished by a series of three enzymes which may form high-energy thiolester linkages between an active-site Cys residue and the C-terminal carboxyl group of Ub (8, 9). Ub is initially activated by a highly conserved Ub activating enzyme (E1) that forms a thiolester adduct in an ATP dependant manner. This is followed by transfer of the Ub molecule to the active-site Cys of a Ub conjugating enzyme (E2) via a transthiolesterification reaction. Substrate specificity is thought to be mediated by at least two families of Ub protein ligases (E3), which in combination with the E2 enzymes are responsible for the formation of an isopeptide bond between Ub and a Lys residue on the surface of the target.

Whereas a monoubiquitination event serves as a signal for certain cellular fates (10), in most cases one observes formation of poly-Ub chains on the target substrate through repetitive conjugation of Ub molecules to each other (11). The Ub molecules are linked to each other through an isopeptide bond formed between the C-terminal carboxy group of an incoming, or donor, Ub and one of seven Lys residues on the surface of a substrate attached, or acceptor, Ub. As a result, there exist a variety of poly-Ub chains defined by the Lys residue linking sequential Ub molecules, and these chains likely adopt unique topologies, and therefore potentially different functional roles (12-17). Poly-Ub chains linked through Lys[48] are the best understood; this chain configuration typically targets proteins for degradation via the 26S proteasome and therefore serves an obviously crucial role in regulation of cellular protein levels (8). The alternative

covalent tethering of Lys^{63}-linked Ub chains to a target substrate, on the other hand, serves not as a proteolytic tag for the target, but instead as a recruitment and/or signaling marker. The importance of Lys^{63}-linked chains is underscored by their role in both NF-κB (*3, 18*) signaling and error-free post-replicative DNA repair processes (*5, 19-22*).

The catalytic mechanisms through which specific poly-Ub chain linkages are assembled and delivered to substrates are poorly understood. Surprisingly, some of the first insights into these processes have come not from well characterized systems involving the assembly of Lys^{48} poly-Ub chains, but from the study of non-canonical Lys^{63} poly-Ub linkages. Lys^{63}-linked poly-Ub chains are assembled through a conserved heterodimer of E2 proteins composed of a catalytically active Ubc13 subunit and an inactive E2-like subunit, or Ub-conjugating enzyme variant (Uev) (*23*). Uev proteins share significant sequence and structural similarities with E2s (*24, 25*), yet lack the requisite active-site Cys required for thiolester formation. Structurally, it appears as though the Ubc13/Mms2 heterodimer serves as a binding scaffold for two Ub molecules: a primarily Mms2 associated "acceptor" Ub and a thiolester-linked "donor" Ub on Ubc13 (*24-27*). A model of the tetrameric complex, based on NMR chemical shift mapping, reveals that this orientation not only favors the formation of Lys^{63}-linked chains through the proximal positioning of Lys^{63} on the acceptor Ub and C-terminus of the donor Ub tethered to the Ubc13 active-site, but also precludes the formation of Lys^{48}-linked chains, as this residue is buried in the acceptor Ub•Mms2 interface (*26, 27*). Therefore, structural studies have allowed us to define a structural rationale for the assembly of specific poly-Ub chain linkages. However, a complete picture for this mechanism necessarily involves unraveling the thermodynamics and kinetics of the underlying protein-protein interactions.

In the current study, we examined the thermodynamics and kinetics of the interactions within the $Ubc13/Mms2/Ub_2$ tetramer using a combination of NMR chemical shift titration and isothermal titration calorimetry (ITC) experiments. This approach has allowed for estimation of the affinity, stoichiometry, specificity,

and kinetics of binding between the acceptor Ub and (i) Mms2, (ii) Ubc13/Mms2, or (iii) Uev1a, as well as between the E2/Uev heterodimer components (Mms2 and Ubc13). The results are crucial for understanding the thermodynamic and kinetic aspects of complex assembly, to understand binding differences between Uev proteins, and to confirm the validity of the previously determined model for the tetrameric complex (*27*). Combined with our previous work, a more complete mechanism for poly-Ub chain formation has been determined, and may serve as a more general mechanism for different poly-Ub chain linkages.

5.3 EXPERIMENTAL PROCEDURES

5.3.1 Protein expression and purification

Cloning, expression, and purification of ^{15}N-labeled and unlabeled human Mms2, human Ubc13, Ub, and E1 were performed as described previously (section 2.3.1). Human Uev1a was purified as a GST-fusion protein and subsequently cleaved from GST in a manner identical to that previously described for Mms2, with the exception that cleavage of the GST moiety proceeded for 4 hours, and protease inhibitors (Calbiotech, setII cocktail) were then immediately added. It should be noted that for Mms2, Uev1a, and Ubc13 proteins, cleavage of the GST moiety leaves a 5-residue linker attached to the N-terminus of the recombinant protein. SDS-PAGE analysis, BCA protein assays, and amino acid analyses were employed to confirm the concentration and purity of the samples prior to and during the titration experiments.

5.3.2 NMR samples

All NMR sample volumes were approximately 500 μL (90% H_2O, 10% D_2O) prior to titration, and included 50 mM HEPES (pH 7.5), 50 mM NaCl, 1mM EDTA, 10 mM DTT, and 1 mM DSS (internal ^{1}H chemical shift standard). The pH of the samples were adjusted to 7.5.

5.3.3 NMR spectroscopy

All NMR spectra were obtained using a Varian Unity INOVA 600 MHz spectrometer operating at 30 °C. The 2D ^{1}H-^{15}N-HSQC NMR spectra were acquired using the sensitivity-enhanced gradient pulse scheme developed by Kay and co-workers (*28, 29*). The ^{1}H and ^{15}N sweep widths were 8000 and 2200 Hz, respectively. A minimum of 64 transients per point in the indirect (^{15}N) dimension were collected for each spectrum. Spectral processing was accomplished with the NMRPipe program. (*30*). The NMRview program (*31*) was employed in the assignment of all 2D ^{1}H-^{15}N-HSQC NMR cross-peaks.

5.3.4 Titration of ^{15}N-Mms2 with Ub

To an NMR sample containing 500 μM ^{15}N-Mms2, 15 μL aliquots of 6.5 mM Ub were successively added for a total of nine titration points. For all titrations carried out in this study, following acquisition of a 2D ^{1}H-^{15}N HSQC NMR spectrum for each titration point, up to 5 μL of the NMR sample was set aside for use in duplicate amino acid analyses, giving [Ub]/[^{15}N-Mms2] ratios of 0, 0.33, 0.65, 0.98, 1.31, 1.65, 1.98, 2.32, 2.67, and 3.01 for the respective titration points. While this technique did result in significant volume increases, changes in concentration for both titrant and analyte were taken into account in the final analysis for all titrations presented herein. The pH of the sample was routinely checked, and maintained at 7.5 throughout this and all titrations conducted in this study. For all titrations, a 1D ^{1}H NMR spectrum was acquired prior to each 2D ^{1}H-^{15}N HSQC NMR spectrum in order to assess potential salt-dependant changes in the ^{1}H pulse width. The 90° pulse width remained unchanged from its initial value (7.0 μs) for this and all other titrations presented herein.

5.3.5 Titration of ^{15}N-Uev1a with Ub

To an NMR sample containing 130 μM ^{15}N-Uev1a, 10, 10, 15, 15, 15, 15, 20, and 20 μL aliquots of 2.8 mM Ub were successively added for a total of nine titration points. For the respective titration points, [Ub]/[^{15}N-Uev1a] ratios of 0,

0.36, 0.72, 1.27, 1.82, 2.38, 2.95, 3.71, and 4.47 were obtained from amino acid analyses.

5.3.6 Titration of ^{15}N-Mms2/Ubc13 with Ub

To an NMR sample containing 151 μM ^{15}N-Mms2/Ubc13, 10, 10, 5, 10, and 7.5 μL aliquots of 3.6 mM Ub were added successively for a total of five titration points, corresponding to [Ub]/[^{15}N-Mms2/Ubc13] ratios of 0, 0.44, 0.89, 1.11, 1.55, 1.89, and 2.20 respectively.

5.3.7 Titration of ^{15}N-Ubc13 with Mms2

Successive aliquots of 10, 10, 5, 10, and 7.5 μL of 950 μM Mms2 were added to an NMR sample containing 344 μM ^{15}N-Ubc13 for a total of five titration points. Molar ratios for [Mms2]/[^{15}N-Ubc13] of 0, 0.12, 0.23, 0.35, 0.48, 0.61, 0.79, 0.91, 1.09, and 1.27 were obtained from amino acid analyses for the respective titration points.

5.3.8 Calculation of dissociation constants

Dissociation constants were determined by following changes in backbone amide ^{1}H$_N$ and ^{15}N chemical shifts for Uev proteins in 2D ^{1}H-^{15}N HSQC NMR spectra upon addition of ligand. The total average change in backbone amide chemical shifts for the entire protein for each point in a titration was calculated using the following equation (32):

$$\Delta\delta_{total} = \frac{\sum_{j=1}^{n}\sqrt{\left(\Delta\delta\,^{15}N_j\right)^2 + \left(\Delta\delta\,^1H_{Nj}\right)^2}}{n}$$

[eq. 5.1]

where $\Delta\delta^{15}N_j$ and $\Delta\delta^1H_{Nj}$ are the chemical shift changes in Hertz for residue j, and the summation extends over all residues ($j = 1$ to n) that were employed in the calculation. The average change in total chemical shift was calculated at the end point of the titration using each of the residues whose chemical shifts changed significantly during titration, and the fractional change in total chemical shift was

determined for each titration point by normalization to the endpoint $\Delta\delta_{total}$. This value was then plotted as a function of the molar ratio of ligand:protein and fit to equation 5.2, to yield a macroscopic dissociation constant ($K_D = k_{off}/k_{on}$) for the interaction between a protein (P) and ligand (L):

$$[\text{PL}] = \frac{1}{2}\left(K_D + L_0 + P_0 - \sqrt{(K_D + L_0 + P_0)^2 - 4L_0P_0}\right)$$ [eq. 5.2]

where K_D is the dissociation constant, P_0 is the total protein concentration, L_0 is the total ligand concentration, and [PL] is the concentration of protein-ligand complex (33). K_D was determined from $\Delta\delta_{total}$ through a non-linear least squares fit using the program Xcrvfit (available at http://canopus.pence.ualberta.ca/ftp/).

5.3.9 Lineshape analysis for determination of off-rate constants

Cross peaks in 2D ^{1}H-^{15}N HSQC NMR spectra during titration of Ub into either ^{15}N-Mms2 or ^{15}N-Uev1a fall into the limit of fast exchange on the NMR time scale, and therefore appear as single resonances that move progressively towards the bound chemical shifts upon addition of Ub according to:

$$\delta_{obs} = (1 - P_b)\,\delta_f + P_b\delta_b$$ [eq. 5.3]

where δ_{obs} is the observed chemical shift of the backbone amide cross-peak, P_b is the fraction of bound Mms2, respectively, and δ_f and δ_b are the chemical shifts for the free and bound species, respectively (32). The program Mathematica (34) was used to simulate ^{1}H NMR lineshapes using the experimentally derived values of $\Delta\upsilon_f$ (linewidth at half-height for free protein), $\Delta\upsilon_b$ (linewidth at half-height for bound protein), δ_f, δ_b, K_D, adjusting k_{off} manually, and using the equations describing effects of site exchange on NMR spectra (32, 35).

5.3.10 Isothermal titration calorimetry of Ubc13/Mms2

A VP-ITC MicroCalorimeter (Microcal, Northampton, MA) was used to analyze binding of Mms2 to Ubc13. Proteins were dialyzed against 50 mM Tris, pH 7.5, 150 mM NaCl, and 1 mM ETDA and degassed prior to analysis. Ubc13 (7 μM) was injected into the sample cell, and Mms2 (70 μM solution) was placed

into the syringe, or vice versa with the exception that a slightly higher concentration of analyte was used (80 μM). The dialysis buffer was placed in the reference cell. Either Mms2 or Ubc13 was titrated against dialysis buffer to obtain the heat of dilution. The following parameters were used in the titration: 30 °C, 10 μl injections, and 4 min between injections with stirring at 305 rpm. These titration data were fit using the program Microcal Origin (v 5.0) to extract thermodynamic parameters.

5.4 RESULTS

5.4.1 Ub binding to Uev proteins: interaction of Ub with Mms2

Examination of the thermodynamics and kinetics for the interaction between non-covalently bound acceptor Ub and the Ubc13/Uev scaffold, involved analysis of 2D ^{1}H-^{15}N HSQC NMR spectra for ^{15}N-Mms2 in the free state and upon successive additions of unlabelled Ub. This scheme allowed for monitoring of the NMR resonance peaks for the ^{15}N-Mms2 component without interference from unlabeled Ub NMR resonance peaks. The 2D ^{1}H-^{15}N HSQC NMR spectrum of ^{15}N-Mms2 alone shows approximately 120 backbone amide cross-peaks that can be used to follow the titration with Ub in detail. Changes in cross-peak resonance frequencies can reflect changes in local chemical environment, and therefore identify residues that are potentially involved in the interaction with Ub.

Contour plots of the ^{1}H-^{15}N HSQC NMR spectra taken during titration of Ub into ^{15}N-Mms2 are shown in Figure 5.1A. Eighteen backbone amide ^{1}H-^{15}N cross-peaks, corresponding to residues Glu^{21}, Gly^{22}, Gly^{25}, Val^{26}, Gly^{29}, Thr^{30}, Val^{31}, Ser^{32}, Gly^{34}, Thr^{47}, Gly^{48}, Met^{49}, Gly^{52}, Asn^{60}, Tyr^{63}, Lys^{65}, Val^{117}, and Gln^{120}, were observed to experience significant changes in chemical shift upon addition of Ub, indicating possible participation in the interface between Mms2 and acceptor Ub. These residues cluster to the α1 and α2 helices, and the first three β-strands of Mms2. These residues map to a concave surface on one face of the protein (Fig. 5.2). These results are in good agreement with previous chemical
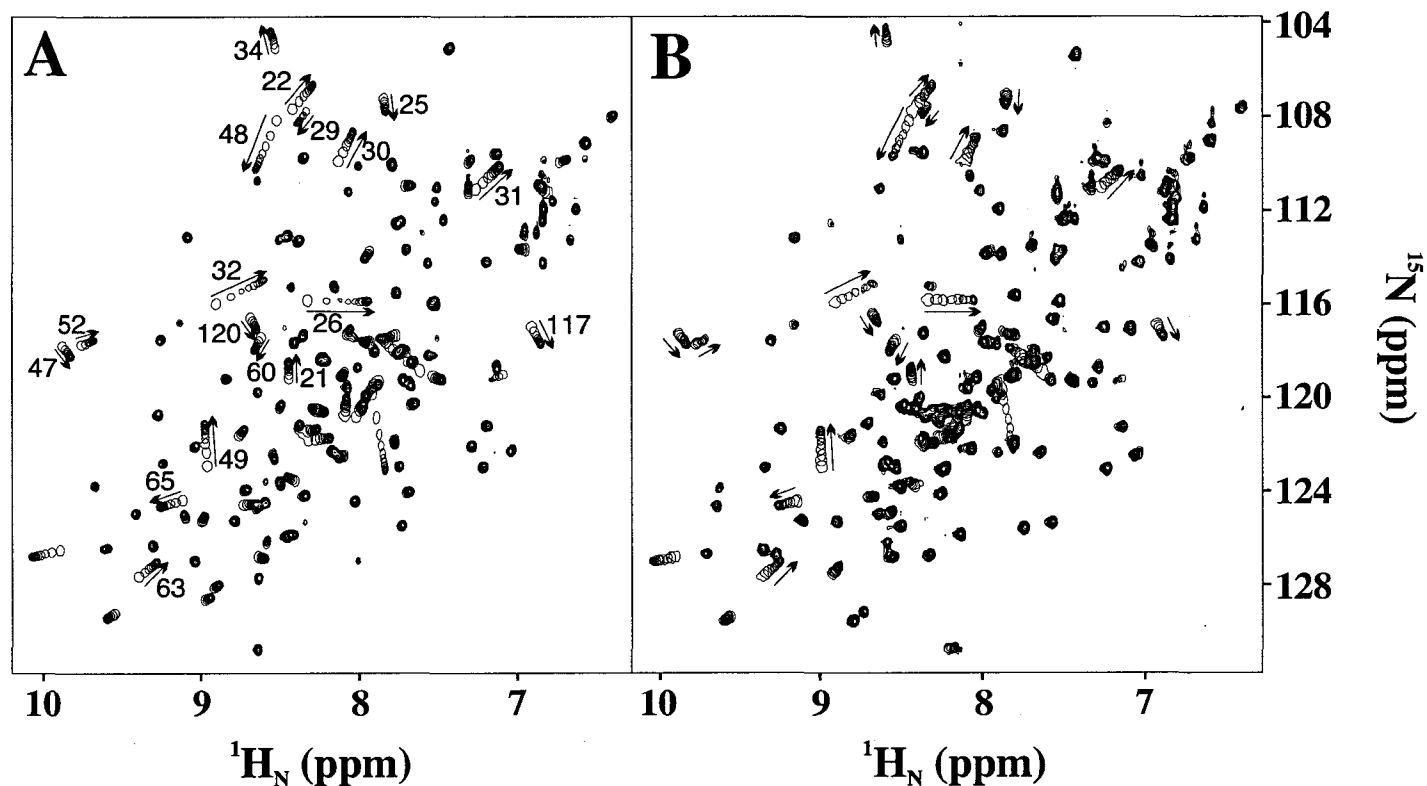
Figure 5.1   Contour plots of 2D ^{1}H-^{15}N HSQC NMR spectra from the backbone amide regions of ^{15}N-labeled Mms2 (A) or Uev1a (B), showing the effect of Ub addition.   The final titration point in each spectrum is shown as multiple contours, whereas all other points are represented by a single contour.   The well resolved cross-peaks which undego significant changes in chemical shift during titration are numbered according to residue,with the progress of the titration labeled with an arrow.   Only those residues labeled with arrows were used in the analysis of the K$_D$ value.
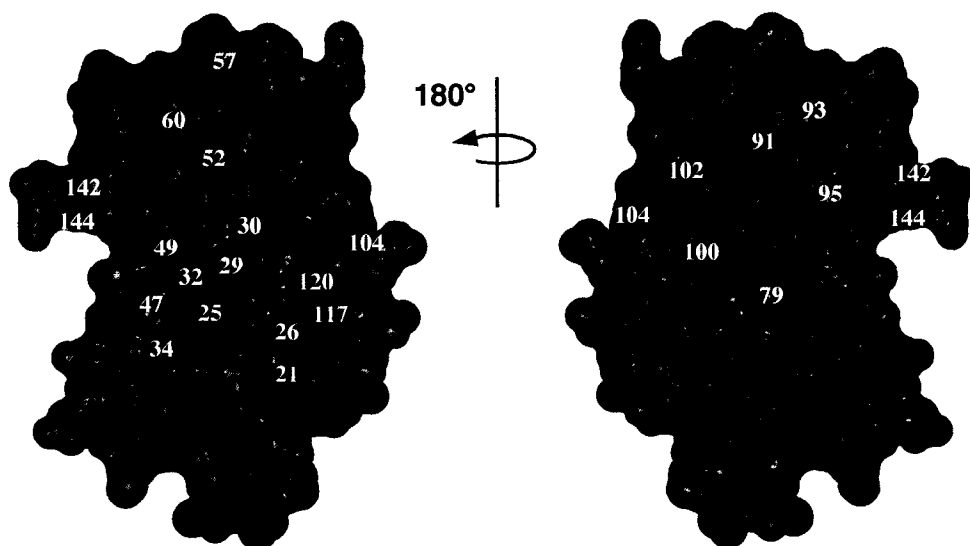
Figure 5.2 Ub binding site on the surface of Mms2. The surface of Mms2 (blue) is presented showing the putative Ub interaction site. Residues affected by non-covalent interaction with Ub, as determined by 2D ^{1}H-^{15}N HSQC NMR chemical shift titrations (see Fig. 5.1), are colored in red. Non-identical residues between Mms2 and Uev1a are colored in purple. Note that these non-identical residues occur at different regions of the protein surface from those involved in Ub binding.

shift perturbation studies which delineated the surfaces of interaction between the protein species (Chapter 4).

On the basis of previous biochemical and NMR data (26, 27), the non-covalent interaction between Ub and a given Uev is expected to be weak (K_D in the μM range). In accordance with this expectation, all of the backbone amide chemical shift changes fall into the fast exchange limit on the NMR time scale to a first approximation (see lineshape analysis below), as is often observed for weaker interactions (36). At any given point during the titration, only a single set of cross-peaks, whose chemical shifts are the weighted average of the free and bound chemical shifts, are observed. The linear trajectories for the shifting cross-peaks in the 2D ^{1}H-^{15}N NMR spectra for ^{15}N-Mms2 are indicative of a 1:1, weak interaction between Ub and Mms2.

Residues that undergo backbone amide ^{1}H$_N$ or ^{15}N chemical shift changes during the titration can be monitored in order to quantitate the thermodynamics and kinetics of binding between two protein species. The fractional change in total chemical shift was determined for each titration point, and these values were plotted as a function of the [Ub]/[^{15}N-Mms2] ratio and fit to equation 5.2 with P = Mms2 and L = Ub, yielding a macroscopic dissociation constant (K_D) of 99 $\pm$ 15 μM for a 1:1 binding complex (Fig. 5.3A, diamonds). The completeness of the titration is evidenced by the fact that the chemical shifts for all eighteen cross-peaks undergoing significant changes during Ub titration cease to do so at an approximate 3-fold excess of Ub relative to Mms2. Furthermore, the dependence of backbone amide Mms2 chemical shifts upon Ub concentration for each of the cross peaks whose chemical shifts change significantly upon titration is virtually identical, consistent with a single binding event.

1D traces through the ^{1}H dimension for numerous cross-peaks for the 2D ^{1}H-^{15}N HSQC spectrum of ^{15}N-Mms2 were taken, and a representative trace corresponding to the backbone amide resonance of Val[26] is shown in Figure 5.3B (top) to display the effect of exchange between free and Ub-bound Mms2 at various points during the titration. For the backbone amide resonance of Val[26],
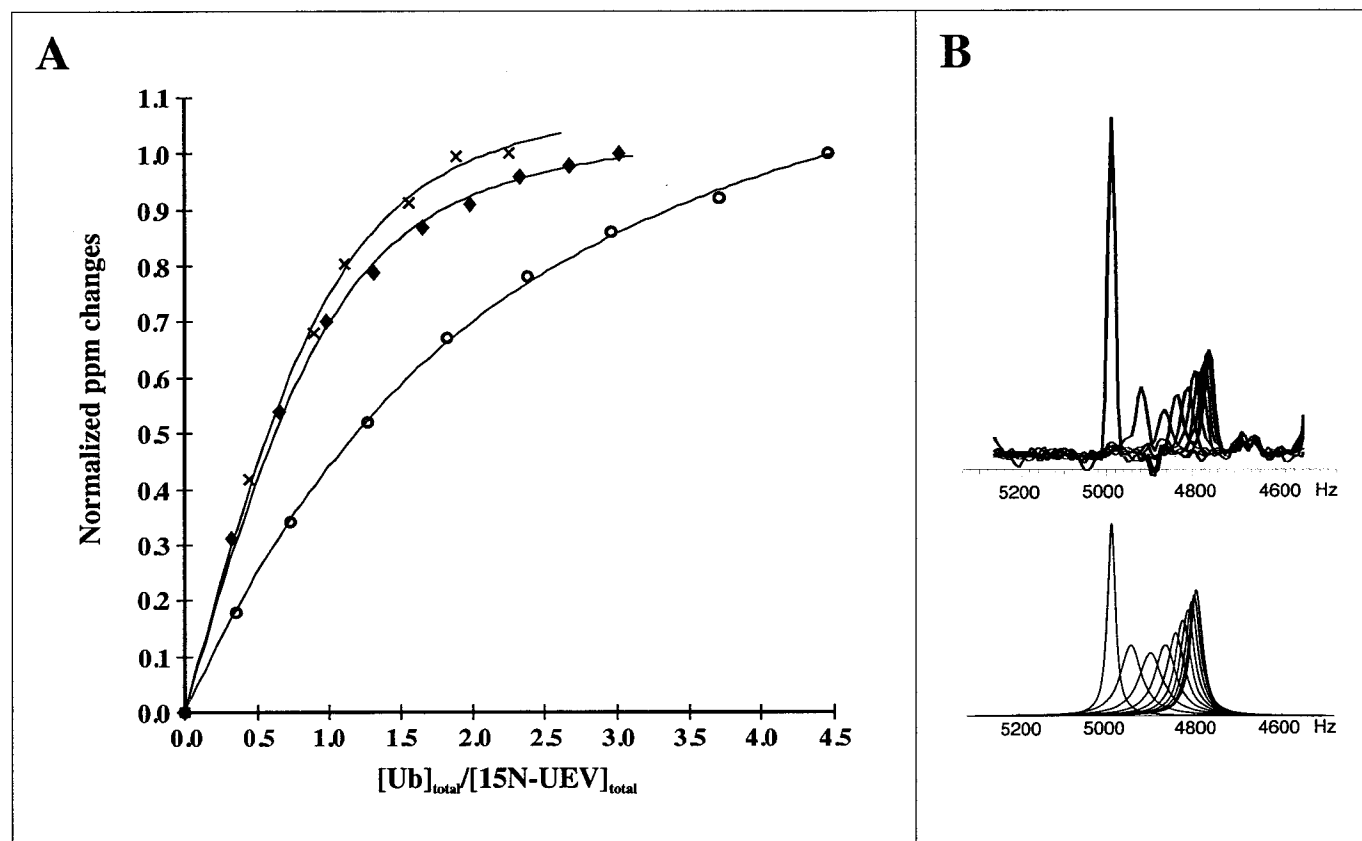
Figure 5.3 Thermodynamic and kinetic analysis of Ub binding by the Uevs. (A) Binding curves derived from 2D ^{1}H-^{15}N HSQC NMR titrations of Ub into ^{15}N-Mms2 (diamonds), ^{15}N-Uev1a (circles), and ^{15}N-Mms2/Ubc13 (crosses). The average normalized ppm changes are plotted as a function of the ratio of [Ub]/[^{15}N-species], with non-linear least squares fits to the data shown as solid lines. The error on the data points are smaller than the size of the corresponding symbols. (B) 1D ^{1}H traces taken through the cross-peaks of Val^{26} from 2D ^{1}H-^{15}N HSQC NMR spectra during titration of Ub into ^{15}N-Mms2 (top). The corresponding lineshape simulation using a k_{on} value of 2250 s^{-1} is also shown (bottom).

the total change in chemical shift in the ^1H dimension is 230 Hz, and significant line-broadening is observed during the titration, but the resonance peak sharpens dramatically when ^{15}N-Mms2 is saturated with Ub. This broadening phenomenon is expected because the effect of chemical exchange on linewidth is dependent upon the chemical shift difference between the free and bound states:

$$\Delta v_{ex} = P_f P_b \tau_{ex} (\delta_f - \delta_b)^2 \qquad \text{[eq. 5.4]}$$

where Δv_{ex} is the observed line width, P_f and P_b are the fraction free and fraction bound ^{15}N-Mms2, and τ_{ex} is the exchange lifetime defined as $(\tau_f \tau_b)/(\tau_f + \tau_b)$. Computer simulations of the observed lineshape changes were performed using the experimentally derived values of Δv_f, Δv_b, δ_f, δ_b, K_D, and manually adjusting k_{off}. A k_{off} value of 2250 ± 500 s^{-1} provides a satisfactory fit with the experimental data (Fig. 5.3B, bottom).

5.4.2 Ub binding to Uev proteins: interaction of Ub with Uev1a

Uev1a, a homologue of Mms2 involved in NF-κB signaling, shares high sequence identity (92%) within the core Uev domain (residues 1-145 of Mms2), but not with the N-terminal extension or 11 scattered amino acid substitutions throughout Uev1a (Fig. 5.4A). Whereas the non-covalent interaction between Ub and Mms2 has been well characterized (26, 27), there is scant information regarding a potential non-covalent interaction between Uev1a and Ub, as well as the potential differences and/or similarities between its mode of Ub binding relative to that of Mms2.

The 2D ^1H-^{15}N HSQC NMR spectrum for ^{15}N-Uev1a is shown in Figure 5.4B (red contours). The backbone amide resonances show the linewidth and dispersion expected for an E2-like protein, with the exception of a cluster of cross-peaks found at chemical shifts typical of random coil secondary structure. Although we have not assigned the backbone amide chemical shifts for ^{15}N-Uev1a, it is apparent that upon superposition with the 2D ^1H-^{15}N HSQC NMR of ^{15}N-Mms2 spectrum (Fig. 5.4B, black contours) that the chemical shifts for the

A

hMms2
hUev1a
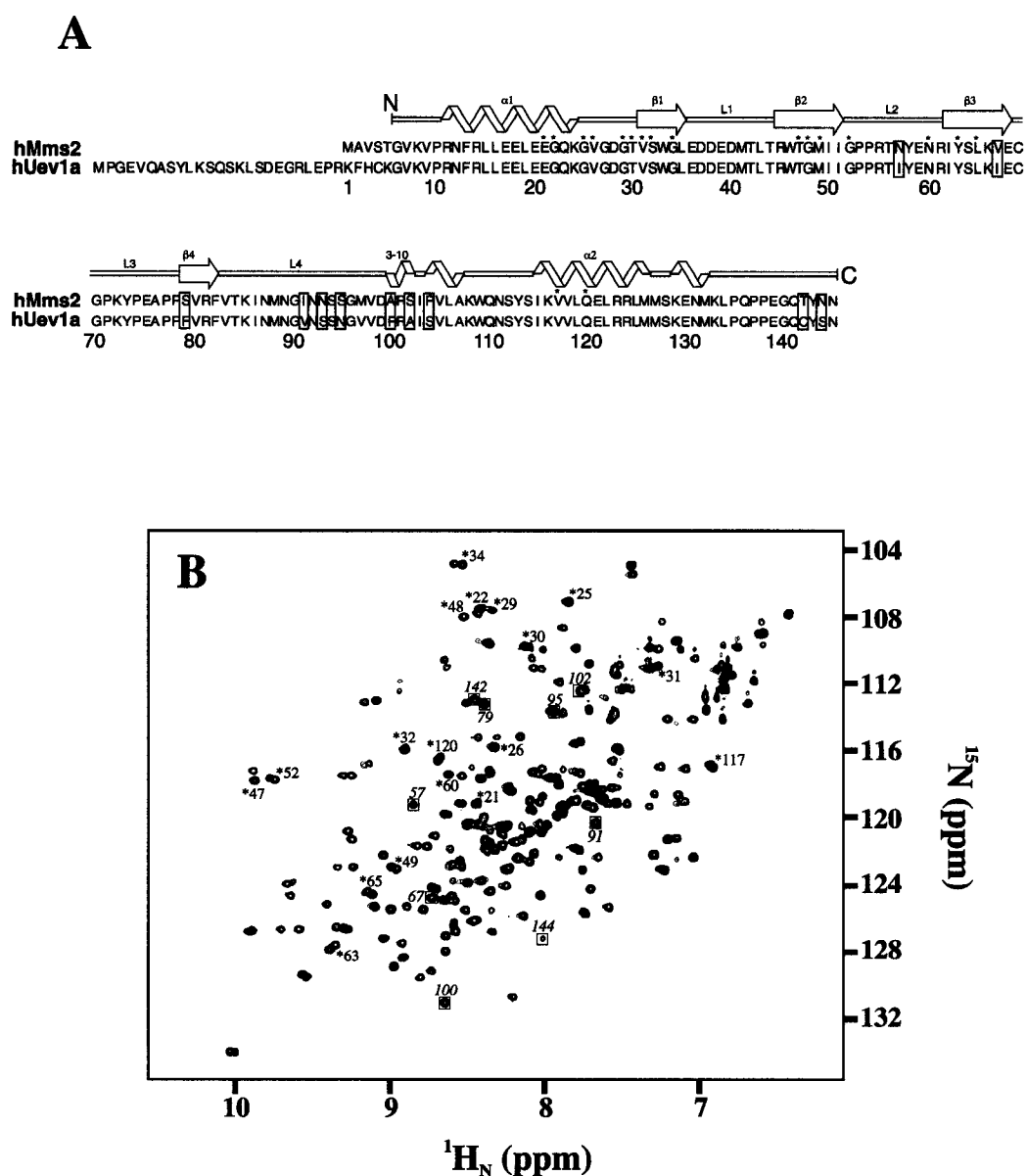
Figure 5.4 Comparison of the Mms2 and Uev1a proteins. (A) Sequence alignment of Mms2 and Uev1a, shown with the corresponding secondary structures. Important residues are labeled as described below. (B) Superposition of 2D ^{1}H-^{15}N HSQC NMR spectra of free ^{15}N-Mms2 (black) and ^{15}N-Uev1a (red). Cross-peaks in ^{15}N-Mms2 which are affected by complex formation with Ub are numbered and indicated with an asterisk, while those which differ between the Uevs are numbered and boxed.

backbone amide cross-peaks for the two proteins are similar. Notable exceptions are the residues that presumably correspond to the N-terminal extension of Uev1a that is likely disordered in solution, and those which are non-identical in the primary amino acid sequence. The disordered conformation of the N-terminal extension for Uev1a likely results in both the difficulty of crystallizing the full length species and its susceptibility to proteolysis during purification[2]. Given the 92% sequence identity for Mms2 and Uev1a for the core domain residues, and the similarity for the 2D ^{1}H-^{15}N HSQC NMR spectra, we hypothesize that the structures of Mms2 and Uev1 are likely to be similar.

2D ^{1}H-^{15}N HSQC NMR spectra were collected for ^{15}N-Uev1a in the free state and upon successive addition of unlabelled Ub. Contour plots of the spectra during titration with Ub are shown in Figure 5.1B. Of the 135 backbone amide cross-peaks that can be used to follow the titration of Ub into Uev1, eighteen of these cross-peaks were observed to shift in a linear fashion upon successive additions of Ub, and fall into the fast exchange limit on the NMR time scale. Upon inspection of the 2D ^{1}H-^{15}N HSQC NMR spectrum of free ^{15}N-Uev1a, it is clear that many of the resonances superimpose with those in the spectrum of free ^{15}N-Mms2 (Fig. 5.4B), indicating that the chemical shift assignments for Uev1a are likely to be similar to those for Mms2. Furthermore, the trajectories for resonances in Uev1a undergoing significant changes in chemical shift upon titration with Ub match well with those observed in Mms2, indicating that a similar binding interface is used by each protein with respect to Ub binding (Figure 5.1). To complement this result, the surface on Ub involved in binding Uev1a, as determined from chemical shift perturbation experiments of ^{15}N-Ub (data not shown) is similar to that found previously for the interaction between ^{15}N-Ub and Mms2 (26). Therefore, we conclude that the weak non-covalent interaction between Ub and Uev1a likely employs a similar mode of binding as that of Ub binding to Mms2.

In order to quantitatively compare the thermodynamics and kinetics of Ub

---

[2] T. Moraes, personal communication (2003).

binding between Mms2 and Uev1a, the average fractional change in total chemical shift was calculated based on the eighteen residues labeled in Figure 1B, plotted as a function of the [Ub]/[^{15}N-Uev1a] ratio, and fit to equation 5.2 with P = Uev1a and L = Ub, giving a K_D value of 214 ± 14 μM for a 1:1 complex (Figure 5.3A, circles). As in the case for Mms2, the rate and linearity for the trajectory of movement for each of the significant cross-peaks is virtually identical, indicating a single binding event requiring an approximate 4.5-fold excess of Ub to saturate Uev1a. However, the observed K_D is 2.2-fold larger than that for the interaction between Ub and Mms2, indicating a weaker interaction despite the fact that presumably similar residues are implicated in the binding event.

One-dimensional traces through numerous cross-peaks of Uev1a were taken, and computer simulations of the experimental line shapes were performed using the experimentally derived values of Δv_f, Δv_b, δ_f, δ_b, K_D, and adjusting k_{off} manually. A k_{off} of 1800 ± 450 s^{-1} provides a satisfactory fit with the experimental data (data not shown), indicating a slight difference compared to that for the Ub•Mms2 interaction.

5.4.3 Interaction of Ub with the Ubc13/Mms2 heterodimer

The heterodimerization of Mms2 (or Uev1a) with Ubc13 is a prerequisite for the synthesis of Lys[63]-linked poly-Ub chains. Therefore, determination of the thermodynamics and kinetics of interaction between Ub and the Ubc13/Mms2 heterodimer is important in order to understand the contribution that Ubc13 makes to non-covalent acceptor Ub binding. This is of particular interest in light of the fact that Mms2 alone makes extensive non-covalent interactions with Ub, while Ubc13 alone has no detectable affinity for Ub molecules (*26*). In employing solution NMR to analyze the interaction of Ub with the Ubc13/Mms2 heterodimer, a complicating factor is the increase in molecular weight for the complex (42.5 kDa) relative to that of Mms2 and Ub alone (25.5 kDa), which results in a decrease in signal to noise for 2D ^{1}H-^{15}N HSQC NMR spectra. Furthermore,

certain backbone amide cross-peak resonances for ^{15}N-Mms2 change and/or disappear upon heterodimerization, and cannot be identified for the analysis.

Titration of Ub into the Ubc13/Mms2 heterodimer employed an NMR sample for which only Mms2 was ^{15}N-lableled, thereby simplifying the spectrum. 2D ^{1}H-^{15}N HSQC NMR spectra were collected for ^{15}N-Ubc13/Mms2 free of Ub, and upon successive additions of unlabelled Ub. Of the 105 observable backbone amide cross-peaks, fifteen were observed to shift significantly: Glu^{21}, Gly^{22}, Val^{26}, Gly^{29}, Thr^{30}, Val^{31}, Ser^{32}, Gly^{34}, Thr^{47}, Gly^{48}, Met^{49}, Gly^{52}, Asn^{60}, Tyr^{63}, Lys^{65}, and Gln^{120}. Each of these peaks moved in a linear fashion upon titration with Ub, and exhibited fast exchange on the NMR time scale. These fifteen residues correspond to those involved in the interaction between Ub and Mms2 subunit alone, indicating that a similar mode of binding between Mms2 and Ub is employed in the heterodimer. This result is in agreement with previous chemical perturbation experiments (27).

In order to quantify the thermodynamics and kinetics of Ub binding to Mms2 within the heterodimer, the average fractional change in total chemical shift was calculated based on the fifteen residues described above, plotted as a function of the [Ub]/[^{15}N-Ubc13/Mms2] ratio, and fit to equation 2 with $P = {}^{15}$N-Ubc13/Mms2 and $L = $ Ub, to give a K_D of 28 ± 6 μM (Fig. 5.3A, crosses). As in the case with binding of Ub to Mms2 alone, the rate of the trajectory of movement for each of the significant cross-peaks is virtually identical, indicating a single binding event requiring an approximate 2-fold excess of Ub to saturate Mms2. The observed K_D is 3.5-fold smaller than that for the interaction between Ub and Mms2 alone, indicating a greater affinity of Ub for Mms2 within the heterodimer. We therefore conclude that Ubc13 contributes to the thermodynamics and kinetics of Ub binding within the Ubc13/Mms2 heterodimer (see Discussion).

A lineshape analysis for the determination of a k_{off} value was not possible due to reduced signal to noise for the spectra of Ub•^{15}N-Ubc13/Mms2 compared to Ub•^{15}N-Mms2.

5.4.4 Thermodynamics of interaction between components of the Ubc13/Mms2 heterodimer

Mms2 and Ubc13 form a stable heterodimer over a range of concentrations and solution conditions (26, 27). An upper limit to K_D for the heterodimer of 2 μM was previously determined by analytical ultracentrifugation (24). The high-affinity limit for quantitative determination of the dissociation constant by solution NMR currently lies around 3 μM (36, 37). A 2D ^{1}H-^{15}N HSQC NMR titration experiment in which Ubc13 was ^{15}N-labeled and unlabeled Mms2 was used as the titrant was performed in order to determine a K_D for the Ubc13/Mms2 interaction (data not shown). The K_D value was estimated to be 1 $\pm$ 1 μM. However, due to the poor fit of the data, this value should be treated as an upper limit. It is worth noting that the chemical shift change maximum occurred between [Mms2]/[^{15}N-Ubc13] molar ratios of 0.91 and 1.09, indicating the formation of an equimolar complex of the two proteins at a molar ratio of close to 1:1.

In order to more accurately probe the thermodynamics of the heterodimer interaction, ITC methodologies were employed (Fig. 5.5). ITC experiments were conducted in which the reaction cell contained either Ubc13 or Mms2, and small equivalent volume injections of the complimentary heterodimer component were progressively added. The heat evolved upon binding is monitored as the titrant is successively injected, allowing for the calculation of thermodynamic parameters. This analysis yielded an average K_D of 49 $\pm$ 7 nM for the interaction between heterodimer components (ΔH= -5946 $\pm$ 59 cal/mol, ΔS= 13.8 $\pm$ 2.3 cal/mol/°C).

5.5 DISCUSSION

Central issues regarding the mechanism responsible for the formation of Lys^{63}-linked poly-Ub chains by the Ubc13/Mms2 heterodimer are the structural features that enable the heterodimer to perform its catalytic function, and the thermodynamics and kinetics of the interactions between donor and acceptor Ub
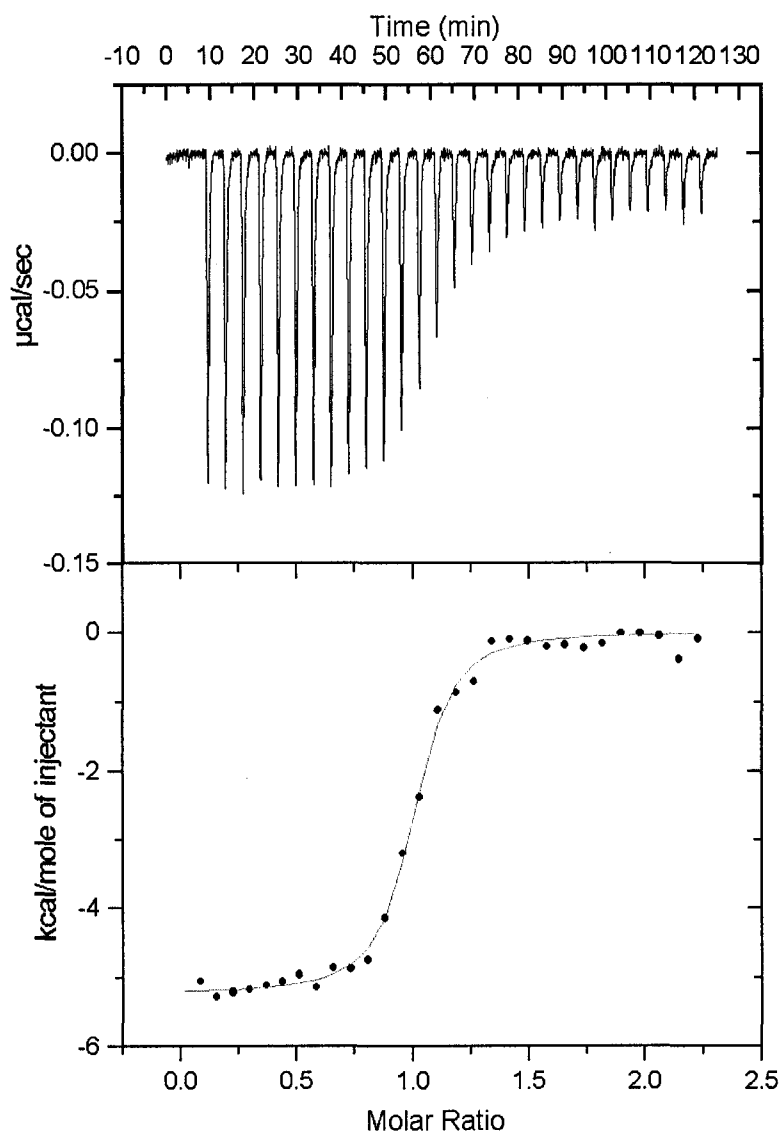
Figure 5.5 Isothermal Titration Calorimetry of the Ubc13/Mms2 heterodimer. ITC thermogram is shown for the titration of Ubc13 (7 μM, sample cell) with Mms2 (70 μM, syringe), with the heat evolved shown on a per injection basis (top). ITC titration curve for the same reaction (bottom), where the heat evolved per injection is shown as a function of the molar ratio of Mms2 to Ubc13.

moieties and the heterodimer scaffold. Backbone amide chemical shift perturbation analysis has allowed the construction of a low resolution model of the interactions between the Ubc13/Mms2 scaffold and two molecules of Ub (the acceptor Ub bound non-covalently primarily by Mms2 and a thiolester-linked donor Ub on Ubc13), which predicts a reasonable mechanism in which Lys[63] of the acceptor Ub is placed in close proximity to both Gly[76] of the donor Ub and the active site Cys[87] on Ubc13 (chapter 4). Here we report the affinity, stoichiometry, specificity, and the kinetics of interaction between various members of the tetrameric complex, as determined using 2D ^{1}H-^{15}N HSQC NMR titration experiments and ITC. The results are important with respect to gaining an understanding of the thermodynamics and kinetics associated with the poly-Ub chain building mechanism.

The thermodynamics and kinetics of Ub binding to two human Uev proteins, Mms2 and Uev1a, were examined in detail and illustrated striking similarities and some subtle differences between their modes of binding. As expected, both Mms2 and Uev1a bind Ub non-covalently in a 1:1 stoichiometry, and use virtually identical residues to mediate the binding event (Fig. 5.1). Uev contacts to Ub involve residues from the N-terminal α-helix, the first 3 stands of the β-sheet, and the C-terminal α-helix, which correspond well with those residues previously determined to be important in the Mms2•Ub interaction (chapter 4). When mapped onto the surface of the known Mms2 structure (24), these residues cluster to a single concave surface of the molecule of appropriate area for Ub binding (Fig. 5.2A). However, Mms2 binds Ub with a 2.2-fold higher affinity than Uev1a, indicating that despite the use of a similar binding surface, subtle differences in terms of the binding interface with Ub may exist. Whereas the majority of the amino acid differences between these two proteins cluster to a surface on the protein opposite that responsible for Ub binding (Fig. 5.2B), a few key differences including Asn[57]Ile, Val[67]Ile, Phe[104]Ser, Thr[142]Cys, Asn[144]Ser, and the 25 residue N-terminal extension may account for the difference in affinity for Ub between the Uevs (Fig. 5.4A). It is also important to consider the fact that we

are looking exclusively at changes in local environment for the backbone amide bond and not directly at side chain structural interactions, which may prove more informative. Furthermore, the difference between the two Uev proteins in affinity for Ub could be minimized upon heterodimerization with Ubc13, though there are not data to support this possibility. Regardless, the K_D values determined are reasonable, and likely support the interaction *in vivo* despite the relatively weak binding observed. The mechanism of chain formation would require efficient release of Ub_2 from the Ubc13/Mms2 heterodimer, necessitating a weak interaction. It should be noted that the interaction with additional protein factors (*i.e.* E3 proteins) may also modulate the affinity towards Ub.

The results presented herein are corroborated by the fact that another Uev, Tsg101, binds Ub non-covalently with a K_D of approximately 600 μM, though the structural basis for this interaction is distinct from that between Mms2 and Ub (*38*). While Mms2 and Uev1a each serve to properly orient Ub in order to achieve synthesis of Lys[63]-linked poly-Ub chains, the cellular pathways in which they are involved are different. Preliminary results have also indicated that Uev1a and Mms2 have different *in vitro* chain building activities[3]. Taken together, these results imply that the different affinities for Ub between these proteins are important in Ub binding/release and thus must account in part for differences in poly-Ub chain building catalyzed by the two proteins.

Previous studies have demonstrated that the Ubc13 subunit alone has no detectable affinity for Ub under conditions and concentrations appropriate for NMR (*26, 27*). Furthermore, Mms2 binds Ub specifically, regardless of its heterodimerization state with Ubc13. We therefore sought to examine in detail whether heterodimerization of Mms2 significantly affects the thermodynamics and kinetics of Ub binding. It was determined that Ub is bound 3.5-fold more tightly by the Ubc13/Mms2 heterodimer when compared to the Mms2 subunit alone, and interact in a 1:1 stoichiometry. This result is striking given that similar residues on the surface of Mms2 within the heterodimer appear to be involved in

---

[3] Trevor Moraes, personal communication (2003).

complex formation. Based on these results, it is clear that either the interaction with Ubc13 modulates the Mms2 binding interface, or Ubc13 is involved in directly binding the acceptor Ub molecule. The latter conclusion seems more plausible on two accounts. First, the NMR-derived model of the tetrameric complex predicts an interaction between the loop containing Lys[63] of the acceptor Ub and a channel above the active site on Ubc13 (27). Second, a Ubc13 substitution Asp[81]Ala situated in this channel attenuates the affinity of the heterodimer for Ub in vitro (25). Therefore, Ubc13 apparently serves three key catalytic functions in Lys[63] chain assembly: (i) the formation of thiolester with donor Ub, (ii) the orientation of Lys[63] on the acceptor Ub towards the active-site, and (iii) the concomitant increased affinity for acceptor Ub.

Mms2 and Ubc13 can be chromatographically co-purified as a heterodimer which remains stable over a wide variety of concentrations and buffer conditions (24, 26, 27). The S. cerevisiae homologues of these proteins also form a stable 1:1 heterodimer (20) with a K_D of 0.4 μM (22). Unfortunately, the quality of the data precluded the rigorous kinetic analysis for the Ubc13/Mms2 heterodimer interaction by 2D ^{1}H-^{15}N HSQC NMR titration experiments. However, using ^{15}N-Ubc13 and unlabeled Mms2, we were able to observe 1:1 stoichiometry for the human proteins and estimate an upper limit of 1 μM for the value of K_D. This result is in good agreement with the previous value of 2 μM determined by analytical ultracentrifugation. In order to accurately determine the affinity of interaction, ITC experiments were performed, and yielded a K_D value of 49 $\pm$ 7 nM for the interaction, indicative of a tight binding event. The in vivo outcome of the difference in K_D values for the yeast and human heterodimers has not been explored. The free energies associated with each of the interactions between Ub and the Ubc13/Mms2 heterodimer are summarized in Figure 5.6. A $\Delta G°$ for binding of Ub and Mms2 is −5.6 kcal/mol, whereas $\Delta G°$ is −6.3 kcal/mol for binding of heterodimer and acceptor Ub. Based on our previous model for the Ubc13/Mms2/Ub$_2$ heterodimer, we propose that the increased affinity of acceptor Ub for Mms2 within the heterodimer compared
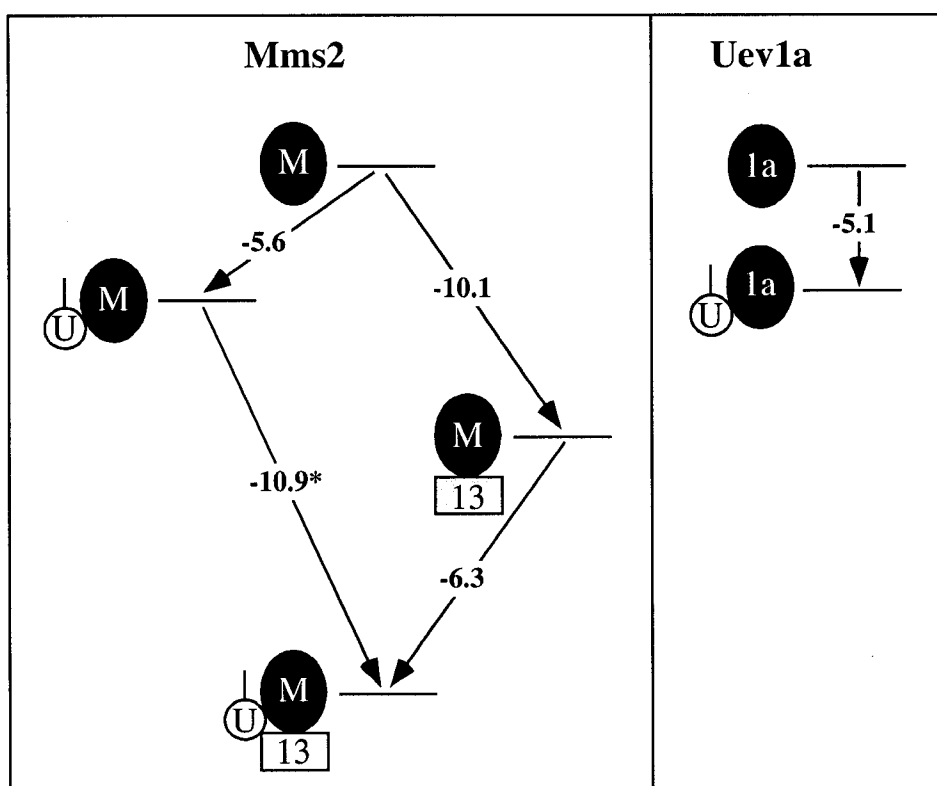
Figure 5.6 Schematic view of the relative free energies (ΔG°binding in kcal/mol) involved in the binding of acceptor Ub by the Ubc13/Uev heterodimer. The free energies are calculated from the NMR- and ITC-derived K_D values (ΔG°binding = RTlnK_D), with the exception of the ΔG°binding value for the Mms2-Ub association with Ubc13 (*), which was calculated based on the coupling with other free energies in the cycle. Labels are as follows: U=Ub, M=Mms2, 13=Ubc13, 1a=Uev1a.

to the interaction between Ub and Mms2 alone results predominantly from the direct binding of a loop from Ub containing Lys[63] to Ubc13. A $\Delta G°$ of -10.1 kcal/mol was determined for the Ubc13/Mms2 interaction, and the hypothetical association of Ubc13 with the Mms2·Ub complex would result in a $\Delta G°$ of -10.9 kcal/mol. This thermodynamic cycle implies that Ubc13 binding to Mms2 likely precedes interaction with the acceptor Ub molecule, serving to increase the affinity of Mms2 (within the heterodimer) for Ub. These results are consistent with previous biochemical studies that have shown that thiolester formation proceeds at different rates depending on the heterodimerization state of the Uev proteins (Chapter 2).

This study, in combination with a wealth of structural information regarding catalysis of poly-Ub chain formation facilitated by the Ubc13/Uev heterodimer, represents an important first step in understanding the thermodynamic and kinetic aspects associated with poly-Ub chain formation. Establishment of a solid structural, thermodynamic, and kinetic base of knowledge with respect to Lys[63]-linked chain formation will hopefully lead to more general insights into the mechanism of poly-Ub chain formation.

5.6 REFERENCES

1.   Peters, J.-M., King, R.W., Deshaies, R.J. (1998) *Ubiquitin and the Biology of the Cell*, Plenum Press, New York.

2.   Chen, Z. J., Parent, L., and Maniatis, T. (1996) *Cell 84*, 853-62.

3.   Deng, L., Wang, C., Spencer, E., Yang, L., Braun, A., You, J., Slaughter, C., Pickart, C., and Chen, Z. J. (2000) *Cell 103*, 351-61.

4.   Jentsch, S., McGrath, J. P., and Varshavsky, A. (1987) *Nature 329*, 131-4.

5.   Hoege, C., Pfander, B., Moldovan, G. L., Pyrowolakis, G., and Jentsch, S. (2002) *Nature 419*, 135-41.

6.   Finley, D., Bartel, B., and Varshavsky, A. (1989) *Nature 338*, 394-401.

7.   Hicke, L., and Riezman, H. (1996) *Cell 84*, 277-87.

8.   Glickman, M. H., and Ciechanover, A. (2002) *Physiol Rev 82*, 373-428.

9.   Hochstrasser, M. (1996) *Annu Rev Genet 30*, 405-39.

10.   Hicke, L. (2001) *Nat Rev Mol Cell Biol 2*, 195-201.

11.   Pickart, C. M. (2000) *Trends Biochem Sci 25*, 544-8.

12.   Chau, V., Tobias, J. W., Bachmair, A., Marriott, D., Ecker, D. J., Gonda, D. K., and Varshavsky, A. (1989) *Science 243*, 1576-83.

13.   Arnason, T., and Ellison, M. J. (1994) *Mol Cell Biol 14*, 7876-83.

14.   Johnson, E. S., Ma, P. C., Ota, I. M., and Varshavsky, A. (1995) *J Biol Chem 270*, 17442-56.

15.   Spence, J., Sadis, S., Haas, A. L., and Finley, D. (1995) *Mol Cell Biol 15*, 1265-73.

16.   Baboshina, O. V., and Haas, A. L. (1996) *J Biol Chem 271*, 2823-31.

17.   Koegl, M., Hoppe, T., Schlenker, S., Ulrich, H. D., Mayer, T. U., and Jentsch, S. (1999) *Cell 96*, 635-44.

18.   Wang, C., Deng, L., Hong, M., Akkaraju, G. R., Inoue, J., and Chen, Z. J. (2001) *Nature 412*, 346-51.

19. Broomfield, S., Chow, B. L., and Xiao, W. (1998) *Proc Natl Acad Sci U S A 95*, 5678-83.

20. Hofmann, R. M., and Pickart, C. M. (2001) *J Biol Chem 276*, 27936-43.

21. Brusky, J., Zhu, Y., and Xiao, W. (2000) *Curr Genet 37*, 168-74.

22. Ulrich, H. D. (2003) *J Biol Chem 278*, 7051-8.

23. Hofmann, R. M., and Pickart, C. M. (1999) *Cell 96*, 645-53.

24. Moraes, T. F., Edwards, R. A., McKenna, S., Pastushok, L., Xiao, W., Glover, J. N., and Ellison, M. J. (2001) *Nat Struct Biol 8*, 669-73.

25. VanDemark, A. P., Hofmann, R. M., Tsui, C., Pickart, C. M., and Wolberger, C. (2001) *Cell 105*, 711-20.

26. McKenna, S., Spyracopoulos, L., Moraes, T., Pastushok, L., Ptak, C., Xiao, W., and Ellison, M. J. (2001) *J Biol Chem 276*, 40120-6.

27. McKenna, S., Moraes, T., Pastushok, L., Ptak, C., Xiao, W., Spyracopoulos, L., and Ellison, M. J. (2003) *J Biol Chem 278*, 13151-8.

28. Kay, L. E., Keifer, P., Saarinen, T. (1992) *J. Am. Chem. Soc. 114*, 10663-10665.

29. Zhang, O., Kay, L. E., Olivier, J. P., and Forman-Kay, J. D. (1994) *J Biomol NMR 4*, 845-58.

30. Delaglio, F., Grzesiek, S., Vuister, G. W., Zhu, G., Pfeifer, J., and Bax, A. (1995) *J Biomol NMR 6*, 277-93.

31. Johnson, B. A., Blevins, R.A. (1994) *J. Chem. Phys. 29*, 1012-1014.

32. McKay, R. T., Tripet, B. P., Hodges, R. S., and Sykes, B. D. (1997) *J Biol Chem 272*, 28494-500.

33. Williams, T. C., Shelling, J.G, Sykes, B.D. (1985) in *NMR in the Life Science* (Bradbury, A. M., Nicolini, C., Ed.) pp 93-104, Plenum Press, New York City.

34. Wolfram, S. (1996) *The Mathematica Book*, 3rd ed., Wolfram Media/ Cambridge University Press, Cambridge.

35. Sutherland, I. O. (1971) *Annual Reports on NMR Spectroscopy*, Vol. 4, Academic Press, New York.

36.   Zuiderweg, E. R. (2002) *Biochemistry 41*, 1-7.

37.   Mercier, P., Li, M. X., and Sykes, B. D. (2000) *Biochemistry 39*, 2902-11.

38.   Pornillos, O., Alam, S. L., Rich, R. L., Myszka, D. G., Davis, D. R., and Sundquist, W. I. (2002) *Embo J 21*, 2397-406.

CHAPTER 6:

Backbone dynamics within the human Ubc13/Mms2 ubiquitination complex

6.1 SUMMARY

Ub-conjugating enzyme variants share significant sequence similarity with typical E2 enzymes of the protein ubiquitination pathway, but lack their characteristic active-site Cys residue. A hypothesized role for the Ubc13/Mms2 ubiquitin conjugation complex is to correctly orient either a target-bound or untethered Ub molecule such that its Lys[63] is placed proximally to the C-terminus of the Ub molecule that is linked to the active-site of Ubc13. The result is the ability of the heterodimeric complex to serve as the catalytic scaffold for the formation of Lys[63]-linked poly-Ub chains required in key cellular pathways, including NF-κB signal transduction and postreplicative DNA repair. In this chapter, the inherent flexibility of (i) the monomeric Ubc13 and Mms2 subunits, and (ii) the Ubc13/Mms2 heterodimer was examined using ^{15}N-T_1, ^{15}N-T_2, and ^{1}H-^{15}N-NOE backbone amide relaxation experiments. These data were analyzed using the Lipari-Szabo formalism in order to calculate order parameters, which specify the degree of motional freedom associated with the backbone amide bond vector. The results presented herein represent a key first step in the determination of the dynamic nature of a ubiquitination complex.

6.2 INTRODUCTION

As described extensively the introductory chapter to this thesis, the human Ubc13/Uev system plays a crucial cellular role in pathways including error-free postreplicative DNA repair (1-5) and NF-κB-dependent signal transduction (6, 7). These functions appear to be mediated by a Lys[63] protein ubiquitination capacity inherent to the heterodimer formed between these two proteins, one of which is the catalytically active Ubc13 subunit, and the other inactive Uev which lacks the

catalytic active-site Cys despite sharing significant sequence and structural similarities with typical E2s (*1, 8, 9*). This specific system has provided unique insights into the mechanism of Lys^{63} poly-Ub chain formation, as it appears as though the Ubc13/Uev heterodimer serves as a binding scaffold for two Ub moieties, the primarily Mms2-associated "acceptor" Ub, and a Ub thiolester "donor" Ub tethered to the active-site Cys of Ubc13. Specifically, the scaffold appears to favor a specific orientation of the Ub molecules such that efficient isopeptide bond formation can proceed between the C-terminal Gly^{76} of the donor and Lys^{63} of the acceptor Ub (*8-11*). Therefore, straightforward structural studies have provided a mechanism whereby the formation of a specific chain linkage (Lys^{63}) can be accomplished.

A number of interesting results stemming from a variety of different methodological approaches have indicated that, not surprisingly, the interactions between acceptor Ub and Uev, as well as the formation of thiolester adduct between donor Ub and Ubc13, are significantly affected by heterodimerization between Ubc13 and Uevs. First, kinetic analysis of *in vitro* thiolester formation revealed that heterodimerization with Mms2 reduces the rate of thiolester formation on Ubc13 (Chapter 2). Second, thermodynamic analyses of acceptor Ub binding using ^{1}H-^{15}N-HSQC titrations have indicated that heterodimerized Mms2 binds Ub with greater affinity ($\Delta\Delta G°=-0.7$ kcal/mol) (Chapter 5). Third, NMR chemical shift perturbation experiments have indicated that, in particular, the loop containing the active-site Cys on Ubc13 experiences significant changes in chemical environment upon heterodimerization, indicating a potential structural rearrangement at the active-site (Chapter 4). Taken together, these observations support the hypothesis that there may well be significant differences at each Ub binding site upon heterodimerization. Unfortunately, based on both the human (*8*) and *S. cerevisiae* (*9*) crystal structures, the only significant structural rearrangement in the protein C_α backbones is the reorientation of the first 9 residues of Mms2 from an open to a closed conformation upon

heterodimerization. Therefore, there is not a simple structural rationale for the functional differences observed upon heterodimerization.

In order to gain a more thorough understanding of the biomolecular recognition events required for the catalytic function of the Ubc13/Uev heterodimer, NMR experiments which examine backbone ^{15}N-^1H_N relaxation phenomenon were exploited in order to obtain information regarding rotational tumbling and internal dynamics (*12, 13*). Specifically, the overall rotational correlation time, an internal correlation time, and an order parameter (S^2) for every observable backbone amide bond vector in a protein can be determined by applying the Lipari-Szabo formalism in order to analyze relaxation data (*14-16*). S^2 represents an extremely useful parameter as it represents the degree of motional freedom associated with a bond vector in the absence of a specific motional model. Analysis of the backbone amide bonds, therefore, provides residue specific information about the conformational freedom associated with the protein backbone. Furthermore, by assuming a specific motional model associated with bond vector diffusion (*i.e.* diffusion-in-a-cone), the order parameter can be interpreted in terms of conformational entropy in a semi-quantitative fashion, but in general should be approached as an upper limit (*17-20*).

In this chapter, we provide an extensive backbone amide relaxation analysis of four protein species (^{15}N-Ubc13, ^{15}N-Mms2, ^{15}N-Ubc13/Mms2, and Ubc13/^{15}N-Mms2) at a single magnetic field strength. First, ^{15}N-^1H_N backbone relaxation analysis of the individual subunits was performed in order to compare the dynamics of a catalytically active E2 (Ubc13) and its inactive paralogue (Mms2). Second, ^{15}N-^1H_N backbone relaxation analysis of the heterodimer species was performed in order to assess whether dynamic changes in backbone conformation could be observed at three crucial protein-protein interfaces upon heterodimerization: the heterodimer interface, the donor Ub thiolester site on Ubc13, and the acceptor Ub binding site on Mms2. Taken

together, these studies represent a first step in an attempt to delineate enthalpic and entropic factors that govern the process of poly-Ub chain formation.

6.3 EXPERIMENTAL PROCEDURES

6.3.1 Protein expression and purification

Cloning, expression, and purification of ^{15}N-labeled and unlabeled human Mms2 and Ubc13 was performed as a GST fusion protein and subsequently cleaved from GST as described previously (section 2.3.1). Cleavage of the GST moiety leaves a five-residue linker attached to the N-terminus of the recombinant protein. Ubc13/Mms2 heterodimer in which only one subunit was ^{15}N-labeled was purified from its monomer components by mixing Ubc13 and Mms2 (500 μL each at approximately 500 μM) at 25 °C, followed by Hi-Load 16/60 Superdex 75 column chromatography in order to separate the subunits from heterodimer. The concentration and purity of the protein samples was determined by using SDS-PAGE analysis in combination with BCA protein assays.

6.3.2 NMR samples

Four separate NMR samples were prepared in order to examine the backbone amide dynamics: ^{15}N-Ubc13 (400 μM), ^{15}N-Mms2 (400 μM), ^{15}N-Ubc13/Mms2 (400 μM), and Ubc13/^{15}N-Mms2 (400 μM). All NMR sample volumes were approximately 600 μL (90% H_2O and 10% D_2O), and included 150 mM HEPES (pH 7.5), 75 mM NaCl, 1 mM EDTA, 10 mM DTT, and 1 mM DSS (internal ^{1}H chemical shift standard). The pH of the samples was adjusted to 7.5 in all cases. Sample and salt concentrations were optimized using preliminary ^{1}H^{15}N-T_1 and -T_2 experiments such that minimal aggregation is observed.

6.3.3 NMR spectroscopy

NMR spectra were acquired using a Varian Unity INOVA 600 MHz spectrometer equipped with 5 mm triple resonance probes and z-axis pulsed field gradients. ^{15}N-T_1, -T_2, and ^{1}H-^{15}N NOE experiments were performed at 30 °C

using enhanced sensitivity, gradient pulse sequences developed by Farrow *et. al.* (*21*). ^{15}N-T_1 data were acquired for the ^{15}N-Ubc13 and ^{15}N-Mms2 subunits using relaxation delays of 11.1, 55.5, 122.1, 199.8, 277.5, 388.5, 499.5, 666.0, 888.0, and 1054.5 ms, whereas relaxation delays of 11.1, 55.5, 122.1, 199.8, 277.5, 388.5, 499.5, 666.0, and 888.0 ms were employed for the heterodimerized samples. For the ^{15}N-T_1 pulse sequence, the delay between transients was 1.5 seconds. ^{15}N-T_2 data were acquired for the ^{15}N-Ubc13 and ^{15}N-Mms2 subunits using relaxation delays of 16.5, 33.1, 49.6, 66.2, 82.8, 99.3, 115.8, and 132.4 ms, whereas relaxation delays of 16.5, 33.1, 49.6, 66.2, 82.8, and 99.3 ms were employed for the heterodimerized samples. For the ^{15}N-T_2 pulse sequence, the delay between transients was 3 seconds in order to reduce the effects of sample heating during the Carr-Purcell-Meiboom-Gill pulse train, as previously noted (*22*). ^{1}H-^{15}N steady-state NOEs were measured by recording two HSQC spectra, one with (NOE experiment) and one without (noNOE experiment) proton saturation prior to the first ^{15}N excitation pulse. The spectrum recorded without proton saturation was acquired with a delay between transients of 6 seconds, whereas that acquired in the presence of proton saturation incorporated a relaxation delay of 3 seconds, followed by a 3 s proton saturation (train of 120° pulses with 5 ms intervals) for a total delay between transients of 6 s.

6.3.4 NMR data processing

All spectral processing was accomplished with the program NMRPipe (*23*). Enhanced sensitivity data were processed using the ranceY.M macro within the NMRPipe software. The NMRView program (*24*) was employed for peak picking of all ^{1}H-^{15}N-HSQC spectra based on the previously completed assignments (Chapter 3). The values of the ellipsoid volume (evolume) associated with each peak were fit to single-exponential, two-parameter decay curves using the rate analysis tool in NMRView in order to determine the ^{15}N-T_1 and ^{15}N-T_2 values associated with each backbone amide. The fit was accomplished using 500 simulations and a confidence level of 0.65, and

incorporated the standard deviation of the noise in the spectrum (evolume value of the region of the spectrum not containing a peak divided by 5). Error in the ^{15}N-T_1 and ^{15}N-T_2 measurements was obtained from non-linear least squares fits of the peak evolumes to two-parameter exponential decays. ^{1}H-^{15}N-NOE values were calculated using the hetNOE panel in NMRView, again using evolumes from both the reference (noNOE) and NOE (NOE) spectra. The standard deviation of noise was calculated as described for the ^{15}N-T_1 and ^{15}N-T_2 analysis.

6.3.5 Relaxation Data Analysis

In most cases, the dominant factors contributing to backbone amide (^{15}N-^{1}H$_N$) relaxation, and hence the T_1 and T_2 relaxation times and the ^{15}N-NOE enhancement, are the dipolar interaction between the ^{15}N nucleus and its attached proton, and the chemical shift anisotropy of the ^{15}N nucleus (25). Expressions for ^{15}N-T_1 and ^{15}N-T_2, and ^{1}H-^{15}N steady state NOE relaxation parameters are given by linear combinations of the spectral density function [$J(\omega)$] at the specific Larmor angular frequencies, and linear combinations thereof, for ^{15}N and ^{1}H$_N$ nuclei (25):

$$\frac{1}{T_1} = D\left[J(\omega_H - \omega_N) + 3J(\omega_N) + 6J(\omega_H + \omega_N)\right] + C\left[J(\omega_N)\right]$$

[eq. 6.1]

$$\frac{1}{T_2} = \frac{D}{2}\left[4J(0) + J(\omega_H - \omega_N) + 3J(\omega_N) + 6J(\omega_H) + 6J(\omega_H + \omega_N)\right] + \frac{C}{6}\left[3J(\omega_N) + 4J(0)\right]$$

[eq. 6.2]

$$\text{NOE} = 1 + \left(\frac{\gamma_H}{\gamma_N}\right)D\left[6J(\omega_H + \omega_N) - J(\omega_H - \omega_N)\right]T_1$$

[eq. 6.3]

where $D = \left(\frac{\mu_0}{4\pi}\right)^2\left(\frac{\gamma_H^2\gamma_N^2\hbar^2}{4r_{NH}^6}\right)$ and $C = \frac{\Delta^2\omega_N^2}{3}$, μ_0 is the permeability constant of free space ($4\pi \times 10^{-7}$ kg m s^{-2} A^{-2}), γ_H is the proton magnetogyric ratio (2.68 $\times 10^8$ rad s^{-1} T^{-1}), γ_N is the ^{15}N magnetogyric ratio (-2.71 $\times 10^7$ rad s^{-1} T^{-1}), r_{NH} is the proton-

nitrogen internuclear separation (1.04 Å), Δ is the difference between the parallel and perpendicular components of the ^{15}N chemical shift tensor (-172 ppm), and h is Planck's constant divided by 2π (1.05 x10^{34} J s). The spectral density functions employed in equations 6.1-6.3 can be represented by the Lipari-Szabo model-free formalism in terms of an order parameter (S^2) that indicates the degree of spatial restriction for the backbone amide bond vector. With the assumptions of isotropic molecular tumbling, a single, overall rotational correlation time for the protein, and an associated internal correlation time, we can define the spectral density function as:

$$J(\omega) = \frac{2}{5}\left[\frac{S^2\tau_m}{\left(1+\omega^2\tau_m^2\right)} + \frac{\left(1-S^2\right)\tau}{\left(1+\omega^2\tau^2\right)}\right]$$

[eq. 6.4]

where $\dfrac{1}{\tau} = \dfrac{1}{\tau_m} + \dfrac{1}{\tau_e}$, τ_m is the correlation time for overall molecular tumbling, and τ_e is the correlation time for internal motion.

The relaxation parameters for each residue can subsequently be fit to a motional model describing the overall molecular tumbling of the protein, including one or two types of internal motions of various time-scales. This basic motional model is separated into 5 specific models which can be independently tested and compared to each other (21). In model 1, τ_e is fixed at zero and is assumed not to contribute to relaxation. As a result, model 1 adopts a simplified form of equation 6.4 which can be described using only the order parameter, S^2, and τ_m. Model 2 assumes that internal motions corresponding to τ_e are within the picosecond timescale ($0 < \tau_e < \tau_m$), and therefore includes optimization of three parameters: S^2, τ_m, and τ_e. Model 3 is identical to model 1 with the added inclusion of the parameter R_{ex} (s^{-1}) that reflects the contribution of microsecond to millisecond time-scale internal motions to the $\dfrac{1}{T_2}$ term from equation 6.2. Similarly, model 4 is simply model 2 with the addition of the R_{ex} parameter.

Model 5, which has not been rigorously derived, takes into account internal motions that occur on two time-scales, and can be used to analyze the relaxation data (26, 27). This model includes an order parameter for fast picosecond internal motions (S_f^2), an order parameter for nanosecond time-scale internal motions that are faster that τ_m but slower than τ_e (S_s^2), and a correlation time for nanosecond time-scale internal motions (τ_s). If we assumed that fast time-scale motions do not contribute significantly to relaxation ($\tau_e \rightarrow 0$), then the extended model spectral density function is given as follows:

$$J(\omega) = \frac{2}{5}\left[\frac{S^2\tau_m}{\left(1+\omega^2\tau_m^2\right)} + \frac{\left(S_f^2 - S^2\right)\tau_s'}{\left(1+\omega^2\tau_s'^2\right)}\right]$$

[eq. 6.5]

where $S^2 = S_f^2 S_s^2$, and $\tau_s' = \dfrac{\tau_s\tau_m}{\left(\tau_s + \tau_m\right)}$.

^{15}N-T_1, ^{15}N-T_2, and ^{1}H-^{15}N-NOE values for each residue were exported from the NMRView software into the Modelfree 4.15 program (28, 29), wherein parameters for each model of the spectral density function were adjusted to minimize the following function:

$$\chi^2 = \frac{\left(T_{1c} - T_{1e}\right)}{\sigma_{T_1}^2} + \frac{\left(T_{2c} - T_{2e}\right)}{\sigma_{T_2}^2} + \frac{\left(\text{NOE}_c - \text{NOE}_e\right)}{\sigma_{\text{NOE}}^2}$$

[eq. 6.6]

where the subscripts c and e indicate the calculated and experimental values, and σ is the error associated with each of the individual relaxation parameters. Statistical selection of the appropriate model (1 through 5) for each amino residue is accomplished through iterative testing of each model using Modelfree 4.15, starting with the simplest, until the proposed model describes the relaxation rates within 95% confidence limits, and represents a significant improvement over simpler models (using an f-test) which cannot be accounted for by increased parameterization (28). Once model selection is complete, a final optimization of the parameters within the selected model is performed.

In situations wherein rotational tumbling anisotropy is present in the protein molecule, the spectral density function has been explained elsewhere, in

which six parameters (D_{xx}, D_{yy}, D_{zz}, θ, ϕ, and ψ) describe the diffusion tensor of the protein molecule (*30*). These diffusion parameters are then optimized by minimizing the following function:

$$\chi^2 = \sum_n \left\{ \frac{\left[\left[\left(\frac{T_1}{T_2} \right)_e - \left(\frac{T_1}{T_2} \right)_c \right]_n \right]^2}{\sigma_n} \right\}$$

[eq. 6.7]

where σ is the error associated with the experimental T_1/T_2 ratio. This summation was performed over all "rigid" residues as outlined by the following three equations:

$$\overline{T_1} + 1\,SD > T_{1,n} > \overline{T_1} - 1\,SD$$

[eq. 6.8]

$$\overline{T_2} + 1\,SD > T_{2,n} > \overline{T_2} - 1\,SD$$

[eq. 6.9]

$$NOE_n = \overline{NOE} - 1\,SD$$

[eq. 6.10]

where SD is the standard deviation associated with each individual relaxation parameter.

In order to assess whether anisotropic reorientation is an appropriate model to describe the motion of our specific protein samples, the Cartesian coordinates of either Ubc13, Mms2, or the Ubc13/Mms2 heterodimer were taken from the existing crystal structure (*8*). Residues that satisfied the criteria established by equations 6.8-6.10 were input into the gridit software program (written in-house by Stéphane Gagné) that was used to fit the components and orientation of the diffusion tensor. The relaxation data was analyzed with respect to isotropic, axially symmetric, and fully asymmetric molecular motions. The simplest motional model which was described in terms of a small χ^2 value as described in equation 6.7 and did not reflect an improvement in the fit due to the addition of increased parameters (f-test) was chosen as appropriate. For each of the protein subunits, Ubc13 and Mms2, an axially symmetric motional model was

appropriate, whereas for the heterodimer, Ubc13/Mms2, an isotropic model was chosen.

The global isotropic correlation time was also optimized prior to relaxation analysis, using those residues that satisfy equations 6.8-6.10 such that residues that display active mobility were excluded.

In the case of rotational diffusion anisotropy with an axially symmetric diffusion tensor, the spectral density function adopts the following form (31-33):

$$J(\omega) = \frac{2}{5} S_f^2 \sum_{j=1}^{3} A_j \left[\frac{S_s^2 \tau_j}{\left(1+\omega^2 \tau_j^2\right)} + \frac{\left(1-S_s^2\right)\tau_j'}{\left(1+\omega^2 \tau_j'^2\right)} \right] \qquad \text{[eq. 6.11]}$$

with $A_1 = \dfrac{\left(3\cos^2\theta - 1\right)}{4}$, $A_2 = 3\sin^2\theta\cos^2\theta$, $A_3 = \left(\dfrac{3}{4}\right)\sin^4\theta$, where θ is the angle between the $^{15}N\text{-}^{1}H_N$ bond vector and the unique axis of the diffusion tensor in the principal axis system, and $\tau_j' = \dfrac{\tau_j \tau_s}{\left(\tau_j + \tau_s\right)}$, $\dfrac{1}{\tau_1} = 6D_\perp$, $\dfrac{1}{\tau_2} = 5D_\perp + D_\parallel$, $\dfrac{1}{\tau_3} = 2D_\perp + 4D_\parallel$.

With the global isotropic correlation time and diffusion tensor parameters, the Modelfree v4.15 program (28) was employed in order to calculate order parameters for the monomeric protein subunits. Identical statistical tests and selection criteria were employed in order to select the appropriate model (1-5) for analysis of relaxation data.

6.4 RESULTS

6.4.1 Human Mms2 $^{15}N\text{-}T_1$, $^{15}N\text{-}T_2$, and NOE data

The backbone amide ^{15}N and $^{1}H_N$ chemical shift resonances for Mms2 have been previously assigned (Chapter 3). 95 non-overlapping residues from the $^{1}H\text{-}^{15}N$-HSQC spectra were employed in the determination of relaxation parameters, and generally yielded an excellent fit to their appropriate parameter (Figure 6.1). Figure 6.1A also illustrates the importance of employing only non-overlapping residues in the determination of relaxation parameters.

The values for $^{15}N\text{-}T_1$, $-T_2$, and $^1H\text{-}^{15}N\text{-}NOE$ as a function of residue number and secondary structure are shown in Figure 6.2, and demonstrates qualitatively good data. The average T_1/T_2 ratio calculated for residues with negligible internal motions was 8.8 $\pm$ 1.3, which agrees well with the expected value (8.5 ns) for a globular protein of 17 kDa. Backbone relaxation experiments yielded an average $^{15}N\text{-}T_1$ of 703 $\pm$ 65 ms, $^{15}N\text{-}T_2$ of 85 $\pm$ 11 ms, and $^1H\text{-}^{15}N\text{-}NOE$ of 0.74 $\pm$ 0.12 respectively. Generally, regions displaying secondary structure possess relaxation parameters with values close to the mean, whereas loop regions and the termini display values either significantly lower (T_1, NOE) or higher (T_2) than the mean, demonstrating a correlation with respect to flexible/rigid segments relative to each other in the protein.

Identical experiments were conducted to determine the relaxation parameters for $^{15}N\text{-}Mms2$ upon heterodimerization with Ubc13 to detect whether differences in backbone dynamics exist between the two states. The values for $^{15}N\text{-}T_1$, $-T_2$, and $^1H\text{-}^{15}N\text{-}NOE$ as a function of residue number and secondary structure are shown in Figure 6.3. Despite increased linewidths as a result of the increased molecular weight of complex formation, upwards of 95 non-overlapping residues were used in the analysis. The average T_1/T_2 ratio calculated for residues with negligible internal motions was 44 $\pm$ 9, and yielded an average $^{15}N\text{-}T_1$ of 1285 $\pm$ 275 ms, $^{15}N\text{-}T_2$ of 33 $\pm$ 7 ms, and $^1H\text{-}^{15}N\text{-}NOE$ of 0.67 $\pm$ 0.23 respectively, all of which reflect the increase in molecular weight in the complex. Again, regions displaying secondary structure possess relaxation parameters with values closer to the mean, whereas loop regions and the termini display values divergent from the average values. However, due to the worse nature of the fit, these trends are less concrete than in the case of $^{15}N\text{-}Mms2$ alone.

To directly compare the backbone amide ^{15}N NMR relaxation data for Mms2 in both its monomeric and heterodimerized forms, the Lipari-Szabo model-independent formalism was employed (14, 15). In order to effectively use this approach, a global correlation time (τ_m) must first be established. The first step in calculating a τ_m value is to remove residues demonstrating internal motions that

A

B

Figure 6.1 Determination of ^{15}N-backbone relaxation parameters. (A) Representative 1D ^{1}H slices taken at a ^{15}N chemical shift of 121.2 ppm from a 2D ^{15}N-T$_2$ ^{15}N-hMms2 backbone amide relaxation experiment, acquired using relaxation delays of 16.5, 33.1, 49.6, 66.2, 82.8, 99.3, 115.8, and 132.4 ms respectively (from top to bottom). Both a residue that was employed for relaxation analysis (Ala^2) and those which were not due to overlap (Glu^{121} and Leu^{125}) are shown. (B) Relative peak ellipsoid volume was calculated for each residue at each relaxation delay indicated in (A), and fit appropriately (see Experimental) in order to determine the ^{15}N-T$_2$ value. Shown graphically are three such residues in ^{15}N-Mms2, Ala^2, Val^{26}, and Arg^{55}, which yielded T$_2$ values of 95$\pm$1, 133$\pm$2, and 92$\pm$2 ms respectively.

Figure 6.2 ¹⁵N-relaxation parameters for the human Mms2 protein. Plots of (A) ¹⁵N-T_1, (B) ¹⁵N-T_2, and (C) ¹H-¹⁵N NOE are shown, as measured at 600 MHz and 30 °C. Each data point is shown with its associated error. The average T_1/T_2 ratio calculated for residues with negligible internal motions (NOE > 0.65) was 8.8 ± 1.3. A schematic diagram of secondary structure is drawn above the panel. The residues in the structured regions are: α1 (11-24), β1 (31-35), β2 (45-51), β3 (62-68), β4 (79-82), 3_{10} helix (100-107), and α2 (115-132).
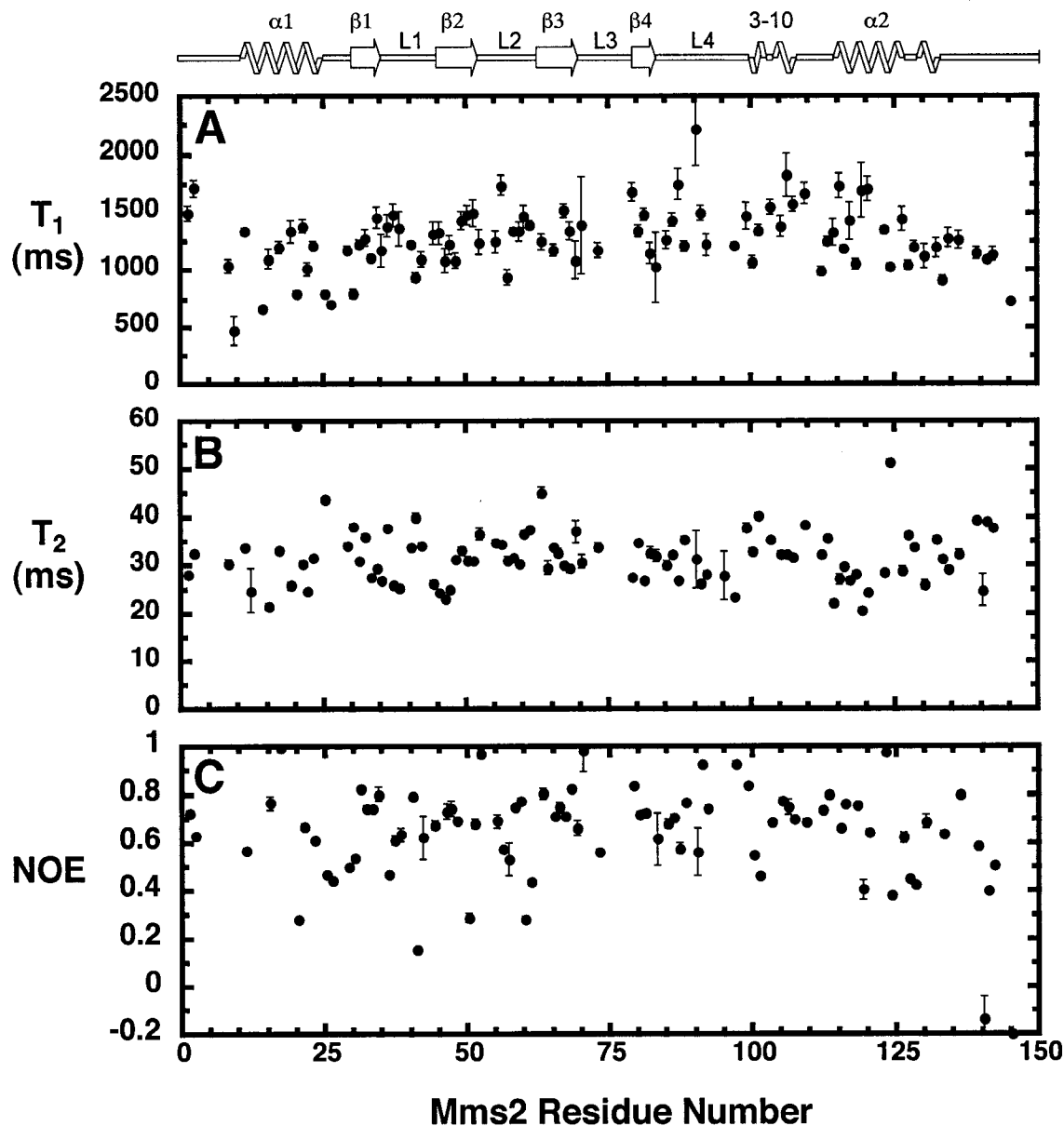
Figure 6.3 **15N-relaxation parameters for the human Mms2 protein heterodimerized with Ubc13.** Plots of (A) $^{15}N-T_1$, (B) $^{15}N-T_2$, and (C) $^1H-^{15}N$ NOE are shown, measured at 600 MHz and 30° C. Each data point is shown with its associated error. The average T_1/T_2 ratio calculated for residues with negligible internal motions (NOE > 0.65) was 44.2 + 9.0. A schematic diagram of secondary structure is drawn above the panel. The residues in the structured regions are: α1 (11-24), β1 (31-35), β2 (45-51), β3 (62-68), β4 (79-82), 3_{10} helix (100-107), and α2 (115-132).

occur on a faster time-scale than τ_m, which is generally done by establishing an NOE threshold and eliminating residues below it. As NOE is sensitive to internal motions on the nanosecond to picosecond time-scale, it can be reliably employed as a gauge for residues displaying exceedingly fast internal motions. An NOE cutoff of 0.65 was employed for ^{15}N-Mms2 and 0.60 for Ubc13/^{15}N-Mms2 samples, which tended to exclude residues from the termini and loop regions. For those residues remaining, the T_1/T_2 ratio was calculated, and those whose value was not within one standard deviation of the mean were also excluded from the τ_m calculation. With the assumption of negligible internal mobility and exchange, the T_1/T_2 ratio is dependent only on the overall rotational tumbling of the protein, and therefore provides a good estimate of τ_m. Using this analysis, an average T_1/T_2 ratio of 8.8 ± 1.3 and 44.2 ± 9.0 was determined for Mms2 alone and in complex with Ubc13, respectively. Global τ_m values of 8.9 ns for ^{15}N-Mms2 and 19.0 ns for Ubc13/^{15}N-Mms2 were established, and represent reasonable values given that the heterodimer is roughly twice the molecular weight of the Mms2 subunit alone.

It has been shown that even a small degree of anisotropy in rotational tumbling of a protein can have a significant impact on the eventual magnitude of order parameters, and therefore must be taken into account (34-37). Using the coordinates of the crystal structures, the relaxation data were analyzed in terms of isotropic, axially symmetric, and fully asymmetric rotational correlation models. The rotational tumbling of Mms2 alone was best represented by an axially symmetric model with an axial ratio ($D_\parallel / D_\perp$) of 1.10, whereas Ubc13/^{15}N-Mms2 was represented by an isotropic tumbling model. Therefore, when optimizing the results of the Lipari-Szabo formalism, the anisotropy in Mms2 was taken into account.

6.4.2 Human Mms2 modelfree analysis

In order to simplify comparisons and quantify the backbone dynamics of Mms2, order parameters (S^2) were calculated on a per-residue basis by fitting the

relaxation parameters (T_1, T_2, NOE) to one of five spectral density models (see materials and methods). S^2 values reflect the degree of motional restriction associated with a particular bond vector, varying from complete motional freedom (S^2=0) to restriction (S^2=1) (*14, 15*).

For the Mms2 subunit, an average S^2 of 0.85 ± 0.12 was determined for all residues, with an S^2 of 0.87 ± 0.06 as the average for residues involved in secondary structural elements. The error accompanying the latter result clearly demonstrates the backbone rigidity associated with the repeating elements of secondary structure. Figure 6.4A shows the S^2 values as a function of residue number, and demonstrates a number of interesting features. First and foremost, regions of secondary structure, as expected, display backbone rigidity (S^2~0.85), whereas the termini and linker regions between secondary structure elements generally display lower order parameters. Of particular interest are the linker regions between α1 and β1, and the region immediately preceding α1, as they appear to represent some of the most flexible regions of the protein.

Models 1 and 2 were not sufficient to fit all of the relaxation data, as several residues required the addition of either the R_{ex} parameter (models 3 and 4) or a two time-scale approach (model 5) to fit the data properly (Figure 6.4B,C). The addition of the R_{ex} parameter generally indicates the presence of slow (microsecond to millisecond time-scale) conformational exchange phenomena (*12*). In particular, the second half of α1 and many residues within α2, as well as residues scattered throughout the β-sheet, required the addition of the R_{ex} parameter (Figure 6.4B). Particularly high values of R_{ex} were also observed in the linker region between β1 and β2, which may be indicative of an exchange process on the ms-μs timescale. Approximately a dozen residues required the two time-scale model (model 5) in order to properly fit the relaxation data.

Upon heterodimerization with Ubc13, ^{15}N-Mms2 displayed an average S^2 of 0.83 ± 0.16 for all residues, with an S^2 of 0.84 ± 0.16 as the mean for residues involved in secondary structural elements. The relatively large error associated with these values is representative of the significantly wider distribution of order
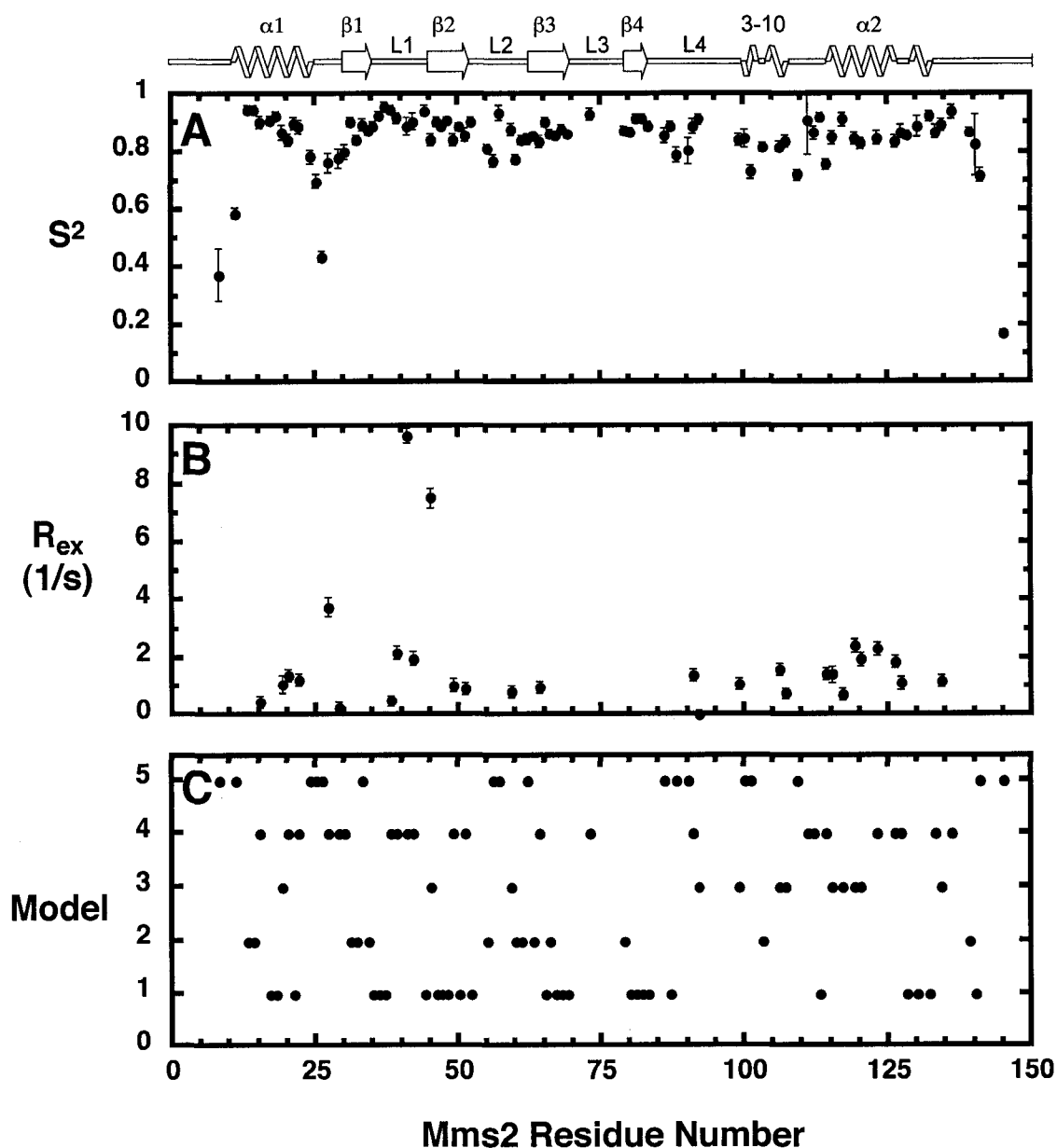
Figure 6.4 Order parameter determination for the human Mms2 protein. Plots of (A) S^2, (B) R_{ex}, and (C) model selection, determined from measurements at 600 MHz and 30 °C using the Modelfree4 program. Models used for optimization of the order parameters are as follows: model 1 (S^2), model 2 (S^2-τ_e), model 3 (S^2-R_{ex}), model 4 (S^2-τ_e-R_{ex}), or model 5 (S_f^2-S_s^2-τ_e). A schematic diagram of secondary structure is drawn above the panel. The residues in the structured regions are: $\alpha 1$ (11-24), $\beta 1$ (31-35), $\beta 2$ (45-51), $\beta 3$ (62-68), $\beta 4$ (79-82), 3_{10} helix (100-107), and $\alpha 2$ (115-132).

parameters that is observed relative to the monomeric protein. Figure 6.5 shows the S^2 values as a function of residue number, and in general, regions of secondary structure display relative backbone rigidity ($S^2\sim0.84$), whereas the termini and linker regions between secondary structure elements display lower order parameters. However, there are some notable exceptions to this observation, namely at the C-terminus of α1, where order parameters below 0.7 are observed, and at Ser[66] in β3 ($S^2=0.58$).

Upon direct comparison of the S^2 values between monomeric and heterodimerized states, the vast majority of the protein does not undergo any significant changes, as the mean ΔS^2 value reported was 0.01 ± 0.15. However, three distinct regions of the protein undergo significant changes in backbone dynamics upon complex formation. The most dramatic changes occur in and around α1, where in particular Arg[14] ($\Delta S^2=+0.80$), Glu[20] ($\Delta S^2=+0.31$), and Gly[22] ($\Delta S^2=+0.16$), which are all part of α1, display significant increases in S^2 values upon heterodimerization. Glu[41] of L1 also displays a significant increase in conformational freedom ($\Delta S^2=+0.18$). These observations are of particular interest, because α1 in combination with residues from L1 are the primary structural motifs responsible for interaction with Ubc13, which may indicate an increased flexibility associated with the interface. Furthermore, Arg[11], which is the residue N-terminal to α1, demonstrates a significant decrease in flexibility ($\Delta S^2=-0.36$), potentially indicative of a key ordering process of the N-terminus upon heterodimerization. Only two other residues throughout the protein display significant changes in backbone flexibility: Ser[66] ($\Delta S^2=+0.29$), and Met[90] ($\Delta S^2=+0.34$).

6.4.3 Human Ubc13 $^{15}N\text{-}T_1$, $^{15}N\text{-}T_2$, and NOE data.

The backbone amide ^{15}N and $^{1}H_N$ chemical shift resonances for Ubc13 have been previously assigned (Chapter 3). 91 non-overlapping residues from the $^{1}H\text{-}^{15}N$-HSQC spectra were employed in the determination of relaxation parameters.
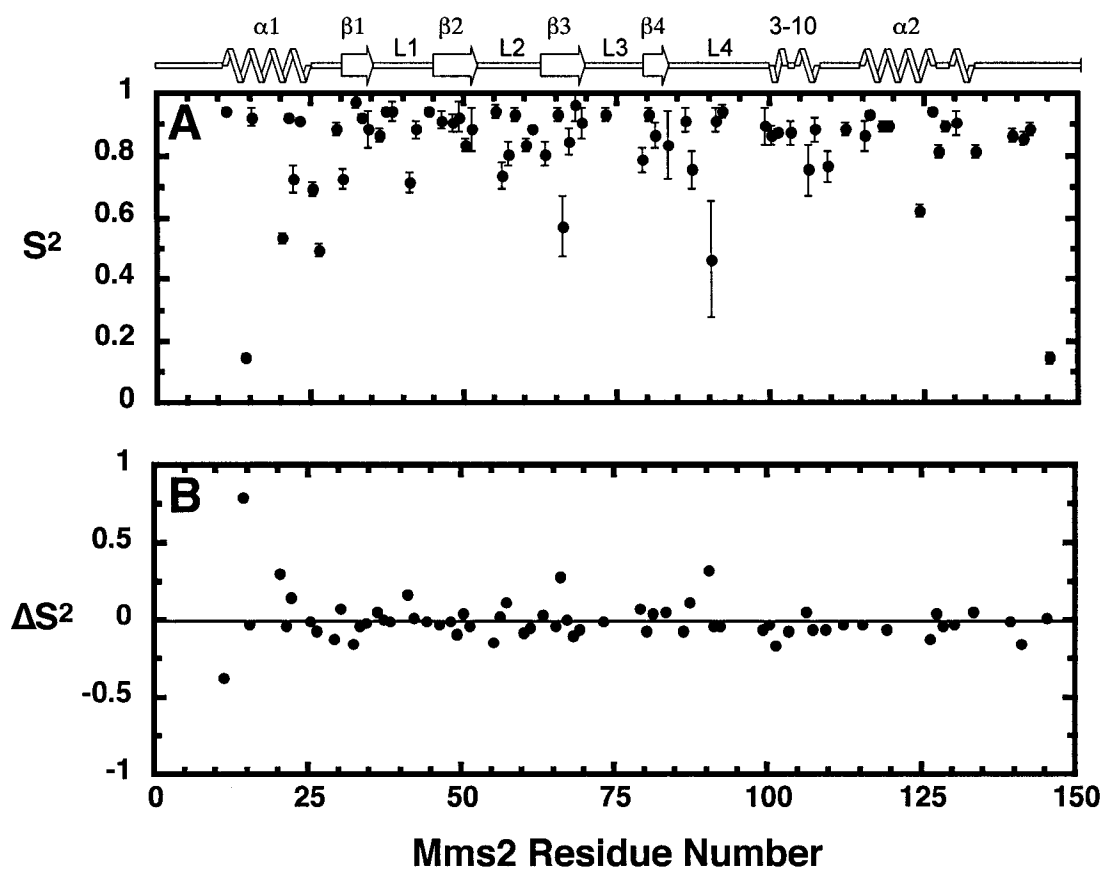
Figure 6.5   Order parameter comparison for the human Mms2 protein in its monomeric and heterodimeric forms. Plots of (A) S^2, and (B) ΔS^2 (S^2 alone-S^2 heterodimer), as measured at 600 MHz and 30 °C using the Modelfree4 program. A schematic diagram of secondary structure is drawn above the panel. The residues in the structured regions are: $\beta 1$ (11-24), $\beta 1$ (31-35), $\beta 2$ (45-51), $\beta 3$ (62-68), $\beta 4$ (79-82), 3_{10} helix (100-107), and $\alpha 2$ (115-132).

The values for ^{15}N-T_1, -T_2, and ^{1}H-^{15}N-NOE as a function of residue number and secondary structure are shown in Figure 6.6. The average T_1/T_2 ratio calculated for residues with negligible internal motions was 9.0 ± 1.8, which agrees well with that expected for a globular protein of 17 kDa (8.5 ns). Backbone relaxation experiments yielded an average ^{15}N-T_1 of 732 ± 80 ms, ^{15}N-T_2 of 79 ± 12 ms, and ^{1}H-^{15}N-NOE of 0.80 ± 0.20 respectively. Secondary structural segments possess relaxation parameters with values close to the mean, whereas loop regions and the termini display values either significantly lower (T_1, NOE) or higher (T_2) than the mean.

Identical experiments were conducted in order to determine the relaxation parameters for ^{15}N-Ubc13 upon heterodimerization with Mms2 to determine whether differences in backbone dynamics exist between the two states. The values for ^{15}N-T_1, -T_2, and ^{1}H-^{15}N-NOE as a function of residue number and secondary structure are shown in Figure 6.7. Despite increased linewidths due to complex formation, 88 non-overlapping residues were used in the analysis. The average T_1/T_2 ratio calculated for residues with negligible internal motions was 43 ± 10, and yielded an average ^{15}N-T_1 of 1354 ± 258 ms, ^{15}N-T_2 of 32 ± 5 ms, and ^{1}H-^{15}N-NOE of 0.78 ± 0.09 respectively, all of which reflect an increase in molecular weight. Again, regions of secondary structure display relaxation parameters with values closer to the mean, whereas loop regions and the termini display values divergent from the mean. However, due to the worse fit of these data, these trends are less concrete than in the case of ^{15}N-Ubc13 alone.

The Lipari-Szabo formalism was employed in order to directly compare the backbone amide ^{15}N NMR relaxation data for Ubc13 in both its monomeric and heterodimerized forms. An NOE cutoff of 0.65 was employed for ^{15}N-Ubc13 and 0.60 for ^{15}N-Ubc13/Mms2 samples, which tended to exclude residues from the termini and loop regions based on the crystal structure (8, 9). For those residues remaining, the T_1/T_2 ratio was calculated, and those whose value was not within one standard deviation of the mean were also excluded from the τ_m calculation. Using this analysis, an average T_1/T_2 ratio of 9.0 ± 1.8 and 42.7 ± 9.7 was
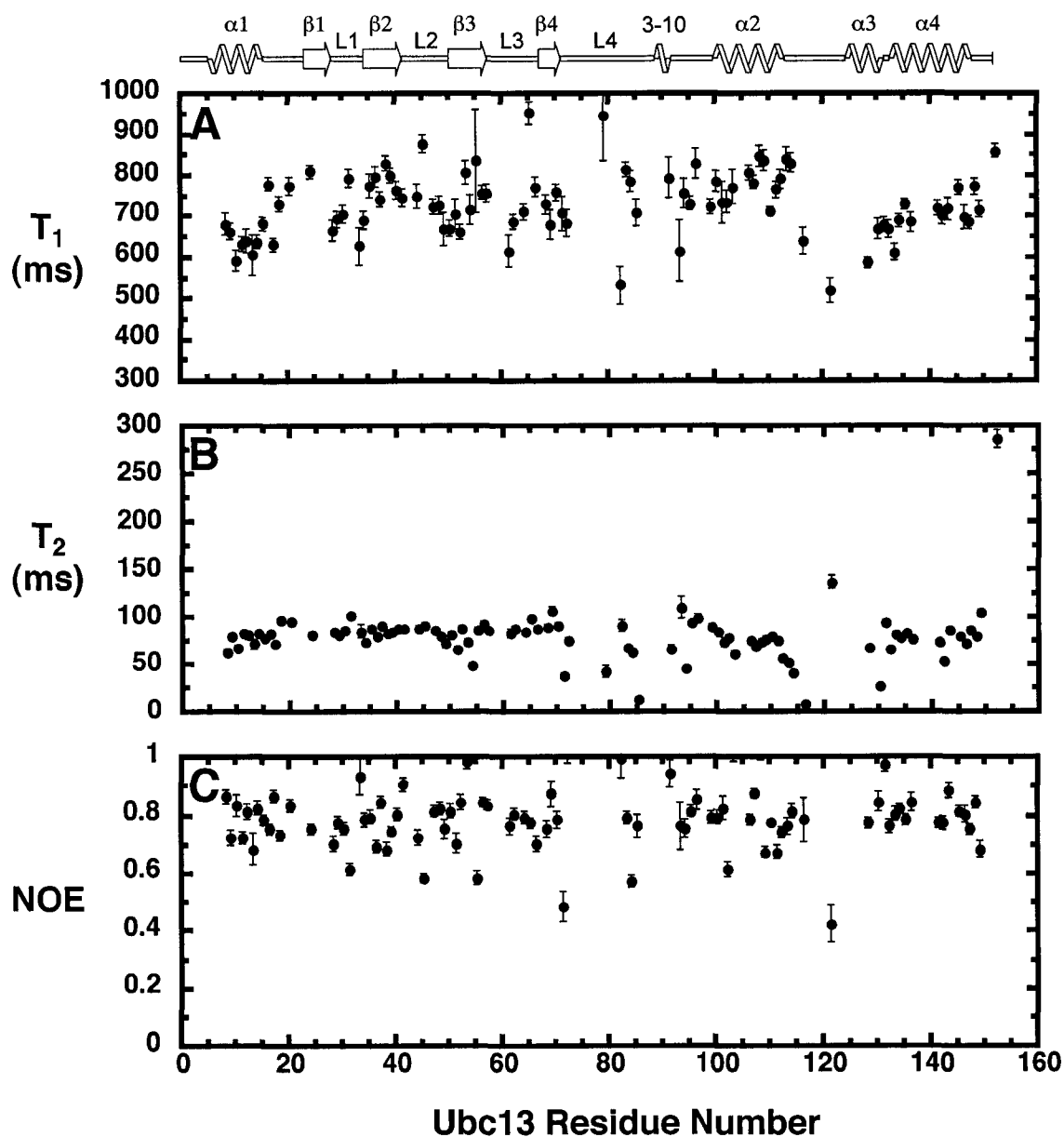
Figure 6.6 ^{15}N-relaxation parameters for the human Ubc13 protein. Plots of (A) ^{15}N-T$_1$, (B) ^{15}N-T$_2$, and (C) ^{1}H-^{15}N NOE are shown, as measured at 600 MHz and 30 °C. Each data point is shown with its associated error. The average T$_1$/T$_2$ ratio calculated for residues with negligible internal motions (NOE > 0.65) was 9.0 ± 1.8. A schematic diagram of secondary structure is drawn above the panel. The residues in the structured regions are: α1 (5-15), β1 (23-28), β2 (34-40), β3 (51-57), β4 (68-71), 3$_{10}$ helix (89-91), α2 (101-113), α3 (125-131), α4 (133-147).
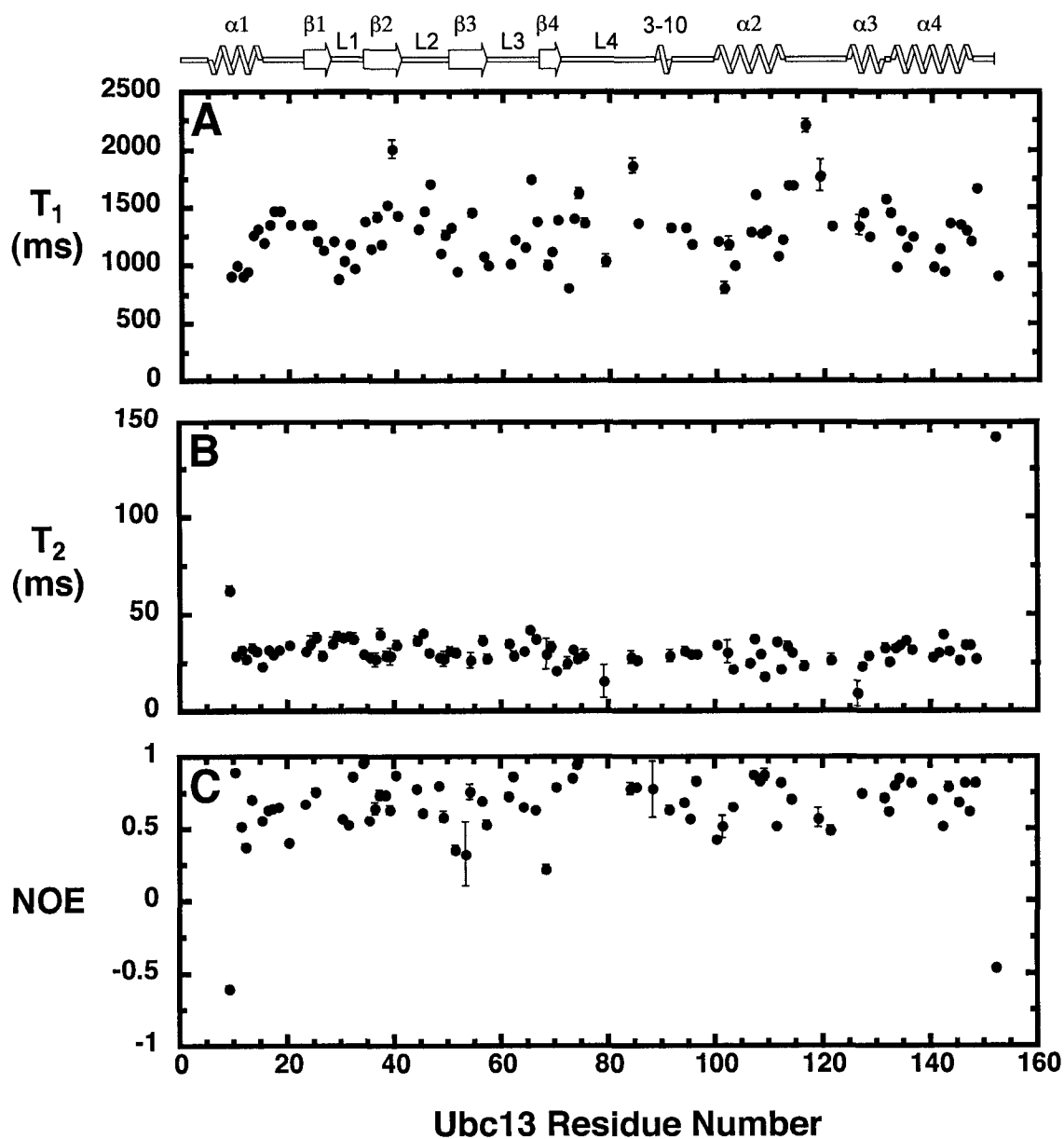
Figure 6.7 ^{15}N-relaxation parameters for the human Ubc13 protein upon heterodimerization with Mms2. Plots of (A) ^{15}N-T_1, (B) ^{15}N-T_2, and (C) ^{1}H-^{15}N NOE are shown, measured at 600 MHz and 30° C. Each data point is shown with its associated error. The average T_1/T_2 ratio calculated for residues with negligible internal motions (NOE > 0.65) was 42.7 ± 9.7. A schematic diagram of secondary structure is drawn above the panel. The residues in the structured regions are: α1 (5-15), β1 (23-28), β2 (34-40), β3 (51-57), β4 (68-71), 3_{10} helix (89-91), α2 (101-113), α3 (125-131), α4 (133-147).

determined for Ubc13 alone and in complex with Mms2, respectively. Global τ_m values of 8.8 ns for ^{15}N-Ubc13 and 19.6 ns for ^{15}N-Ubc13/Mms2 were established, and represent reasonable values given that the heterodimer is roughly twice the molecular weight of the Ubc13 subunit alone.

Using coordinates of the crystal structures, the relaxation data were analyzed in terms of isotropic, axially symmetric, and fully asymmetric rotational correlation models. Using this approach, the rotational tumbling of Ubc13 alone was best represented by an axially symmetric model with an axial ratio ($D_\parallel / D_\perp$) of 1.25, whereas ^{15}N-Ubc13/Mms2 was best represented by an isotropic tumbling model. Therefore, when optimizing the results of the Lipari-Szabo formalism, the anisotropy in Ubc13 was taken into account.

6.4.4 Human Ubc13 modelfree analysis

Order parameters were calculated on a per-residue basis by fitting the relaxation parameters (T_1, T_2, NOE) to one of five spectral density models for both ^{15}N-Ubc13 alone and in complex with unlabeled Mms2. For the Ubc13 subunit alone, an average S^2 of 0.84 ± 0.09 was determined for all residues, with an S^2 of 0.86 ± 0.08 as the mean for residues involved in secondary structural elements. The error associated with each of these values is quite reasonable, and indicates that the majority of the residues in Ubc13 behave in a fairly typical manner. Figure 6.8 shows the S^2 values as a function of residue number, and demonstrates that regions of secondary structure display relative backbone rigidity (S^2~0.85), whereas the linker regions between secondary structure elements display lower order parameters. Although all of the linker regions display backbone flexibility, a few residues in L4 display significantly lower order parameters than most (Figure 6.8A).

As opposed to Mms2, models 1 and 2 fit the majority of the residues in Ubc13. However, some residues required the addition of either the R_{ex} parameter (models 3 and 4) or a two time-scale approach (model 5) to fit the data properly (Figure 6.8B,C).
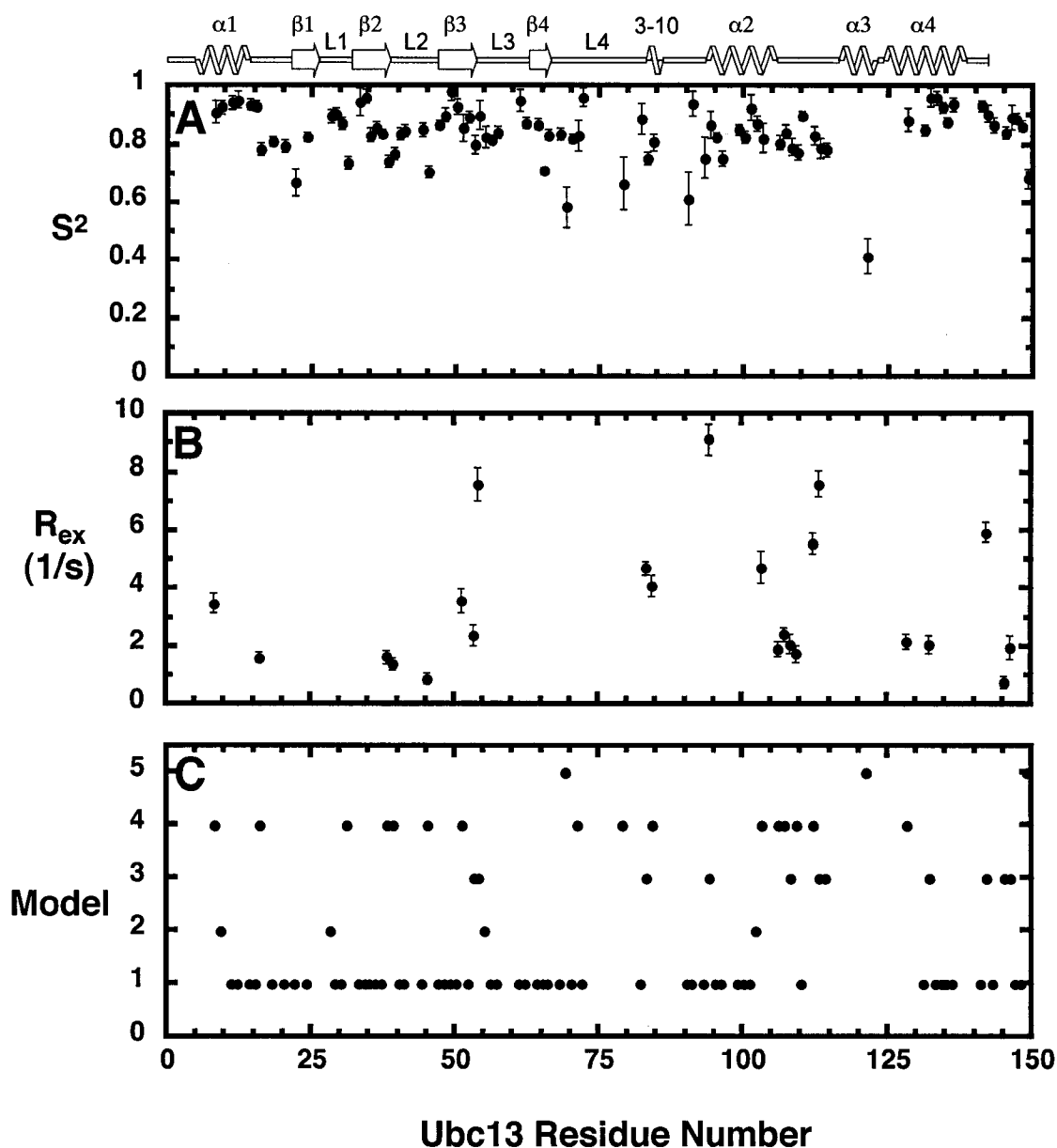
Figure 6.8 Order parameter determination for the human Ubc13 protein. Plots of (A) S^2, (B) R_{ex}, and (C) model selection, as measured at 600 MHz and 30 °C using the Modelfree4 program. Models used for optimization of the order parameters are as follows: model 1 (S^2), model 2 (S^2-τ_e), model 3 (S^2-R_{ex}), model 4 (S^2-τ_e-R_{ex}), or model 5 (S_f^2-S_s^2-τ_e).A schematic diagram of secondary structure is drawn above the panel. The residues in the structured regions are: $\alpha1$ (5-15), $\beta1$ (23-28), $\beta2$ (34-40), $\beta3$ (51-57), $\beta4$ (68-71), 3_{10} helix (89-91), $\alpha2$ (101-113), $\alpha3$ (125-131), $\alpha4$ (133-147).

Upon heterodimerization with Mms2, ^{15}N-Ubc13 displayed an average S^2 of 0.86 ± 0.10, with an S^2 of 0.86 ± 0.09 for residues involved in secondary structural elements (*8*). Unfortunately, due to increased linewidth compared to the monomeric protein, numerous peaks were either unobservable or too broad to be used reliably for Modelfree analysis. As a result, only a partial picture of the backbone dynamics is observed. Figure 6.9 shows the S^2 values as a function of residue number, and regions of secondary structure display relative backbone rigidity (S^2~0.85), whereas the linker regions between secondary structure elements display lower order parameters. However, there are some notable exceptions to this observation, namely at the C-terminus of α1, and within α2, where numerous order parameters below 0.8 are observed.

Upon direct comparison of the S^2 values between monomeric and heterodimerized states, the vast majority of the protein does not undergo any significant changes, as the average ΔS^2 was –0.01 ± 0.13. Due to the partial completeness of the heterodimer data, particularly with respect to residues surrounding the active-site Cys^{87}, this comparison should be approached with caution. However, distinct regions of the protein did apparently undergo significant changes in dynamics upon complex formation, and may therefore give us some useful information. The most dramatic changes occur in α1, where in particular Ile^9 (ΔS^2=+0.40), Glu^{11} (ΔS^2=+0.16), and Thr^{12} (ΔS^2=+0.18), display significant increases in backbone dynamics upon heterodimerization. The interpretation of these results is, however, not terribly straightforward because α1 is not apparently involved in directly mediating any known protein-protein interactions. A second region of interest involves the increased flexibility observed around the active-site of Ubc13, namely Gly^{84} (ΔS^2=+0.12), Ser^{96} (ΔS^2=+0.30), and Ile^{101} (ΔS^2=+0.20). These residues may indicate an increase backbone flexibility around the donor Ub binding site upon heterodimerization. Leu^{121}, which is the N-terminal to α3, demonstrates a significant decrease in flexibility (ΔS^2=-0.51), however the interpretation of this result is unclear in the context of the known structural interactions within the system.
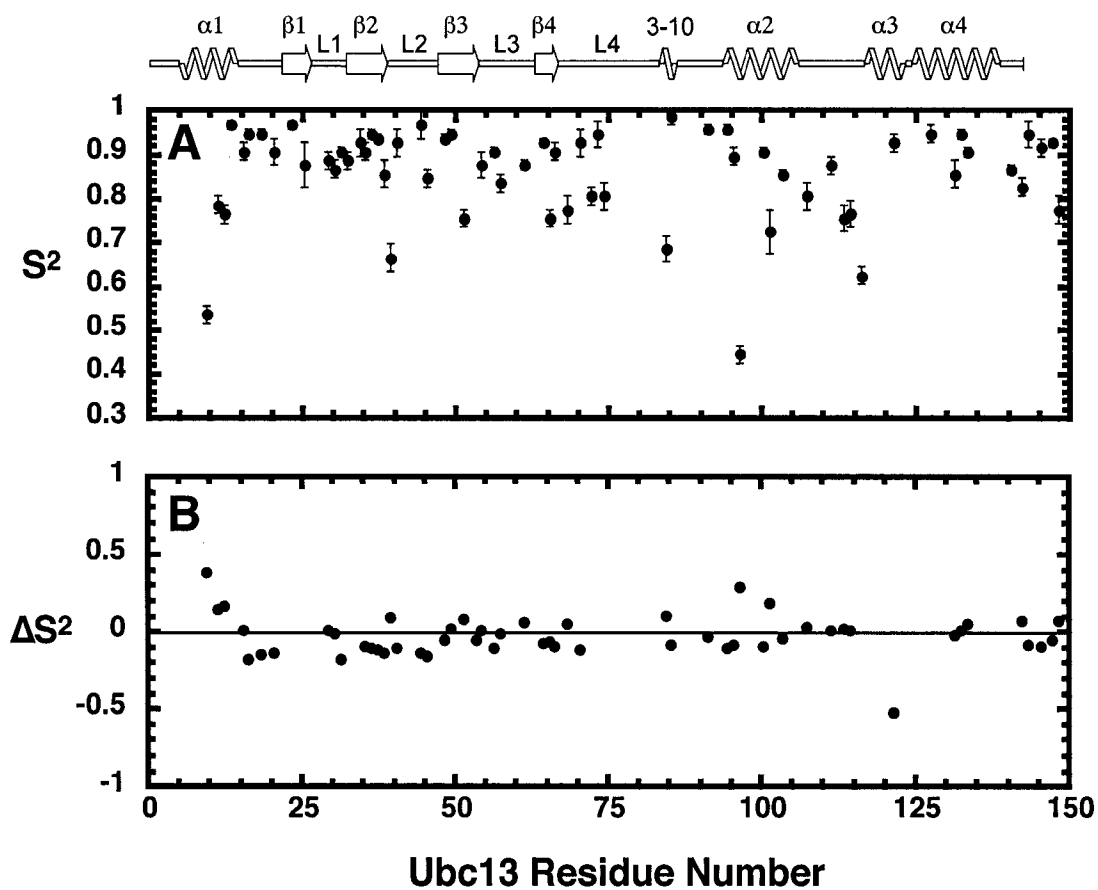
Figure 6.9   Order parameter comparison for the human Ubc13 protein in its monomeric and heterodimeric forms. Plots of (A) S^2, and (B) ΔS^2 (S^2 alone-S^2 heterodimer), as measured at 600 MHz and 30 °C using the Modelfree4 program. A schematic diagram of secondary structure is drawn above the panel. The residues in the structured regions are: $\alpha 1$ (5-15), $\beta 1$ (23-28), $\beta 2$ (34-40), $\beta 3$ (51-57), $\beta 4$ (68-71), 3_{10} helix (89-91), $\alpha 2$ (101-113), $\alpha 3$ (125-131), $\alpha 4$ (133-147).

6.5 DISCUSSION

^{15}N-T_1, -T_2, and ^{1}H-^{15}N-NOE backbone dynamics experiments can provide extremely useful information about the inherent conformational flexibility in regions of secondary structure within a protein. These experimental results are often interpreted through the calculation of order parameters (S^2), which can be used for comparison of backbone dynamics between two different states of a protein (*i.e.* ligand bound vs. unbound), or between two different proteins of interest. With respect to the Ubc13/Mms2 system, we sought to characterize and compare the backbone dynamics of (i) each protein in its monomeric and heterodimeric states, and (ii) each protein relative to each other in order to examine the differences between a catalytically active and inactive homologue.

Prior to a discussion of the results, two key problems regarding this form of analysis should be discussed in order to place the results presented in their proper context. First, while backbone NMR relaxation experiments can serve as a useful first step in characterizing dynamic regions of a protein, they are extremely limited in terms of characterizing protein-protein interfaces when compared to ^{13}C-methyl side chain dynamics. Second, while the relaxation data for the monomeric proteins is quite satisfactory, the number of overlapping or unobservable peaks upon heterodimerization represents a serious limit to the proper analysis of these proteins. This problem could be overcome by deuteration strategies and increased concentration, but was not performed due to time and material constraints. In spite of these shortcomings, the relaxation data presented in this chapter represent an excellent preliminary step towards characterizing the dynamics of this interesting biological system.

The characterization of the Ubc13/Mms2 heterodimer interface by backbone relaxation approaches proved most interesting, as significant changes in conformational freedom, particularly in Mms2, appear to play a role in mediating the Ubc13/Mms2 interaction. Significant increases in backbone dynamics were observed for numerous residues in α1 (Arg^{14}, Glu^{20}, Gly^{22}) and L1 (Glu^{41}) of Mms2, whereas a noticeable decrease in backbone dynamics was

observed at Arg[11], the residue immediately preceding α1. Given that the crystal structures of monomeric and heterodimerized Mms2 display a distinct reorientation of α1 such that it forms the primary surface of interaction with the β-sheet of Ubc13, the observed increase in conformational entropy within this region of Mms2 combined with a distinct ordering of the residue preceding the helix may suggest a significant entropic contribution to the binding. Although some complementary increases in backbone flexibility were observed in the β-sheet of Ubc13, the overall values for ΔS^2 in this region remain close to zero. Therefore, while these results do point towards a potentially interesting phenomenon, more work, particularly side chain dynamics, could prove more informative.

The acceptor Ub binding site on Mms2 does not appear to be mediated by dynamic regions of the protein but rather by rigid secondary structural elements (β-sheet). Furthermore, this interface does not demonstrate significant changes in dynamics upon heterodimerization. Therefore, the dynamic properties of this Uev do not appear to play a central role in mediating non-covalent Ub binding.

An RMSD of 0.8 Å for superimposition of all backbone C_α atoms between free and Mms2-bound Ubc13 has been reported, with their active site clefts structurally superimposable (9). Ubc13 thiolester formation with donor Ub, however, appears to employ regions of the protein, which are both inherently dynamic (L4 and the 3_{10} helix) as well as relatively rigid secondary structural elements (α2). Unfortunately, the region surrounding the active-site of Ubc13 was remarkably difficult to characterize using backbone dynamics as very few resonance cross-peaks in this region were observable. This problem is highlighted when Ubc13 is heterodimerized, as linewidth broadening becomes a factor.

A third initiative with respect to characterizing these proteins dynamically was the fact that we could compare a catalytically active and inactive homologue to each other by using S^2 values as a measure of ^1H_N-^{15}N bond rigidity. Overall, the general trend that is observed in most proteins was also seen for both Ubc13

and Mms2: secondary structural elements were rigid ($S^2 \sim 0.85$), whereas linker regions between these elements possessed lower S^2 values. Two differences, however, between these two proteins were discernable. First, the linker between $\alpha 1$ and $\beta 1$ in Mms2 is significantly more flexible than its Ubc13 counterpart. This result could reflect the requirement for the conformational reorientation of $\alpha 1$ upon heterodimerization. Second, although the data is not complete around the active-site region of Ubc13, there is significantly greater backbone flexibility in this region than near the corresponding vestigial active-site on Mms2. As there has yet to be a functional role characterized for the vestigial active-site on Mms2, it is not surprising that the potential need for flexibility in the formation of thiolester on Ubc13 is not required for Mms2.

Overall, the results presented in this chapter present a solid foundation for the future study of dynamics within the Ubc13/Mms2 system. An obvious next step is the examination of side chain dynamics, which should prove more informative and render a more complete data set than those presented here.

6.6 REFERENCES

1.   Hofmann, R. M., and Pickart, C. M. (1999) *Cell 96*, 645-53.

2.   Hoege, C., Pfander, B., Moldovan, G. L., Pyrowolakis, G., and Jentsch, S. (2002) *Nature 419*, 135-41.

3.   Broomfield, S., Chow, B. L., and Xiao, W. (1998) *Proc Natl Acad Sci U S A 95*, 5678-83.

4.   Brusky, J., Zhu, Y., and Xiao, W. (2000) *Curr Genet 37*, 168-74.

5.   Ulrich, H. D. (2003) *J Biol Chem 278*, 7051-8.

6.   Deng, L., Wang, C., Spencer, E., Yang, L., Braun, A., You, J., Slaughter, C., Pickart, C., and Chen, Z. J. (2000) *Cell 103*, 351-61.

7.   Wang, C., Deng, L., Hong, M., Akkaraju, G. R., Inoue, J., and Chen, Z. J. (2001) *Nature 412*, 346-51.

8.   Moraes, T. F., Edwards, R. A., McKenna, S., Pastushok, L., Xiao, W., Glover, J. N., and Ellison, M. J. (2001) *Nat Struct Biol 8*, 669-73.

9.   VanDemark, A. P., Hofmann, R. M., Tsui, C., Pickart, C. M., and Wolberger, C. (2001) *Cell 105*, 711-20.

10.   McKenna, S., Spyracopoulos, L., Moraes, T., Pastushok, L., Ptak, C., Xiao, W., and Ellison, M. J. (2001) *J Biol Chem 276*, 40120-6.

11.   McKenna, S., Moraes, T., Pastushok, L., Ptak, C., Xiao, W., Spyracopoulos, L., and Ellison, M. J. (2003) *J Biol Chem 278*, 13151-8.

12.   Kay, L. E. (1998) *Biochem Cell Biol 76*, 145-52.

13.   Palmer, A. G., 3rd. (1993) *Curr Opin Biotechnol 4*, 385-91.

14.   Lipari, G., Szabo, A. (1982) *J. Am. Chem. Soc. 104*, 4546-4559.

15.   Lipari, G., Szabo, A. (1982) *J. Am. Chem. Soc. 104*, 4559-4570.

16.   Kay, L. E., Torchia, D. A., and Bax, A. (1989) *Biochemistry 28*, 8972-9.

17.   Akke, M., Bruschweiler, R., and Palmer, A.G. (1993) *J. Am. Chem. Soc. 115*, 9832-9833.

18.   Li, Z., Raychaudhuri, S., and Wand, A. J. (1996) *Protein Sci 5*, 2647-50.

19. Yang, D., and Kay, L. E. (1996) *J Mol Biol 263*, 369-82.

20. Yang, D., Mok, Y. K., Forman-Kay, J. D., Farrow, N. A., and Kay, L. E. (1997) *J Mol Biol 272*, 790-804.

21. Farrow, N. A., Muhandiram, R., Singer, A. U., Pascal, S. M., Kay, C. M., Gish, G., Shoelson, S. E., Pawson, T., Forman-Kay, J. D., and Kay, L. E. (1994) *Biochemistry 33*, 5984-6003.

22. Gagne, S. M., Li, M. X., McKay, R. T., and Sykes, B. D. (1998) *Biochem Cell Biol 76*, 302-12.

23. Delaglio, F., Grzesiek, S., Vuister, G. W., Zhu, G., Pfeifer, J., and Bax, A. (1995) *J Biomol NMR 6*, 277-93.

24. Johnson, B. A., Blevins, R.A. (1994) *J. Chem. Phys. 29*, 1012-1014.

25. Abragam, A. (1961) *Principles of Nuclear Magnetism*, Clarendon Press, Oxford, U.K.

26. Clore, G. M., Driscoll, P. C., Wingfield, P. T., and Gronenborn, A. M. (1990) *Biochemistry 29*, 7387-401.

27. Clore, G. M., Szabo, A., Bax, A., Kay, L.E., Driscoll, P.C., and Gronenborn, A.M. (1990) *J. Am. Chem. Soc. 112*, 4989-4991.

28. Mandel, A. M., Akke, M., and Palmer, A. G., 3rd. (1995) *J Mol Biol 246*, 144-63.

29. Palmer, A. G., Rance, M., Wright, P.E. (1991) *J. Am. Chem. Soc. 113*, 4371-4380.

30. Tjandra, N., Kuboniwa, H., Ren, H., and Bax, A. (1995) *Eur J Biochem 230*, 1014-24.

31. Woessner, D. E. (1962) *J. Chem. Phys. 37*, 647-654.

32. Wennerström, H. (1972) *Mol. Phys. 24*, 69-80.

33. Barbato, G., Ikura, M., Kay, L. E., Pastor, R. W., and Bax, A. (1992) *Biochemistry 31*, 5269-78.

34. Gagne, S. M., Tsuda, S., Spyracopoulos, L., Kay, L. E., and Sykes, B. D. (1998) *J Mol Biol 278*, 667-86.

35. Tjandra, N., Feller, S.E., Pastor, R.W., Bax, A. (1995) *J. Am. Chem. Soc. 117*, 12562-12566.

36. Luginbuhl, P., Pervushin, K. V., Iwai, H., and Wuthrich, K. (1997) *Biochemistry 36*, 7305-12.

37. Lee, L. K., Rance, M., Chazin, W. J., and Palmer, A. G., 3rd. (1997) *J Biomol NMR 9*, 287-98.

CHAPTER 7:

Comparison of Ub-binding within the Ub-conjugating enzyme family

7.1 SUMMARY

Previous studies have indicated that E2 enzymes and their variants may possess two distinct but equally important Ub binding sites. Thiolester formation between the active-site Cys of the E2 and a Ub molecule is required to transfer activated Ub moieties to an elongating chain. A second, and potentially novel role for the E2 enzymes is the ability to accommodate a second molecule of Ub, which may serve to facilitate either poly-Ub chain formation (*e.g.* Ubc13/Uev systems) or interaction with other proteins containing Ub-like domains (*e.g.* E1). In order to examine the similarities and differences amongst E2 family members, three additional E2 enzymes from *S. cerevisiae* (Cdc34, Ubc1, and Rad6) were investigated with respect to these two potential Ub-binding sites. ^{1}H-^{15}N-HSQC NMR chemical shift perturbation assays were employed in order to detect both thiolester intermediate and non-covalent Ub binding, and were complemented by both *in vitro* chain building and *in vivo* complementation assays. While the results are preliminary, the data suggest that the structural features required for thiolester formation by E2 family members is highly conserved, although slightly different surfaces mediate the interaction on different E2s. Preliminary evidence also suggests that E2s may bind Ub non-covalently, although the biological role of this Ub-binding event remains to be determined.

7.2 INTRODUCTION

As discussed extensively in previous chapters, the covalent attachment of poly-Ub chains to target substrates involves a series of three enzymatic steps mediated in succession by the E1 (Ub-activating enzyme), E2 (Ub-conjugating enzyme) and E3 (Ub-protein ligase) proteins (*1, 2*). The first step involves the

ATP-dependent activation of Ub to form a high-energy thiolester linkage between the C-terminal tail of Ub (Gly^{76}) and the active site Cys of E1. The activated Ub moiety is subsequently transferred from E1 to the active-site Cys of an E2 via a transthiolesterification reaction. Ultimately, often in combination with an E3 enzyme, Ub is transferred from the E2 to the ε-amino group of a surface exposed Lys residue on the target protein, forming a covalent isopeptide bond. Poly-Ub chains are formed by the repetitive conjugation of Ub molecules onto a Lys residue (e.g. Lys^{48} vs. Lys^{63}) of the terminal Ub moiety in the existing chain (1, 2). However, the catalytic mechanism whereby Ub chain extension is mediated remains mostly uncharacterized.

Target substrate specificity is dependent largely on the specific combination of E2 and E3 proteins which are employed (3-6). This combinatorial feature of ubiquitination is also responsible for the type and length of poly-Ub chain linkage that is assembled on a particular target substrate. For example, in S. cerevisiae, the use of a particular Ub-conjugation complex (Ubc13/Mms2) is responsible for the assembly of Lys^{63}-linked chains (7-10), and its interaction with an appropriate E3 (Rad5) results in the ubiquitination of a specific target substrate, PCNA (11, 12). Conversely, the use of a different E2-E3 combination (Rad6-Rad18) results in monoubiquitination of the same target (11, 13, 14). Another layer of complexity exists as analogous protein conjugation systems exist which share conserved mechanisms with protein ubiquitination (2). For example, a structural homologue of Ub, SUMO, is conjugated onto PCNA by a unique E2 (Ubc9) (11, 15).

What is remarkable about the protein ubiquitination system is that despite the diversity in substrate recognition and poly-Ub chain linkages, the basic cascade mechanism appears to be highly conserved, particularly with respect to the E2s. Within the family of known E2s, all share a highly similar catalytic core domain of ~150 amino acid residues, and are classified based on the presence or absence of C- and N-terminal extensions, which are thought to potentially help mediate E2-E3 interactions, or serve auto-regulatory roles (16). Type I enzymes

lack extensions, whereas type II, III, and IV E2s have respective C-terminal, N-terminal, or both C- and N-terminal additions to the core domain (Fig. 7.1) (*17*). Numerous overlapping structural studies have confirmed that the fold of the core domain is highly conserved amongst family members (*18-26*), although a structural understanding of the tail regions and distinctive loops (Fig. 7.1) have remained largely elusive. Interactions between Ub and E2s within thiolester intermediates also appear to be highly conserved (*9, 10, 27-31*). Furthermore, evidence is emerging that E2 self-association and/or heterodimerization may play a key role in E2 function (*8, 32-38*). Therefore it appears as though the vast majority of an E2's functional abilities are conserved amongst family members, and raises the intriguing possibility that other features that have only been observed for some of the family members may represent a general trend (*i.e.* non-covalent Ub binding).

In the current chapter, we sought to examine the differences and similarities amongst the E2 family members by investigating the role of their N- and C- terminal extensions, thiolester formation, and non-covalent interactions with Ub from a structural perspective. In this pursuit, a comparison between human Ubc13 and Mms2 (which build non-canonical Lys^{63}-linked chains) and three *S. cerevisiae* E2s, Ubc1, Rad6 and Cdc34 (which each build Lys^{48}-linked chains) was undertaken.

Ubc1, a class II E2 with a 65-residue C-terminal extension, is a necessary component of the stress-response in the absence of Ubc4 and Ubc5 (*39*). The C-terminus of this tail has been demonstrated essential for the G_0-G_1 transition during sporulation (*40*). Rad6 (Ubc2) is a class IV E2 with a 2-residue N-terminal and an acidic 22-residue C-terminal addition to the core domain (*2*). Rad6's ubiquitin-conjugation activity is essential for a variety of DNA repair pathways, as is highlighted by *rad6* mutants' sensitivity to UV light and other DNA damaging agents (*41-43*). Cdc34 (Ubc3) is a class IV E2 with an 8-residue N-terminal and 126-residue C-terminal addition to the core domain, each of which play a role in its cell cycle function (*44-47*). Cdc34 is responsible for the G_1 to S phase

	Insertions		Extensions	
	a	b	N-terminal	C-terminal
UBC4	–	–	–	–
UBC5	–	–	–	–
UBC13	–	–	1	–
UBC1	1	–	–	65
UBC9	5	2	1	–
UBC8	–	–	-1	58
UBC12	–	–	28	–
UBC11	–	–	6	–
RAD6	–	–	2	22
CDC34	1	12	8	126
UBC7	1	13	2	–
UBC6	–	3	3	98
MMS 2	4	2	3	-20
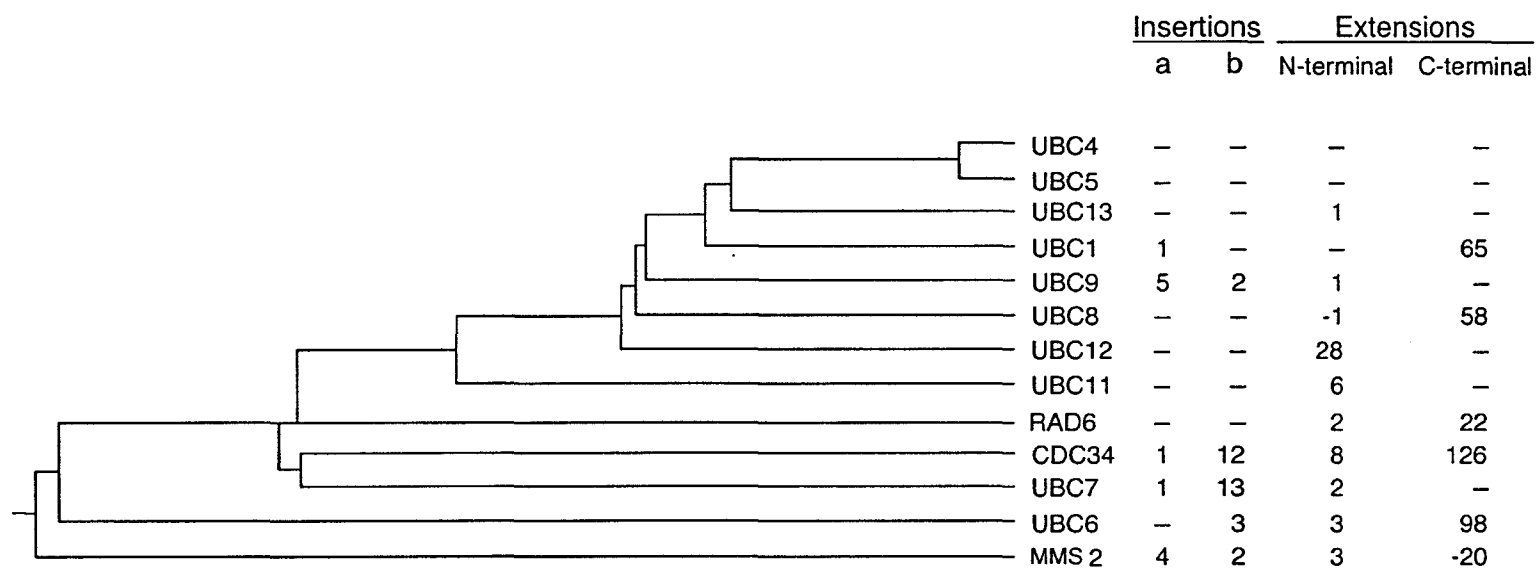
Figure 7.1 Evolutionary relationships among E2s from S. cerevisiae. Indicated are the lengths of the major sequence landmarks for each E2, and include insertion lengths (a and b), as well as N- and C-terminal extensions. Figure adapted from (47).

transition in the *S. cerevisiae* cell cycle, and is responsible for the degradation of several short-lived cell cycle-related proteins (*3, 48*).

We highlight in this chapter that despite the variety in the type, length, and biological outcomes of poly-Ub chain assembly, members of the E2 family share more commonalities than they do differences.

7.3 EXPERIMENTAL PROCEDURES

7.3.1 Expression and purification of recombinant Cdc34 and its derivatives

S. cerevisiae Cdc34 open reading frames for the wild-type protein as well as two C-terminal truncations (*cdc34Δ_{244}* and *cdc34Δ_{209}*) were originally excised from yeast high copy plasmids as *SstI-KpnI* fragments (*37*), and cloned into the corresponding sites of a modified pET-3a overexpression vector (*49*).

These expression plasmids were transformed into the *E. coli* strain *BL21(DE_3)-pLysS* (Stratagene) using standard chemical transformation methodologies. 2 L cultures were grown at 37° C to $OD_{590}= 0.3$ in LB media containing ampicillin (50 μg/ml) and chloramphenicol (34 μg/ml) followed by induction with IPTG (0.4 mM) for 5 hours at 37° C. Cells were harvested by centrifugation, and stored at –80° C. All subsequent steps were performed at 4° C.

Cell pellets were resuspended in 30 mL of Q-Sepharose Buffer A (50 mM Tris/Cl pH 7.5, 1 mM EDTA, 1 mM DTT), lysed by sonication at maximum setting until clarified, followed by centrifugation (40,000 rpm for 1 hour). The filtered lysate was applied at 2.5 mL/min to a HiLoad Q-Sepharose 26/10 ion exchange column (Pharmacia), previously equilibrated with Q-Sepharose Buffer A. The column was washed with 50 mL of Q-Sepharose Buffer A, and the retained protein was eluted with a gradient that ranged from 0 to 2 M NaCl by using linear combinations of Q-Sepharose Buffer A and Buffer B (50 mM Tris/Cl pH 7.5, 2 M NaCl, 1 mM EDTA, 1 mM DTT). Each derivative eluted as a major protein peak at a specific NaCl concentration: Cdc34 at 460 mM, cdc34Δ_{244} at 390 mM, cdc34Δ_{209}, and at 275 mM.

The eluate was concentrated to 2 mL using an Ultrafree Centrifugal Filter Device (Millipore- 10 kDa molecular mass cutoff) and applied to a Hi-Load 16/60 Superdex 75 column (Pharmacia) equilibrated with 200 mL of Superdex 75 buffer (50 mM HEPES pH 7.5, 75 mM NaCl, 1 mM EDTA, 1 mM DTT). Proteins were eluted at a flow rate of 1 mL/min, and collected in 1 mL fractions. Cdc34 and its derivatives were judged to be pure by SDS-PAGE. Samples were subsequently pooled and concentrated.

7.3.2 Expression and purification of recombinant ubc1Δ

The *S. cerevisiae* ubc1Δ open reading frame was originally excised from yeast high copy plasmids as *SstI-KpnI* fragments, and cloned into the corresponding sites of a modified pET-3a overexpression vector in a manner identical to that described for *Cdc34* and its derivatives in the preceding section. The ubc1Δ truncation represents the deletion of codons 151 to 215, encoding unconserved the C-terminal tail of the protein (*50*). Numerous derivatives of the ubc1Δ plasmid were created for the purposes of testing their *in vitro* and *in vivo* properties, each representing a single point mutation that was introduced by PCR site-directed mutagenesis. These included the following substitutions: $Thr^{73}Ala$, $Thr^{73}Arg$, $Lys^{74}Ala$, $Ser^{82}Cys$, $Ser^{97}Cys$, $Ser^{115}Cys$, and $Ala^{111}Arg$. A further mutant was constructed in which five Ala substitutions were included (Ala^{125}): $Glu^{125}Ala/ His^{129}Ala/ Leu^{131}Ala/ Arg^{132}Ala/ Glu^{135}Ala$. In order to perform NMR experiments in which thiolester assembly was probed the additional substitution of $Lys^{93}Arg$ was introduced into both ubc1Δ and each of the aforementioned mutants so as to eliminate the formation of Ub-E2 conjugate formation.

These expression plasmids were transformed into the *E. coli* strain *BL21(DE₃)-pLysS* (Stratagene) using standard chemical transformation methodologies. 2 L cultures were grown at 37° C to $OD_{590}= 0.5$ in LB media containing ampicillin (50 μg/ml) and chloramphenicol (34 μg/ml) followed by induction with IPTG (0.4 mM) for 5 hours at 37° C. Cells were harvested by

centrifugation, and stored at −80° C. All subsequent steps were performed at 4° C.

Cell pellets were resuspended in 15 mL of Q-Sepharose Buffer A (50 mM Tris/Cl pH 7.5, 1 mM EDTA, 1 mM DTT), lysed by sonication at maximum setting until clarified, followed by centrifugation (40,000 rpm for 1 hour). The filtered lysate was applied at 2.5 mL/min to a HiLoad Q-Sepharose 26/10 ion exchange column (Pharmacia), previously equilibrated with Q-Sepharose Buffer A. ubc1Δ is not retained by the ion exchange column, and therefore upon washing with Q-Sepharose Buffer A, ubc1Δ and its derivatives can be collected as flow-through.

The broad flow-through peak was pooled, and concentrated to 2 mL using an Ultrafree Centrifugal Filter Device (Millipore- 10 kDa molecular mass cutoff). The concentrated sample was dialyzed against 1 L of Superdex 75 buffer (50 mM HEPES pH 7.5, 75 mM NaCl, 1 mM EDTA, 1 mM DTT) overnight at 4° C and clarified through a 0.45 μm low protein binding filter (Millipore). The sample was then applied to a Hi-Load 16/60 Superdex 75 column (Pharmacia) equilibrated with 200 mL of Superdex 75 buffer (50 mM HEPES pH 7.5, 75 mM NaCl, 1 mM EDTA, 1 mM DTT). Proteins were eluted at a flow rate of 1 mL/min, and collected in 1 mL fractions. ubc1Δ typically elutes with a major peak centered at fraction 80. ubc1Δ and its derivatives were judged to be pure by SDS-PAGE. Samples were subsequently pooled and concentrated.

7.3.3 Expression and purification of recombinant rad6Δ

The *S. cerevisiae rad6Δ* open reading frame was originally excised from yeast high copy plasmids as *SstI-KpnI* fragments, and cloned into the corresponding sites of a modified pET-3a overexpression vector in a manner identical to that described for *Cdc34* and its derivatives in a preceding section. The rad6Δ truncation represents the deletion of the 18 amino acids in the unconserved the C-terminal tail of the protein, leaving the core domain consisting of the N-terminal 153 amino acid residues.

The expression plasmids were transformed into the *E. coli* strain *BL21(DE₃)-pLysS* (Stratagene) using standard chemical transformation methodologies. 2 L cultures were grown at 37 °C to OD_{590}= 0.5 in LB media containing ampicillin (50 μg/mL) and chloramphenicol (34 μg/mL) followed by induction with IPTG (0.4mM) for 5 hours at 37 °C. Cells were harvested by centrifugation, and stored at –80° C. All subsequent steps were performed at 4° C.

Cell pellets were resuspended in 50 mL of Q-Sepharose Buffer A (50 mM Tris/Cl pH 7.5, 1 mM EDTA, 1 mM DTT), lysed by sonication at maximum setting until clarified, followed by centrifugation (40,000 rpm for 1 hour). The filtered lysate was applied at 2.5 mL/min to a HiLoad Q-Sepharose 26/10 ion exchange column (Pharmacia), previously equilibrated with Q-Sepharose Buffer A. rad6Δ is retained by the ion exchange column, and was therefore eluted (at an approximate [NaCl] = 250 mM) by using an identical NaCl gradient to that described for Cdc34 (Section 7.3.1).

The eluate peak fractions were pooled, and concentrated to 2 mL using an Ultrafree Centrifugal Filter Device (Millipore- 10 kDa molecular mass cutoff). The concentrated sample was dialyzed against 1 L of Superdex 75 buffer (50 mM HEPES pH 7.5, 75 mM NaCl, 1 mM EDTA, 1 mM DTT) overnight at 4 °C and clarified through a 0.45 μm low protein binding filter (Millipore). The sample was then applied to a Hi-Load 16/60 Superdex 75 column (Pharmacia) equilibrated with 200 mL of Superdex 75 buffer (50 mM HEPES pH 7.5, 75 mM NaCl, 1 mM EDTA, 1 mM DTT). Proteins were eluted at a flow rate of 1 mL/min, and collected in 1 mL fractions. rad6Δ and its derivatives were judged to be pure by SDS-PAGE. Samples were subsequently pooled and concentrated.

7.3.4 NMR spectroscopy

All NMR spectra were obtained using a Varian Unity INOVA 600 MHz spectrometer at 30°C, with the exception of ubc1Δ data which was performed on an analogous 500 MHz machine. The 2D ^{1}H-^{15}N-HSQC NMR spectra were

acquired using the sensitivity-enhanced gradient pulse scheme developed by Kay and co-workers (51, 52). The ^{1}H and ^{15}N sweep widths were 8000 and 2200 Hz, respectively. A minimum of 64 transients were collected for each spectrum. All NMR samples were prepared to include HEPES (50 mM, pH 7.5), NaCl (75 mM), EDTA (1 mM), DTT (1 mM), and DSS (1 mM) in the presence of 9:1 $H_2O:D_2O$.

Spectral processing was accomplished with the NMRPipe program (53). The NMRview program (54) was employed in the assignment of all 2D ^{1}H-^{15}N-HSQC NMR crosspeaks. The total average change in backbone amide ^{1}H^N and ^{15}N chemical shifts for each resonance was calculated and quantitated as described in equation 4.1.

7.3.5 ^{15}N-Ub thiolester formation with Ub conjugation enzymes.

An initial 2D ^{1}H-^{15}N-HSQC NMR spectrum was acquired for ^{15}N-UbLys^{48}Arg (400 μM) as a point of reference for all thiolester reactions, and correlated well with the previously assigned protein (30).

Thiolester-linked interactions between ^{15}N-Ub (400 μM) and Cdc34 (450 μM) were examined in situ by inclusion of S. cerevisiae E1 (1 μM), ATP (5 mM), and MgCl$_2$ (5 mM) as described in section 2.3.9. The onset of conjugate formation can be clearly identified based on the accumulation of new peaks emanating from the mixed population of Ub species, and occurs fairly rapidly (hours), and therefore only initial ^{1}H-^{15}N-HSQC spectra (<2 hours) were employed. UbLys^{48}Arg was employed as the Ub species in order to eliminate the possibility of chain formation, and hence eliminate further complication of the spectra. Identical experiments were performed using cdc34Δ_{244} instead of wild-type Cdc34 at identical concentrations.

Thiolester-linked interactions between ^{15}N-Ub (400 μM) and rad6Δ (450 μM) were examined using an identical experimental procedure as that described for Cdc34 derivatives in the preceding paragraph.

All thiolester reactions involving ubc1Δ were performed at 30 °C, and *in situ* thiolester formation was induced by including ubc1Δ (~0.8 mM), UbLys^{48}Arg (~0.8 mM), E1 (10 μM), ATP (10 mM), and MgCl$_2$ (5 mM) in following buffer: HEPES pH 7.5 (40 mM), NaCl (450 mM), and EDTA (1 mM). In each reaction, either the E2 or Ub was ^{15}N-labeled and the other remained unlabeled. Initial ^{1}H-^{15}N HSQC spectra of the ^{15}N-labeled protein were collected, the samples were reduced in volume by Speedvac, and an equimolar amount of the unlabeled partner was added such that the overall volume in the NMR tube remained constant (500 μL). ^{1}H-^{15}N HSQC spectra were then acquired under identical conditions to that described for the ^{15}N-labeled protein alone in order to assess the presence/absence of a non-covalent interaction. The sample volume was subsequently reduced, and the ATP, MgCl$_2$, and E1 enzyme were added to the reaction mixture, and mixed thoroughly. ^{1}H-^{15}N HSQC spectra were acquired periodically in order to assess the kinetics of thiolester formation.

7.3.6 ^{15}N-Ub non-covalent interactions with Ub conjugation enzymes.

Non-covalent interactions between ^{15}N-UbLys^{48}Arg (400 μM) and Cdc34 (450 μM) were examined by mixing the two proteins and allowing equilibration for 30 minutes prior to acquisition of a 2D ^{1}H-^{15}N-HSQC NMR spectrum. Experiments were also conducted using rad6Δ under identical experimental conditions to those described for Cdc34.

7.3.7 Conjugation reactions

All Ub conjugation reactions (1 mL) were performed at 30 °C for 8 hours, as described in section 2.3.8. The concentration of each component is noted in the figure legends. Reactions were terminated by the addition of trichloroacetic acid (10%- final) and processed for SDS-PAGE (18%) and autoradiography.

7.3.8 In vivo complementation experiments

S. cerevisiae MHY508 cells (Ubc4⁻Ubc5⁻) were transformed with plasmids harboring the wild-type or mutant ubc1Δ, grown overnight at 30 °C to an OD_{600} of approximately 0.5, and serially diluted from between 10^6 to 10^3 cells/10 μL. 10 μL of each serial dilution was subsequently plated onto Trp⁻ plates, and growth was allowed to proceed for 3 days at 30 °C. The pES12 plasmid was also included as a negative control. Previous experiments have shown that the ubc1Δ plasmid partially complements the lack of growth associated with the MHY508 strain.

7.4 RESULTS

7.4.1 NMR spectroscopy of Cdc34 and its C-terminal tail truncations

In order to investigate whether general trends for E2•Ub interactions exist, several such Ub interactions with different E2s were probed for comparison purposes. We decided first to examine key structural and protein-protein interactions of the *S. cerevisiae* Cdc34 protein *in vitro*. This particular E2 was chosen because of the ease of over-expression and purification of a number of C-terminal truncations, which have been examined extensively in terms of their associated biological functions; namely chain building (*37*), E3 interaction (*55*), and self-association (*32*).

Prior to examining E2•Ub interactions, our initial goal was to solve the solution structure of the full length (preferably) or a C-terminal truncation (if necessary) of Cdc34. Crystallization of these proteins by both our group and others has proven unsuccessful, likely due to inherent disorder in the tail region (*37*). As such, an NMR approach was undertaken in an attempt to gain potential insights into the structure of Cdc34. Cdc34, cdc34Δ_{244}, and cdc34Δ_{209} proteins were purified in amounts appropriate for NMR experiments (~ 1 mM), and were determined to be stable to proteolysis at both 25 °C and 37 °C over the span of 48 hours (Figure 7.2). Therefore, as with other E2 proteins, Cdc34 is quite stable over the range of temperatures and time periods required for structural

A

B
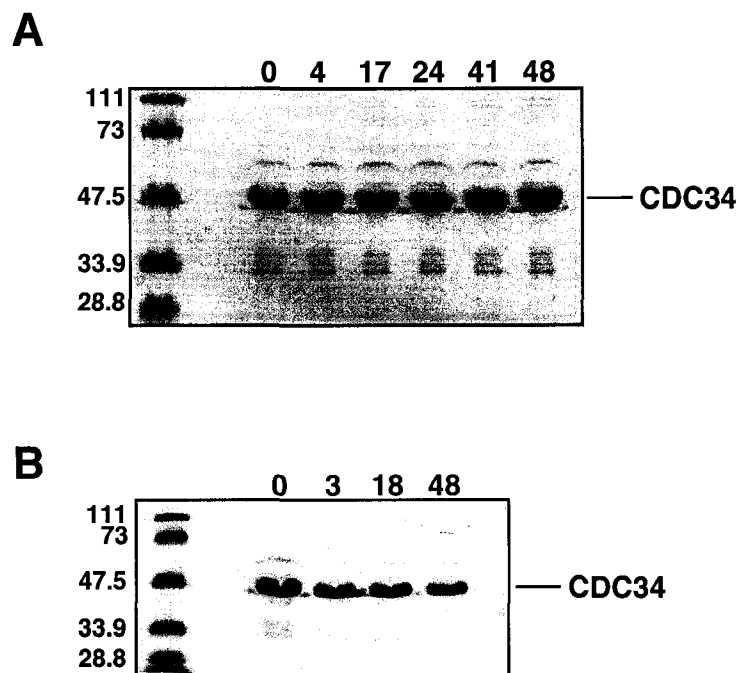
Figure 7.2 Stability and suitability of the Cdc34 protein for the purposes of NMR experimentation. Purified Cdc34 protein was concentrated to approximately 200 μL, incubated at either (A) 37 °C, or (B) 25 °C, aliquots removed at various time points (shown above the gel, in hours), and were subjected to SDS-PAGE. This, in combination with size exclusion chromatography (not shown), were used to assess the degradative and aggregative properties of Cdc34, which was shown to be stable under all conditions examined. $cdc34\Delta_{244}$ was also examined, and produced identical results.

determinations by NMR. The aggregation state of each of the Cdc34 derivatives was also assessed by size exclusion chromatography after incubation of each derivative at NMR concentrations, and it was determined that cdc34Δ_{209} aggregated significantly, whereas full-length Cdc34 and cdc34Δ_{244} remained monomeric.

As a first step, we sought to determine whether an NMR-based determination of Cdc34 structure was feasible. To test this approach, a ^{1}H-^{15}N HSQC NMR experiment was established in order to determine whether or not significant resolution of cross peaks would allow for such a determination (Fig. 7.3A). A large number of the chemical shifts of the amide cross-peaks for the full length protein were dispersed as was expected for a protein possessing significant secondary structural elements. Unfortunately a number of the observable cross-peaks also appear to cluster to the region of the spectrum typically associated with random coil and were significantly more intense than the well-dispersed peaks. This observation is consistent with the fact that Cdc34 possesses a 125 residue C-terminal tail (42% of the protein) which has previously been hypothesized to adopt, at least partially, a random coil orientation (*37*). Based on these observations, in combination with the fact that numerous amide cross-peaks are not observed (likely due to the size, 34 kDa, of Cdc34 and exchange in extremely flexible regions of the protein), we concluded that solving the solution structure of Cdc34 would prove unfeasible by conventional NMR approaches.

An ^{1}H-^{15}N HSQC NMR experiment was next performed on a C-terminal truncation, cdc34Δ_{244}, which deletes 51 C-terminal residues, but maintains its ability to complement for a wild-type disruption mutant (*37*) (Fig. 7.3B). As was the case with the full length protein, numerous amide cross-peaks were observed in both the typical regions of the spectrum associated with a well-folded protein possessing secondary structure, and a central region of the spectrum typically associated with random coil. Upon comparison of the 2D ^{1}H-^{15}N HSQC spectra of Cdc34 and cdc34Δ_{244}, it is apparent that the 51 C-terminal amino acids of
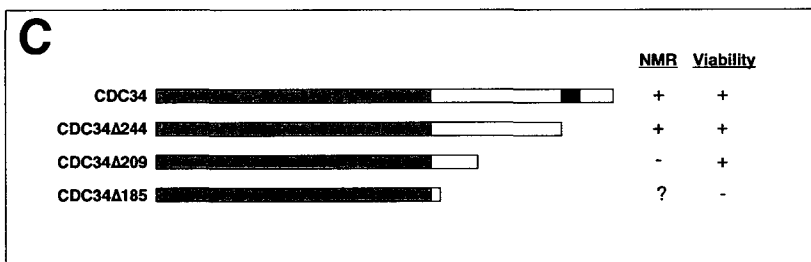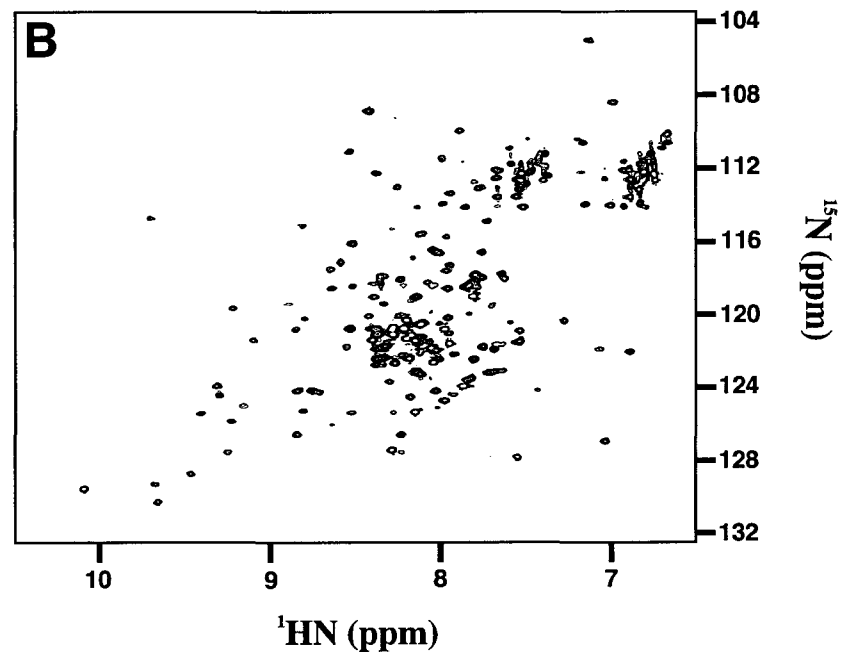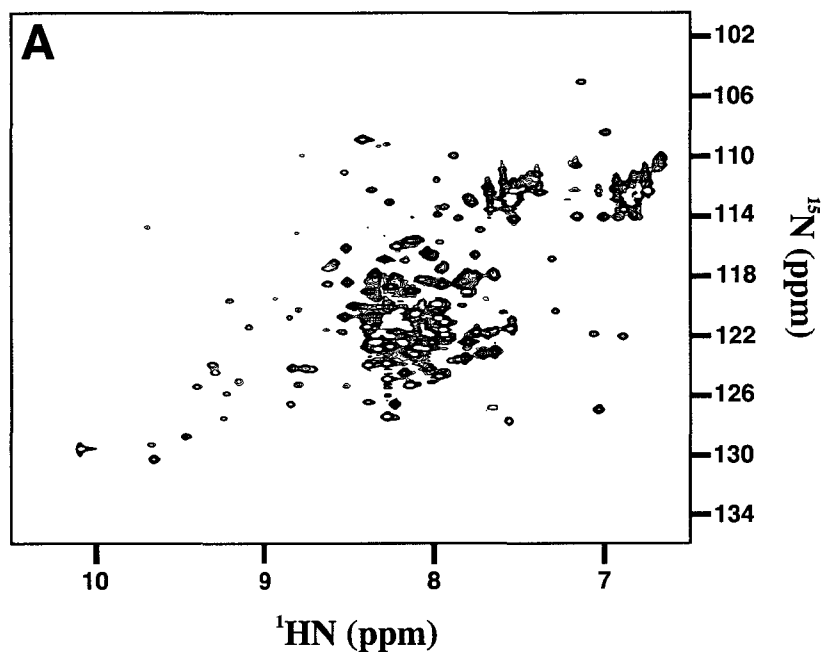
Figure 7.3 NMR spectroscopy of Cdc34 and its C-terminal tail truncations. ^{1}H-^{15}N HSQC NMR spectrum of (A) Cdc34, and (B) cdc34Δ_{244} at 30 °C and 600 MHz. (C) Schematic alignment of Cdc34 and its C-terminal tail derivatives. The ability to acquire structured and non-aggregated HSQC spectra and the ability of the truncation to complement a Cdc34 disruption in S. cerevisiae (37) are also indicated.

Cdc34 are either adopting a non-canonical secondary structure or are not observable, as only the number and intensity of the cross-peaks clustering to the random coil portion of the spectrum are being reduced in the case of cdc34Δ_{244}. This observation also underscores the fact that it is highly unlikely that the 51 C-terminal residues of Cdc34 are interacting to a significant degree with the E2 core, as very few changes in chemical shift of cross-peaks adopting typical secondary structure were observed. Unfortunately, because longer C-terminal truncations than cdc34Δ_{244} (e.g. cdc34Δ_{209}) were observed to aggregate under NMR conditions, we cannot unequivocally state that the tail region of Cdc34 does not make contacts with the core E2 fold.

The cdc34Δ_{244} spectrum represents a significant improvement relative to the full length protein given the smaller number and greater intensity of peaks clustering to the random coil region of the spectrum, and therefore presented an opportunity to probe the feasibility of structure determination. ^{2}H-^{15}N-^{13}C-labeled cdc34Δ_{244} was purified, and preliminary 2D-HNCA and -HNCO experiments (first plane of 3D experiment only) were performed in order to determine whether reasonable signal could be detected. Unfortunately, due to the combination of low yields associated with triply labeled sample, the high number of random coil residues, and the size of the protein (~ 28 kDa) we were not optimistic after performing these preliminary experiments, particularly with respect to assigning the backbone amide resonances.

7.4.2 Thiolester interaction between Cdc34 and Ub

Although the solution structure determination of Cdc34 derivatives proved untenable, chemical shift perturbation methodologies in which Ub was ^{15}N-labeled have been employed to successfully map the surface of Ub that interacts with E2s (9, 30), and was therefore applied to Cdc34. The full backbone chemical shift assignments for S. cerevisiae ^{15}N-UbLys^{48}Arg at pH 7.5 have previously been determined (30) and exhibits well dispersed and resolved ^{1}H-^{15}N HSQC NMR spectra at 600 MHz (Fig. 7.4, black contours).

Upon *in situ* thiolester formation between Cdc34 and ^{15}N-UbLys^{48}Arg, a handful of residues whose backbone amide ^{1}H and ^{15}N chemical shifts exhibited a perturbation upon complex formation were identified (Fig. 7.4, red contours), and quantified in terms of the total change in chemical shift, $\Delta\delta_{total}$. The most significant $\Delta\delta_{total}$ upon thiolester formation include: Arg^{42}, Arg^{48}, Gln^{49}, His^{68}, Val^{70}, Leu^{71}, Arg^{72}, Leu^{73}, and Gly^{76}. When mapped onto the surface of Ub, these residues form a solvent-exposed face stretching from the C-terminal Gly^{76} of Ub towards the centrally positioned Lys^{48} (Fig. 7.5, top left). No other significant $\Delta\delta_{total}$ were observed elsewhere on the protein. These chemical shifts return to those of ^{15}N-UbLys^{48}Arg alone upon treatment with DTT, a thiolester reducing agent, which confirms that these chemical shifts are associated with thiolester intermediate and not an autoubiquitination of Lys residues on Cdc34.

In order to compare the surfaces of interaction on Ub that are formed/lost upon C-terminal truncation of Cdc34, identical experiments were performed using unlabeled cdc34Δ_{244} for *in situ* thiolester reactions. Nearly identical residues were observed to undergo the most significant $\Delta\delta_{total}$ when compared to the thiolester reaction involving the full-length protein, and occurred qualitatively at the same rates (data not shown). Based on these results, we can conclude that deletion of the 51 C-terminal residues has no significant effect on thiolester formation, nor does it appear to interact with Ub.

7.4.3 Potential non-covalent interactions between Cdc34 and Ub

2D ^{1}H-^{15}N-HSQC NMR spectroscopy was also used to determine whether Ub associates with full length Cdc34 in a non-covalent fashion; that is in the absence of E1 and ATP/Mg^{2+}. At the concentrations employed (see figure legends), slight changes in the ^{1}H-^{15}N-HSQC NMR spectrum of ^{15}N-UbK48R are observed upon addition of a slight 1.1-fold excess of Cdc34 (Fig. 7.6A), indicative of a potential non-covalent interaction between these two proteins. The most significant $\Delta\delta_{total}$ were observed for the following residues: Ile^{13}, Asp^{24}, Gln^{40}, Leu^{43}, Gly^{47}, Arg^{48}, Gln^{49}, His^{68}, Leu^{69}, Val^{70}, and Leu^{71}. When mapped onto the
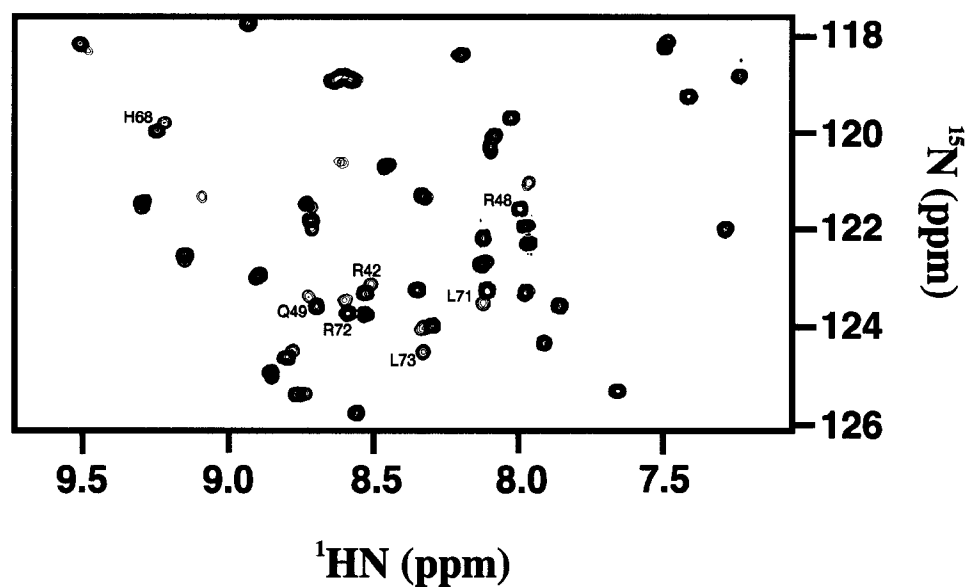
Figure 7.4 Superposition of ^{1}H-^{15}N HSQC NMR spectra of ^{15}N-labeled Ub, free and in a thiolester complex with Cdc34. 500 μL NMR samples including either ^{15}N-UbLys^{48}Arg (400 μM, black), or ^{15}N-UbLys^{48}Arg (400 μM), E1 (1 μM), and Cdc34 (450 μM) (red) were studied at 30 °C, pH 7.5. Only selected backbone cross-peaks that were affected by complex formation are labeled in the close-up view of the amide region in the spectrum.
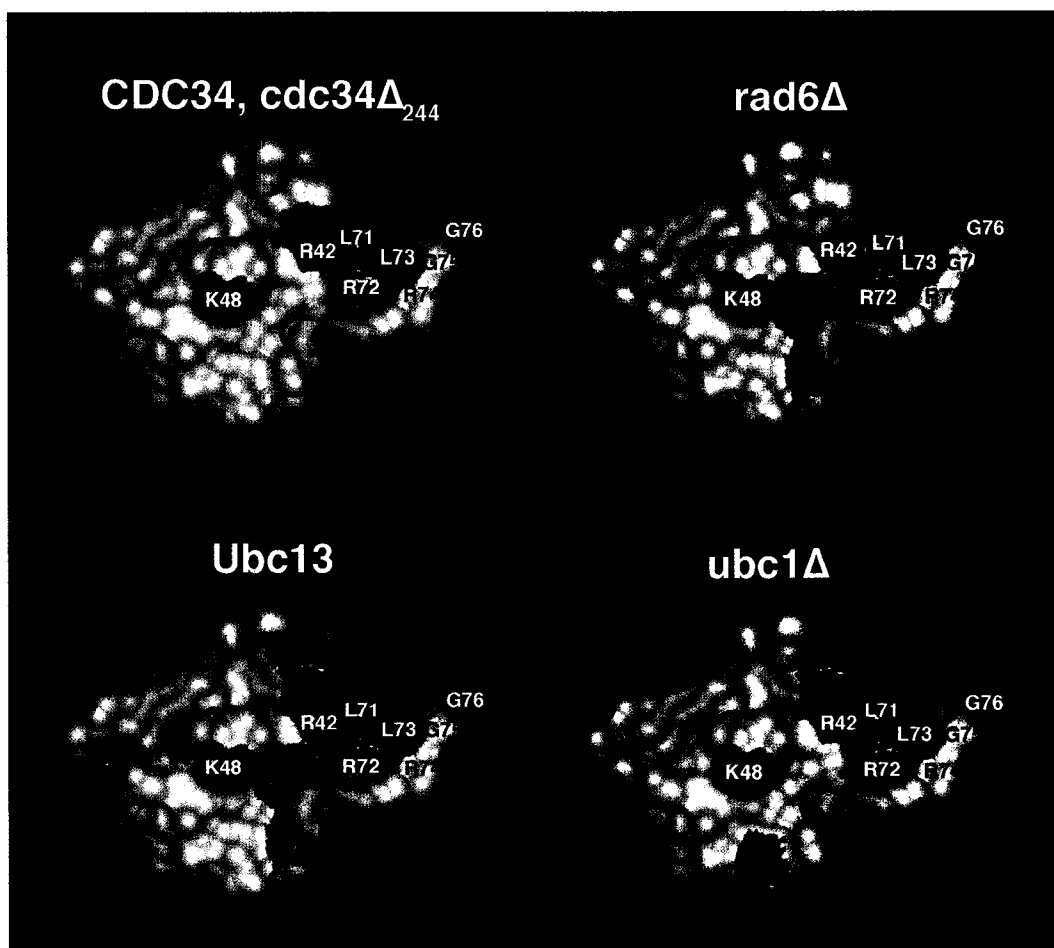
Figure 7.5 A common surface on Ub is responsible for mediating its thiolester interactions with E2 enzymes. The surface of Ub is presented, and residues which undergo significant $^{1}H-^{15}N$ HSQC NMR chemical shift changes (as measured by calculating the $\Delta\delta_{total}$, and determining those residues which are one standard deviation unit above the average) upon the formation of a thiolester complex with the designated E2 enzyme are colored in red. All truncations refer to C-terminal derivatives. Residues important for thiolester formation which are common to the E2's studied are labeled in white, as well as Arg^{74} and Gly^{75} which are not observed in the $^{1}H-^{15}N$ HSQC NMR experiment but assumed to participate in the interface.
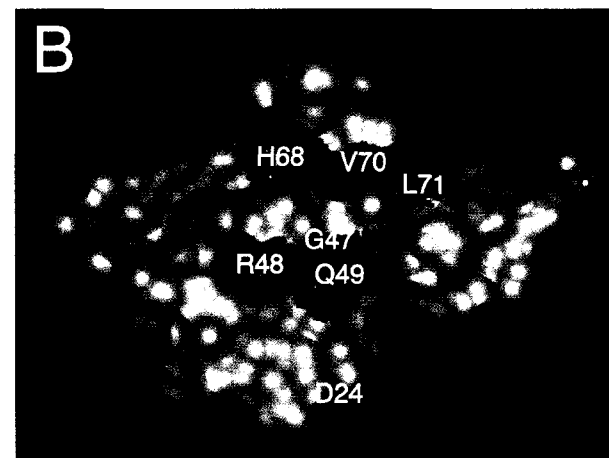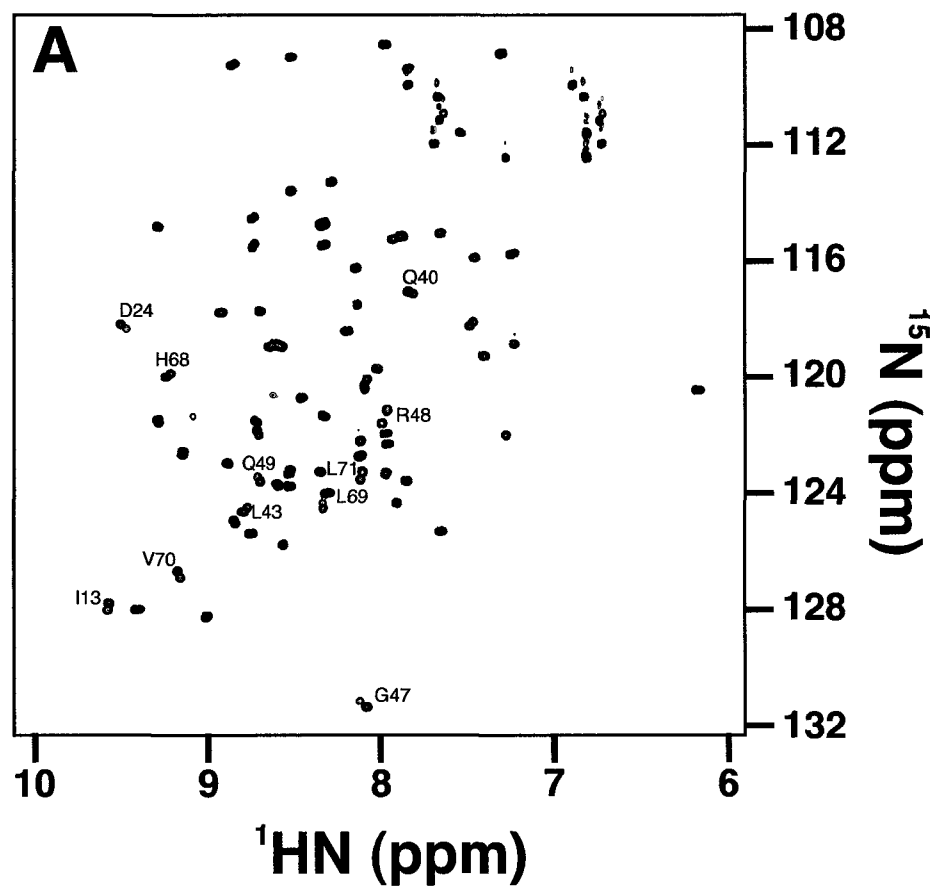
Figure 7.6 A non-covalent interaction between Ub and Cdc34 as detected by NMR spectroscopy. (A) Superposition of ^{1}H-^{15}N HSQC NMR spectra of ^{15}N-labeled Ub, free and in the presence of Cdc34. 500 μL NMR samples including either ^{15}N-UbLys^{48}Arg (400 μM, black), or ^{15}N-UbLys^{48}Arg (400 μM), and Cdc34 (450 μM) (blue) were studied at 30° C, pH 7.5. Only backbone cross-peaks that underwent significant changes in chemical shift upon complex formation are labeled. (B) The surface of Ub is presented, and those residues which were highlighted in (A) and are surface exposed are colored red on the surface. Gly^{76} is also indicated as a point of reference.

surface of the structure of Ub, the majority of these residues cluster to a face centrally located on one side of the Ub molecule, although some are scattered on distal surfaces as well (*i.e.* Asp[24]). While these results do appear to indicate a potential non-covalent interaction, they should be treated with caution for a couple of reasons. First and foremost, only a slight excess of Cdc34 relative to ^{15}N-UbLys[48]Arg was employed, and as a result only slight changes in chemical shifts were observed. In order to increase the reliability of these results, a higher excess of Cdc34 should be employed, but experimental difficulties including precipitation prevented this analysis. Second, without independent confirmation (*i.e.* accompanying biochemical data, K_D determination) these results should be approached skeptically.

7.4.4 Interactions between Rad6 (Ubc2) and Ub

The surface of Ub involved in the interaction with another E2, Rad6, was also determined for the purpose of comparison with other E2s. Specifically, a tail truncation of the 18 C-terminal amino acids was employed (rad6Δ), as it consists of the core E2 fold, and its C-terminal tail is not essential for its DNA repair function (*56*). As with Cdc34, an NMR based approach was employed in order to detect the thiolester and potential non-covalent interactions between ^{15}N-UbLys[48]Arg and rad6Δ.

The 2D ^{1}H-^{15}N-HSQC NMR spectrum of ^{15}N-UbLys[48]Arg alone is indistinguishable from the spectrum acquired in the presence of rad6Δ. This observation indicates the lack of a non-covalent interaction between Ub and rad6Δ at a concentration of 400 μM (data not shown).

Upon *in situ* thiolester formation between rad6Δ and ^{15}N-UbLys[48]Arg, as with the other E2 enzymes, numerous cross-peaks exhibited a significant $\Delta\delta_{total}$ values, representative of residues that may be involved in mediating the thiolester interaction (data not shown). The major $\Delta\delta_{total}$ upon thiolester formation include: Ile[23], Arg[42], Leu[43], Arg[48], Gln[49], Leu[50], Glu[51], His[68], Leu[71], Arg[72], Leu[73], and Gly[76]. When mapped onto the surface of Ub, these residues form a solvent-

exposed face stretching from the C-terminal Gly[76] of Ub to the centrally positioned Lys[48] (Fig. 7.5, top right). No other significant $\Delta\delta_{total}$ were observed elsewhere on the protein.

7.4.5 Interactions between Ub and Ubc1 as probed by site-directed mutagenesis.

Previous studies by our group led to the determination of a model structure of the thiolester intermediate between a 64 residue C-terminal tail truncation of Ubc1 (ubc1Δ) and ^{15}N-UbLys[48]Arg using an NMR-based molecular modeling approach (29). The 3D model of this intermediate thiolester complex utilizes similar surfaces of interaction as the Ubc13~Ub thiolester complex, as discussed in detail in section 4.4.3 of this dissertation. Furthermore, ubc1Δ function may be probed using both in vitro and in vivo methods. As such, ubc1Δ was an ideal candidate to use in structure/function studies relating to the E2~Ub thiolester intermediate. Determination of these structure/function relationships employed mutants carrying surface residue substitutions. These mutants can be subjected to in vitro thiolester formation and chain building assays, as well as in vivo complementation of their stress-related function in S. cerevisiae. These results can subsequently be correlated with structural changes within thiolester intermediates as determined by NMR. Therefore, our goal was to assess whether specific structural determinants in ubc1Δ could be identified that carry out a specific function (i.e. chain building, thiolester formation).

The first group of ubc1Δ derivatives that were examined included those that have no discernable effect on thiolester formation, but result in attenuation of poly-Ub chain formation. Previous studies in our laboratory have determined that the Ala[111]Arg point mutant and the Glu[125]Ala/ His[129]Ala/ Leu[131]Ala/ Arg[132]Ala/ Glu[135]Ala quintuple mutant (referred to as the Ala[125] mutant for the remainder) satisfy these conditions[1] (Fig. 7.7). These substitutions are therefore of interest

---

[1] Dr. C. Ptak, personal communication

because they represent changes within an E2 that specifically affect Ub transfer to a lengthening poly-Ub chain. In order to investigate whether altered structural features of the thiolester intermediate could be responsible for the attenuated ability to form poly-Ub chains, each of these mutants were ^{15}N-labeled, and the interaction surfaces involved in *in situ* thiolester formation with Ub were characterized using 2D ^{1}H-^{15}N HSQC NMR chemical shift perturbation experiments. In each case, significant $\Delta\delta_{total}$ were observed upon thiolester formation, however, these $\Delta\delta_{total}$ were identical to those observed upon thiolester formation with ubc1Δ (Fig. 7.8 and Table 7.1). The corollary experiments were also performed using ^{15}N-Ub and unlabeled mutant ubc1Δ, and similar results were obtained. Therefore, it is clear that these mutants are not directly affecting thiolester formation, but rather a process further downstream in the chain building process.

The second group of mutations, which include Thr^{73}Ala, Thr^{73}Arg, and Lys^{74}Ala, were constructed for two distinct purposes. First, these residues lie on the face opposite from that proposed to be involved in the formation of the ubc1Δ~Ub thiolester intermediate. Second, based on previous data presented in this thesis for the Mms2 protein, these residues could correspond to a patch responsible for the Ub non-covalent binding of Ub to ubc1Δ. Of particular interest is the fact that intermediate changes in chemical shifts were observed for Thr^{73} and Lys^{74} upon thiolester formation (29) (Fig. 7.7, yellow), which may reflect a novel conformational change exposing a second Ub binding site. *In vitro* assays were performed using [^{35}S]-Ub as the detectable species, and demonstrated that each of the backside mutants demonstrated only minor differences in efficiency when compared to ubc1Δ in terms of both chain building (Fig. 7.9A) and thiolester formation (data not shown). Furthermore, *in vivo* complementation experiments demonstrated that each of these mutants were equally capable of complementing its stress-related function in *S. cerevisiae* as the normal ubc1Δ protein (Fig. 7.9B). Taken together, these results indicate that positions Thr^{73} and Lys^{74} likely do not represent important residues in the function of ubc1Δ.
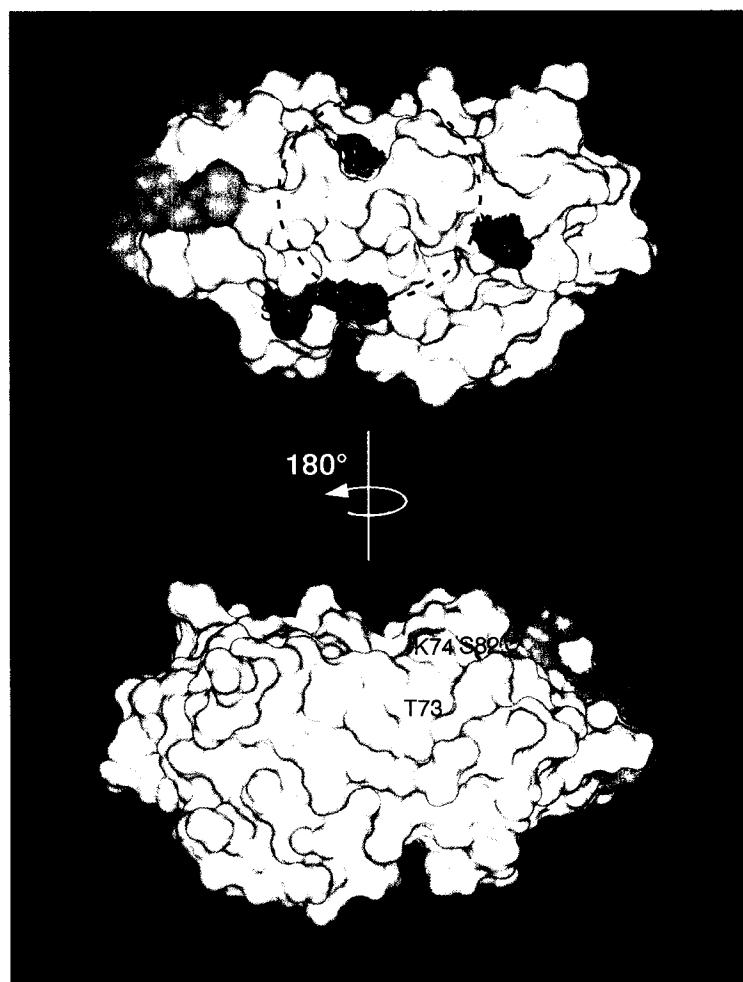
Figure 7.7 Summary of the mutagenesis sites in ubc1Δ for the purposes of examining the thiolester and potential non-covalent interactions with Ub. The Connolly surface of ubc1Δ is presented, rotated along the horizontal axis by 180°. The active-site Cys[88] (green) as well as the proposed thiolester interaction site with Ub (dashed circle) are indicated as a point of reference. Sites of mutagenesis include those designed to probe the thiolester interaction directly (red) and indirectly (orange). Residues hypothesized to affect the non-covalent binding of Ub as determined by preliminary NMR experiments are colored yellow.
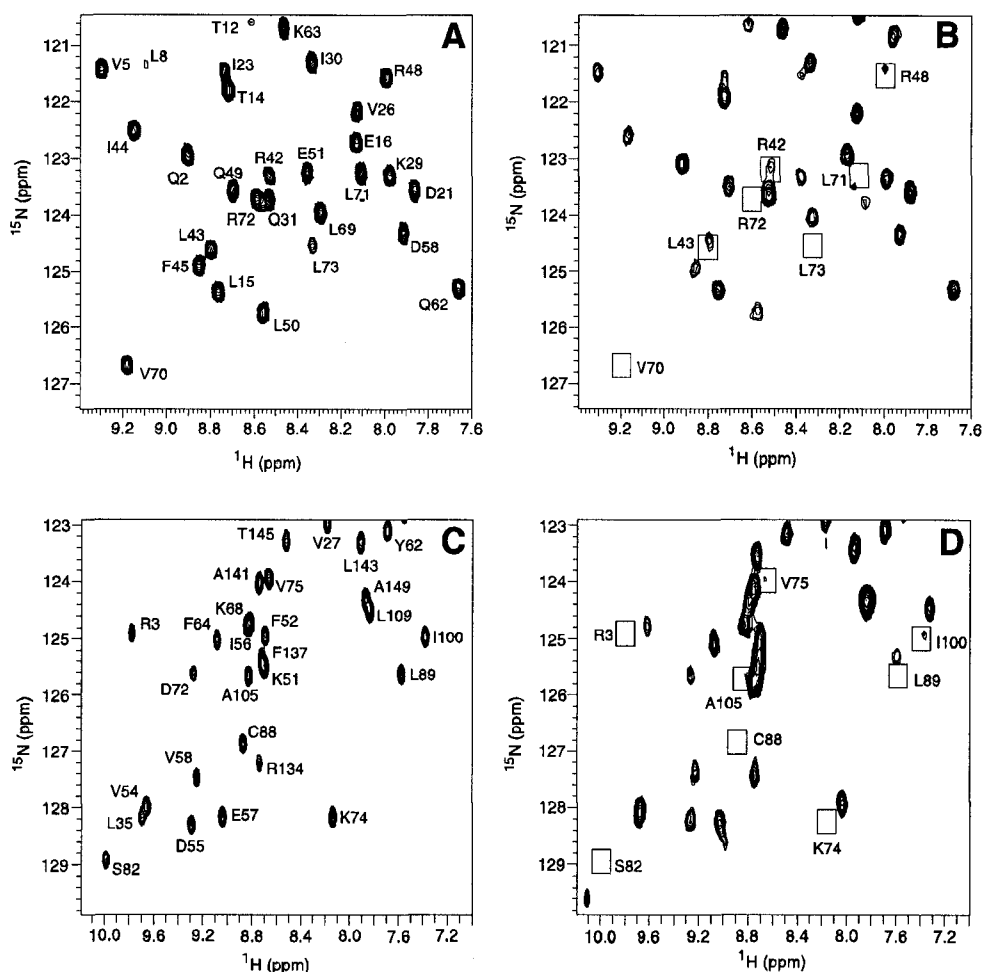
Figure 7.8 Control spectra of ubc1Δ thiolester formation probed by NMR spectroscopy. Selected regions of a 500 MHz ¹H-¹⁵N HSQC spectra showing the effect of thiolester formation on chemical shift. (A) ¹⁵N-UbLys⁴⁸Arg (0.8 mM) and unlabeled ubc1Δ (0.8 mM) collected prior to thiolester formation. (B) Spectrum acquired 1 hour after *in situ* thiolester formation for the sample used in (A). (C) An identical experiment is shown for ¹⁵N-ubc1Δ (0.8 mM) prior to thiolester formation, and (D) 1 hour after *in situ* thiolester formation with unlabeled UbLys⁴⁸Arg (0.8 mM). In both cases, resonances are indicated with boxes to indicate the residues which demonstrated a significant change in chemical shift upon thiolester formation. Figure adapted from Hamilton *et. al.* (29).

In order to confirm that these residues do not play a crucial role in thiolester formation, the Lys[74]Ala mutant was ^{15}N-labeled, and subjected to ^{1}H-^{15}N-HSQC NMR chemical shift perturbation experiments prior to and after *in situ* thiolester formation. As expected, the changes in $\Delta\delta_{total}$ upon thiolester formation are indistinguishable from those determined for the ubc1Δ protein, indicating that these residues occur at amino acid positions which are not responsible for forming the interface between ubc1Δ and Ub (Table 7.1).

A third group of mutations were designed to confirm the hypothesized 3D model of the thiolester interaction between Ub and ubc1Δ. Three mutants were designed which encompassed regions previously determined to play a peripheral role in mediating the thiolester interaction, and contained a surface exposed Ser which could be substituted with Cys: Ser[82]Cys, Ser[97]Cys, and Ser[115]Cys (Fig. 7.7). A spatially conservative substitution (Ser to Cys) was chosen such that the protein structure would remain largely unaffected, while introducing minor changes in chemical environment due to the increased electronegativity of the sulfhydryl over hydroxyl group. Therefore, if the mutagenized residues were playing a role in maintaining the structure of the thiolester intermediate, NMR approaches would detect these small changes in chemical environment. If specific changes in chemical shift could be associated with a particular mutant, then orientational information could be obtained which would confirm or refute the model determined.

In order to confirm that the introduction of Cys substitutions did not affect the activity of ubc1Δ, *in vitro* assays were performed. No major differences in efficiency when compared to ubc1Δ in terms of both chain building and thiolester formation were (data not shown). In order to determine whether differences in the surface of interaction within the thiolester intermediate could be observed, either the mutant ubc1Δ proteins were ^{15}N-labeled and converted to thiolester with unlabelled UbLys[48]Arg, or vice versa. Each complex was then subjected to ^{1}H-^{15}N-HSQC NMR chemical shift perturbation experiments and compared to the
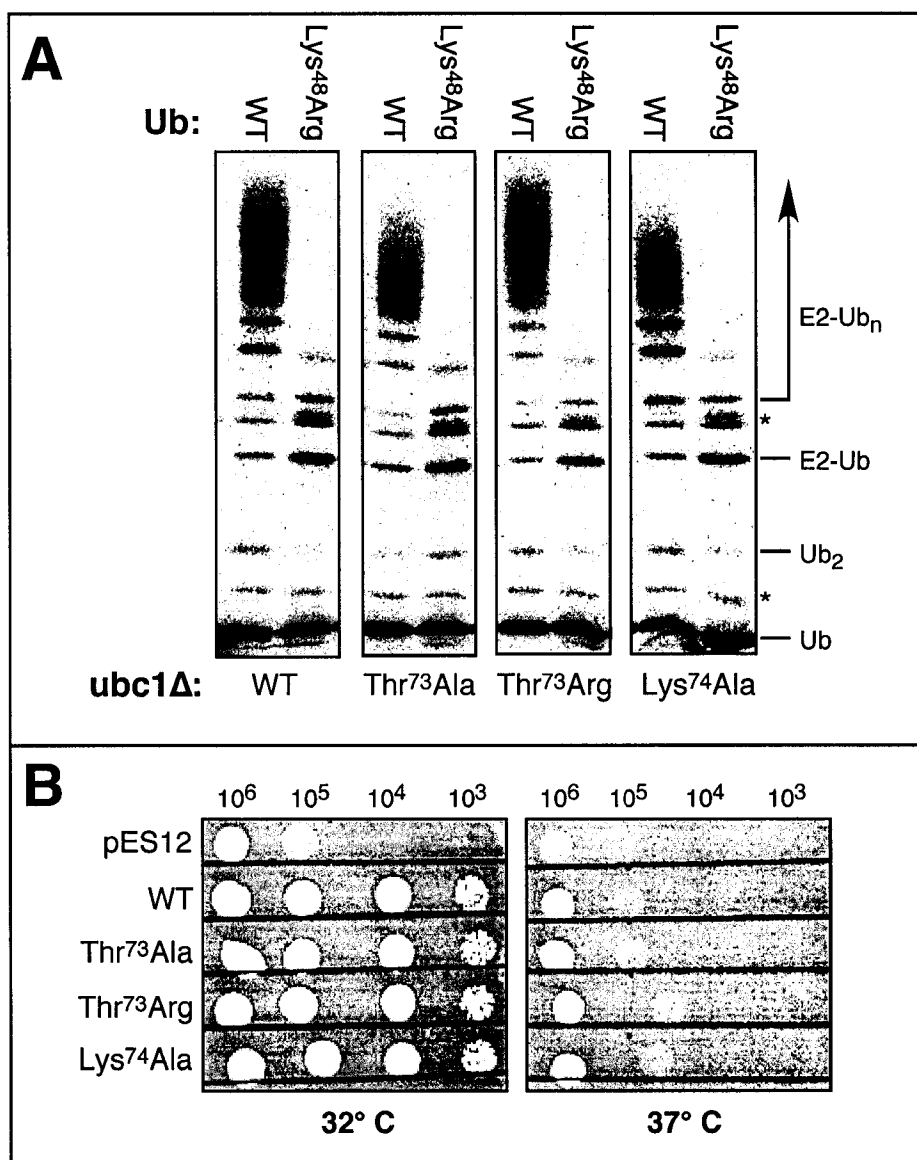
Figure 7.9 Mutation of residues not involved in the ubc1Δ~Ub thiolester interface results in wild-type activity. (A) *In vitro* ubiquitination assays were performed using ^{35}S-Ub in combination with 18% SDS-PAGE and autoradiography in the presence of DTT. In all cases, 100 nM ^{35}S-Ub, 100 nM E2, and 10 nM E1 were employed in the reaction mixture (1 mL), which was incubated at 30 °C for 8 hours. Contaminants present in the ^{35}S-Ub preparation are denoted (*). (B) Serial dilutions examining the *in vivo* ability of the ubc1Δ mutant plasmids to partially complement the MHY508 strain (Ubc4⁻/Ubc5⁻) in *S. cerevisiae*. MHY508 cells were transformed with plasmids harboring wild-type or mutant ubc1Δ, grown overnight, and serially diluted onto Trp⁻ plates. Cell growth proceeded for a period of 3 days. The pES12 plasmid was included as a negative control.

Table 7.1 NMR examination of ubc1Δ mutants. ^{1}H-^{15}N-HSQC NMR experiments were performed as indicated in the tables below, and compared to the associated wild-type spectrum of ubc1Δ in terms of changes in chemical shift. (A) ^{15}N-E2 alone, the non-covalent interaction between Ub and ^{15}N-E2, and the thiolester interaction between Ub and ^{15}N-E2 were probed. (B) ^{15}N-Ub alone, the non-covalent interaction between E2 and ^{15}N-Ub, and the thiolester interaction between E2 and ^{15}N-Ub were investigated.

A

^{15}N-ubc1Δ Protein	^{15}N-ubc1Δ spectrum	^{15}N-ubc1Δ + Ub spectrum	^{15}N-ubc1Δ + Ub + E1 spectrum
Lys^{74}Ala	Residues in proximity to the mutation display altered chemical shifts, otherwise identical to wt.	As with wt protein, no non-covalent interaction observed.	No significant difference in chemical shifts relative to wt.
Ala^{111}Arg	Residues in proximity to the mutation display altered chemical shifts, otherwise identical to wt.	As with wt protein, no non-covalent interaction observed.	No significant difference in chemical shifts relative to wt.
Glu^{125}Ala/His^{129}Ala/ Leu^{131}Ala/Arg^{132}Ala/ Glu^{135}Ala	Due to large number of mutations, the spectrum is significantly different than wt.	Not attempted	Not attempted
Ser^{82}Cys	Residues in proximity to the mutation display altered chemical shifts, otherwise identical to wt.	As with wt protein, no non-covalent interaction observed.	No significant difference in chemical shifts relative to wt.
Ser^{97}Cys	Residues in proximity to the mutation display altered chemical shifts, otherwise identical to wt.	As with wild-type protein, no non-covalent interaction observed.	No significant difference in chemical shifts relative to wt.
Ser^{115}Cys	Residues in proximity to the mutation display altered chemical shifts, otherwise identical to wt.	As with wt protein, no non-covalent interaction observed.	No significant difference in chemical shifts relative to wt.

B

ubc1Δ Protein	ubc1Δ + ^{15}N-Ub spectrum	ubc1Δ + ^{15}N-Ub +E1 spectrum
Ser^{82}Cys	As with wild-type protein, no non-covalent interaction observed.	Glu^{16}, Asp^{24}, Lys^{33}, Glu^{51}, and Leu^{69} do not shift upon thiolester formation. Arg^{42}, Gln^{49}, and Arg^{72} display different chemical shifts from both wild-type and Ser^{115}Cys.
Ser^{115}Cys	As with wild-type protein, no non-covalent interaction observed.	Glu^{16}, Asp^{24}, and Lys^{33} do not shift upon thiolester formation. Arg^{42}, Gln^{49}, and Arg^{72} display different chemical shifts from both wild-type and Ser^{82}Cys.

^{15}N-labeled protein prior to *in situ* thiolester formation. The residues affected most significantly by thiolester formation on the E2 were very similar to those observed for ubc1Δ (Table 7.1A). However, the residues experiencing the greatest $\Delta\delta_{total}$ on the ^{15}N-Ub moiety upon thiolester formation with the mutants were significantly different than when normal ubc1Δ was employed (Table 7.1B). Specifically, a handful or backbone amide resonances which normally experience large $\Delta\delta_{total}$ values were not observed to shift when the mutant proteins were employed (Glu^{16}, Asp^{24}, Lys^{33}), and three critical residues involved in thiolester formation (Arg^{42}, Gln^{49}, and Arg^{72}) experience similar $\Delta\delta_{total}$ magnitudes but shift in different directions than when ubc1Δ is used. Taken together, these results appear to support the hypothesized ubc1$\Delta\sim$Ub thiolester model.

7.5 DISCUSSION

All chapters preceding this one have dealt with issues involved in the Ubc13/Mms2 mediated protein ubiquitination cascade, specifically characterizing two apparently crucial interactions with Ub: a thiolester intermediate (donor Ub) and a non-covalent interaction (acceptor Ub). A novel mechanism has been proposed in which the acceptor Ub is correctly oriented such that the high energy thiolester bond from the donor Ub can be specifically attached to a surface exposed Lys residue on the acceptor Ub, thereby directing chain formation and eventually the biological outcome of such an event. In this chapter, our goal was to examine the nature of both thiolester and potential non-covalent interactions between Ub and other E2 enzymes in an attempt to highlight commonalities and differences between members of the E2 family.

In this pursuit we employed three E2s from *S. cerevisiae* (Cdc34, Ubc1, and Rad6) and thiolester formation was monitored by standard chemical shift perturbation assays in order to map the surface of interaction on the Ub molecule. A comparison of the surface of Ub being employed to mediate the thiolester interaction with the *S. cerevisiae* E2s and human Ubc13 reveals that a

core patch, consisting of residues in the C-terminal tail (Leu[71], Arg[72], Leu[73], and Gly[76]), as well as Arg[42], and Arg[48] are required by each (Fig. 7.5). This result is not terribly surprising given the high sequence and structural similarities shared amongst members of the E2 family (*1, 2*). We would therefore expect a common motif on the surface of Ub to mediate the thiolester interaction. However, empirical data have demonstrated differential rates of thiolester formation amongst E2 family members (data not shown), which could suggest a slight modulation of the core motif in each individual case. As hypothesized, the data presented herein indicates that each individual E2 appears to require additional but unique surface features on Ub in order to support the thiolester interaction. For example Cdc34 and its derivatives require only Val[70] in addition to the core patch, whereas Rad6 additionally requires Ile[23], Leu[43], Leu[50], and Glu[51] (Fig. 7.5). This data is consistent with the corollary experiments which have demonstrated that the surface patches on the E2 enzymes upon thiolester formation share a common motif, but display marked differences specific to each E2 (*10, 28, 29*). Even more striking is the apparent correlation between the additional surface requirements and the evolution of the E2 family of proteins, as E2s further downstream on the evolutionary chain require more complex surface patches (Fig. 7.1 and 7.5).

As most E2 enzymes examined to date share similar structural and enzymatic features, it is not unreasonable to hypothesize that the non-covalent interaction between Mms2 and Ub may reflect a general mechanism required for poly-Ub chain building. This hypothesis is underscored by cross-linking of Ub to an E2 in the absence of thiolester formation that has been observed for both Cdc34 (*57*) and ubc1Δ^2, indicative of potential non-covalent interactions. Potential use of a non-covalent Ub binding site on an E2 suggests that poly-Ub chain assembly could employ a mechanism analogous to that of Ubc13/Mms2, where thiolester-linked (donor) and non-covalently associated (acceptor) Ub molecules are positioned in order to effect specific poly-Ub chain formation. The

---

[2] Dr. C. Ptak, personal communication.

identification of E2 self-association or heterodimerization suggests that one E2 may function to form thiolester complex while the second positions the acceptor Ub. *In vivo* evidence for Cdc34 (*32*) or Ubc7 (*38*) self-association, and Ubc6/Ubc7 heterodimerization (*38*) suggests that these interactions may be required for catalytic activity. Supporting *in vitro* evidence of higher-order complex formation amongst E2's has also been reported for many of the E2s (*33-37*).

2D ^{1}H-^{15}N HSQC chemical shift perturbation experiments on other E2 enzymes have proven inconclusive with respect to identification of a non-covalent binding site for Ub or Ub-like modifiers, as an interaction has been detected for both human Ubc9 (*27*) and human Ubc2b (*28*), whereas non-covalent Ub binding was not detected for human Ubc13 (*9, 10*) or yeast ubc1Δ (*29*). The results documented in this chapter are consistent with these previous studies, as a potential non-covalent interaction with Ub was detected for Cdc34 (Fig. 7.6) but not for Rad6 or any of the ubc1Δ mutants. In the absence of corroborating functional evidence, such non-covalent interactions should be treated as preliminary. However, based on the accumulating body of evidence, the intriguing possibility remains that a second Ub binding site exists on a single E2 molecule. The exact functional role of this potential binding site remains to be elucidated, although two possibilities include: (i) the orientation of a Ub molecule such that poly-Ub chain formation is favoured, as has been demonstrated for the Ubc13/Uev system (*9, 10, 31*), and (ii) the interaction with a domain in E1 proteins, which appears to contain the Ub superfold (*58*).

Although the 3D structural determination of the Cdc34 protein and its C-terminal truncations proved unsuccessful, useful insights into structural features of the C-terminal tail were gained. First and foremost, at least a portion of the C-terminal tail adopts random coil secondary structure. Second, it appears as though the 51 C-terminal amino acids of Cdc34 do not make significant contacts with the core E2 domain. This observation is further supported by the fact that the residues of Ub required for thiolester formation (Fig. 7.4) and the rate of

thiolester formation are not affected by truncation of the C-terminal tail (*32*). Recent studies of the Ubc1 C-terminal tail indicate that it both possesses some recognizable secondary structural elements, and that it interacts with the core E2 domain near the active-site Cys (*59*). Although other E2s with C-terminal extensions may also exhibit such an interaction, our data suggests that Cdc34 and Ubc1 tails function significantly differently. More work is clearly needed to establish the exact role of each of these tails in poly-Ub chain formation.

Mutagenesis of ubc1Δ at a variety of locations revealed some basic information regarding both its structure and function (Table 7.1). Mutations on ubc1Δ that surrounded the active site spatially were demonstrated to slightly modulate the nature of the Ub thiolester interaction, without drastically affecting chain building or the rate of thiolester formation. As expected, mutations distal from the active site were shown to have no effect on thiolester formation, chain building, or the structure of thiolester intermediate. Another mutant, $A^{111}R$, demonstrated no significant difference in terms of the surfaces of interaction within the thiolester complex. These observations complemented biochemical data for these derivatives that had shown attenuation of chain building but not thiolester formation. Taken together, these results appear to confirm the proposed model of the ubc1Δ~Ub thiolester intermediate previously determined (*29*).

Overall, our investigations into the function of E2s outside the scope of the Ubc13/Mms2 pathway provided some interesting insights into the mechanism of poly-Ub chain assembly. However, much work remains if we are to establish the commonalities and differences between members of this highly conserved family of enzymes.

7.6 REFERENCES

1. Hochstrasser, M. (1996) *Annu Rev Genet 30*, 405-39.

2. Glickman, M. H., and Ciechanover, A. (2002) *Physiol Rev 82*, 373-428.

3. Deshaies, R. J. (1999) *Annu Rev Cell Dev Biol 15*, 435-67.

4. Feldman, R. M., Correll, C. C., Kaplan, K. B., and Deshaies, R. J. (1997) *Cell 91*, 221-30.

5. Kumar, S., Kao, W. H., and Howley, P. M. (1997) *J Biol Chem 272*, 13548-54.

6. Nuber, U., Schwarz, S., Kaiser, P., Schneider, R., and Scheffner, M. (1996) *J Biol Chem 271*, 2795-800.

7. Hofmann, R. M., and Pickart, C. M. (2001) *J Biol Chem 276*, 27936-43.

8. Hofmann, R. M., and Pickart, C. M. (1999) *Cell 96*, 645-53.

9. McKenna, S., Spyracopoulos, L., Moraes, T., Pastushok, L., Ptak, C., Xiao, W., and Ellison, M. J. (2001) *J Biol Chem 276*, 40120-6.

10. McKenna, S., Moraes, T., Pastushok, L., Ptak, C., Xiao, W., Spyracopoulos, L., and Ellison, M. J. (2003) *J Biol Chem 278*, 13151-8.

11. Hoege, C., Pfander, B., Moldovan, G. L., Pyrowolakis, G., and Jentsch, S. (2002) *Nature 419*, 135-41.

12. Deng, L., Wang, C., Spencer, E., Yang, L., Braun, A., You, J., Slaughter, C., Pickart, C., and Chen, Z. J. (2000) *Cell 103*, 351-61.

13. Ulrich, H. D. (2003) *J Biol Chem 278*, 7051-8.

14. Ulrich, H. D., and Jentsch, S. (2000) *Embo J 19*, 3388-97.

15. Schwarz, S. E., Matuschewski, K., Liakopoulos, D., Scheffner, M., and Jentsch, S. (1998) *Proc Natl Acad Sci U S A 95*, 560-4.

16. Schulman, B. A., Carrano, A. C., Jeffrey, P. D., Bowen, Z., Kinnucan, E. R., Finnin, M. S., Elledge, S. J., Harper, J. W., Pagano, M., and Pavletich, N. P. (2000) *Nature 408*, 381-6.

17. Jentsch, S. (1992) *Annu Rev Genet 26*, 179-207.

18.   Cook, W. J., Martin, P. D., Edwards, B. F., Yamazaki, R. K., and Chau, V. (1997) *Biochemistry 36*, 1621-7.

19.   Giraud, M. F., Desterro, J. M., and Naismith, J. H. (1998) *Acta Crystallogr D Biol Crystallogr 54 (Pt 5)*, 891-8.

20.   Jiang, F., and Basavappa, R. (1999) *Biochemistry 38*, 6471-8.

21.   Tong, H., Hateboer, G., Perrakis, A., Bernards, R., and Sixma, T. K. (1997) *J Biol Chem 272*, 21381-7.

22.   Cook, W. J., Jeffrey, L. C., Xu, Y., and Chau, V. (1993) *Biochemistry 32*, 13809-17.

23.   Worthylake, D. K., Prakash, S., Prakash, L., and Hill, C. P. (1998) *J Biol Chem 273*, 6271-6.

24.   Huang, L., Kinnucan, E., Wang, G., Beaudenon, S., Howley, P. M., Huibregtse, J. M., and Pavletich, N. P. (1999) *Science 286*, 1321-6.

25.   Moraes, T. F., Edwards, R. A., McKenna, S., Pastushok, L., Xiao, W., Glover, J. N., and Ellison, M. J. (2001) *Nat Struct Biol 8*, 669-73.

26.   VanDemark, A. P., Hofmann, R. M., Tsui, C., Pickart, C. M., and Wolberger, C. (2001) *Cell 105*, 711-20.

27.   Liu, Q., Jin, C., Liao, X., Shen, Z., Chen, D. J., and Chen, Y. (1999) *J Biol Chem 274*, 16979-87.

28.   Miura, T., Klaus, W., Gsell, B., Miyamoto, C., and Senn, H. (1999) *J Mol Biol 290*, 213-28.

29.   Hamilton, K. S., Ellison, M. J., Barber, K. R., Williams, R. S., Huzil, J. T., McKenna, S., Ptak, C., Glover, M., and Shaw, G. S. (2001) *Structure (Camb) 9*, 897-904.

30.   Hamilton, K. S., Ellison, M. J., and Shaw, G. S. (2000) *J Biomol NMR 18*, 319-27.

31.   McKenna, S., Hu, J., Moraes, T., Xiao, W., Ellison, M. J., and Spyracopoulos, L. (2003) *Biochemistry 42*, 7922-7930.

32.   Varelas, X., Ptak, C., and Ellison, M. J. (2003) *Mol Cell Biol 23*, 5388-400.

33.   Girod, P. A., and Vierstra, R. D. (1993) *J Biol Chem 268*, 955-60.

34.   Pickart, C. M., and Rose, I. A. (1985) *J Biol Chem 260*, 1573-81.

35. Gwozd, C. S., Arnason, T. G., Cook, W. J., Chau, V., and Ellison, M. J. (1995) *Biochemistry 34*, 6296-302.

36. Leggett, D. S., and Candido, P. M. (1997) *Biochem J 327 (Pt 2)*, 357-61.

37. Ptak, C., Prendergast, J. A., Hodgins, R., Kay, C. M., Chau, V., and Ellison, M. J. (1994) *J Biol Chem 269*, 26539-45.

38. Chen, P., Johnson, P., Sommer, T., Jentsch, S., and Hochstrasser, M. (1993) *Cell 74*, 357-69.

39. Seufert, W., and Jentsch, S. (1990) *Embo J 9*, 543-50.

40. Seufert, W., McGrath, J. P., and Jentsch, S. (1990) *Embo J 9*, 4535-41.

41. Jentsch, S., McGrath, J. P., and Varshavsky, A. (1987) *Nature 329*, 131-4.

42. Watkins, J. F., Sung, P., Prakash, S., and Prakash, L. (1993) *Genes Dev 7*, 250-61.

43. Prakash, S., Sung, P., and Prakash, L. (1993) *Annu Rev Genet 27*, 33-70.

44. Kolman, C. J., Toth, J., and Gonda, D. K. (1992) *Embo J 11*, 3081-90.

45. Liu, Y., Mathias, N., Steussy, C. N., and Goebl, M. G. (1995) *Mol Cell Biol 15*, 5635-44.

46. Silver, E. T., Gwozd, T. J., Ptak, C., Goebl, M., and Ellison, M. J. (1992) *Embo J 11*, 3091-8.

47. Ptak, C., Gwozd, C., Huzil, J. T., Gwozd, T. J., Garen, G., and Ellison, M. J. (2001) *Mol Cell Biol 21*, 6537-48.

48. Goebl, M. G., Yochem, J., Jentsch, S., McGrath, J. P., Varshavsky, A., and Byers, B. (1988) *Science 241*, 1331-5.

49. Studier, F. W., Rosenberg, A. H., Dunn, J. J., and Dubendorff, J. W. (1990) *Methods Enzymol 185*, 60-89.

50. Hodgins, R., Gwozd, C., Arnason, T., Cummings, M., and Ellison, M. J. (1996) *J Biol Chem 271*, 28766-71.

51. Kay, L. E., Keifer, P., Saarinen, T. (1992) *J. Am. Chem. Soc. 114*, 10663-10665.

52. Zhang, O., Kay, L. E., Olivier, J. P., and Forman-Kay, J. D. (1994) *J Biomol NMR 4*, 845-58.

53. Delaglio, F., Grzesiek, S., Vuister, G. W., Zhu, G., Pfeifer, J., and Bax, A. (1995) *J Biomol NMR 6*, 277-93.

54. Johnson, B. A., Blevins, R.A. (1994) *J. Chem. Phys. 29*, 1012-1014.

55. Mathias, N., Steussy, C. N., and Goebl, M. G. (1998) *J Biol Chem 273*, 4040-5.

56. Morrison, A., Miller, E. J., and Prakash, L. (1988) *Mol Cell Biol 8*, 1179-85.

57. Prendergast, J. A., Ptak, C., Arnason, T. G., and Ellison, M. J. (1995) *J Biol Chem 270*, 9347-52.

58. Walden, H., Podgorski, M. S., and Schulman, B. A. (2003) *Nature 422*, 330-4.

59. Merkley, N., and Shaw, G. S. (2003) *J Biomol NMR 26*, 147-55.

CHAPTER 8:

Conclusion

8.1 CONCLUSION

The work that has been described in this dissertation constitutes primarily a structural investigation into the Ub-conjugation enzyme family (E2s) and the interfaces that help to mediate the interactions between these E2s and Ub in a variety of capacities. The data presented have extended the base of knowledge with respect to the differences and similarities between the E2 proteins and their closely related Uev paralogues. And finally, I believe that fundamental structural insights into the mechanisms of both chain building and thiolester formation have been gained via an examination of the Ubc13/Uev Ub-conjugation machinery.

Chapter 2 serves as the foundation for all of the work concerning the Ubc13/Uev pathway, as it establishes from both a biochemical and structural perspective that the role of the human Mms2 protein is to (i) non-covalently associate with a "acceptor" Ub molecule, and (ii) mediate an interaction with Ubc13~Ub thiolester such that Lys^{63}-linked chains are preferentially formed. These results represent one of the first insights into the mechanism whereby a specific chain linkage can be accommodated, and established a role for the previously enigmatic Uev proteins.

Chapter 3 represented the largest time investment towards the completion of this thesis. The chemical shift assignments of two proteins from humans, Ubc13 and Mms2, are described in detail, and are a necessary prerequisite for the structural studies that followed. Secondary structural determinations were accomplished for each protein, and corroborated previously determined structural information (1).

Chapter 4 confirmed and extended the proposed structural scaffold of the Ubc13/Mms2 heterodimer in humans. Using NMR-derived constraints and an unbiased docking approach, a 3D model of the Ub-bound human Ub-conjugation

complex Ubc13/Mms2 was generated, which provided a structural basis for Lys^{63}-linked chain catalysis.

Chapter 5 outlined the energetics and specificity of the interactions within Ubc13/Uev/Ub human Ub conjugation complexes. Specifically, crucial dissociation constants and kinetic parameters were established for the interactions between acceptor Ub and Mms2, which increased our confidence in the model proposed in Chapter 4. Furthermore, the surfaces of interaction and dissociation constants were established for the interactions between Uev1a and acceptor Ub. This demonstrated for the first time that a parallel mechanism to Mms2, which had previously only been implied, was employed by this Uev protein. These studies also allowed for a preliminary investigation into the differences and similarities between two Uev proteins, Mms2 and Uev1a, with respect to Ub binding.

Chapter 6 described the determination of backbone amide dynamics within the Ubc13/Mms2 heterodimer. ^{15}N-T_1, ^{15}N-T_2, and ^{1}H-^{15}N-NOE backbone amide relaxation experiments were performed on each protein in both their monomeric and heterodimerized forms in order to effect a comparison between the two states. Although side chain dynamics experiments were not performed, these studies represented a first insight into the dynamic nature of a protein ubiquitination complex.

Chapter 7, the final data-containing chapter, outlined a comparison of the Ub-binding capabilities amongst members of the E2 enzyme family. Chemical shift perturbation experiments detailed both the nature of thiolester intermediates and potential non-covalent interactions between Ub and each of Ubc1, Cdc34, and Rad6 from S. cerevisiae. While the data presented is preliminary, it appears as though similar but non-identical surfaces on Ub are employed by each of these E2s in order to effect Ub binding. Further structural insight into the tail of Cdc34, and the thiolester intermediate between Ub and Ubc1, were also gained.

Taken together, the data presented herein represent a comprehensive examination into structural features of the Ub-conjugation machinery. The most

important insights came with respect to the Ubc13/Mms2 heterodimer, which was demonstrated conclusively to employ each member of the heterodimer to interact in a specific manner with a Ub molecule such that a specific chain linkage (Lys[63]) was effected. These results may reflect a more general feature of the E2 enzymes, particularly because of the recent demonstration that E2 enzymes may in fact self-associate into higher order complexes (2), which would be capable of potentially utilizing a similar mechanism to effect canonical chain building as described for Ubc13/Mms2.

^{1}H-^{15}N HSQC chemical shift perturbation experiments were used extensively and effectively to characterize the interactions between Ub and E2s. While this technique does not represent the most sophisticated or high-resolution approach to solving structural biology questions, it does represent one of the most rapid and versatile techniques available. For example, all of the protein complexes examined were either extremely short-lived (e.g. thiolester intermediates) or quite weak (e.g. acceptor Ub binding), and therefore chemical shift perturbation was a most appropriate technique. Using this procedure, in combination with classical biochemistry, several key insights into the E2 enzymes were gained. First, the surfaces on interaction on both Ub and the E2s (particularly Ubc13) were mapped with respect to thiolester formation. In both cases, a common and complimentary surface is employed to mediate the interaction, with slight but significant differences depending on the specific E2 examined. As for a non-covalent interaction between E2s and Ub representing a general feature, the results remain inconclusive at best. Whereas some E2s demonstrate a clear and biologically relevant non-covalent interaction with Ub or Ub-like proteins (3-7), others demonstrate either a moderate interaction which is uncorroborated (i.e. Cdc34) or do not demonstrate any non-covalent interaction with Ub at the detectability limit of NMR (4, 5, 8, 9).

Further studies are required in order to determine whether only specific E2s employ non-covalent associations with Ub, and whether these interactions are of biological significance to chain building (as is clearly the case for the

Ubc13/Mms2 system). Furthermore, the work outlined in this thesis represents a low-resolution picture of the interaction between the Uevs and Ub, and as such the higher resolution determination of these structures by NMR based techniques such as partial protein alignment for measuring residual dipolar couplings (*10*) remains a goal.

A series of structural determinations would be worth investigating, as they are feasible and would represent significant improvement in our understanding of the protein ubiquitination machinery. Whereas X-ray crystallography is clearly superior with respect to the determination of higher order complexes involving the interactions between the heterodimer and either E1 or E3 proteins, solution structure determination by NMR could prove invaluable with respect to mapping the associations between Ub and these proteins. In particular, the interactions between the E1 proteins and Ub have remained elusive. The interactions between the E3s Rad5 (*S. cerevisiae*) and Traf6 (human) and Ub could be mapped by chemical shift perturbation approaches, as could the effect of E2 association with E3 on both thiolester and acceptor Ub interactions. Recent improvements to NMR methodologies have significantly reduced its size limitations, making the potential for the experiments a reality.

The beginning of a detailed comparison between the different Uev proteins, in particular Uev1a and Mms2, was presented in this thesis and should be extended. Structural and functional studies in the same vein to those presented for Mms2 should be pursued for Uev1a in order to characterize their differences and similarities. The 3D structure of the Uev1a protein, free and in complex with Ubc13 should be investigated in order to examine the role of the N-terminal extension on Uev1a. And finally, the intracellular differences between these two proteins (*i.e.* nuclear localization, phosphorylation, E3 interactions) should be elucidated.

The biological role of non-canonical poly-Ub chains has been implied (*i.e.* structure modulation, recruitment) but has yet to be demonstrated conclusively. Solving the solution and/or crystal phase structures of alternative poly-Ub chains

may prove informative with respect to understanding how these protein markers are recognized and differentiated from each other. In this vein, uncovering non-canonical poly-Ub chain binding proteins would also prove beneficial.

Structural features of the E2 N- and C-terminal extensions, while difficult, should be examined. These extensions often play crucial *in vivo* roles, but remain remarkably poorly understood from a structure/function point of view. Attempts to crystallize E2s containing these extensions have not proven successful, whereas preliminary NMR-based studies have at least provided some reason for optimism (*11*). The viability of studying an E2 such as Cdc34 was presented in Chapter 7, and the results indicated that such studies may prove quite time consuming. However, I do believe that information contained in these structures would be valuable.

While information regarding the backbone dynamics of the Ubc13/Mms2 system provided some insights into the nature of these proteins, I believe that in order to fully correlate the dynamic nature of these proteins with their function(s), side chain methyl dynamics could represent the most informative approach. This methodology would require the complete assignment of all side chain and backbone resonances, which should prove feasible based on those assignments presented in Chapter 3 of this thesis.

The final area of interest that I believe may be worth investigating is the biological relevance of E2 conjugate formation and autoubiquitination. It still remains unclear as to whether these modifications represent a real regulatory mechanism or are simply an artifact of the high concentrations typically used in *in vitro* experiments. Apart from *in vivo* experiments to determine the relevance of this modification, structural and functional studies could characterize this interesting species.

Overall, I believe that the data outlined in this thesis represents a sound body of work that has contributed valuable information regarding the nature of poly-Ub chain building to the scientific community, and has established a basis upon which future investigations can be successfully based.

8.2 REFERENCES

1. Moraes, T. F., Edwards, R. A., McKenna, S., Pastushok, L., Xiao, W., Glover, J. N., and Ellison, M. J. (2001) *Nat Struct Biol 8*, 669-73.

2. Varelas, X., Ptak, C., and Ellison, M. J. (2003) *Mol Cell Biol 23*, 5388-400.

3. McKenna, S., Hu, J., Moraes, T., Xiao, W., Ellison, M. J., and Spyracopoulos, L. (2003) *Biochemistry 42*, 7922-7930.

4. McKenna, S., Moraes, T., Pastushok, L., Ptak, C., Xiao, W., Spyracopoulos, L., and Ellison, M. J. (2003) *J Biol Chem 278*, 13151-8.

5. McKenna, S., Spyracopoulos, L., Moraes, T., Pastushok, L., Ptak, C., Xiao, W., and Ellison, M. J. (2001) *J Biol Chem 276*, 40120-6.

6. Miura, T., Klaus, W., Gsell, B., Miyamoto, C., and Senn, H. (1999) *J Mol Biol 290*, 213-28.

7. Liu, Q., Jin, C., Liao, X., Shen, Z., Chen, D. J., and Chen, Y. (1999) *J Biol Chem 274*, 16979-87.

8. Hamilton, K. S., Ellison, M. J., Barber, K. R., Williams, R. S., Huzil, J. T., McKenna, S., Ptak, C., Glover, M., and Shaw, G. S. (2001) *Structure (Camb) 9*, 897-904.

9. Hamilton, K. S., Ellison, M. J., and Shaw, G. S. (2000) *J Biomol NMR 18*, 319-27.

10. Zuiderweg, E. R. (2002) *Biochemistry 41*, 1-7.

11. Merkley, N., and Shaw, G. S. (2003) *J Biomol NMR 26*, 147-55.